Development and Discovery of Treatments for Mitochondrial Disease

This thesis is submitted for the degree of Doctor of Philosophy to Newcastle University

Oliver Michael Russell

BSc (Hons), MRes

Wellcome Trust Centre for Mitochondrial Research

Institute for Ageing and Health

Newcastle University

September 2013

Declaration

This thesis is submitted for the degree of Doctor of Philosophy to Newcastle University. The research was performed within the Wellcome Trust Centre for Mitochondrial Research, Institute for Ageing and Health, Newcastle University, and is my own work. The research was carried out under the supervision of Professor D. M. Turnbull and Professor R. N. Lightowlers between October 2010 and September 2013.

I certify that none of the material offered in this thesis has been previously submitted by me for a degree or any other qualification at this or any other university.

Abstract

Although mitochondrial disorders are the most common inherited form of neuromuscular disease, there are currently limited effective treatments that directly improve mitochondrial function – either by modulation of the effects of mutated genes or by increasing the proportion of healthy mitochondria. In this work, two different approaches were employed to develop treatments for mitochondrial diseases: the design of mitochondrially targeted anti-sense oligonucleotides and the development of a high throughput screen of a unique library of bacterial extracts.

The heteroplasmic nature of mitochondrial DNA (mtDNA) enables the use of anti-genomic strategies to specifically prevent the replication, transcription or translation of mutated molecules of mtDNA or mitochondrial mRNA in patients with heteroplasmic mtDNA mutations. In conjunction with an industrial partner (Ugichem GmbH), a mitochondrial targeting oligonucleotide was developed using cell membrane crossing oligomers (CMCOs) – a new class of oligonucleotide with the ability to enter and accumulate within the cytoplasm. By conjugating "mitochondrial targeting" molecules to the CMCOs, translocation to mitochondria was shown, potentially enabling the use of anti-sense therapies in the treatment of mtDNA diseases.

To complement the mutation specific approach of anti-sense oligonucleotide therapies a large scale screen was carried out to discover compounds that could cause a general improvement in mitochondrial function. A library of unique bacterial extracts, provided by Demuris Ltd, was screened for effects on mitochondrial biogenesis in HeLa cells. To that end, a high throughput assay, which used fluorescent markers to detect changes in relative mitochondrial mass, was designed and validated using mitochondrially active control compounds. The screen of bacterial extracts discovered several one extract which caused mitochondrial mass to increase 2 fold after 48 hours incubation.

Acknowledgements

There are so many people who have made the last three years possible, all of which I need to thank. Firstly, I would like to thank Doug and Bob for giving me the opportunity to start my career in the MRG and for trusting me with such an interesting project. There have been difficult times over the last three years and without your help and guidance I doubt this project would have ever managed to actually get some results!

I would also like to thank my collaborators at Ugichem, Dr Thomas Lindhorst and Dr Birgit Werner, without whom this project would not have been possible. Your input has been instrumental in the continuation of this project even when it looked like we weren't getting anywhere. The guys at Demuris have also been great for all their help with the drug screen. I can't thank you enough for being so helpful and teaching me about the wonders of soil bacteria! Dr Alex Laude for all his help with microscopy and for trusting me with his expensive confocal! Thanks to Dr Peter Banks for teaching me how to use the robots and for helping me design the programmes, hopefully I didn't break anything!

Everyone in the MRG who has helped me over the last three years, especially my office chum(p)s Eve, John and Georgia for making writing up so much fun. Even when writing seemed like a Sisyphean task we still managed to have a laugh, apologies for constantly trying your patience with a lot of inappropriate comments. Thanks to John G for helpful stats advice and joining me in some hard earned procrastination.

Big thanks to my family, without who I wouldn't have made it this far, I can't thank you enough for all the support you have given me over the years. I really appreciate it even if I don't always show it. To Lucy, I'm sorry I have forgotten your birthday… again! As I write this your card is hurtling towards you in the post! To the Stags, the five best friends that anyone can have, without our wolf pack I would not have kept my sanity. Harroo! And to Amy, who I know is going to be annoyed at being last on this list, I cannot put into words how much your help and support has kept me going over the last

few years. Without you none of this would have been possible and I would be a lesser man. Thank you.

Table of Contents

List of Figures

List of Tables

Abbreviations

A-site	Aminoacyl acceptor site
ATP	Adenosine Triphosphate
ATPase	ATP synthase
bp	Base pair
BSA	Bovine Serum Albumin
CO_2	Carbon dioxide
CoA	Coenzyme A
COX	Cytochrome *c* oxidase
DAPI	4',6-diamidino-2-phenylindole
ddH_2O	Double distilled water
dH_2O	Distilled water
D-loop	Displacement loop
DMSO	Dimethyl Sulphoxide
DNA	Deoxyribonucleic acid
e^-	Electron
E-site	Exit site
FAD	Flavin adenine dinucleotide
$FADH_2$	Reduced flavin adenine dinucleotide
FAM	6-carboxyfluorescein
FBS	Foetal bovine serum

FCCP	Trifluorocarbonylcyanide Phenylhydrazone
FITC	Fluorescein isothiocyanate
g	Grams
g	Force of gravity
H^+	Proton
HSP	Heavy strand promoter
H-strand	Heavy strand
kDa	Kilo Dalton
L	Litre
LSP	Light strand promoter
L-strand	Light strand
M	Molar
MELAS	Mitochondrial encephalomyopathy and stroke-like symptoms
MEM	Modified Eagle's Medium
MERRF	Myoclonic epilepsy with ragged-red fibres
mg	Milligram
ml	Millilitre
MNGIE	Mitochondrial neurogastrointestinal encephalopathy syndrome
mRNA	Messenger ribonucleic acid

mtDNA	Mitochondrial deoxyribonucleic acid
mtEF	Mitochondrial elongation factor
mTERF	Mitochondrial termination factor
mtIF	Mitochondrial initiation factor
mtRF	Mitochondrial release factor
mt-rRNA	Mitochondrial ribosomal ribonucleic acid
mtSSB	Mitochondrial single-stranded DNA binding protein
NAD^+	Nicotinamide adenine dinucleotide
NADH	Reduced nicotinamide adenine dinucleotide
NaOH	Sodium hydroxide
nDNA	nuclear deoxyribonucleic acid
NDUFS	NADH dehydrogenase ubiquinone iron-sulphur
NEAA	Non-Essential Amino Acids
NGS	Normal goat serum
nt	Nucleotide
O_2	Molecular oxygen
$O_2^{\cdot -}$	Superoxide anion
O_H	Origin of heavy strand replication
O_L	Origin of light strand replication
OXPHOS	Oxidative phosphorylation
PBS	Phosphate buffered saline
PBST	Phosphate buffered saline with 0.1% Tween

PCR	Polymerase chain reaction
PFA	Paraformaldehyde
PFS	Perfect focus system
PGC-1α	PPAR gamma coactivator -1α
PMT	Photomultiplier tube
POLG	Polymerase gamma (γ)
POLRMT	Mitochondrial RNA polymerase
PPAR	Peroxisome proliferator-activated receptor
P-site	Peptidyl site
PVDF	Polyvinylidene fluoride
Q	Ubiquinone
QH_2	Ubiquinol
rCRS	Revised Cambridge reference sequence
RNA	Ribonucleic acid
ROS	Reactive oxygen species
RT-PCR	Reverse transcription polymerase chain reaction
SDH	Succinate dehydrogenase
SDS	Sodium dodecyl sulphate
TAE	Tris acetate EDTA
TAMRA	Carboxytetramethylrhodamine
TBS	Tris buffered saline

TCA cycle	Tricarboxylic acid cycle
TFAM	Mitochondrial transcription factor A
TFB1M	Mitochondrial transcription factor B1
TFB2M	Mitochondrial transcription factor B2
TIM	Translocase of the inner membrane
TMRM	Tetramethylrhodamine
TOM	Translocase of the outer membrane
tRNA	Transfer RNA
TTBS	Tris-buffered saline with 0.1%Tween 20
µl	Microlitre
µm	Micrometer
UV	Ultra-violet
v/v	Volume per volume
VDAC	Voltage gated ion channel
w/v	Weight per volume

Introduction

Introduction

1.1. MITOCHONDRIA

The mitochondrion is a cytoplasmic organelle found within a large reticular network in eukaryotic cells. Each organelle has a double membrane structure, which houses the machinery needed for mitochondria to not only produce ATP (adenosine triphosphate), but also to fulfil their roles in apoptosis, calcium handling and the formation of iron sulphur clusters along with numerous other functions. Mitochondria are the only non-nuclear source of DNA in humans and although the mitochondrial genome encodes vital proteins for mitochondria function, the vast majority of mitochondrial proteins are nuclear encoded (Anderson et al. 1981). However, the fact that mitochondria encode their own proteins also means that they are susceptible to a set of diseases caused by mutations in mitochondrial DNA (mtDNA), which not only affect mitochondria, but cellular function as a whole (Park and Larsson 2011).

1.2. ORIGINS OF MITOCHONDRIA

The origin of mitochondria is generally believed to stem from a symbiotic relationship between a eubacterium and a primitive eukaryotic cell in order to take advantage of increasing concentrations of atmospheric O_2, which eventually led to the bacterium being permanently housed within the cell. The original hypothesis for this was proposed by Margulis in 1971 who suggested that this relationship occurred after the formation of the nucleus (Margulis 1971). Martin and Muller offered an alternative theory that the mitochondrion and nucleus were formed simultaneously as a result of fusion between a hydrogen dependent archaebacterium and a hydrogen producing eubacterium (Martin and Muller 1998). These theories, known as the endosymbiotic theory and hydrogen hypothesis respectively, both believe that the majority of the genetic material contained within mitochondria was transferred to the nucleus. Whole genome sequencing of the α-proteobacterium, *Rickettsia prowazekii*, found that a complete set of tricarboxylic acid cycle (TCA) genes and respiratory-chain enzymes were encoded, genes that are essential for mitochondrial based respiration (Andersson et al. 1998).

1.3. STRUCTURE

The mammalian mitochondrion has been traditionally viewed as an ovoid organelle compartmentalised by a double plasma membrane. The “baffle” model of mitochondrial structure was developed using early electron microscopy (EM) studies and described a folded inner membrane contained within an outer membrane. The broad folds of inner membrane were named “cristae” (Palade 1952). This model has since been updated using EM tomography studies, which shows that the cristae do not have wide openings at the intermembrane space, but in fact show a much narrower and tubular like structure (Mannella et al. 1994) (figure 1.1).

The outer mitochondrial membrane compartmentalises the organelle from the cytosol and contains abundant levels of the mitochondrial voltage dependant anion channel (VDAC). This protein forms a channel through which molecules up to 10kDa can enter the intermembrane space (Alberts et al. 2008). The inner membrane is cardiolipin rich and separates the intermembrane space from the matrix and consequently contains a number of transport proteins that regulate the flow of material into the matrix (these proteins are vital as the membrane is essentially impermeable). The inner membrane not only forms the scaffold for oxidative phosphorylation proteins, but also helps maintain the electrochemical gradient between the intermembrane space and the matrix, which is essential for ATP formation (Mitchell 1961).

The mitochondrial matrix is the site of many of the enzymatic processes required for oxidative metabolism, such as the TCA cycle and β-oxidation of fatty acids. It also contains mtDNA and is the site of replication, transcription and translation of this genome.

Transport of compounds into the matrix is highly regulated in order to maintain the proton electrochemical gradient (Alberts et al. 2008). As the majority of mitochondrial proteins are produced in the cytosol, there is a dedicated peptide transport system across the outer and inner membranes; TOM (translocase of the outer membrane) and TIM (translocase of the inner membrane), respectively. These multi-subunit translocases recognise mitochondrial targeting sequences located primarily at the N-terminal of the

peptide, allowing the peptide to enter the matrix, after which the targeting sequence is cleaved by a matrix processing peptidase (Hawlitschek et al. 1988; Pfanner et al. 1988). The most abundant transport protein in the inner membrane is the adenine nucleotide translocator (ANT). This protein enables the transport of ATP and ADP between the matrix and inner membrane space (Pfaff and Klingenberg 1968).

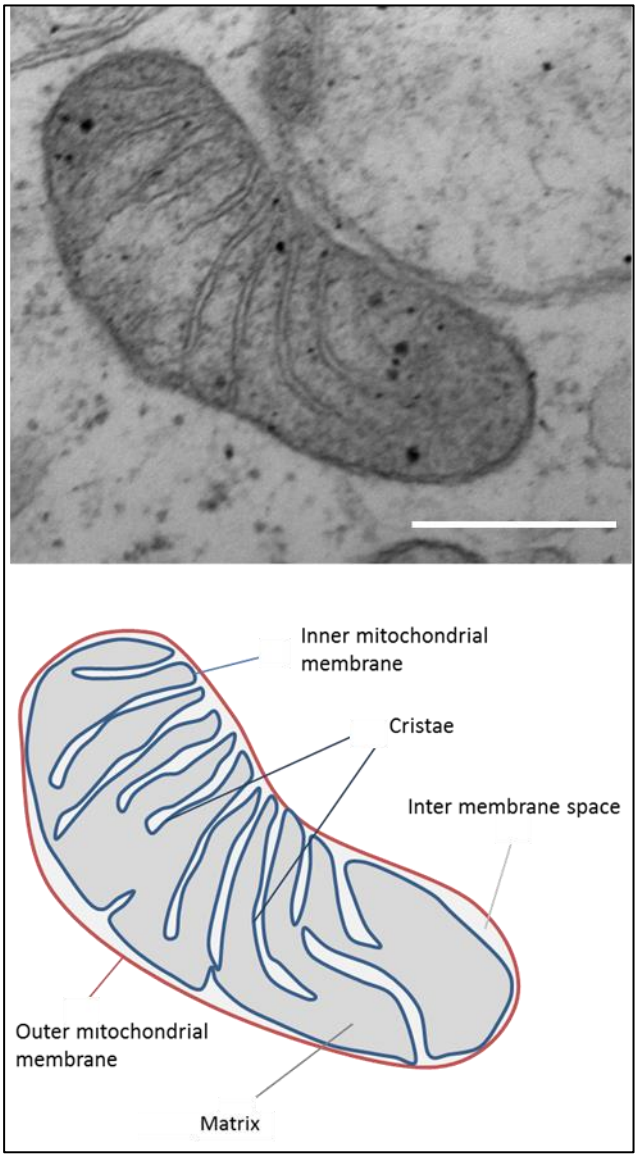

Figure 1.1 – Mitochondrial structure.
An electron micrograph (upper panel) shows the fine structure of an ovoid mitochondrion. The lower panel shows a schematic of the image with labelled compartments and structures. Scale represents 500nm. *Image courtesy of Dr. Amy Reeve*.

1.3.1. **Mitochondrial dynamics**

With the advent of live cell microscopy studies, it became clear that mitochondria are not static organelles, but are in fact highly dynamic and undergo processes of fission and fusion (Bereiter-Hahn 1978; Nunnari et al. 1997). Fusion and fission are essential for the transport of mitochondria into daughter cells, removal of damaged mitochondria and may also play a role in modulation of ATP production (Skulachev 2001).

1.3.1.1. *Mitochondrial fusion*

Mitochondrial fusion is mediated by members of the Dynamin family of proteins, the first of which to be characterised was outer mitochondrial membrane protein Fzo (fuzzy onion), found in *Drosophila* sperm cells where it controls the formation of giant mitochondria (Hales and Fuller 1997). A second outer membrane protein that was characterised in other *Drosophila* cell types was Marf, which also mediates fusion (Dorn et al. 2011).

The Mitofusins – Mfn1 & Mfn2 – are the mammalian outer membrane fusion proteins. These proteins are large GTPases which interact via hydrophobic heptad repeat regions (HR2) that are found on the cytosolic face of the protein. Mitofusins tether to each other via HR2 interactions, after which GTPase is involved in the fusion of mitochondria, (Koshiba et al. 2004). Although they are expressed in the same cell lines, each protein is capable of controlling fusion on its own (Chen et al. 2003). Fusion of the inner mitochondrial membrane is controlled by the GTPase Opa1 in humans (so called for its involvement in dominant *Op*tic *a*trophy), which requires Mfn1 in order to promote fusion, but not Mfn2 (Cipolat et al. 2004).

1.3.1.2. *Mitochondrial fission*

Unlike fusion proteins that require both an inner and outer membrane protein in order for complete fusion to occur, the process of fission is controlled in yeast by one Dynamin protein (Dnm1). Genetic screens of yeast found that Dnm1 was responsible for mitochondrial fission (Bleazard et al. 1999), as is its mammalian homolog; Drp1 (Shin et al. 1997). All of the homologs contain a GTPase domain and a variable domain, which is required to bind to a target membrane. Drp1 is thought to be recruited to the

mitochondrial membrane by another protein (possibly Fis1). It is postulated that it then forms a ring like structure and pinches mitochondria using its GTPase domain (Hoppins et al. 2007). Fis1, a small outer membrane bound protein, is required for the recruitment of Dmn1 in yeast (Mozdy et al. 2000), however its function in mammalian fission is not clear as its depletion does not affect Drp1 (Otera et al. 2010).

1.3.2. **Mitochondrial Biogenesis**

As the energy requirements of the cell change, so does its need for mitochondria, therefore mitochondrial biogenesis is tightly regulated (figure 1.2) in order to produce sufficient ATP. The primary controller of biogenesis is the peroxisome proliferator-activated receptor γ coactivator 1α (PGC-1α) a cofactor for transcription factors that regulate the expression of nuclear-encoded mitochondrial proteins; nuclear respiratory factors (NRF1 and 2) and oestrogen related receptor α (ERRα), as well as forkhead box class-O (FoxO1) and peroxisome proliferator activated receptors (PPARs) (Puigserver and Spiegelman 2003). Overexpression of PGC-1α in "mutator mouse" models (see section 1.7.6) has been shown to increase the quantity of mitochondrially encoded OXPHOS subunits detected by western blotting by up to 50%. mtDNA copy number doubled in the overexpression mice, and there was also a decrease in the number of COX-deficient fibres seen in their skeletal muscle (Dillon et al. 2012).

1.3.3. **Transcriptional control**

Control of PGC-1α is tightly regulated and its activity essentially depends on the energy requirement of the cell at a given time. For example, in skeletal muscle during exercise, PGC-1α can be activated in response to Ca^{2+} signalling through either Ca^{2+}/calmodulin dependent kinase IV (CaMKIV) or calcineurin A (CnA). CaMKIV phosphorylates CREB (cAMP response element binding protein), which binds CRE (CREB response element) and increases PGC-1α expression (Herzig et al. 2001). CnA activates the myocyte enhancer factors (MEF2C & D) that drive myogenesis and also induce PGC-1α. The mitogen activated protein kinase p38 (MAPK) can also activate MEF2 during exercise, along with ATF2 (activating factor 2) which both go on to induce expression (Michael et al. 2001; Handschin et al. 2003; Akimoto et al. 2005).

In brown adipose tissue cold temperatures are sensed by the sympathetic nervous system and activate β3 adrenergic receptors (Puigserver et al. 1998). This increases cAMP activating PKA (protein kinase A). PKA's primary target is CREB, which activates and subsequently goes on to increase PGC-1α expression (Cao et al. 2004).

1.3.4. **Functional control**

During exercise the level of AMP in relation to ATP increases, which triggers the activation of AMPK (AMP activated protein kinase) (Jorgensen et al. 2005). This kinase activates cellular processes in order to increase ATP production, one of which is to increase mitochondrial biogenesis. The amount of PGC-1α has been shown to increase in an AMPK dependent manner in skeletal muscle, as has the proportion that is activated (Jager et al. 2007). Although the mechanism of PGC-1α induction by AMPK is unclear, treatment of skeletal muscle cells with AICAR (5-aminoimidazole-4-carboxamide 1-β-D-ribofuranoside), an AMPK activator, has also been shown to increase PGC-1α activation (Jorgensen et al. 2005).

Acetylation also plays a role in the regulation of PGC-1α as the deacetylase enzyme Sirtuin 1 (SIRT1) has been shown to increase its activity. SIRT1 is largely thought to sense the energy status of the cell, as it needs the cofactor NAD^+ in order to function (Houtkooper et al. 2010). The NAD^+/NADH ratio swings in favour of high NAD^+ in low energy situations, which increases the activity of SIRT1 and therefore PGC-1α (Canto et al. 2009). Work in mice has shown that SIRT1 knockdowns have lower levels of PGC-1α induced gluconeogenesis proteins, whereas SIRT1 overexpression mice have increased levels. β-oxidation of fatty acids, in response to starvation, also increases the level of NAD^+ and increases the activity of SIRT1 (Rodgers et al. 2005; Rodgers and Puigserver 2007).

Down-regulation of PGC-1α is caused by histone acetyltransferase (GCN5) both *in vitro* and *in vivo* when the cell has a high energy status (Lerin et al. 2006). Insulin also plays a role in PGC-1α regulation. In the presence of insulin (when the cell has a high energy status) Akt (protein kinase B) phosphorylates FoxO1, preventing it from inducing PGC-1α and sequestering it into the cytosol (Southgate et al. 2005).

Figure 1.2 - Transcriptional and functional control of PGC-1α in response to various cell stimuli.

Activation of PGC-1α is controlled by AMP-activated protein kinase (AMPK) which phosphorylates PGC-1α in response to high AMP. Sirtuin 1 (SIRT1) deacetylates PGC-1α in response to high NAD^+. Histone acetyltransferase (GCN5) acetylates PGC-1α in response to caloric excess, inhibiting its action. Mammalian target of rapamycin (mTOR) inhibits AMPK in response to insulin or excess amino acids, preventing phosphorylation. AMPK is also inhibited by high levels of ATP / low AMP levels.

Transcription of PGC-1α occurs in response to exercise by increasing calcium signalling via calcineurin A (CnA) and calmodulin dependent protein kinase IV (CaMKIV). p38 signalling also increases in response to exercise activating myocyte enhancer factor 2 (MEF2) activation along with activation of activating transcription factor 2 (ATF2). As part of thermogenesis during cold conditions stimulation by β3 adrenergic receptors (β-AR) activates transcription of PGC-1α via cyclic AMP (cAMP), protein kinase A (PKA) and cAMP response element binding protein (CREB) binding. Glucagon activation of glucagon receptors (GLGN-R) via the PKA /CREB pathway also causes transcription of PGC-1α. Insulin is thought to cause cytosolic sequestration of forkhead box class –O (FoxO1) via protein kinase B (Akt), decreasing transcription.

Figure adapted from (Andreux et al. 2013)

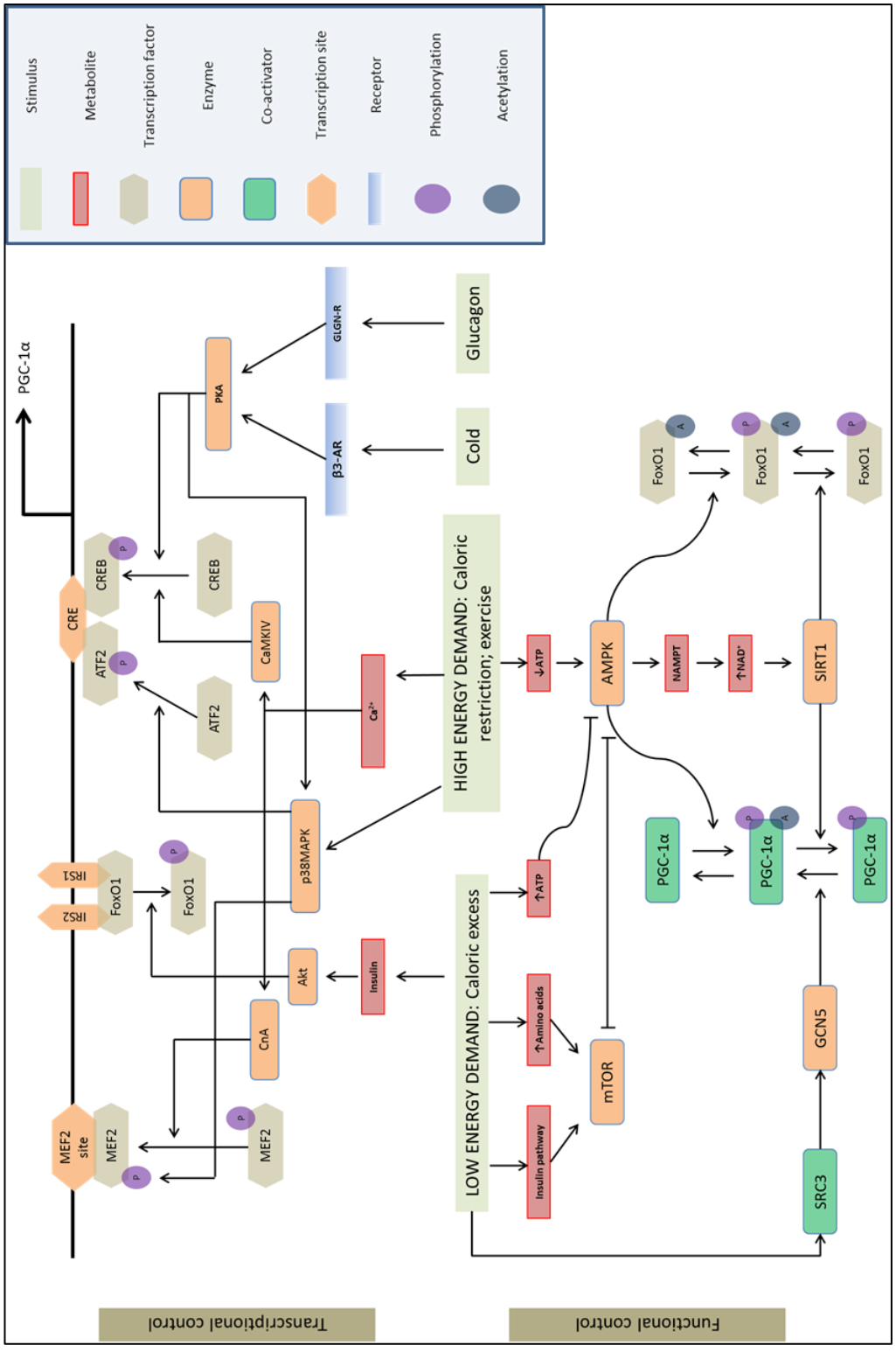
Stimulus
Metabolite
Transcription factor
Enzyme
Co-activator
Transcription site
Receptor
Phosphorylation
Acetylation
PGC-1α
GLGN-R
Glucagon
PKA
β3-AR
Cold
CRE
CREB
ATF2
CaMKIV
Ca2+
HIGH ENERGY DEMAND: Caloric restriction; exercise
↓ATP
AMPK
NAMPT
↑NAD+
SIRT1
FoxO1
PGC-1α
p38MAPK
IRS1
IRS2
FoxO1
Akt
Insulin
CnA
MEF2 site
MEF2
LOW ENERGY DEMAND: Caloric excess
↑ATP
↑Amino acids
Insulin pathway
mTOR
GCN5
SRC3
Transcriptional control
Functional control

1.4. MITOCHONDRIAL FUNCTIONS

Mitochondria are most commonly associated with the production of ATP; however they are also the site of reactive oxygen species generation and iron-sulphur cluster formation. They also play important roles in calcium handling, β-oxidation of fatty acids and apoptosis, all of which makes mitochondria an essential organelle for the health of the cell.

1.4.1. Respiration

Mitochondria are sometimes referred to as the "powerhouses" of the cell, an apt description as they are the production sites of the majority of cellular ATP. Several intermediate steps are required to produce substrates for oxidative phosphorylation (OXPHOS), the major ATP source. This begins in the cytosol with the conversion of glucose into pyruvate during glycolysis (equation 1.1), which also generates a net gain of 2 ATP molecules (Berg 2011).

$$glucose + 2NAD^+ + 2ADP + 2P_i \rightarrow 2\,pyruvate + 2NADH + 2H^+ + 2ATP + 2H_2O$$

Equation 1.1 – Glycolysis

Pyruvate is transported across the double mitochondrial membrane into the matrix where it is converted into acetyl CoA by pyruvate dehydrogenase (equation 2).

$$pyruvate + CoA + NAD^+ \rightarrow acetylCoA + NADH + H^+ + CO_2$$

Equation 1.2 – Pyruvate decarboxylation

Acetyl CoA feeds into the matrix localised TCA cycle, a series of reactions that produce reduced electron carriers: NADH and $FADH_2$ along with ATP and CO_2. Acetyl CoA enters the cycle by reacting with oxaloacetate to form citrate. Several intermediate reactions occur until oxaloacetate is reformed. The overall reaction is shown in equation 1.3 (Berg 2011).

$$acetyl\ CoA + 3NAD^+ + FAD + ADP + P_i + 2H_2O \rightarrow CoA + 3NADH + 2H^+ + FADH_2 + ATP + 2CO_2$$

Equation 1.3 - Overall TCA cycle

The production of the electron carriers NADH and $FADH_2$ is essential for the final stage of respiration – OXPHOS. During this process they donate electrons to complexes I and II, which are transferred to complexes III and IV, releasing energy which is used to transport H^+ into the intermembrane space, generating an electro-chemical gradient which is harnessed by the ATP synthase (complex V) to produce ATP (figure 1.3) (Berg 2011).

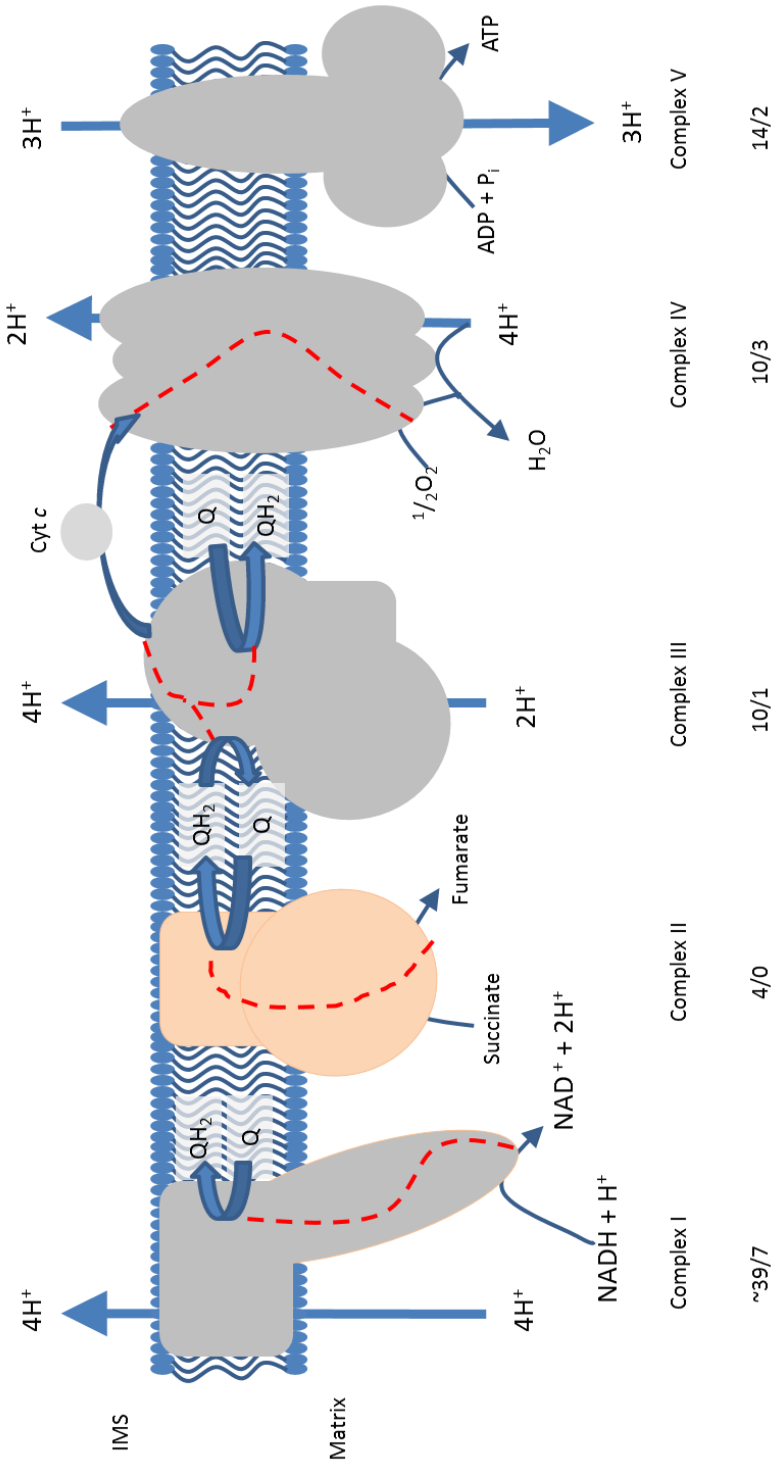

Figure 1.3 – Oxidative phosphorylation.
OXPHOS proteins are embedded in the inner mitochondrial membrane. Electrons enter OXPHOS via complex I & II and transported across complex III to complex IV. The electrons (red lines) provide energy to drive the transport of protons into the inter membrane space, creating an electrochemical gradient. The final complex, ATP synthase uses the proton gradient to produce ATP. The ratio of nuclear to mitochondrially encoded subunits in each complex is show by the numbers below each complex name. For example ~38/7 shows that Complex I has ~38 nuclear encoded and 7 mitochondrially encoded subunits. Figure based on (Nijtmans *et.al.*, 2004).

1.4.1.1. *Oxidative Phosphorylation*

Complex I (NADH: Ubiquinone Oxidoreductase) is made up of ~38 subunits, 7 of which are encoded by mtDNA (Hirst et al. 2003). The complex comprises of three modules (N, Q and P) each with a different function. NADH is oxidised in a reaction occurring in module N, during which two electrons are donated to flavin mononucleotide (FMN) (Walker et al. 1992). The electrons are transferred along a chain of iron sulphur (Fe-S) clusters through to module Q where the electrons are used to reduce ubiquinone (Q) to ubiquinol (QH_2), creating a pool of ubiquinol in the intermembrane space (Sazanov 2007).

During electron transport it is thought that a conformational change occurs in complex I enabling module P, which is embedded in the inner membrane, to open pores and allow 4 protons to cross into the intermembrane space (Efremov et al. 2010; Baradaran et al. 2013). The overall reaction is shown in equation 1.4.

$$NADH + Q + 5H^+_{matrix} \rightarrow NAD^+ + QH_2 + 4H^+_{ims}$$

Equation 1.4 – Complex I reaction

Complex II (Succinate ubiquinone oxidoreductase) is entirely encoded by the nuclear genome and consists of 4 subunits (SDHC & SDHD, which anchor the complex to the inner membrane and SDHA & SDHB - the matrix located catalytic core) (Hagerhall 1997).

No protons are transferred into the intermembrane space by complex II, however it does play a crucial role in the TCA cycle as it catalyses the conversion of succinate to fumarate, generating $FADH_2$ in the process (Berg 2011). $FADH_2$ is then oxidised to FAD^+, the electrons from which are transported along Fe-S clusters and then used to reduce ubiquinone to ubiquinol (equation 1.5) (Hagerhall 1997).

$$succinate + Q \rightarrow fumarate + QH_2$$

Equation 1.5- Complex II reaction

Complex III- (Ubiquinol: cytochrome *c* oxidoreductase) consists of 11 subunits, only one of which (apocytochrome *b*) is encoded by the mitochondrial genome, and is responsible for the transfer of 2 electrons from ubiquinol to cytochrome *c*. Its function requires a number of cytochromes that contain haem along with a Rieske Fe-S cluster (Xia et al. 1997).

The transfer of electrons is carried out during the Q cycle, which couples the reduction of ubiquinol to the movement of two H^+ ions into the intermembrane space (Mitchell 1976). A ubiquinol binds the Q_0 site where it releases two electrons and two H^+ ions, one electron binds the Rieske Fe-S and passes onto cytochrome c_1 before reducing cytochrome *c* and releasing it. The other is transferred to cytochrome *b* where it passes across haem groups before reducing ubiquinone to form ubisemiquinone at the Q_1 site. The second ubiquinol then binds the Q_0 site releasing two electrons and H^+ ions. One electron is transferred to new cytochrome *c* and the other is used to fully reduce the ubisemiquinone to ubiquinone (Berg 2011). This is summarised by equation 1.6.

$$2QH_2 + Q + 2Cytc_{ox} + 2H^+_{matrix} \rightarrow 2Q + QH_2 + 2Cytc_{red} + 4H^+_{ims}$$

Equation 1.6- The Q cycle

Complex IV- Cytochrome *c* oxidase is comprised of 13 subunits (subunits I - III are encoded by mtDNA) and is responsible for the reduction of O_2 and the formation of H_2O. Electrons are initially transferred from cytochrome *c* to the primary electron donor Cu_A and then to $haem_a$. The electron is then transferred to the catalytic site of $haem_{a3}$ and Cu_B (Tsukihara et al. 1996; Faxen et al. 2005).

The formation of H_2O occurs in two stages of electron transfer – one molecule of H_2O requires the transfer of 4 electrons from 4 cytochrome *c* molecules (one electron each). The first two electrons travel to the catalytic site where the first electron reduces Cu_B and the second reduces $haem_{a3}$. A peroxide bridge is formed between the two groups by the addition of molecular oxygen (Faxen et al. 2005).

The next round of electrons follows the same pattern, however this time the metal groups are bound by $2H^+$ ions, releasing the peroxide bridge. The formation of two molecules of H_2O is completed by the addition of $2H^+$ ions. As this occurs, $4H^+$ ions are transferred to the intermembrane space (Faxen et al. 2005). This is summarised in equation 1.7.

$$4Cytc_{red} + 8H^+ + O_2 \rightarrow 4Cytc_{ox} + 2H_2O + 4H^+_{ims}$$

Equation 1.7 – Complex IV reaction

Complex V- the F_oF_1 ATP Synthase utilizes the proton gradient that is generated by three of the four complexes to produce ATP. Complex V is composed of two domains; F_o which is located in the membrane and F_1 which extends into the matrix (Yoshida et al. 2001). F_o contains 8 hydrophobic c-subunits forming a c-ring through which protons pass. F_1 consists of five subunits in total (α, β, γ, δ and ε), with a stationary ring consisting of 3α and 3β subunits with the remaining subunits forming the central rotary stalk (Wittig and Schagger 2008; Wittig et al. 2008).

The movement of H^+ ions through F_o generates rotary torque that is used by F_1 to drive the formation of ATP from ADP and P_i. As H^+ ions move through the c-ring, glutamate residues on the c-subunits are protonated and deprotonated which causes rotation of F_1 subunits γ and ε. As F_1 rotates, the β subunits (to which ATP and P_i bind) undergo conformational changes (Noji et al. 1997). Continued rotation generates enough energy to convert ADP and P_i to ATP, after which ATP is released. A full 360^o rotation generates 3 molecules of ATP for the transfer of 8 H^+ ions; therefore each molecule of ATP produced costs 2.7 H^+ ions (Watt et al. 2010; Berg 2011).

1.4.2. **Generation of reactive oxygen species**

Reactive oxygen species (ROS) produced by mitochondria play an important role in redox signalling from the organelle to the rest of the cell, and are also implicated in causing oxidative damage to the organelle. Work by Loschen and colleagues in isolated pigeon heart mitochondria showed that production of H_2O_2 is linked to OXPHOS respiration (Loschen et al. 1971). Subsequent work has shown that H_2O_2 is produced after the action of superoxide dismutase II on superoxide anions ($O_2^{\cdot -}$) in the matrix (Brand 2010). Complex I produces the majority of $O_2^{\cdot -}$, which is produced in a reaction of molecular oxygen with fully reduced FMN (Kussmaul and Hirst 2006). Although it has been shown that complex III can produce more ROS than complex I under conditions such as antimycin inhibition, the physiological relevance of this is unclear (Murphy 2009). However, it is likely that basal levels of ROS are produced during normal OXPHOS (Murphy 2009). It should be noted that superoxide produced by complex III is released on both sides of the inner membrane unlike complex I which releases superoxide into the matrix (St-Pierre et al. 2002), potentially making complex III ROS more important for cell signalling as ROS have easier access to the cytosol than other ROS sources – they do not have to cross the inner mitochondrial membrane. Glycerol 3-phosphate dehydrogenase, an inner membrane bound enzyme which is involved in lipid metabolism, has also been shown to be produce ROS on both sides of the inner membrane, although the exact production site is unclear (Brand 2010).

Hydroxyl radicals are produced during the Fenton reaction in which H_2O_2 reacts oxidises iron to form hydroxide ions and hydroxyl radicals. The hydroxyl radical is particularly reactive and has been shown to damage most biological molecules. Due to its reactivity it is relatively short lived with a half-life of 10^{-9} seconds when compared to superoxide anions and H_2O_2 which both have half lives in the microsecond range, although these depend on their enzymatic detoxification rates (Sies 1993). Nitric oxide is also produced in the mitochondria by conversion of L-arginine to L-citrulline by nitric oxide synthase. It can bind in a reversible and dose dependent manner the O_2 binding site of cytochrome *c* synthase, preventing the flow of electrons and decreasing OXPHOS. Reaction of NO with superoxide generates peroxynitrite (half-life 0.05-1s), accounting for consumption of 15% of the superoxide produced by mitochondria. This radical can damage mitochondria by oxidising lipid membranes and has also been linked to the induction of apoptosis (Ghafourifar and Cadenas 2005).

Redox signalling from mitochondrially produced ROS is important for reporting the status of mitochondria to the rest of the cell. H_2O_2 can oxidise thiol groups on cysteine residues, altering the activity of proteins involved in signalling cascades. Regulation by H_2O_2 has been shown to occur by oxidising residues in the catalytic site of phosphatases such as PTPb1, PTEN and MAPK, inhibiting their ability to dephosphorylate their respective targets (Rhee et al. 2000; Tonks 2005). MAPK is part of the signalling cascade which leads to the transcription of PGC1α –the master regulator of mitochondrial biogenesis as discussed previously. Interestingly, it has also been shown that PGC1α also acts as a transcription factor of antioxidants, enabling the balance between ROS and mitochondria to be maintained (St-Pierre et al. 2006).

To prevent cell damage or aberrant cell signalling, ROS are tightly regulated. Consequently there are several mechanisms to reduce ROS in order to detoxify them. Reduction of $O_2^{\cdot -}$ to H_2O_2 is catalysed by SOD1 in the intermembrane space and cytosol, SOD2 in the matrix and SOD3 in the extracellular space. Several mechanism are used to reduce H_2O_2.Catalse is present in peroxisomes and converts H_2O_2 to H_2O and O_2 (Sena and Chandel 2012). The peroxiredoxins (PRX), of which there are 6 isoforms in mammalian cells, also reduce H_2O_2. Reduced PRX is converted to an inactive, oxidised form via the oxidation of a cysteine residue by H_2O_2, converting it to H_2O. Oxidised PRX is converted back into its active reduced form by thioredoxin. Glutathione peroxidases are also responsible for reduction of H_2O_2, catalysing the oxidation of glutathione to glutathione disulphide by H_2O_2 (Sena and Chandel 2012).

1.4.3. **Calcium Handling**

Cellular Ca^{2+} signalling is essential for the control of inter cell communication, programmed cell death and ATP production (Duchen 2000). Mitochondria act as Ca^{2+} buffers in the cell, preventing changes in extracellular Ca^{2+} concentration from damaging cellular components. Mitochondria have the ability to accumulate up to 1000nmol Ca^{2+}/mg of mitochondrial protein via the calcium uniporter located in the inner membrane (Kirichok et al. 2004). Modulation of Ca^{2+} is critical in neuronal pre-synaptic terminals where Ca^{2+} plays a crucial role in synaptic transmission (Jacobson and Duchen 2004; Abramov and Duchen 2010). Increased mitochondrial Ca^{2+} has also

been shown to increase the activity of the TCA cycle and ATP production (McCormack et al. 1990; Jouaville et al. 1999).

1.4.4. **Apoptosis**

Apoptosis, or programmed cell death, is controlled by an extrinsic, cell receptor mediated pathway, or an intrinsic, cell damage mediated pathway. Cytochrome *c* is an integral factor of apoptosis, the release of which from mitochondria enables the formation of an apoptosome with APAF1 which goes on to activate caspase-9, leading to apoptosis (Wang and Youle 2009).

Release of cytochrome *c* is a stringently regulated process that requires the binding of pro-apoptotic Bcl2 family proteins Bax and Bak to the outer mitochondrial membrane, causing membrane permeablisation and cytochrome *c* release (Wei et al. 2001). Oligomerisation and membrane localisation of these proteins is normally inhibited by Bcl-2, however during apoptosis Bcl-2 is inhibited by the BH3 family of proteins (Willis et al. 2007). Exactly how these pores form is currently unknown.

1.4.5. **Iron Sulphur cluster formation**

Iron sulphur clusters are essential cofactors for OXPHOS, facilitating the transfer of electrons by repeatedly changing the redox status of iron from Fe^{2+} to Fe^{3+}. Reduced iron is transported into the mitochondrial matrix by mitoferrins (Paradkar et al. 2009), after which iron is donated to scaffold proteins Isu1 and Nfu via frataxin and an iron-sulphur cluster is formed (Tong et al. 2003; Yoon and Cowan 2003). Sulphur is provided in the form of sulphide ions formed from the release of sulphur from cysteine by cysteine desulphurase (Tong and Rouault 2000). The production of iron sulphur clusters is the only conserved function of mitochondria and mitosomes (primitive mitochondria) across all eukaryotes.

1.5. MITOCHONDRIAL DNA

Mitochondria contain their own 16,569bp circular, intronless genome situated in the mitochondrial matrix. Of the 37 genes encoded by the genome, 13 encode hydrophobic proteins that are essential for OXPHOS. To enable translation of these proteins, mtDNA also encodes 22tRNAs and 2rRNAs (Anderson et al. 1981). The majority of the genes (12 proteins, 14tRNAs and both rRNAs) are transcribed from the outer "heavy" strand- so called because of the abundance of guanine. The remaining protein-encoding gene (*MTND6*) and 8 tRNAs are transcribed from the "light" strand figure 1.4.

Unlike the nuclear genome, which contains two copies of most genes, mitochondrial genomes are found in multiple copies within the cell. Depending on cell type this number can range from no mtDNA copies in erythrocytes to 100,000s in oocytes (Shoubridge and Wai 2007). Within the matrix but associated with the inner membrane (Albring et al. 1977), current work by Brown and colleagues using super resolution microscopy suggests that single genomes are packaged together in nucleoprotein complexes termed nucleoids, which contain some of the protein machinery essential for the replication and transcription of mtDNA (mitochondrial transcription factor A, single-stranded DNA binding protein and twinkle helicase) (Garrido et al. 2003; Wang and Bogenhagen 2006; Brown et al. 2011). Mgm101p is also present in the nucleoids of yeast and is thought to play a role in mtDNA repair (Meeusen et al. 1999).

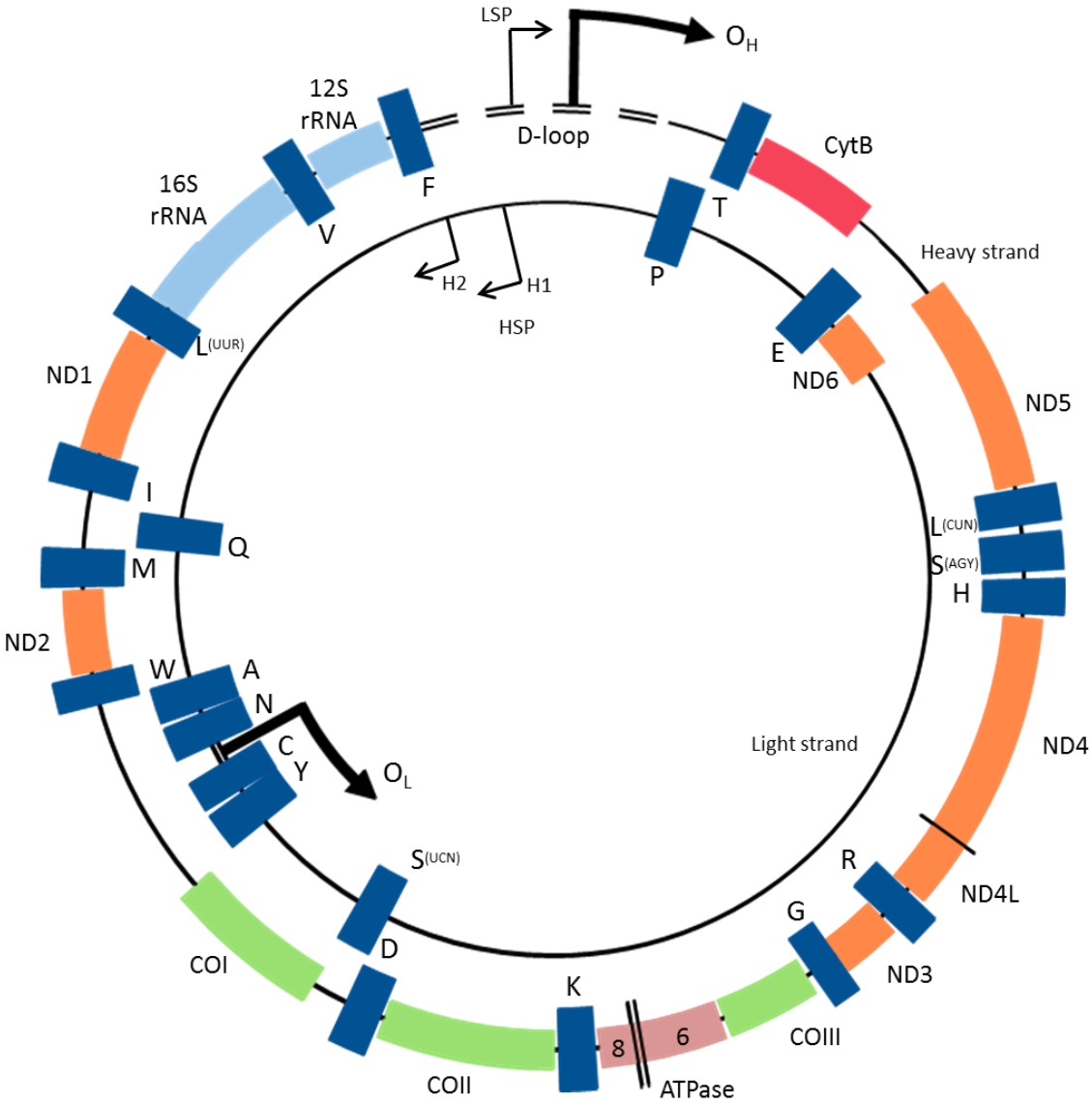

Figure 1.4 – The mitochondrial genome.
Protein encoding genes are colour coded to signify which complex they produce subunits for: Complex I (orange), Complex III (red), Complex IV (green), Complex V (brown). Ribosomal RNAs genes are light blue, tRNA genes are dark blue. The origins of replication; O_H (heavy strand) and O_L (light strand) and transcription are also shown (HSP – heavy strand promoter which contains two translation initiation sites; H1 and H2 and LSP- light strand promoter). Black lines signify the boundary of protein encoding genes when they are not separated by tRNA genes.

1.5.1. **Transcription**

Transcription of mtDNA occurs bi-directionally and is initiated from three promoter sites. The light strand promoter (LSP) initiates transcription of the light strand and the heavy strand promoter (HSP) initiates transcription for the heavy strand at two sites (H1 and H2). Initiation at H1 generates a short transcript containing the two rRNAs, $tRNA^{Phe}$ and $tRNA^{Val}$, whereas initiation at H2 generates a transcript covering almost the full genome (Montoya et al. 1982; Chang and Clayton 1984; Zollo et al. 2012). According to the tRNA punctuation model, cloverleaf folds induced in the polycistronic transcripts by tRNA act as targets for RNA processing enzymes after transcription (Ojala et al. 1981) with RNase P and RNase Z cleaving the 5' and 3' ends of the tRNAs respectively (Dubrovsky et al. 2004; Holzmann et al. 2008). However this model does not apply to all mitochondrial mRNA species and it is still unclear how *MT-ATP6/8* and *MT-ND6* transcripts are processed as they are not separated by a tRNA gene. Due to the overlap of *MT-ATP6* and *MT-ATP8*, it is essential that this bicistronic mRNA is not cleaved by RNases as it would involve the truncation of either of the proteins or removal of the *MT-ATP6* start codon. It is currently unclear how translation of ATP6 occurs to produce a separate protein, as its start codon is contained within *MT-ATP8*, but it if the mitochondrial ribosome scans mRNA and binds start codons, it may be possible to translate *MT-ATP6* from the intact bicistronic mRNA.

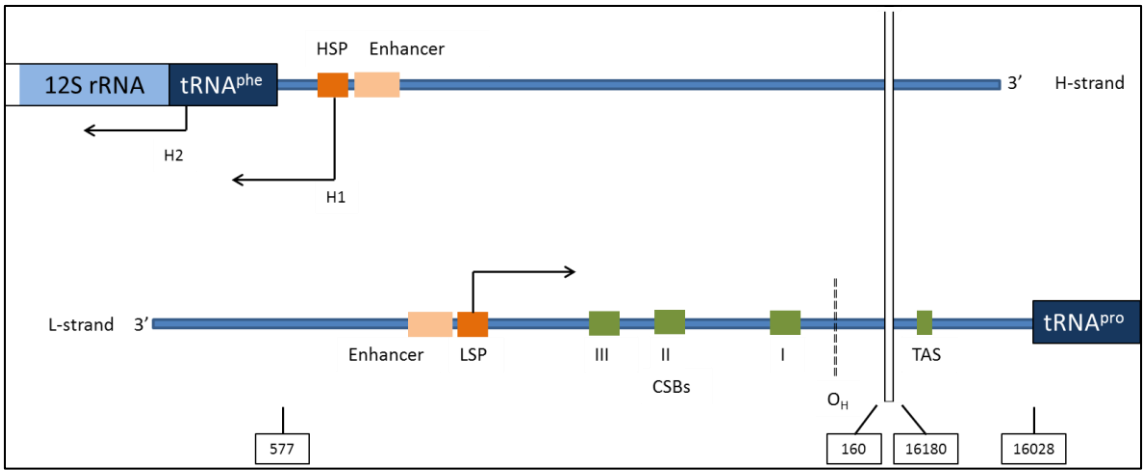

Figure 1.5 – A schematic of mitochondrial translation promoter sites.
Transcription is initiated from three distinct sites. Heavy (H) strand transcription initiates from two sites - H1 (which generates short transcripts) and H2 (which generates whole genome transcripts). Light strand transcription is initiated at LSP. Conserved sequence blocks (CSBs) and termination associated sequence sites are also shown. Image adapted from (Taanman 1999). Numbers represent the nucleotide positions of the sites within mtDNA.

Transcripts are produced by the mitochondrial RNA polymerase (POLMRT) that works in conjunction with other key components of the transcription machinery: mitochondrial transcription factor A (TFAM) and mitochondrial transcription factor B2 (TFB2M) (Falkenberg et al. 2002; Litonin et al. 2010).

When TFAM was originally identified, it was found that it bound LSP and HSP and it was therefore assumed that its activity was essential for transcription initiation (Fisher and Clayton 1988). However recent work suggests that TFAM may not be an essential component. While it has been shown that TFAM unwinds DNA to expose promoter regions (Fisher et al. 1992), overexpression of TFAM inhibits transcription by causing increased packaging into nucleoids, which is thought to prevent the access of other transcription factors to mtDNA (Rebelo et al. 2009). The yeast homologue of TFAM, Abf2, is not required for transcription (Xu and Clayton 1992), and work in *E. coli* has shown that different levels of TFAM within nucleoids influence which promoter site is used, but is not essential for initiation (Shutt et al. 2010; Lodeiro et al. 2012). However, this has been disputed by Shi *et al*. who believe that TFAM is in fact essential for initiation of transcription in conditions that closely replicate physiological conditions (Shi et al. 2012). Recent work using ChIP-seq has shown that TFAM coats the whole mitochondrial genome as part of its role in packaging mtDNA (Wang et al. 2013).

For transcription to occur, POLRMT has to form a heterodimer with either TFB1M or TFB2M, however the levels of transcription are 10-fold lower when the heterodimer consists of TFB1M and POLRMT rather than with TFB2M. It has been suggested that TFB1M may assist in promoter melting at the transcription start site (Sologub et al. 2009) while TFB2M has been postulated to stabilize ssDNA formed during mtDNA unwinding (Falkenberg et al. 2007). Thus the evidence suggests that the only two essential components of the initiation complex are TFAM and TFB2M (Litonin et al. 2010).

Termination of transcription is controlled by the mitochondrial termination factors, of which four have been identified (mTERF 1-4). The first factor to be discovered, mTERF1, was thought to be essential for termination of transcripts from all three

promoters, as it was shown to bind a 28bp region down-stream of the 16SrRNA where the H1 transcript terminates (Kruse et al. 1989). Binding of mTERF1 is thought to cause DNA unwinding and base flipping, as shown by the crystal structure of DNA bound mTERF1 (Yakubovskaya et al. 2010), which is likely to interfere with the elongation machinery. It has also been shown to have a role in the pausing of replication after it was determined that overexpression of mTERF1 increased the incidence of replication intermediates (Hyvarinen et al. 2007). Recently it has been shown that mTERF1 knockouts in mice are viable, indicating that mTERF1s main function may be to prevent L-stand transcripts from proceeding around mtDNA (Terzioglu et al. 2013).

Two of the mTERF1 homologues, mTERF2 and mTERF3, are thought to be involved in the regulation of termination and have been shown to bind to promoter regions (Wenz et al. 2009), however another report also suggests that mTERF2 is a nucleoid component which binds mtDNA in a non-sequence specific manner with one mTERF2 monomer present every ~265bp (Pellegrini et al. 2009). Decreases in mTERF2 have been shown to cause decreased mitochondrial transcription in mice (Wenz et al. 2009), which leads to OXPHOS impairment. However, depletion of mTERF3 actually increases transcription levels, suggesting that it may be an inhibitor of transcription (Park et al. 2007), although their exact functions are unknown. Experiments in *mTERF3* heart knockout mice have shown that mTERF3 may have a role in ribosomal biogenesis due to the decreased presence of the assembled large ribosomal subunit, the authors also showed that mTERF3 may have this effect by binding to 16S rRNA (Wredenberg et al. 2013). The final member of this family, mTERF4, has been shown to be involved in the regulation of mRNA translation. Work in mice has shown that mTERF4 forms a complex with NSUN4 (a member of the m5C RNA methyltransferases family), recruiting NSUN4 to the mitochondrial ribosome, a process essential for ribosome assembly (Camara et al. 2011).

1.5.2. **Translation**

Mitochondrial mRNA translation has a number of key differences from cytosolic translation. First, it utilises only 22 tRNAs compared to the 31 essential for translation of the nuclear genome. This difference is explained by the “wobble hypothesis” which proposes that the first base of the anti-codon can form non Watson-Crick pairs with the third base of the codon, enabling flexible codon reading of mRNA (Crick 1966; Barrell

et al. 1980). Secondly, the mitochondrial ribosome is has a lower sedimentary coefficient at 55S when compared to bacterial ribosomes (70S), which is surprising considering the bacterial origin of mitochondria. The mammalian mitochondrial ribosome contains less than half the quantity of RNA that is seen in prokaryotic ribosomes but more protein (O'Brian 1971). The process of mitochondrial translation is discussed below and is shown in figure 1.6.

Initiation of translation in mitochondria is controlled by two factors, $IF2_{mt}$ and $IF3_{mt}$. Prior to mRNA binding, the ribosome is split into 39S and 28S subunits by mitochondrial ribosome recycling factor (mtRRF) and kept apart by the binding of $IF3_{mt}$ to the small ribosomal subunit (Koc et al. 2001; Suzuki et al. 2001). After mRNA has bound (in an orientation that ensures the start codon is located at the P (peptidyl) site), $IF2_{mt}$ facilitates the binding of $tRNA^{fmet}$ (the initiating tRNA) (Ma and Spremulli 1996; Smits et al. 2010) to the ribosomal P-site. The formylated $tRNA^{fmet}$ is only used for initiation and so mitochondria also maintain a pool of non-formylated $tRNA^{met}$ for elongation (Takeuchi et al. 2001). Defects in formylation caused by mutations in *MTFMT* have recently been shown to cause Leigh syndrome, highlighting the importance of $tRNA^{fmet}$ for efficient mitochondrial translation (Tucker et al. 2011).

The mitochondrial elongation factor Tu (mtEFTu) forms a complex with GTP and then binds individual tRNAs, potentially protecting them from degradation. The tRNAs bind to the A (acceptor) site of the ribosome, hydrolysing GTP and releasing mtEFTu (which is subsequently recycled by mtEFTs) (Jeppesen et al. 2005). Elongation is achieved by the binding of mitochondrial elongation factor G1 (mtEFG1), which causes a conformational change in the ribosome, shifting mRNA by three nucleotides (Katunin et al. 2002). The codon that was at the P-site is replaced by the codon that was previously at the A-site, meanwhile the polypeptide moves through the ribosome and is inserted into the inner mitochondrial membrane (Smits et al. 2010).

The presence of a stop codon in the A-site is required for the correct termination of translation. Rather than binding a tRNA, stop codons are recognised by mitochondrial translational release factor 1a (mtRF1a), which hydrolyses the ester bond holding the

polypeptide to the P-site tRNA. Initially four codons were assigned as stop codons (AGA, AGG, UAA & UAG) however mtRF1a only recognises the final two codons in this list, even though the first two (which were reassigned from arginine) are the final codons for *MTCO1* and *MTND6* mRNA (Soleimanpour-Lichaei et al. 2007). It has since been shown that AGA/AGG may in fact cause a -1 frameshift which moves the ribosome to a UAG stop codon, terminating translation (Temperley et al. 2010). Ribosomal disassembly is mediated by mtRRF and mitochondrial elongation factor G2 (mtEFG2) which cause release of mRNA and tRNA (Rorbach et al. 2008; Tsuboi et al. 2009).

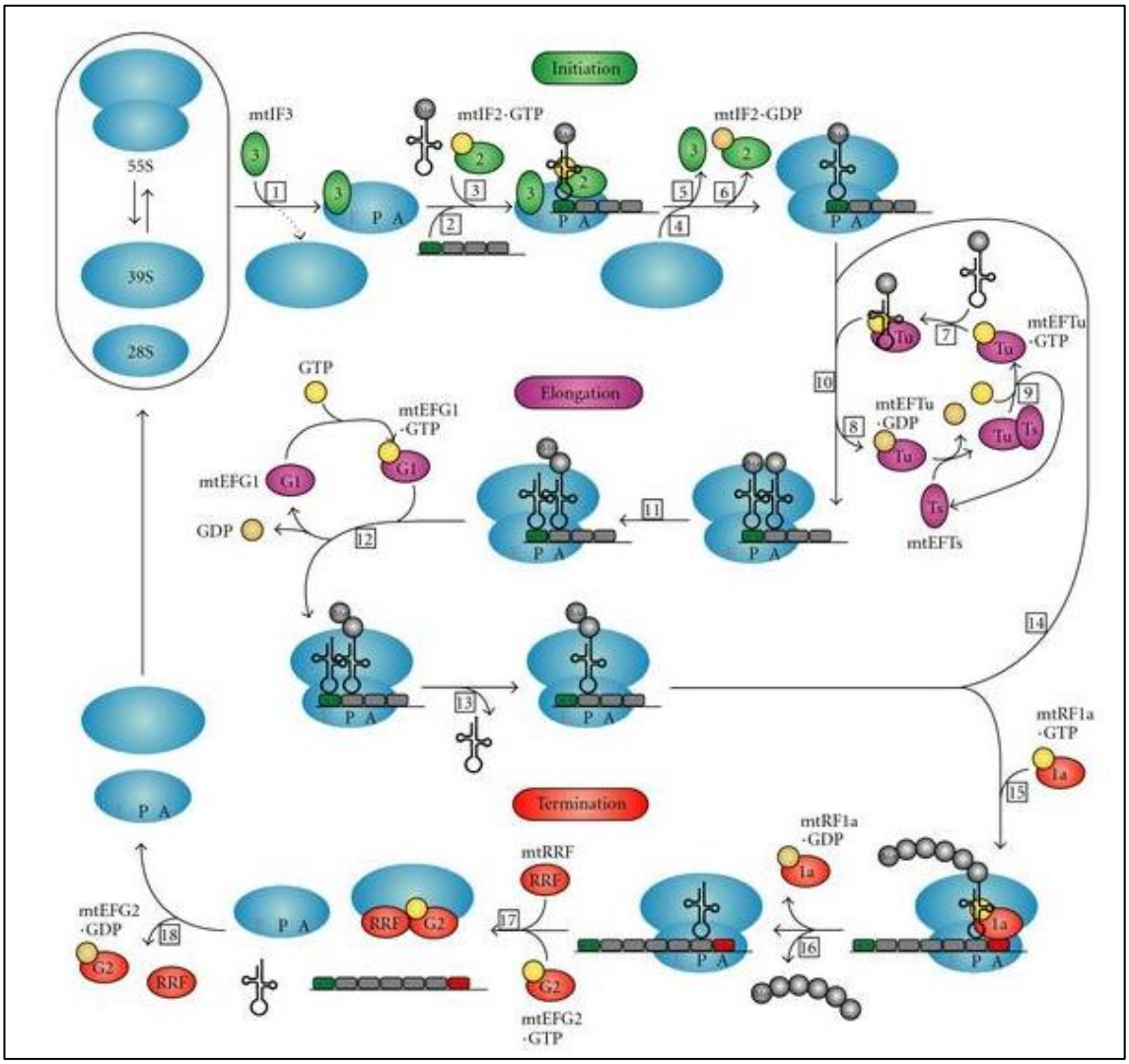

Figure 1.6 – Mitochondrial translation.
The process of translation is shown above and is split into three distinct phases, initiation (green), elongation (purple) and termination (red). The mitochondrial ribosome is shown as blue ovals, E, P and A represent the various active sites of the ribosome. The various steps of translation are discussed in section 1.5.2. Image taken from (Smits et al. 2010)

1.5.3. **Replication of mitochondrial DNA**

Replication of mtDNA propagates from the origin of H-strand replication (O_H) and is initiated by RNA primers produced during transcription originating at the LSP (Chang and Clayton 1984). A region containing three conserved sequence blocks (CSB I, II and III), discovered using sequence analysis of vertebrates, is situated downstream of the LSP. Transition from the RNA primer to newly synthesised mtDNA has been mapped to regions near CSB II, which has also been found to increase the stability of RNA:DNA hybrids (Xu and Clayton 1996). Originally it was thought that the primers were formed by site specific cleavage of RNA by RNase MRP (Chang and Clayton 1987) but recently it has been suggested that as the CSBII region is transcribed, a G-quadruplex structure forms, weakening the interaction with POLRMT and terminating transcription (Wanrooij et al. 2010). The mitochondrial replisome is shown in figure 1.7.

The human mitochondrial DNA polymerase, POLγ, consists of a heterotrimer of three subunits; the catalytic subunit POLγA, is a 140kDa enzyme which has polymerase, 3'-5' exonuclease and 5'-deoxyribose phosphate (dRP) lyase activities and two accessory subunits POLγB, a 55kDa protein which binds regions of dsDNA longer than 45bp and increases both the catalytic activity and processing speed of POLγA (Gray and Wong 1992; Carrodeguas et al. 1999; Carrodeguas et al. 2002).

The mitochondrial helicase (TWINKLE) catalyses the unwinding of the DNA duplex in an ATP dependent manner and together with POLγA, TWINKLE represents the essential components of the mtDNA replication machinery, capable of synthesising regions of DNA up to 2kb in the absence of single stranded binding protein (mtSSB) (Falkenberg et al. 2007). In order to synthesise the entire mitochondrial genome, mtSSB is required (Korhonen et al. 2004). This 13-16kDa protein binds single stranded regions of mtDNA in a tetramer, protecting it from degradation and preventing the formation of stable secondary structures after unwinding by TWINKLE (Chase and Williams 1986). The interaction between mtSSB and TWINKLE stimulates the rate at which TWINKLE unwinds mtDNA and stimulates mtDNA synthesis by POLγ.

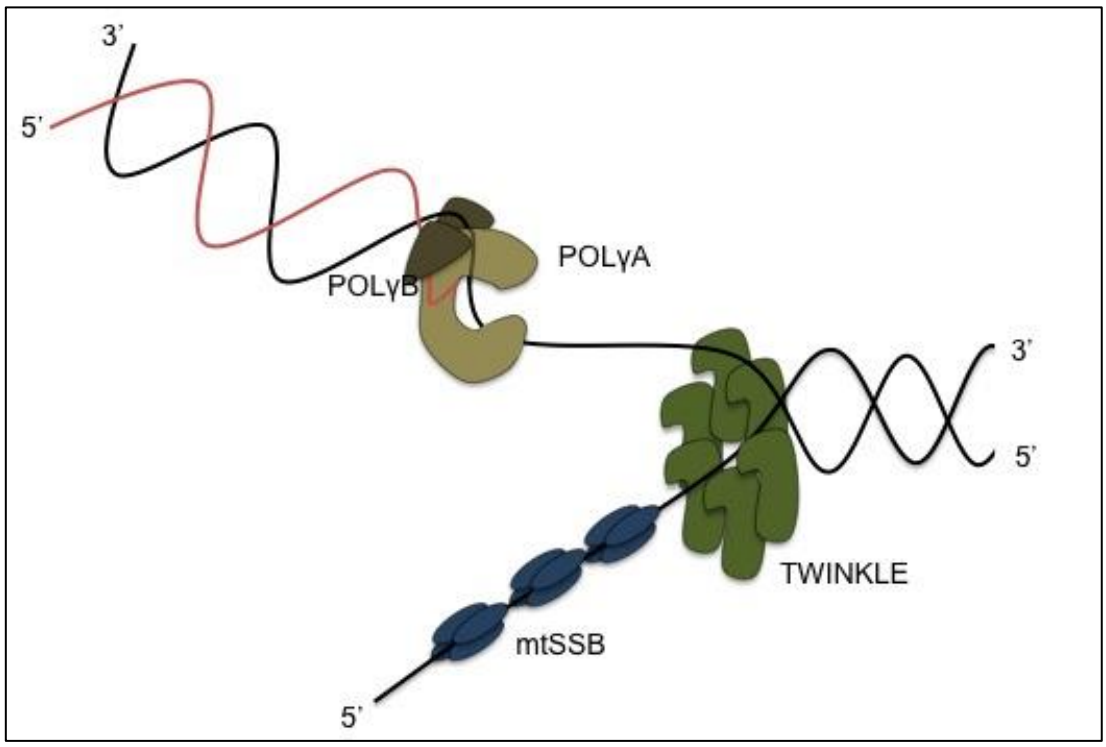

Figure 1.7 –Mitochondrial DNA replisome.
The replisome is shown synthesising in the 5' to 3' direction; all the components are discussed in section 1.5.3.

1.5.4. **Modes of mtDNA replication**

Replication of mtDNA is independent of the nuclear replication and occurs throughout the cell cycle (Bogenhagen and Clayton 1977). It is thought to occur using one or more modes of replication; asynchronous and synchronous.

1.5.4.1. *Asynchronous replication*

This model was first proposed by Clayton and colleagues in 1982. They showed that replication is initiated at O_H and two thirds of the heavy strand is replicated before the O_L is exposed, leaving the O_L unbound and single stranded, which initiates light strand replication (Clayton 1982) via the formation of a stem loop structure (Hixson and Clayton 1985). More recently it has been shown that the formation of this stem loop structure enables the binding of POLRMT and the creation of a short ~25bp RNA primer which is used by Polγ to initiate replication (Wanrooij et al. 2008). Heavy strand replication continues in a clockwise direction, opposite to the direction of light strand replication. Light strand replication is completed after replication of the heavy strand. When the strands are completed they are circularised and supercoiled turns are introduced by mitochondrial topoisomerases. The D-loop is then replicated after the

formation of this supercoil, which is believed to serve as a template for its replication (Clayton 1982).

1.5.4.2. *Synchronous replication*

Replication of the mitochondrial genome has also been shown to follow a synchronous, strand coupled mechanism of replication. Using 2D gel electrophoresis Holt and colleagues described a replication intermediate (RI) species, which showed resistance to digestion by a single strand nuclease (Holt et al. 2000). It was shown that mtDNA replication initiates at the O_H where the heavy strand is replicated around the genome, which initiates light strand replication from nucleotide 16,184. Replication of the light strand was postulated to make use of short oligonucleotide Okazaki fragments as in replication of nuclear DNA. However the presence of Okazaki fragments has yet to be demonstrated in mitochondria (Wanrooij and Falkenberg 2010). Replication of both strands continues around the genome until both strands are complete (Holt et al. 2000). Evidence of a related mechanism, RITOLS (ribonucleotide incorporation throughout the lagging strand) has also been identified as a possible mechanism for mtDNA replication. The authors of this work discovered that RNA hybridises to the single stranded lagging strand during replication possibly to prevent transcription complexes from accessing mtDNA during replication. The authors hypothesised that after RNA incorporation, a RNase enzyme, possibly RNase H1, processed the RNA to create short RNA:DNA lagging strand hybrids which may act as primers for DNA polγ, completing lagging strand replication (Yasukawa et al. 2006).

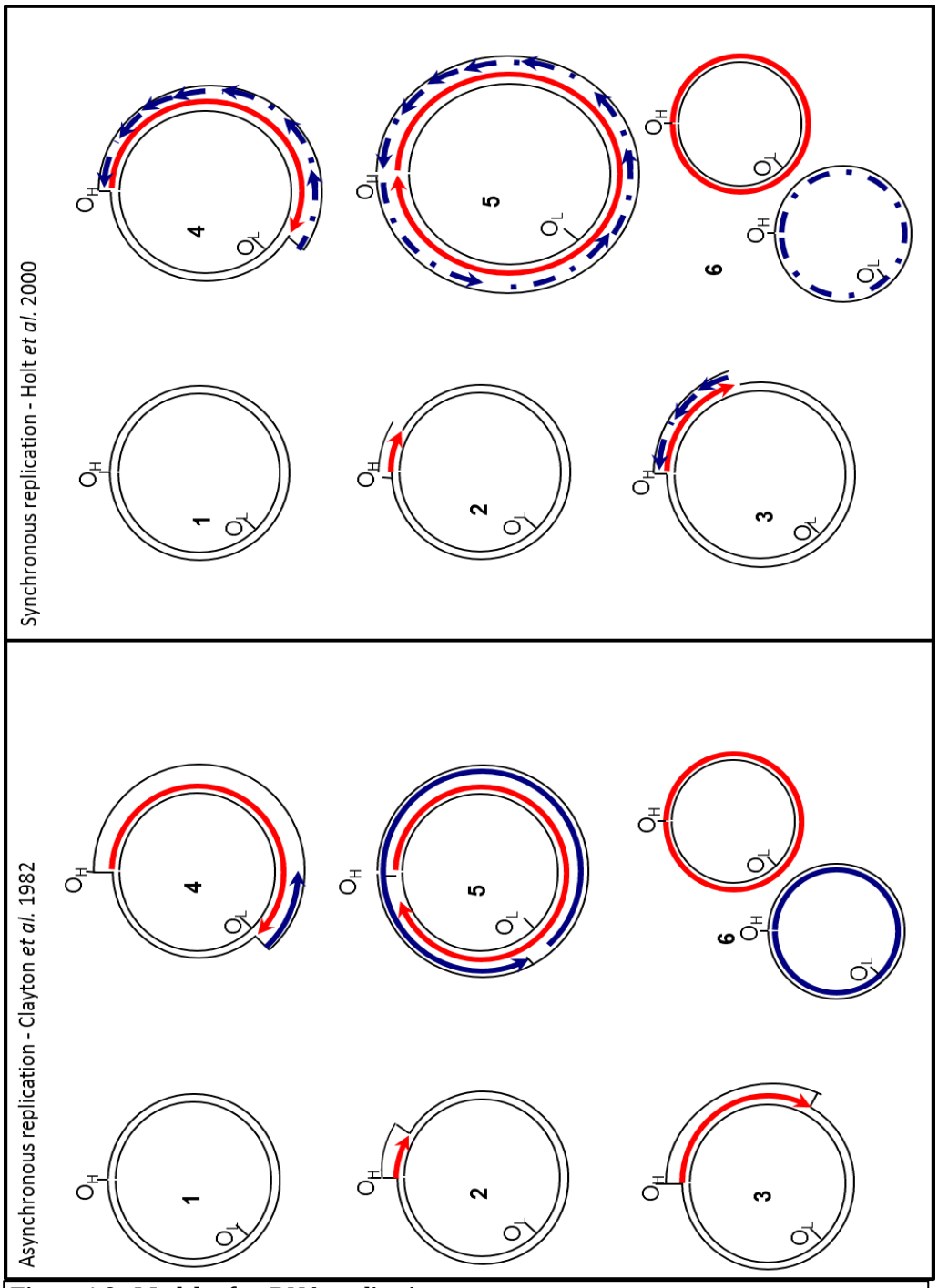

Figure 1.8 –Models of mtDNA replication.
The figure shows the two models of replication described in section 0 (Asynchronous replication) and section 1.5.4.2 (Synchronous replication).
The left panel shows the O_H (1) and the displacement of the L-strand as replication initiates (2) and replicates until it reaches O_L (3 &4) where replication of the L-strand commences (4)and the remaining genome is replicated (5) until replication is complete (6).
The right panel shows replication commencing from O_H (2) after which L-strand synthesis commences. The dashed blue lines represent the generation of Okazaki fragments as replication proceeds bi-directionally (4 & 5) until two genomes are produced (6). Figure adapted from (Reeve 2007).

1.6. MITOCHONDRIAL GENETICS

1.6.1. **Heteroplasmy**

Cells contain multiple copies of the mitochondrial genome, some of which can contain polymorphic or even pathogenic variations. If an individual cell contains different mitochondrial genomes, it is said to be heteroplasmic. The level of heteroplasmy depends on the percentage of mutated molecules in relation to the person's wild type sequence. In order to maintain a relatively constant number of molecules in the cell, mtDNA can be randomly replicated or degraded. Due to the stochastic nature of this process, a mutated molecule can be replicated until it reaches high levels in the cell (Taylor and Turnbull 2005).

Initial investigations used Holstein cows, to monitor the change in heteroplasmy level of a point mutation across four generations. These animals were chosen as they had been shown in a previous study to harbour the mutation (Hauswirth and Laipis 1982). The study found that heteroplasmy levels change between generations, to a point where the mutation can be lost after just one generation. The study also reported that heteroplasmy can differ widely in siblings, with one cow with 35% heteroplasmy producing offspring with mutant heteroplasmy ranging from 20% to 80% (Ashley et al. 1989). It is also possible for mtDNA mutations to randomly segregate within tissues. These results indicated that there is unequal portioning of mtDNA mutations within the female germline, making it difficult to predict the likelihood of a mother passing on a mtDNA mutation to her offspring.

1.6.2. **Clonal Expansion**

The proportion of mutation containing mtDNA genomes within a cell can change over time through a process called clonal expansion. Although the mechanisms of this change are not clear, several theories have tried to explain this phenomenon. The first theory was put forward in 1992 by Wallace and colleagues and investigated the expansion of deleted species of mtDNA within single cells. They postulated that because these molecules were shorter than their wild type counterparts, they were replicated at a faster rate and could therefore expand their numbers within the cell

(Wallace 1992). The second model was evidenced by the observation that cybrid cells generated from patients with heteroplasmic m.3243A>G mutation showed a shift towards higher mutant heteroplasmy (Yoneda et al. 1992). The mechanism of this increases was discussed by the authors who postulated that mitochondria with high levels of mtDNA damage proliferated in an attempt to overcome the respiratory chain defect caused by the mutation, causing clonal expansion of the mutated mtDNA within a cell the so called "sick mitochondria" theory (Yoneda et al. 1992).

In 1997 de Grey proposed that mitochondria with a mutation in mtDNA have lower oxidative phosphorylation and therefore produce less reactive oxygen species. They are therefore damaged less than 'normal' mitochondria which are degraded at a higher rate, as a result of this they expand within non-dividing cells (de Grey 1997). However, lower OXPHOS is also likely to cause a drop in membrane potential as less H^+ ions are transported across the inner mitochondrial membrane. Lower membrane potential has been shown to cause autophagy of mitochondria, suggesting that mutated mtDNA would actually cause an increase in autophagy, rather than being preserved as the theory states.

Clonal expansion could however be caused by random genetic drift where mutated and wild type molecules have an equal chance of replication. Elson and colleagues developed a model of post-mitotic cells based on 1,000 genomes per cell with a half-life of 10 days per genome. Genomes were randomly selected for degradation or replication and a constant number of gnomes per cell maintained in each cell. Each genome was also assigned a mutation rate which would induce a mutation after a defined number of bases had been replicated. The model simulated 600 cells over a period of 30 years. The majority of cells showed a gradual loss of mutated genomes over the 30 year period, however when mutations occurred early in the life of the cell clonal expansion to higher heteroplasmy levels occurred (Elson et al. 2001). This model showed that mutations in childhood or early adulthood were more detrimental as they were more likely to clonally expand to pathogenic levels.

1.6.3. **Threshold Effect**

Although mutations can increase in cells to a point where they reach high levels (>60%) or even homoplasmy, a threshold of mutated mtDNA needs to be reached before a cell shows a deficient phenotype (figure 1.9). Below this threshold, wild type mtDNA can compensate for the mutated molecules so the cell shows no biochemical deficit, above it the cell is unlikely to produce sufficient ATP to function correctly (Sciacco et al. 1994). The threshold varies between mutations and tissues, with tRNA mutations generally needing to be above 80% before wild type mtDNA can no longer compensate for their deficiencies (Taylor and Turnbull 2005). Low heteroplasmy pathogenic mutations have also been reported such as the mt-tRNA^{Glu} m.14723 T>C mutation which was shown to be pathogenic at 7% mutation heteroplasmy (Alston et al. 2010) and the tRNA^{Trp} m.5545C>T mutation which is pathogenic at <25% mutation heteroplasmy (Sacconi et al. 2008).

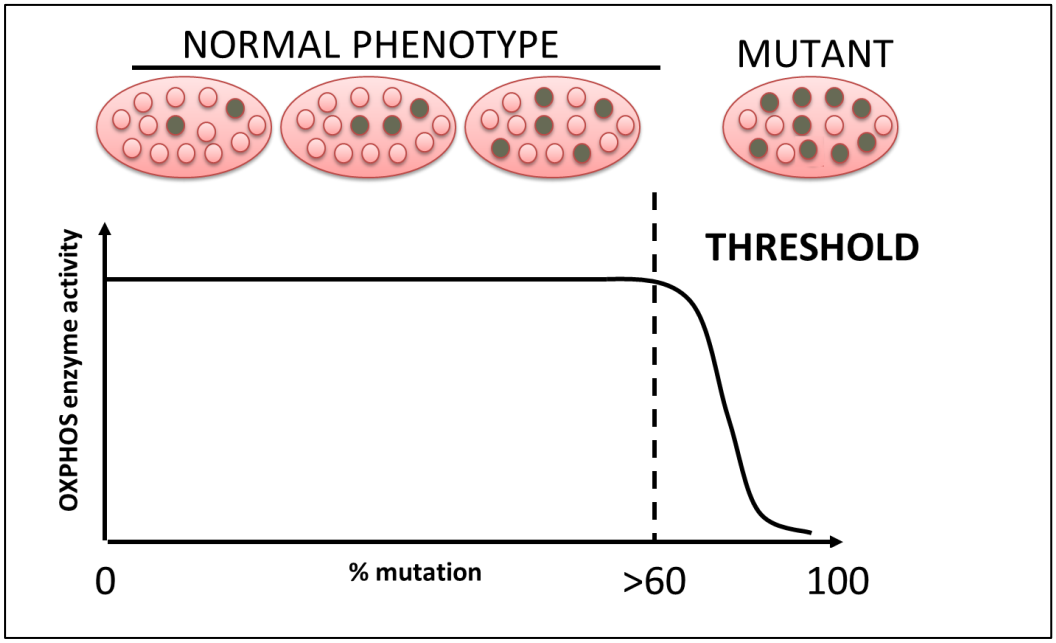

Figure 1.9 – The threshold effect.
Wild type mtDNA (red circles) can compensate for the effects of mutated genomes (brown circles) until a threshold is reached. Although this level varies depending on mutation and the patient, for deletions it is around 60% heteroplasmy. Point mutations tend to have a higher threshold due to the lower number of affected genes. Mitochondrial enzyme activity refers to OXPHOS enzymes.

1.6.4. **Inheritance in Mammals**

mtDNA is clonally inherited down the maternal lineage (Giles et al. 1980), except in one documented case. A patient presented with a 2bp deletion (m.5132delAA) within *MTND2* at homoplasmic levels in his skeletal muscle but undetectable in other tissues. Further investigation showed that his skeletal muscle mtDNA was the same as his father's haplogroup and that he must have acquired the mutation early in embryogenesis, which subsequently segregated into the patient's skeletal muscle (Schwartz and Vissing 2002). It was also found that the patient's blood contained only mtDNA from his mother, showing that he had inherited mitochondria from both parents (Schwartz and Vissing 2002). After fertilisation the father's mitochondria, present in the sperm, are degraded by ubiquitination (Sutovsky et al. 2000) although a recent paper showed that sperm mitochondria can also be degraded by non-ubiquitination mediated autophagy after entry of the spermatozoon into the oocyte (Al Rawi et al. 2011). Subsequent has shown that motile sperm in mice may also lose their mitochondria by an autophagic process prior to fertilisation (Luo et al. 2013).

1.7. MITOCHONDRIAL DISEASE

Mitochondrial diseases represent a range of disorders caused by mutations in either mtDNA or nuclear encoded mitochondrial genes that affect the ability of mitochondria to produce ATP. There are 577 reported mutations in mtDNA that have been associated with disease, some of which are highlighted in Figure1.10 (Mitomap, 2013). An epidemiological study in the North East of England found that 1 in 3500 adults are at risk of developing mitochondrial disease, with up to 1 in 200 carrying pathogenic mtDNA mutations, potentially making them one of the most commonly inherited neuromuscular diseases (Schaefer et al. 2008). This section will discuss the most common mitochondrial mutations.

1.7.1. **Phenotypic expression**

The ubiquitous nature of mitochondria means that multiple organs are often affected by mitochondrial disease, regardless of the mutation. Neuronal tissue is greatly affected due to its high energy requirements and unsurprisingly the most common symptoms in adults are seizures, myoclonic epilepsy and ataxia. However there is also large clinical variation in patients with identical mutations and heteroplasmy. Other common

symptoms include cardiomyopathy, diabetes, ophthalmoplegia and ptosis (McFarland et al. 2002). Children affected by mitochondrial disorders are more likely to experience severe symptoms such as liver failure along with seizures and developmental delay (Chi et al. 2010).

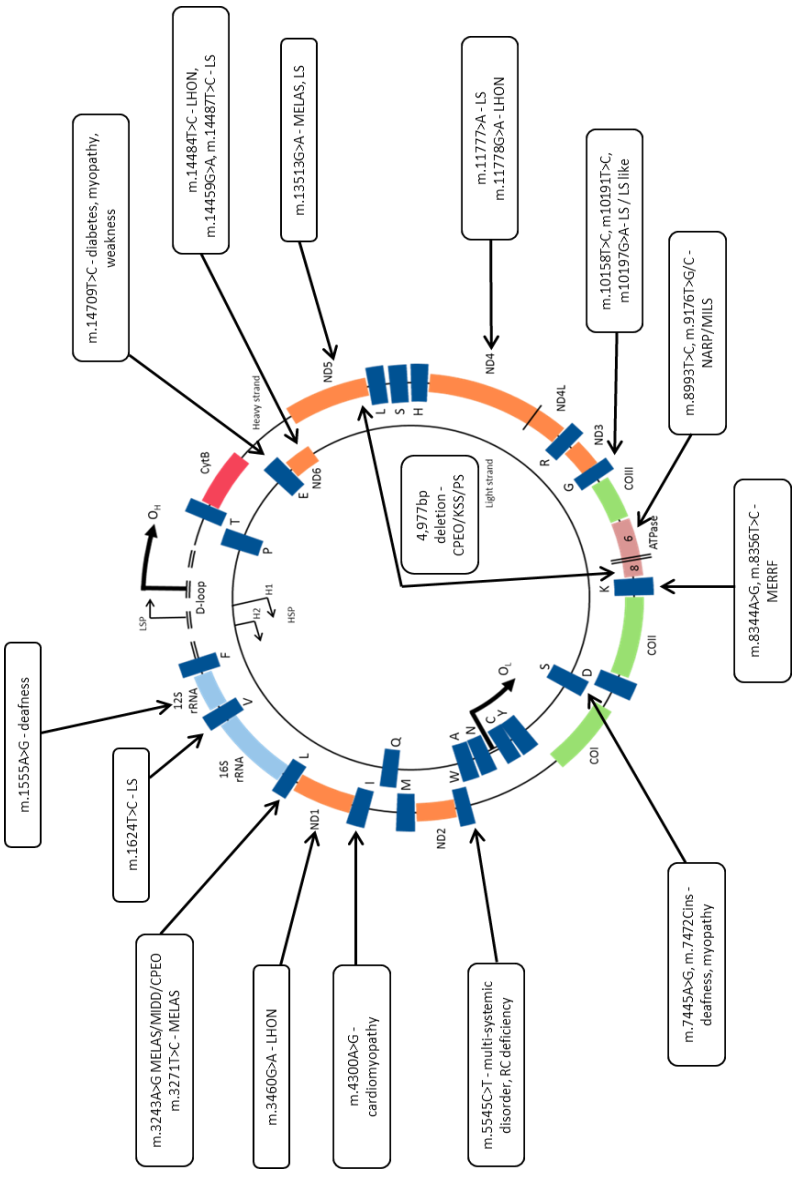

Figure 1.10 - Locations of the disease causing mtDNA mutations.
Point mutations are represented by the arrows, the "common deletion" is shown in the centre of the genome. Abbreviations: CPEO – chronic progressive external ophthalmoplegia, LHON – Leber's hereditary optic neuropathy, LS – Leigh syndrome, MELAS – mitochondrial myopathy, encephalopathy, lactic acidosis, stroke-like episodes, MERRF – Myoclonic epilepsy and ragged red fibres, MILS – maternally inherited Leigh syndrome, NARP – neurogenic weakness, ataxia and retinitis pigmentosa, PS – Pearson's syndrome. Adapted from Tuppen *et al.* 2010.

1.7.2. **m.3243A>G mt-tRNA$^{Leu(UUR)}$ mutation**

This mutation accounts for ~80% of cases of MELAS disease (mitochondrial encephalomyopathy with lactic acidosis and stroke like episodes) (Goto et al. 1990), although it is also associated with other mitochondrial diseases such as maternally inherited diabetes and deafness (MIDD) (Figure 1.10). The mutation prevents 5-taurinomethyluridine modification of the uridine wobble-position in tRNA$^{Leu(UUR)}$, which leads to a reduction in the translation. This was highlighted by the investigations of Kirino and colleagues which showed that wild-type tRNA$^{Leu(UUR)}$ without the taurine modification have a reduced translation rate of UUG codons (Kirino et al. 2004). The authors also noted that when the m.3243A>G mutation is present, the translation of UUA and UUG were both reduced. Prevention of this modification has also been shown in other mutations associated with MELAS (m.3244A>G, m.3258T>C, m.3217T>C and m3219T>C) (Kirino and Suzuki 2005).

Interestingly, the mutation occurs at the mTERF1 binding site, which decreases binding affinity *in vitro*, however there is no evidence that this has a pathogenic effect *in vivo*, possibly due to increased mTERF1 expression compensating for decreased affinity (Kruse et al. 1989; Chomyn et al. 1992).

The level of aminoacylated tRNA$^{Leu(UUR)}$ and total tRNA$^{Leu(UUR)}$ are both decreased in cybrid cells, with work showing that the m.3243A>G mutation can cause the dimerization of the tRNA by encoding a self-complimentary region in the D-loop of the tRNA, which reduces the aminoacylation of the mutated species, which decreases the level of tRNA$^{Leu(UUR)}$ available for translation (Wittenhagen and Kelley 2002). Decreased protein synthesis rate leads to a decrease in the availability of OXPHOS complexes available for oxidative phosphorylation, therefore lowering the overall OXPHOS activity (Ciafaloni et al. 1992).

Symptoms commonly associated with MELAS include short statue, hemiparesis, seizures and lactic acidosis (Pavlakis et al. 1984) as well as ataxia and dementia (Hirano et al. 1992). Ragged red muscle fibres, caused by accumulation of mitochondria under the sarcolemma membrane are also found in muscle biopsies in affected patients

(Ciafaloni et al. 1992). There is also evidence to suggest that higher mutation loads may cause an earlier disease onset (Morgan-Hughes et al. 1995). Interestingly, analysis of type 2 diabetic populations has shown that between 1-3% of cases are due to the m.3243A>G mutation (Vionnet et al. 1993; Alcolado et al. 1994; Ohkubo et al. 2001).

1.7.3. **m.8344A>G tRNA^{Lys} mutation.**

First identified in 1990, this mutation is most commonly associated with MERRF (Myoclonic Epilepsy with Ragged Red Fibres) (Shoffner et al. 1990; Yoneda et al. 1990). The mutation is found in the TψC loop of mitochondrial tRNA^{Lys} and like m.3424A>G affects taurine modification of the uridine wobble-position (Yasukawa et al. 2000). Defective modification has been shown to decrease correct codon-anticodon binding due to a decreased stability of the codon-anticodon interaction, increasing lysine misincorporation into nascent peptides (Yasukawa et al. 2001).

The exact cause of the decreased translation rate is not clear, however abnormal proteins have been detected in cybrids with the m.8344A>G mutation. This could be due to ribosome failure and detachment, which would lead to truncated proteins (Masucci et al. 1995). Another possibility is that the poor codon-anticodon interaction causes ribosomal frame shifting leading to abnormal or truncated proteins (Masucci et al. 1995).

MERRF patients show decreased OXPHOS which in turn leads to ataxia, convulsion and muscular atrophy (Fukuhara et al. 1980). Some patients also exhibit lipomas in areas associated with brown fat such as the upper back and neck regions, which have been shown to be homoplasmic for the m.8344A>G mutation (Holme et al. 1993).

1.7.4. **Mutations in mtDNA encoded protein genes**

The m.8993T>G mutation in ATPase subunit 6 was first associated with NARP (Neuropathy, ataxia, retinitis pigmentosa) disease, and has more recently been found to also cause MILS (maternally inherited Leigh's syndrome), although MILS is also associated with m.9176T>C and m.9176T>G mutations (Thyagarajan et al. 1995; Carrozzo et al. 2001). Patients with MILS are usually paediatric cases that present with

respiratory abnormalities, dystonia and optic atrophy. Unfortunately the disease is often fatal and post mortem analysis shows necrotic lesions of the brain stem, basal ganglia and thalamus (Leigh 1951).

The mutation causes a Leu 156 Arg amino acid change in ATP synthase subunit 6, which leads to the symptoms associated with NARP when heteroplasmy levels reach 90-95% mutant or MILS when mutant heteroplasmy is greater than 95% (Tatuch et al. 1992). It is generally accepted that these disorders arise due to impairment in the synthesis of ATP. The mutated amino acid is in close proximity to Glu-58 in subunit *c* of ATP synthase, an essential residue for the transport of protons, and it was originally hypothesised that the mutation affected the protonation and deprotonation of this residue, altering proton flow, however subsequent work has shown this to not be the case (Hartzog and Cain 1993). More recently it has been shown that the mutation alters the ability of the *c* ring subunits to rotate (Sgarbi et al. 2006) thus preventing the utilisation of rotational torque by the F_1 subunit to generate ATP from ADP and P_i.

At least 95% of cases of Leber's hereditary optic neuropathy (LHON) are caused by mutations in mtDNA encoded complex I subunits. m.3460G>A, m.11778G>A and m.14484T>C mutations are found in *MTND1*, *MTND4* and *MTND6* respectively and cause the loss of retinal ganglion cells in the optic nerve. This leads to symptoms such as acute or subacute visual loss, with both eyes being affected generally within 2 months, which primarily affects males aged 15-35 (Chinnery et al. 2000). LHON is one of the most common mitochondrial diseases with prevalence in the north east of England of ~1 in 25,000 (Chinnery et al. 2000).

1.7.5. **Rearrangements of mtDNA**

Mitochondrial diseases can also be caused by large scale rearrangements of mtDNA, such as single large scale deletions, multiple deletions and duplications. Deletions are thought to occur during replication, which may explain the high incidence of deletions occurring in the major-arc (Shoffner et al. 1989), although recent work has postulated that they may also occur during mtDNA repair (Krishnan et al. 2008). Single large scale deletions are typically inherited through the germ-line and are responsible for some

paediatric onset mitochondrial diseases such as Kearns-Sayres syndrome (KSS) (Lestienne and Ponsot 1988; Zeviani et al. 1988). This disorder is multi-systemic causing cerebellar ataxia and cognitive impairment and is linked to the development of PEO (retinitis pigmentosa and progressive external ophthalmoplegia) before the age of 20 (Tuppen et al. 2010).

Multiple deletions are associated with mutations in *POLG* or *PEO1* and have been associated with CPEO (chronic progressive external ophthalmoplegia) – a disease characterised by progressive paresis of the eye, proximal weakness, bilateral ptosis and in some causes cardiac conduction problems (Agostino et al. 2003). This was first reported in 1989 with the discovery of an autosomal dominant inherited mutation that caused multiple mitochondrial deletions (Zeviani et al. 1989).

Depletion of mtDNA is exhibited in patients with Alpers' syndrome, a relatively uncommon autosomal recessive mitochondrial disorder caused by mutations in Polγ genes, which lower the activity of the enzyme (Naviaux et al. 1999). More than 180 mutations in Polγ are associated with the Alpers' phenotype; intractable seizures, developmental regression and liver dysfunction. Paediatric onset of Alpers' disease is often fatal due to liver failure rather than any other symptom (Saneto et al. 2013).

1.7.6. **Animal models of mitochondrial disease**

Although cell culture models are available for mitochondrial disease such as *trans*mitochondrial cybrids cells, cells which contain mtDNA mutations with a relevant nuclear background, the need to study mitochondrial disease in whole organisms prompted the generation of mouse models (Wallace 2001).

Although models of nuclear mutations are relatively easy to generate (TFAM, TWINKLE and *ANT1* mutation models have been produced previously, each causing severe mitochondrial dysfunction) (Graham et al. 1997; Larsson et al. 1998; Tyynismaa et al. 2005), it is difficult to introduce mtDNA mutations into the germline due to an inability to transfect mitochondria (Wallace 2001; Lightowlers 2011). Mice with single

large scale deletions were generated by fusing zygotes with enucleated mutation containing cybrid cells. It was found that the mutation could be passed down the germline, the mutation led to respiratory defect in multiple tissues (Inoue et al. 2000). The "mtDNA mutator mouse", which has a proof-reading deficient Polγ subunit α, progressively accumulates mutations in mtDNA over time creating a phenotype which has been suggested to mimic an early ageing/progeroid phenotype. This is the most successful model of mtDNA disease created so far, and may enable the generation of stable mtDNA mutations through crossing with wild type mice to select for certain mutations (Trifunovic et al. 2004).

1.8. TREATMENTS

The lack of effective treatments for the causes of mitochondrial disease means clinicians can only treat the symptoms of the disorders. There have been very few randomised clinical trials in which directly acting compounds have been investigated, none of which are suitable for treatment due to either low efficacy or toxicity in mitochondrial patients (Horvath et al. 2008). This section will discuss the treatment of the most common symptoms of mitochondrial diseases; a schematic diagram highlights potential and currently used treatments in figure 1.11, (page 44).

1.8.1. **Symptomatic therapy**

1.8.1.1. *Treatments for neurological symptoms of mitochondrial disease*

As mentioned previously one of the most common symptoms of mitochondrial disease in adults is seizures. There are several anticonvulsants on the market with valproate being one of the most commonly used. This has been shown to be effective in the treatment of seizures in mitochondrial patients. However, it is no longer indicated for use as it has been shown to prevent the uptake of carnitine, which can increase lactic acidosis in mitochondrial patients, particularly in those suffering from MELAS where it exacerbates both fatigue and lactic acidosis (Tein et al. 1993). In Alpers' syndrome patients (those with mutations in *POLG*), the use of valproate is linked to liver failure, although the mechanism is not clear (Horvath et al. 2008).

Seizure control is essential, particularly in patients with *POLG* mutations as epilepsy is a key factor in patient mortality (Tzoulis et al. 2006). The use of benzodiazepine, phenytoin and levetiracetam have shown efficacy at controlling seizure occurrence in *POLG* patients. It has also been indicated that ketogenic diets may be a viable treatment for patients at risk of epileptic seizures; however the evidence for the effectiveness of this treatment is circumstantial. It has been postulated that the diet may up-regulate the production of antioxidants such as glutathione in mitochondria, potentially having a protective effect (Milder and Patel 2012).

Some patients with mutations in *POLG* have shown Parkinsonian-like symptoms, predominately tremor, which is treatable with the use of Levodopa, which increases dopamine signalling in dopaminergic neurons. The use of L-arginine in MELAS has been shown to improve stroke like episodes (Koga et al. 2005), however the mechanism of the effect is unclear. It is likely that L-arginine increases the synthesis of nitric oxide (a potent vasodilator) which increases blood flow to affected areas (Koga et al. 2012).

1.8.1.2. *Treatments for non-neurological symptoms in mitochondrial disease*

Several mitochondrial disorders exhibit skeletal muscle weakness as a symptom such as MELAS, MERRF, LHON and Alpers' syndrome. Although it is often debilitating and can lead to breathing difficulties if respiratory muscles are involved, there is very little scope for treatment. Patients who suffer from breathing difficulties can use ventilators at night and in general patients are advised to avoid overexertion and remain hydrated in order to avoid kidney related complications (McFarland and Turnbull 2009).

Cardiomyopathy is a common complication in MELAS and MERRF, progression of which may take place over a period of years. Rapid progression in MELAS can be managed by the use of β-blockers or ACE (angiotensin converting enzyme) inhibitors. Conduction defects may also require the use of a cardiac pacemaker (McFarland and Turnbull 2009). Patients with MIDD (maternally inherited diabetes and deafness) can have their condition managed by dietary controls or by the use of diabetes treatments such as insulin or metformin (Malecki et al. 2006). Deafness in MIDD patients can be

ameliorated with the use of hearing implants to limit the severity of hearing loss, improving patient well-being (Sinnathuray et al. 2003).

1.8.1.3. *Surgical approaches*

Ptosis (drooping of the eye-lids caused by OXPHOS defects in ocular muscles) is one of the most common and obvious symptoms of mitochondrial disease. As ptosis becomes more severe it can lead to postural and neck problems, which arise as the patient compensates for the defect. This can be relieved using surgery to increase the degree of opening of the eye-lids (Horvath et al. 2008).

Pearson's syndrome is a paediatric form of mitochondrial disease caused by a single large scale deletion or duplication of mtDNA, which causes hypoblastic macrocytic anaemia, exocrine and endocrine deficiency and lactic acidosis (Smith et al. 1995). It is an incredibly debilitating disease and unfortunately death usually occurs in early infancy. The use of bone marrow transplants has been used to replace haematopoietic stem cells and cure the associated haematological symptoms. This was used in a 4 month old child and was found to have completely removed deleted mtDNA species from her haematopoietic system (Faraci et al. 2007). While the patient unfortunately died due to other complications, this treatment may be used in other cases. Patients with MNGIE (mitochondrial neurogastrointestinal encephalomyopathy) may also show an improvement after bone marrow transplant. MNGIE is caused by mutations in *TYMP* gene (encoding thymidine phosphorylase), leading to high levels of circulating thymidine and deoxyuridine, which have been shown to cause mtDNA damage over time. The high levels of thymidine phosphorylase found in platelets means that bone marrow transplants from healthy individuals lead to an increase in the amount of functioning enzyme and therefore a decrease in the levels of thymidine and deoxyuridine (Garone et al. 2011; Halter et al. 2011).

Patients with mitochondrial cardiomyopathy can be given heart transplants to correct the defect. Transplants are normally contraindicated in patients with multi-systemic disorders; however in patients with mitochondrial deficiency that has segregated to the heart, transplants have been shown to be successful at extending the life of affected children (Bonnet et al. 2001).

1.8.1.4. *Mitochondrially acting treatments*

Endogenous ubiquinone (coenzyme Q10) is an effective electron carrier from complex I or II to complex III (Crane 1977). Ubiquinol (reduced ubiquinone) can act as an efficient anti-oxidant by donating a hydrogen atom to lipid peroxyl radicals to form ubisemiquinone. Ubisemiquinone can then either deprotonate into ubiquinol or ubiquinone or it can react with oxygen to form a superoxide radical (which is detoxified by superoxide dismutase and peroxidases) and ubiquinone (Land and Swallow 1970). While many mitochondrial patients have been reported to take ubiquinone (possibly due to its beneficial anti-oxidant effects), and there is anecdotal evidence to suggest that their symptoms were relieved (Horvath et al. 2008), there is little clinical data to support the use of ubiquinone as a general therapy. In patients with mutations in genes encoding enzymes that function in the ubiquinone biosynthesis pathway, such as *COQ2* and *PDSS1*, which have been shown to decrease the amount of CoQ10 and the length of CoQ10 prenyl chain respectively, there is evidence to suggest that OXPHOS improves with ubiquinone treatment (Horvath 2012).

The bioavailability of ubiquinone is problematic as it is a highly lipophilic molecule. Recent attempts to create a mitochondrial targeted, bioavailable form of ubiquinone by conjugating it to TPP (triphenylphosphonium), a lipophilic cation, have led to the creation of MitoQ (Kelso et al. 2001). However, the ability of MitoQ to transport electrons from complex I was shown to be impaired by the addition of the TPP molecule, making it nonviable for use in ubiquinone replacement therapy (James et al. 2007). The antioxidant properties were not impaired and uptake tests on mice have shown that MitoQ and similar molecules can accumulate into mitochondria in as little as 5 minutes post intravenous injection (Ross et al. 2008). This speed of uptake is useful in applications such as modulation of reperfusion injury after cardiac ischemia. During ischemia OXPHOS is inhibited leading to an accumulation of lactic acid, phosphates and fatty acids. Once blood flow is restored, oxygen reacts with the damaged mitochondrial components causing a flood of ROS, which can have devastating downstream effects (Zweier et al. 1987). Exposure to MitoQ over a period of two weeks led to an accumulation of the antioxidant in the mitochondria of rats that subsequently protected their hearts from ischemia-reperfusion injury (Adlam et al. 2005). Although this is more relevant to ischemia than mitochondrial disease, the development of this drug highlights that it is possible to design mitochondrially acting pharmaceuticals.

Manipulation of mitochondrial biogenesis to increase proliferation also has the potential to alleviate the symptoms of mitochondrial disease (Dillon et al. 2012). Several drugs have been shown to modulate the signalling pathways that control mitochondrial biogenesis. As mentioned previously (section1.3.2) PGC-1α is the master regulator of mitochondrial biogenesis and as a consequence drugs that act either directly on PGC-1α or its regulators have been trialled as potential therapeutics. The pan PPAR agonist bezafibrate activates the PGC-1α/PPARγ pathway (Tenenbaum et al. 2005) and has been shown to improve the symptoms of mitochondrial dysfunction in "mutator" mouse models (Dillon et al. 2012). However, there was no apparent increase in the quantity of OXPHOS subunits. AMPK increases PGC-1α expression in response to exercise and caloric restriction. Pharmaceutical activation of AMPK by AICAR may also act to increase biogenesis. Incubation of AICAR with complex I deficient patient fibroblasts increased their O_2 consumption and also caused a 20% increase in mitochondrial volume when compared to untreated cells (Golubitzky et al. 2011). Activation of SIRT1 by resveratrol has been postulated to increase PGC-1α activity by increasing its deacetylation. Work in 2006 showed an increase in citrate synthase activity and a doubling of mitochondrial area in skeletal muscle in mice treated with resveratrol (Lagouge et al. 2006; Andreux et al. 2013). In the same study it was also found that there was an increase in the expression of genes associated with the control of mitochondrial biogenesis such as PGC-1α. Although the data is often not clear regarding drugs that increase biogenesis, it is apparent that there is a need to create compounds that can modulate the mitochondrial biogenesis pathways.

1.8.1.5. *Exercise therapy*

Exercise therapy has been postulated to improve OXPHOS in mitochondrial myopathies caused by single large scale mtDNA deletions. In a study completed in 2006, it was found that endurance training improved the mobility and quality of life of mitochondrial disease patients without influencing levels of deletion heteroplasmy or copy number (Taivassalo et al. 2006). Resistance training has been shown to improve OXPHOS capacity of muscles and decrease the proportion of COX negative fibres in muscle biopsies. This effect was due to satellite cells (which have low levels of deletion heteroplasmy) replacing muscle cells damaged during training, thus improving the muscle phenotype (Murphy et al. 2008).

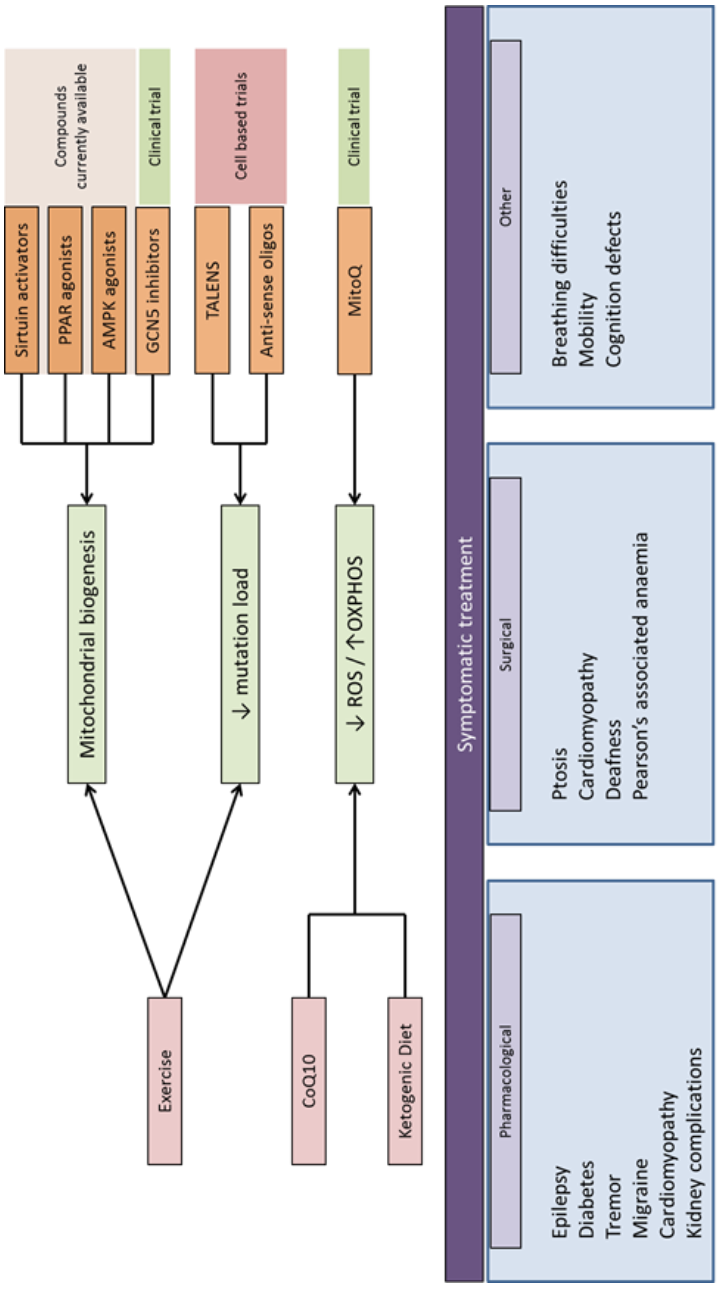

Figure 1.11 - Treatments for mitochondrial disease.
The figure shows various treatments that act directly on mitochondria to improve the disease phenotype. The outcome of the treatments is shown by the green boxes, red boxes to the left of this represent currently used therapies. Orange boxes highlight potential future targets and therapies for mitochondrial dysfunction. Currently treated symptoms of mitochondrial disease are highlighted in the blue boxes. Abbr: peroxisome proliferator activating receptor (PPAR), AMP-activated protein kinase (AMPK), deacetylase enzymes (GCN5), transcription like effector nucleases (TALENS).

1.8.2. **Gene therapy**

The use of gene therapy with the aim of shifting heteroplasmy in favour of wild type in mtDNA disease has been postulated since the mechanism of the diseases was known. The following describes several approaches that have had varying degrees of success, despite this there are currently no effective gene therapies used in the treatment of mitochondrial disease. While some of the approaches listed below have shown efficacy in cell lines, the delivery of the gene therapies for use in multi-systemic diseases prevents their use in man.

1.8.2.1. *Endonucleases*

Endonuclease restriction enzymes have the ability to specifically recognise sequences in DNA and induce double strand breaks. This makes them attractive in the treatment of mtDNA disease as there are two distinct populations of mtDNA, mutated and wild-type. By targeting an endonuclease with the ability to specifically recognise and cleave only mutant mtDNA, a proportionate increase of wild-type mtDNA levels could be achieved following degradation of digested molecules.

Srivastava *et al*. attempted to use *Pst*I endonuclease to specifically cleave mtDNA at either of the two *Pst*I sites contained within human (m.6914 & 9024) and mouse mtDNA. Addition of a COX VIII targeting sequence to bacterial *Pst*I enzyme caused effective colocalisation with mitochondria in transiently transfected HeLa cells (Srivastava and Moraes 2001). The authors created a hybrid cell line containing mouse mtDNA (which contained two *Pst*I sites) and rat mtDNA (which contained none) to investigate the selective removal of *Pst*I containing mtDNA. In hybrid cells which contained a ratio of 3:1 mouse to rat mtDNA and transfected with mitochondrial *Pst*I, the heteroplasmy of mouse mtDNA fell from 75% to 38%, indicating that the mouse mtDNA was specifically degraded after digestion, whereas the rat mtDNA, which did not contain a *Pst*I site, was unaffected.

Although proven in principle, the usefulness of using endonuclease enzymes to treat mtDNA disease is fundamentally limited by the availability of a unique restriction site created by the disease causing mutation. The disease mutation m.8993T>G found in

neurogenic muscle weakness, ataxia and retinitis pigmentosa (NARP) and Leigh's syndrome results in the creation of a unique *Sma*I restriction site in the mutated mtDNA, enabling the use of *Sma*I enzyme to remove mutated genomes (Tanaka et al. 2002).

To target *Sma*I to mitochondria Tanaka *et al*. made a mitochondrially targeted version of the enzyme by adding a COXIV presequence. After transfection into patient cell lines containing the m.8993T>G point mutation, the restriction enzyme eliminated all mutated mtDNA from the cells by digestion; however this required repeated transfections, something that is undesirable in patients (Tanaka et al. 2002). To improve the efficacy of this work Alexeyev and colleagues used the *Sma*I isoschizomer *Xma*I, modified for mitochondrial targeting by the addition of the COX VIII targeting sequence in an adenovirus transfection system (Alexeyev et al. 2008). As with the work done by Tanaka *et al*. mutant mtDNA was completely depleted.

Although this approach to targeting mutated mitochondrial genomes is promising for NARP and Leigh's syndrome, there are issues with the use of these strategies in patients, particularly the development of a reliable and safe cellular delivery method.

1.8.2.2. *Zinc fingers*

Zinc finger peptides (ZFPs) are small protein motifs characterised by finger like protrusions that enable the specific binding of a target molecule. While they have the ability to bind various different molecules, one class in particular, Cys_2His_2, has had its ability to bind DNA in a sequence specific manner well characterised (Wolfe et al. 2000; Persikov et al. 2009). Found in many mammalian transcription factors the Cys_2His_2 class has become particularly useful in the engineering of novel proteins that can bind specific regions of DNA enabling targeted modification and changes in expression. ZFPs readily localise to the nucleus where they interact and bind with DNA, a localisation that is so strong that it does not always require a nuclear localisation motif to be present on certain ZFPs (Minczuk et al. 2006).

Strong nuclear localisation presents a problem for using ZFPs to treat mitochondrial DNA disease, as to exhibit a therapeutic effect they need to efficiently localise to the mitochondrial matrix. It is also important that there is minimal nuclear localisation in order to prevent "off target" toxicity. To try and achieve this Minczuk *et al* conjugated either the N-terminal mitochondrial targeting sequence (MTS) of the F1β subunit of human ATP synthase or COX VIII subunit to three or four fingered ZFPs. While some of the peptides were translocated to mitochondria, none showed exclusive localisation (Minczuk et al. 2006). To try and prevent nuclear accumulation, the authors added a nuclear export sequence (NES), a small peptide that signals the ZFP for export from the nucleus, to the peptides. Immunofluorescent studies showed an exclusive localisation to mitochondria, something that was only achieved in ZFPs that had both the NES and MTS conjugated (Minczuk et al. 2006).

Once in the mitochondria, ZFPs need to fold correctly and incorporate Zinc into their structure to become active. Minczuk and colleagues showed that a ZFP-methyalse can be specifically targeted to mitochondria where it folds correctly and methylates mtDNA (Minczuk et al. 2006). Subsequently this group have developed a ZFP-nuclease (ZFN) that can induce double strand breaks specifically in mtDNA with the m.8993T>G NARP mutation. This was achieved by joining two Fok1 nucleases with a flexible linker, which are then conjugated to a ZFP that has been previously shown to specifically bind mtDNA. This new ZFN had the ability to not only localise within mitochondria but also to specifically target and cut mutant mtDNA. This led to a stable decline in heteroplasmy in cells transfected with the ZFN which was maintained up to 30 days after the initial depletion (Minczuk et al. 2008). Although this approach has shown some potential in the specific recognition and removal of mutated mtDNA, targeting to the mitochondria is hindered by the strong nuclear localisation of Zinc fingers.

1.8.2.3. *TALENS*

TALENS (Transcription Activator-Like Effector Nucleases) are a family of proteins that can bind DNA in a sequence specific manner and induce a double strand break (Hockemeyer et al. 2011). Unlike ZFNs they do not possess a tendency to localise to the nucleus, which enables them to efficiently target mitochondria using protein import

sequences. Bacman *et al.* engineered TALENS with mitochondrial targeting sequences to bind and cleave the 4977bp "common deletion" breakpoint (m.8483_13459) in patient derived cell lines (Bacman et al. 2013). The authors used FokI nucleases that dimerise in order to cleave mtDNA, this required the use of two TALENS each designed to bind different regions of mtDNA, which when bound to species of mtDNA containing the deletion will be in close enough proximity for the nucleases to cleave DNA (Bacman et al. 2013). The authors showed a decrease in heteroplasmy from 70% to 30% in cell lines which contained both TALENS, without affecting the overall copy number of the cells, indicating a compensatory increase in mtDNA replication, which favoured an accumulation of wild type mtDNA as these were not removed by the TALENS. Although this technique showed excellent efficacy, the delivery of gene or protein therapies to patients limits its potential uses in man.

1.8.2.4. *Mitochondrial Transfection*

Development of an effective nucleic acid delivery mechanism for mitochondria has so far proved elusive. While delivering oligomers into the cytoplasm has now become commonplace, the targeting and crossing of the charged mitochondrial double membrane is a technical challenge. Traditionally, liposomes have been used to facilitate the transport of oligomers across the cell membrane. However to use a liposomal approach to mitochondrial drug delivery, a mitochondrial targeting moiety will have to be employed to translocate the liposome to the mitochondrial membrane subsequent to cytoplasmic delivery.

Initial successes were claimed in this area using cationic DQAsomes as a transfection agent. DQAsomes are formed by the sonication of dequalinium (Weissig et al. 1998), an anti-microbial drug that has been previously shown to accumulate in mitochondria (Weiss et al. 1987). An overall cationic charge that is distributed across the molecule makes DQAsomes very attractive for targeting negatively charged mitochondria. D'Souza *et al*. created DQAsome-DNA complexes with plasmid DNA and then incubated these complexes with BT20 epithelial cells. The authors showed delivery of the plasmid into mitochondria by staining cells with the dsDNA stain SYBR green I, cells incubated with the DQAsome-DNA complex showed minimal SYBR green colocalisation to mitochondria (D'Souza et al. 2003). Subsequent work has claimed that

delivery of a green fluorescent protein (GFP) gene to mitochondria is also possible using a DQAsome delivery system (Lyrawati et al. 2011), however the results in this paper are far from conclusive. Although DQAsomes showed initial promise at delivering DNA to mitochondria, currently there are no published articles showing delivery of gene therapy agents to cells affected by mtDNA disease.

Further advances in the design of mitochondria targeting liposomes have taken place since the discovery of DQAsomes. The conjugation of Rhodamine 123, a mitochondrial selective dye, to liposomes was used to deliver drugs to mitochondria and caused a significant increase in not only cellular internalisation of the liposome but also in mitochondrial localisation (Biswas et al. 2011).

Recently, Yamada *et al*. have developed the dual function mito-porter consisting of an outer and inner liposome (Yamada et al. 2011). The complete mito-porter enters the cells via endocytosis after which the outer membrane fuses with the endosome releasing the drug containing inner liposome into the cytoplasm. The targeted inner liposome then fuses with mitochondria delivering the drug into the mitochondrial matrix.

Mitochondrial targeting is achieved by modifying the liposomes with positively charged octaarginine (R8), enabling uptake into the cell via macropinocytosis and also forcing localisation to mitochondria via electrostatic interactions with the negatively charged mitochondrial membrane. The approach has the potential to deliver a wide range of bioactive molecules into the mitochondria including oligomers and peptides (Yamada et al. 2011). To test the concept of mitochondrial matrix delivery, Yamada encapsulated DNase I in the DF-mito-porter and tested the level of mtDNA depletion caused by the enzyme. The authors detected DNase I in mitochondria and also found that there was a decrease in mtDNA when measured using qPCR (Yamada and Harashima 2012). Although this result is promising, further work needs to be completed to assess the efficacy of their approach.

1.8.2.5. *Oligomer therapies*

The use of oligomer therapies in mtDNA disease could offer not only a treatment but also a cure for the diseases. While previous attempts such as endonuclease therapies have been centred on just one mutation in humans (Srivastava and Moraes 2001; Tanaka et al. 2002), oligomers have the potential to be designed to target any mutated region of mtDNA, thus enabling the treatment of all mtDNA disease.

Heteroplasmic mtDNA mutations preserve a pool of wild-type mtDNA that could potentially rescue the mutant phenotype. By designing an oligomer that is complementary to the sense strand of an mtDNA mutation, be it a point mutation or a deletion, the oligomer has the potential to bind both the mutated mtDNA and also the mt-RNA that is transcribed from the mutated region. This strategy potentially offers a therapeutic effect against both mutated mtDNA and mutated mitochondrial mt-RNA or mt-tRNA. Experiments *in vitro* have shown that binding of an oligomer to mtDNA can halt the replication fork thus preventing replication of the mutated genome (Taylor et al. 1997). If this were to happen *in vivo* then it is likely that the mtDNA molecules with a stalled replication fork would be degraded in order to prevent genome instability, or at the very least that it would lead to a preferential increase in the wild type genomes. As described previously, the level of wild type mtDNA drives the cellular phenotype, so a small increase in the proportion of wild type to mutated mtDNA could lead to a greater improvement in the biochemical defect of the mitochondria.

Peptide nucleic acids (PNAs) showed early promise at inhibiting mtDNA replication *in vitro*. Developed to be both nuclease and DNase resistant, PNAs are formed by substituting the deoxyribose-phosphate backbone of DNA with aminoethyl-glycine groups to create a molecule that can also outcompete DNA:DNA interactions to preferentially bind complementary DNA sequences, due to the absence of a negatively charged phosphate group on the PNA backbone increasing the stability of PNA:DNA hybrids relative to DNA:DNA binding (Nielsen et al. 1991). As with all mitochondrial therapies, targeting PNAs to the mitochondrial matrix is challenging. Biotinylated PNAs complementary to the m.8344A>G MERRF mutation were conjugated to the mitochondrial targeting protein presequence of COX VIII to try and facilitate entry into the mitochondrial matrix (Chinnery et al. 1999). Although staining for biotin showed a

mitochondrial colocalisation, it was deemed that entry into the mitochondrial matrix was not occurring due to an absence of functional effect (Chinnery et al. 1999; Filipovska et al. 2004).

Recent developments in this field have focused on improving the ability of PNAs to cross cell membranes. This has led to the emergence of a new class of oligomers termed cell membrane crossing oligomers (CMCOs) (Posch et al. 2012). Modifications on the backbone of CMCOs (phosphonic esters) enable them to enter the cell without the need for delivery mechanisms such as liposomal transfection. This ability to cross cell membranes and accumulate in the cytosol means that there is the potential to cause accumulation in the mitochondria if the CMCOs can be conjugated to a lipophilic cation such as TPP. On-going work to test the efficacy of such an approach forms a significant portion of this thesis (Chapters 3 and 4).

1.8.2.6. *RNA import*

As mentioned previously, nuclear encoded RNAs are imported into the mitochondria and have important roles in both replication and the cleaving of mitochondrial tRNAs from RNA transcripts. It has also been shown that mitochondria have a conserved ability to import cytosolic tRNAs. *S. cerevisiae* yeast import the nuclear encoded $tRNA^{Lys}$ (CUU) into mitochondria and although the mechanism is not clear, the requirement of an intact TOM/TIM set of proteins for successful import suggest that $tRNA^{Lys}$ (CUU) is chaperoned with a protein, possibly an aminoacyl-tRNA synthetase (Tarassov et al. 2007). Overexpression of the nuclear-encoded $tRNA^{Lys}$ (CUU) has been shown to rescue respiratory defects in MERRF immortalized cybrids cells however tests on patient fibroblasts with the MERRF mutation only demonstrated a partial rescue of mitochondrial function (Kolesnikova et al. 2004). Successful import of the $tRNA^{Lys}$ has led to attempts to treat cells affected by the MELAS m.3243A>G $tRNA^{Leu(UUR)}$ mutation. By modifying the aminoacylation identity of $tRNA^{Lys}$ (which has previously been shown to be imported by mitochondria (Tarassov et al. 2007)) from lysine to leucine a tRNA with the ability to correct m.3243A>G $tRNA^{Leu(UUR)}$ mutations can be imported. The modified tRNA has been shown to increase the level of transcription of mitochondrial proteins in cybrids with the m.3243A>G mutation (Karicheva et al. 2011).

Elucidation of the secondary structures needed to facilitate import of $tRNA^{Lys}$ (CUU) and 5S rRNA into mitochondria have led to the creation of recombinant RNAs that can be imported into mitochondria, bind a specific region of mtDNA and prevent replication. In cells derived from Kearns Sayre syndrome patients with a single large scale 7075bp mtDNA deletion and a unique breakpoint, m.8363_15438, treatment with an oligomer complementary to the breakpoint caused a fall in heteroplasmy from 65% to 40% thus rescuing the mutant phenotype (Comte et al. 2013).

Import of the RNA component of RNase P (*H1* RNA) into mitochondria is modulated by PNPase, which recognises a 20bp stem-loop sequence present on the RNA, enabling its entry into the mitochondrial matrix (Wang et al. 2010). The nuclear encoded mRNA of human mitochondrial ribosomal protein S12 (*MRPS12*) has also been shown to contain regulatory sequences in its 3'UTR which are thought to cause localisation to the mitochondrial outer membrane (Russo et al. 2008). The addition of the 20bp stem-loop structure and 3'UTR regulatory sequence onto transfected wild-type mtRNAs could correct defects caused by mutations of mtDNA *in vivo* by driving import of the wild type tRNA into mitochondria.

Targeted RNA import has been used to try and correct decreased translation rates in cybrids containing either the m.3243A>G MELAS or m.8344A>G MERRF mutations. Addition of the stem-loop targeting sequence onto wild-type tRNAs that are mutated in the MELAS (mt-$tRNA^{Leu(UUR)}$) or MERRF (mt-$tRNA^{Lys(AAA)}$) cybrids cell lines led to import into isolated mitochondria and a subsequent increase in peptide steady state levels (Wang et al. 2012). This approach has also been shown by these authors to work with the import of *MTCO2* mRNA enabling correction of defects caused by mutations in mtDNA encoded proteins (Wang et al. 2012). Importantly the stem-loop structure is cleaved from the RNAs after importation enabling, in the case of tRNAs, allowing them to function correctly or, in the case of mRNAs, for them to be translated by the mitochondrial translation machinery. To achieve tRNA mediated rescue of respiration in whole cybrid cells, the import sequence was modified by the addition of the *MRPS12*

3'UTR targeting sequence, along with the PNPase realted stem-loop sequence to cause mitochondrial localisation (Wang et al. 2012).

1.8.3. **Prevention of mitochondrial disease**

Transmission of mtDNA disease through the germline can be prevented using pro-nuclear transfer techniques, which involve removing the pro-nuclei from the fertilised oocyte of a mitochondrial disease affected mother and inserting it into the enucleated donor embryo of an unaffected individual (Craven et al. 2010). The use of the technique is currently being debated in the UK Houses of Parliament. Mitotic spindle transfer techniques in which the chromosomes from an unfertilised oocyte are transferred into an enucleated donor oocyte have been demonstrated in non-human primates. Although this has not been shown in humans, it offers another potential option for preventing transmission of the diseases (Tachibana et al. 2009).

Alternatively, pre-implantation genetic diagnosis can be used to investigate the mutation load of blastocysts, selecting those that are at low risk of having high heteroplasmy of the disease mutation for implantation into the mother during IVF (Steffann et al. 2006).

1.9. AIMS

Despite extensive research over the last 14 years into modulating heteroplasmy in mtDNA diseases, no practical treatments have been created. Over the same period there has been an absence of the development of mitochondrially acting pharmaceuticals. These two factors mean that treatment options for patients have not been greatly advanced, and as a consequence the prognosis for patients has not improved.

To address these issues this project aimed to investigate potential therapies for mitochondrial disease. First, I investigated an anti-genomic approach using CMCOs, oligomers that have previously shown efficacy at inhibiting mtDNA replication in cell culture models, to selectively target mtDNA mutations, preventing the replication of mutated mtDNA and the translation of mutated mRNA. To achieve this, a strategy for targeting CMCOs to mitochondria was developed. Based on previous work in the field, which highlighted the difficulty of exploiting mitochondrial transport proteins to allow oligomer accumulation into the matrix, I exploited the mitochondrial membrane potential to drive accumulation of the oligomers into the matrix, after which their functional effects were investigated.

The second part of the project focused on a large scale screen of compounds to investigate effects on mitochondrial mass. With work in the field indicating that mitochondrial biogenesis may improve mitochondrial myopathies (either through exercise or pharmacologically), it is important to discover compounds with better efficacy at increasing mitochondrial mass than currently available treatments. An assay was developed to screen for changes in mitochondrial mass in a quick and reproducible manner. This assay was then used to screen a library of compounds, after which any "hit" compounds were investigated further.

Materials And Methods

Materials and Methods

2.1. MATERIALS

2.1.1. Equipment

ABI 3100 Genetic Analyser	Applied Biosystems.
ABI Gene Amp 9700 Thermal Cycler	Applied Biosystems.
ABI Prism 7000 sequence detection system	Applied Biosystems.
Autoclave	Astell
Automated fluorescent plate reader	BMG-Omega
Automated plate reader EIx800	Bio-Tek
Balance: Sartorius Basic	Sartorius
Bench-top Microcentrifuge	Sigma
Bench-top Centrifuge 3-15	Sigma
Binder General Purpose Incubator	Philip Harris
Dry Heat Block	Techne
Electrophoresis power supply model 250EX	Life Technologies
Fluorescent plate reader	Bmg labtech
Geldoc system	BioRad
Horizontal Agarose Gel Electrophoresis Systems	Amersham
InCu SafeTM CO2 Incubator	Sanyo
Liquid handling robot	Beckman Coulter
Microflow Biological Safety Cabinet	Bioquell
Nanodrop ND-1000 Spectrophotometer	Labtech International
ND-1000 Software	
Nikon A1R point scanning confocal microscope	Nikon

Nikon Elements software	
3510 pH Meter	Jenway
StepOne plus Real-time PCR	Applied Biosystems
U.V hood	BioAir
Zeiss Axiovert 200M fluorescence microscope	Zeiss

2.1.2. **Consumables**

0.2ml Thin-Walled PCR tubes	Starlabs
0.5ml Thin-Walled PCR tubes	Starlabs
1.5ml Eppendorf tubes	Starlabs
2.0ml Eppendorf tubes	Starlabs
Multi-well optical bottom plates	Greiner
Aerosol resistant Pipette tips	Starlabs
Coverslips (22x22mm)	Merck
Cellstar® Disposable Pipettes (5ml, 10ml, 25ml)	Greiner
Cellstar® Tissue Culture flasks ($25cm^3$, $75cm^3$, $225cm^3$)	Greiner
Cryotubes	Nunc
Falcon tubes (15ml and 50ml)	Starlabs
Gilson Pipetteman (P2, P10, P20, P200, P1000)	Anachem
Liquid handling tips	Beckman Coulter
Western blotting equipment	BioRad

2.1.3. **Solutions**

This list gives solutions not detailed in the methods section.

DNA Loading buffer	0.25% (w/v) Bromophenol Blue 0.25% (w/v) Xylene Cyanol 30% (v/v) Glycerol
Electrophoresis Buffer	100ml 10x TAE 900ml ddH_2O 80µl ethidium bromide
5% Milk solution in TTBS	5g Skimmed Milk powder 100ml TTBS
4% Paraformaldehyde	20g paraformaldehyde in 250ml ddH_2O 250ml 0.2M phosphate buffer
Phosphate Buffered Saline	Prepared from tablets; 1 Tablet in 100ml water
Running Buffer (western) 5x	15g Trisma base 72g Glycine 5g SDS
TTBS pH 7.6	2.42g Trisma base 8g NaCl Made up to 1l with dH_20 0.1% Tween 20 (v/v)

2.2. METHODS

2.2.1. Adherent cell-line culture

Fibroblast or HeLa cells were cultured in either T75cm^2 or T225cm^2 vented Costar flasks in an appropriate amount of media specific to each cell line (Table 2.1) and incubated at 37^{o}C in a humidified atmosphere with 5% CO_2. Once cells reached 90% confluency, the cells were washed once in PBS and passaged using 0.5% Trypsin-EDTA. Trypsin was quenched by addition of complete media and cells transferred to a 30ml universal prior to centrifugation at 160*g* for 4 minutes. Cells were resuspended in their complete media and seeded in fresh flasks or dishes at an appropriate confluency. Cells to be frozen were placed in the complete media with 10% (v/v) DMSO, and frozen at -80^{o}C for 24 hours in Cryotubes (Nunc), after which they were transferred to liquid nitrogen. HeLa cells were provided by Dr. Francesco Bruni (Newcastle University, UK), immortalised fibroblasts were provided by Ms. Marysia Wesolowska (Newcastle University, UK).

Table 2.1 – Cell culture media

Cell line	Media	Supplements
HeLa	EMEM with Earle's salts	10% FBS (v/v), 2mM L-glutamine, 1xNEAA
Fibroblasts	EMEM with Earle's salts	10% FBS (v/v), 2mM L-glutamine, 1xNEAA, 1mM sodium pyruvate, 0.41µM Uridine

2.2.2. Cell counts

Prior to cell counting, 10µl cell suspension was mixed with 10µl Trypan blue. 10µl of the Trypan solution was then placed under the cover slip on a haemocytometer and cell number per ml calculated.

2.2.3. **Live cell staining**

Mitochondrial network stains were diluted to the appropriate concentration in complete media for the cell line to be stained, unless otherwise stated the final concentrations of the dyes are stated in Table 2.2. Cells were incubated with the dye for 30 minutes at 37^{o}C in a humidified atmosphere of 95% air, 5% CO_2. Dye containing media was aspirated and the cells washed in PBS three times, after which they were covered with complete media without Phenol Red. Cells were imaged using the appropriate excitation and emission profiles according to Table 2.2. Concentrations were determined using manufacturers guidelines, all stock solutions were made up in DMSO and stored at -20^{o}C. Final concentrations were diluted in media appropriate for the cell line.

Table 2.2 – Concentration and properties of dyes used for live cell imaging.

Dye	Wavelength Ex/Em (nm)	Stock concentration	Final concentration
Atto 674N	644/669	5mM	1µM
Calcein Blue	360/448	2.1mM	2.1µM
Hoechst 33258	346/460	18mM	7.2µM
Mitotracker Deep Red FM	644/655	1mM	50nM
Mitotracker Green FM	490/516	1mM	50nM
Picogreen	480/520	Unknown	1µl/ml
TAMRA	553/576	10mM	250nM
TMRM	549/573	5mM	15nM

2.3. MICROSCOPY

2.3.1. **Wide-field microscopy**

Wide-field microscopy was carried out using an inverted Zeiss Axiovert 200M fluorescent microscope with the following filters: DAPI 359ex/461em, FITC 490/525, Texas Red 595/620. To image cells, an appropriate filter was chosen to capture signal from the fluorophores used for staining. To capture the image, Axiovision software was used to measure the signal emitted from the excited fluorophore and automatically determine the correct exposure time. Exposure time was manually adjusted to capture a minimal amount of background signal. Images were captured using a 60x oil immersion lens.

2.3.2. **Confocal microscopy**

Confocal microscopy was carried out using an inverted Nikon A1R point scanning confocal microscope equipped with 405nm, 457nm, 488nm, 514nm, 561nm and 647nm laser lines. Images were captured using photomultiplier (PMT) tubes and Nikon Elements software. Unless otherwise stated, images were captured using a 60x oil immersion objective (1.4 numerical aperture (NA)). Live cells were imaged in a bio-chamber set at 37^{o}C and 5% CO_2 after an equilibration of 10 minutes to remove condensation. Appropriate laser lines were selected to image the cells based on the excitation wavelength of the fluorophores (Table 2.2).

Imaging conditions were set up manually by adjusting laser power, PMT voltage and image offset to ensure the best possible image was obtained. Although there was variation between settings for each laser line and experiment, in general the laser power was set as low as possible to prevent fluorophore bleaching and photo-toxicity to the cells. PMT voltage was kept below 100V (1-150V range) where possible, to prevent introduction of noise into the image as this may lead to degradation in image quality. Image offset was adjusted to set the "black" level, for example this can be adjusted to remove background signal from samples. The confocal pinhole was set to the optimum diameter depending on the wavelength to be captured; this was set up automatically by the software.

Prior to imaging, perfect focus system (PFS) was enabled to ensure that the focal plane did not drift during image capture. Images were captured by sequentially exciting the sample using an individual laser line, capturing emitted photons and repeating for each laser line in use. Depending on the quality of staining, line averaging was also used to remove noise from the image. This works by scanning the image a set number of times to determine if a signal is obtained from the same place each time. If the signal is not present on each scan then it is classed as noise and removed from the image, however the increase in scanning also increases exposure time and therefore bleaching and photo-toxicity.

For single plane imaging the cell to be imaged was scanned from top to bottom and the widest part of the cell was imaged. 3D images were obtained by capturing a series of images across a Z-stack. The top and bottom of the cell to be imaged was found by scanning through the cell and storing the locations in Nikon elements software. The number of slices to be imaged was then calculated based on the confocal aperture pinhole diameter, unless otherwise stated the image slice was 0.5µm. For general scanning of the sample, 512x512 pixels were imaged to decrease frame time, captured images had a 1024x1024 pixel resolution.

2.3.3. **High throughput imaging**

High throughput imaging was used to take bright field images of cells grown in 96 well plates as part of a drug screen; all images were obtained using a Nikon Eclipse wide field microscope with bio-chamber and automated stage, the microscope was controlled using Nikon Elements software with Nikon Jobs package Prior to imaging, HeLa cells were seeded in 96 well plates, left overnight and dosed with bacterial extracts according to section 6.3.2. The plate to be imaged was loaded onto the microscope stage and a 10x air (0.3 NA) objective selected.

The following experimental workflow was set up using Nikon Jobs wizard. The appropriate 96 well plate was selected and the stage calibrated by moving the field of view to wells A1 and H12, enabling the software to map the layout of the plate. To compensate for focus drift as the plate moved around during imaging, an autofocus of 100µm was used. This adjusted the focus of the microscope over a range of 100µm, after which the correct focal plane is selected automatically by measuring changes in the image contrast. An exposure time of 100ms and bulb voltage of 3V was selected before all wells were imaged in sequence.

2.3.4. **Colocalisation analysis**

Colocalisation of mitochondria with fluorescently tagged CMCOs was calculated using Volocity (Perkin Elmer) imaging software; all images were captured using a Nikon A1R point scanning confocal microscope. Volocity was used to determine the threshold of the fluorophores according to the method described by Costes and colleagues which

subtracts non-specific background fluorescence (Costes et al. 2004). This is essential to ensure that non-specific background staining is not classed as colocalised. The degree of colocalisation was calculated by Volocity and given as a Pearson's correlation coefficient; therefore perfect colocalisation gives a value of 1 and no relationship between mitochondria and the fluorophore conjugated CMCO gives a value of 0.

2.3.5. **Mitochondrial volume analysis**

Investigation of active extracts after the drug screen was carried out using confocal microscopy. HeLa cells were seeded (1×10^4 cells/well) in a class bottomed 24 well plate and placed in an incubator overnight. Active extracts were filter sterilised and added to the HeLa media at an appropriate concentration and incubated for 48 hours. HeLa cells were stained with 10nM TMRM and 2.1µM Calcein blue for 30 minutes, before washing in PBS and being placed in fresh, Phenol Red free media. Imaging was performed using a Nikon A1R microscope. All images were analysed using Imaris software (Bitplane AG), briefly each colour channel was detected by the software and a new image rendered. The volume of each stain was determined and the proportion of mitochondria per cell calculated.

2.4. PROTEIN EXPRESSION

2.4.1. **Protein extraction**

Adherent cells were passaged according to section 2.2.1 and centrifuged at 160*g* for 4 minutes to pellet the cells. Cell pellets were resuspended in PBS and centrifuged at 160*g* for 4 minutes after which PBS was removed. Pellets were resuspended in 50µl protein lysis buffer (0.05M Tris-HCl pH7.5, 0.13M NaCl, 2mM $MgCl_2$, 2% Igepal CA-360, 1x protease inhibitors) and vortexed for 30secs. Samples were centrifuged at 560*g* for 2 minutes to pellet nuclei and unbroken cells. Supernatant was removed and placed in a fresh 1.5ml tube and 50µl 10mM Tris HCl pH7.5 added. Protein lysates were aliquoted and flash frozen in liquid nitrogen.

2.4.2. **Bradford assay**

Protein concentration was determined using a BSA (bovine serum albumen) standard curve. A standard curve was produced using BSA concentrations of 0, 2, 5, 10, 20µg/µl

made in 800µl dH_2O, 200µl Bradford reagent was then added to these. Samples were prepared by adding 1µl protein lysate to 800µl dH_2O and 200µl Bradford reagent. 200µl of the standards and samples were added in duplicate to a 96 well plate and absorbance was read at 595nm using a BioTEK ELx895 plate reader. Sample protein concentration was extrapolated from the standard curve.

2.4.3. **Polyacrylamide gel electrophoresis**

Protein samples were separated by size using BioRad Mini-PROTEAN TGX Precast gels. Prior to gel loading, samples were diluted 1:1 with 2x Laemmli buffer (60 mM Tris-HCl pH 6.8, 2% SDS, 10% glycerol, 100mM DTT, 0.01% bromophenol blue) and incubated at 37^{o}C for 30 minutes. Gels were placed in an electrophoresis tank filled with an appropriate amount of running buffer (25mM Tris HCl, 192mM glycine, 0.1%SDS, pH8.3). Samples were loaded on to the gel along with 5µl Spectra pre-stained, broad range protein ladder (Thermo Fisher, USA) and run at 150V, 30mA for 1hour or until separation of the ladder was complete.

2.4.4. **Protein Transfer**

For protein transfer on to PVDF membrane, BioRad Turbo blot kits were used according to the manufacturer's instructions. Briefly, Turbo blot filter paper containing the PVDF membrane was placed membrane side up on the bottom of a Turbo blot transfer tray. The precast gel was then removed from the casket and placed on the PVDF membrane and rolled to ensure no air bubbles were present. The top section of filter paper was then laid on the gel and the lid attached to the running tray. Transfer was run at 2.5A, 25V for 4 minutes. Transferred proteins were stained by immersing the PVDF membrane in Ponceau S (0.1% Ponceau S (w/v) in 1% acetic acid (v/v)) for 10 minutes before washing excess off using dH_2O. Stained proteins were visualised by eye to determine if protein detection should be carried out. The transferred gel was stained with Coomassie brilliant blue (1% Coomassie Brilliant Blue, 500ml methanol, 100ml glacial acetic acid, 400ml dH_2O) for 30 minutes at room temperature. Stain was removed and washed in dH_2O before incubation with de-stain solution (500ml methanol, 400ml dH_2O, 100ml glacial acetic acid) overnight at 4^{o}C. Protein staining by Coomassie was assessed to determine efficacy of protein transfer.

2.4.5. **Protein Detection**

PVDF membranes were blocked in 5% milk in TTBS for 1 hour at room temperature on a shaker to prevent non-specific antibody binding. Primary antibody was diluted in 5% milk in TTBS and incubated on the membrane overnight on a shaker at 4^{o}C. After primary antibody incubation the membrane was washed 3 times in TTBS for 5 minutes and the appropriate secondary antibody conjugated to HRP diluted in 5% milk in TTBS incubated with the membrane on a shaker for 1 hour at room temperature. The membrane was then washed 3 times in TTBS for 5 minutes and placed on an acetate sheet, protein side up. Signal development was carried out using ECL Prime according to the manufacturer's instructions and 1ml of the solution was used to cover the membrane for 5 minutes. A luminescent product was produced by reaction with the HRP conjugated bound 2^{o} antibody. This product was detected using a BioRad ChemiDOC MP CCD camera set at an appropriate exposure time. Antibody concentrations are shown in Table 2.3.

Table 2.3 – List of antibodies used for western blotting

Antibody	Stock concentration	Dilution for protein detection
Anti-COX I	1mg/ml	1:1000
Anti-SDHA	1mg/ml	1:500

2.5. MITOCHONDRIAL DNA ANALYSIS

2.5.1. **Adherent Cell DNA extraction**

Culture media was removed from the wells of cells grown in plates. Wells were washed in PBS before the addition of an appropriate volume of DNA lysis buffer (250µl 1%Tween, 195µl ddH_2O, 50µl Tris-HCl (pH 8.5) and 5µl Proteinase K). Plates were incubated at 55^{o}C for 2 hours and lysis buffer transferred into fresh 200µl tubes. Proteinase K was denatured by incubating at 95^{o}C for 10 minutes. DNA concentration and purity was analysed using a Nanodrop ND-1000 spectrophotometer and stored at -20^{o}C.

2.5.2. **Real-time PCR copy number analysis**

Copy number of mtDNA was determined by comparing the relative expressions of the nuclear encoded *B2M* (β2 microglobulin) and the mitochondrial gene *MTND1* using the primer sets described in Table 2.4. All reactions were prepared in a UV PCR hood to prevent contamination. For each sample to be investigated, a tenfold serial dilution was produced ranging from 1:10 to 1:100000, to enable the production of a standard curve. Relative expression of both genes for each sample was measured on the same plate; however the assays cannot be multiplexed (due to the high efficiency of the ND1 reaction). For the ND1 assay 1µl of each sample was added to individual wells in triplicate to which 24µl real-time master mix was also added (12.5µl Taqman Universal master mix, 0.5µl ND1 VIC probe, 0.75µl 10µM forward and reverse primer, 9.0µl ddH_2O). B2M assays were set up in the same way using B2M master mix (12.5µl Taqman Universal master mix, 0.5µl B2M FAM probe, 0.75µl 10µM reverse primer, 0.08µl 10µM forward primer, 10.17µl ddH_2O). A no template control was added to ensure no contamination from the master mix. After loading, 96 well plates were sealed with StarLab film and vortexed. Plates were briefly centrifuged to remove drops from the film. The plate was placed in a StepOnePlus real-time PCR machine (Applied Biosystems). Reaction conditions were an initial cycle of 2 minutes at 50^{o}C, 10 minutes at 95^{o}C followed by 40 cycles of 15secs at 95^{o}C and 1min at 60^{o}C. Copy number of *MTND1* in relation to *B2M* was worked out using the C_T (threshold cycle) value obtained.

2.5.3. **DNA Sequencing**

2.5.3.1. *Polymerase chain reaction*

PCR was used to amplify regions of the mitochondrial genome to provide enough DNA for sequencing. Extracted DNA was amplified using primer pairs designed to span the region of interest (Table 2.4), all primers were tagged with the M13 sequence (Forward - 5'-TGTAAAACGACGGCCAGT-3', Reverse - 5'-CAGGAAACAGCTATGACC-3') to facilitate sequencing, and were designed to anneal optimally at 58^{o}C. PCR was carried out using a 25µL mastermix of 16.87µL ddH_2O, 2.5µL 10x PCR buffer, 2.5µL 10x dNTPs, 0.13µL AmpliTaq Gold and 1µl extracted DNA. A no template control and positive control reaction was also amplified. Reactions were placed in a thermal cycler under the following conditions: 95^{o}C for 10 minutes then 30 cycles of 94.0^{o}C for 45

seconds, 58°C for 45 seconds and 72°C for 1 minute. A final extension of 72°C for 8 minutes was carried out.

2.5.3.2. *Gel Electrophoresis*

Following PCR, 5µL product was mixed with 1µL loading buffer (0.25% (w/v) bromophenol blue, 0.25% (w/v) xylene cyanol, 30% (v/v) glycerol) and loaded on to a 1.5% agarose gel containing 0.4µg/ml ethidium bromide to enable DNA visualization, along with PCRRanger 100bp ladder. Electrophoresis was carried out in 1X TAE buffer for 40 minutes at 70 volts. Subsequent to electrophoresis, PCR products were visualized in ultraviolet light using a BioRad ChemiDOC MP and a digital image obtained. Failed reactions or reactions that showed a positive signal in the negative control were repeated.

2.5.3.3. *Cycle Sequencing*

After visualization, 5µL of the product was placed in a 96 well sequencing plate to which 1.5µL TSAP alkaline phosphatase (Promega) (containing exonuclease I and alkaline phosphatase) was added over ice to remove unreacted nucleotides and primers from the sample. This was incubated in a thermal cycler for 15 minutes at 37°C to enable digestion and 15 minutes at 80°C to denature the enzymes. A 12µL master mix containing 7µL dH_2O, 3µL 5x Sequencing buffer, 1µL Universal forward primer, 1µL BigDye v3.1 was added to each sample after clean up. Samples were placed in a thermal cycler under the following conditions; 96°C for 1 minute then 25 cycles of 96°C for 10 seconds, 50°C for 5 minutes and 60°C for 4 minutes.

Prior to sequencing, PCR products were precipitated by the addition of 2µl of 3M sodium acetate, 2µl of 125mM EDTA and 70µl of 100% Analar ethanol to each sample. This was mixed by inversion and left for 15 minutes prior to centrifuge at 2090*g* for 30 minutes. The supernatant was discarded; 70µL of 70% Analar ethanol was added to each sample and centrifuged at 1650*g* for 15 minutes. The supernatant was discarded and the samples allowed to air dry for 20 minutes in the dark. Before sequencing, 10µL of HiDi formamide was added to each sample to facilitate the separation of DNA

strands and incubated for 2 minutes at 95°C. The plate was then placed in an ABI 3100 Automated DNA sequencer for sequencing. Sequenced fragments were analysed using SeqScape software by comparing sequences to the revised Cambridge Reference sequence (rCRS) (Andrews et al. 1999).

Table 2.4 – PCR primer sets.

Real-time PCR primers	
B2M F	CCAGCAGAGAATGGAAAGTCAA
B2M R	TCTCTCTCCATTCTTCAGTAAGTCAACT
ND1 F	CCCTAAAACCCGCCACATCT
ND1 R	GAGCGATGGTGAGAGCTAAGGT
Real-time PCR probes	
B2M-FAM	ATGTGTCTGGGTTTCATCCATCCGACA
ND1-VIC	CCATCACCCTCTACATCACCGCCC
Sequencing primers: 5875-6410	
12 F	CACTCAGCCATTTTACCTCAC
12 R	ATGGCAGGGGGTTTTATATTG

2.6. CELL MEMBRANE CROSSING OLIGOMERS

2.6.1. CMCO preparation

CMCOs were delivered in a lyophilised form. All CMCOs were resuspended in a volume of PBS that should give a final CMCO concentration of 1mM according to the molecular weight and mass of the CMCO. Due to the manufacturing process, it is likely that the CMCOs are not pure and the concentration is likely to be lower than 1mM. After re-suspension, the concentration of CMCO was determined by measuring the optical density (OD) Absorbance at 260nm over a 1cm light path using a quartz cuvette. The following additive A260 EmM.cm^{-1} for PNA monomers was used: A=13.7, C=6.06, G=11.7, T=8.6. Following calculation of the final concentration, the CMCOs were aliquoted into appropriate volumes and frozen at -20°C. Fluorescently conjugated CMCOs were protected from light.

2.6.2. Dosing

Prior to dosing, HeLa cells were seeded at low density on a plate appropriate for the experiment to be completed. Biotinylated CMCO detection was carried out on cells grown on coverslips in 6-well plates,

2.6.3. **Fixation & biotin detection**

After incubation with biotinylated CMCOs, HeLa cells grown on glass coverslips in 6-well plates were washed three times in PBS and fixed in ice cold 70% ethanol for 30 minutes. After incubation, ethanol was removed and the coverslip air-dried on ice for 10 minutes. The coverslip was removed from the 6-well plate and 200µl blocking solution (10% FBS in PBST) added for 30 minutes. Streptavidin conjugated Alexa Fluor 488 was diluted 1:500 in blocking solution. Blocking solution was then replaced with streptavidin solution and incubated in the dark at room temperature for 90 minutes. This solution was removed and coverslips washed three times in PBST for 5 minutes each followed by three washes in PBS for 5 minutes. Coverslips were mounted on slides using DAPI mount (Vectashield). Slides were stored at -20^{o}C in the dark if not imaged immediately after staining. Images were captured using wide-field microscopy section 2.3.1 and analysed using Volocity software.

2.7. HIGH THROUGHPUT DRUG SCREEN

2.7.1. **Cell seeding**

HeLa cells were grown in T225cm^2 flasks as described in section 2.2.1 until they reached 80% confluency. Cells were then dissociated and counted using a haemocytometer after which they were diluted to 5000 cells/150µl in complete HeLa cell growth media and placed in a Falcon tube. A total volume of 15ml was required per plate to be seeded. Cells were seeded onto HT 96 well plates using a Beckman Biomek FX Liquid Handling robot contained in a Class II cabinet. Beckman Coulter P250 sterile tips were loaded by the robot on to the 96 well arm and 150µl of the cell containing media loaded into each well on the plate. After seeding, plates were re-lidded and placed in a humidified incubator at 37^{o}C and 95% air, 5% CO_2. Plates were not stacked for the first hour of incubation to ensure even warming.

2.7.2. **Extract and control addition**

24 hours after initial seeding, cell containing plates were dosed with either bacterial extracts or control molecules. Prior to addition, a control plate was made by adding HeLa media with either 450µM Bezafibrate or 5µM FCCP to one third of a HT 96 well plate. The final third of the plate contained HeLa media only. Plates containing bacterial

extracts were centrifuged at 2000*g* for 30 minutes to pellet precipitates and prevent pipette tip blockage.

Cell plates were loaded on to the robot, de-lidded and extracts were added to them to a final dilution of either 1 in 10 or 1 in 100. Each concentration of extract was added to 4 cell plates creating 4 repeats of each dose. The final cell plate had its media removed and 150µl/well from the control plate added. Plates were re-lidded and placed in a humidified incubator at 37^{o}C and 95% air, 5% CO_2.

2.7.3. **Mitochondria detection**

Cells were incubated with either the extracts or control molecules for 48 hours after which their media was removed by the robot in the dark and replaced with HeLa media without Phenol red with 75nM TMRM. Plates were re-lidded and placed in a humidified incubator at 37^{o}C and 95% air, 5% CO_2 for 1 hour. After incubation the plates were placed on the robot and the TMRM containing media was removed. Plates were then washed 3 times with warm PBS before the addition of 100µl HeLa media without Phenol red. Plates were then placed in a BMG labtech omega plate reader and the signal emitted by TMRM after excitation at 561nm was measured. Each well was measured in 6 different areas and the average fluorescent signal recorded.

2.7.4. **Cell Fixation and Nuclei Counting**

After mitochondrial measurement the plates were fixed in 4% PFA using the robot. Briefly, media was removed and 100µl per well 4% PFA in PBS added and incubated for 10 minutes. PFA was removed and plates washed 3 times in PBS with the final wash being left on. At this stage plates can be left at 4^{o}C before nuclei staining.

Chapter Three

Development of a mitochondrial targeting system for anti-genomic mtDNA disease therapies

3.1. INTRODUCTION

Mitochondrial DNA (mtDNA) diseases are caused by an accumulation of inherited mutated mtDNA molecules and a subsequent reduction in the proportion of wild-type mtDNA. Although there are treatments for many of the symptoms of these disorders (for example insulin for the treatment of diabetes or surgical correction of ptosis), there are currently no therapeutics that target the cause of these diseases. To effectively treat these diseases, molecules that can interact with mutated mtDNA and prevent its negative downstream effects must be developed. Several mechanisms could be exploited to achieve this, including: prevention of mutated mtDNA replication, degradation of mutated mtDNA, increasing the replication of wild-type mtDNA, prevention of mutated mtDNA transcription or prevention of translation of mitochondrial mRNA (for a more in-depth assessment of the current work in this field please see section 1.8).

Currently the most successful systems to selectively degrade mutated mtDNA, such as the use of mitochondrial targeted restriction enzymes (Tanaka et al. 2002) or the use of zinc finger nucleases and the use of TALENS (Minczuk et al. 2006; Minczuk et al. 2008; Bacman et al. 2013), have not been developed to a point where they can be used in man. The use of RNA import mechanisms to deliver anti-sense molecules to the mitochondrial matrix have also been claimed to show efficacy in cell culture models (Comte et al. 2013). Although in theory these approaches could be used to treat mtDNA disease, in reality the delivery of these therapies to affected tissues in multi-systemic diseases currently prevents their use. However, there is the possibility of using anti-genomic therapies in Leber's hereditary optic atrophy as the ocular location of the disease makes delivery much easier.

The use of anti-sense oligomers to treat mtDNA diseases has previously been attempted in this research group (Taylor et al. 1997; Chinnery et al. 1999). Peptide nucleic acids (PNAs), complementary to mtDNA disease mutations, were targeted to mitochondria using mitochondrial peptide targeting sequences conjugated to the PNA oligomer.

Although *in vitro* inhibition of mtDNA replication proved the concept of selective inhibition (Taylor et al. 1997), delivery of PNAs into the mitochondrial matrix proved elusive. Subcellular localisation studies showed that although the PNAs were delivered to the mitochondria; there was no appreciable effect on mtDNA expression (Chinnery et al. 1999). Based on imaging and molecular studies on mitochondrially localised PNAs, the authors of this work speculated that the PNAs had become embedded in the inner mitochondrial membrane, preventing their accumulation in the matrix and therefore binding to mtDNA. The use of anti-sense therapies still provides an attractive option for the treatment of mtDNA diseases. However, the efficacy of their delivery into the cell needs to be increased, as does the efficiency of mitochondrial targeting and in particular the problem of unequivocal access to the mitochondrial matrix needs to be resolved.

3.1.1. **Cell membrane crossing oligomers**

To improve the likelihood of accumulation within the mitochondrial matrix, a new class of PNA based oligomers has been developed by our industrial partner Ugichem GmbH (Innsbruck, Austria). They have modified the solubility of PNA monomers by adding phosphonic ester side chains, creating a new type of monomer - the Ugimer. The addition of phosphonic esters confers amphiphilic properties to the Ugimers, enabling them to be soluble in both water and lipids. By hybridising mixtures of PNA and Ugimer monomers, Ugichem have developed nucleobase oligomers that can cross plasma membranes and accumulate in the cytosol without the need for transfection – "cell membrane crossing oligomers" (CMCOs). The difference in structure between PNA oligomers and CMCOs is shown in figure 3.1.

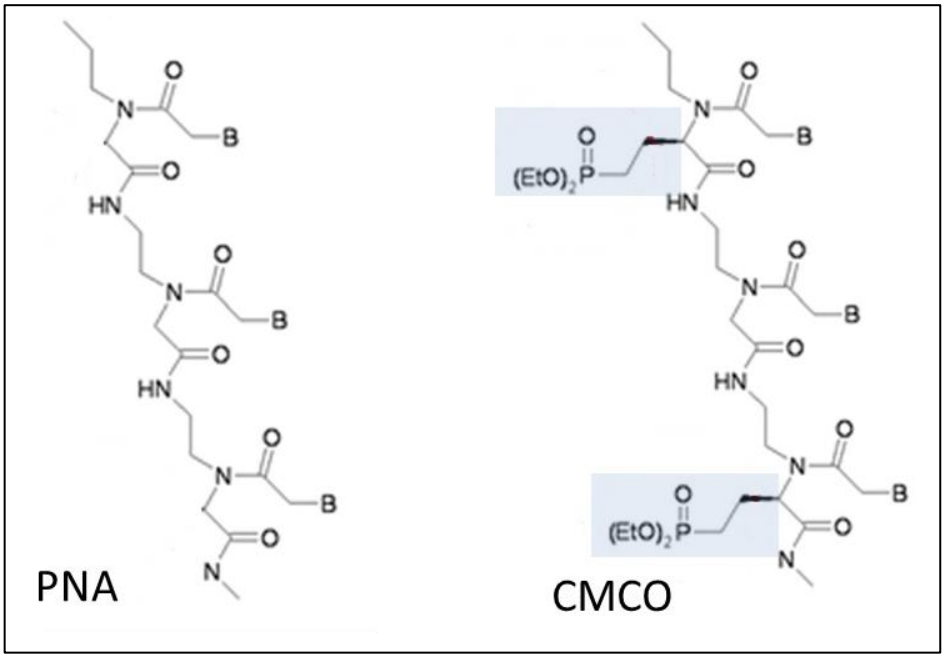

Figure 3.1-The backbone structure of PNAs and CMCOs.
The addition of phosphonic acid is highlighted by the blue boxes; the letter B denotes a DNA nucleobase (adenine, cytosine, guanine or thymine).

The use of phosphonic ester side chains generates an uncharged molecule that has the ability to cross cell membranes, a so called "self-transfecting" oligomer (Posch et al. 2012). Although the ability to cross cell membranes has not been fully investigated for CMCOs, Stein and colleagues recently reported that "locked nucleic acids" (RNA based anti-sense oligomers) can be modified to cross cell membranes without transfection agents (Stein et al. 2010). The phosphonic esters are protected from enzymatic degradation due the phosphorus atom being directly linked to the adjacent carbon atom, something that is not found in biological systems where an oxygen atom is usually required to join the two. Furthermore the CMCOs are designed to enable conjugation of other molecules at their termini, conferring properties that may enable subcellular localisation.

Other approaches currently used to target RNA, DNA or proteins to mitochondria utilise one of the transport mechanisms found within mitochondria, such as the TOM/TIM protein import system. Although there have been some claims of success at exploiting these import mechanisms to drive accumulation of molecular therapies into mitochondria (Srivastava and Moraes 2001; Comte et al. 2013), the fact that transfection of the cell is required to deliver the treatment to mitochondria makes these

treatments un-practical. By using CMCOs we aimed to address these issues by designing a self-transfecting oligonucleotide that could specifically target and accumulate in the mitochondrial matrix. By exploiting the ability of the CMCOs to passively cross plasma membranes, it was decided to conjugate a targeting molecule to the CMCO to drive its accumulation specifically within the matrix. The targeting molecules were selected based on their ability to accumulate within mitochondria as a function of their charge, a process that has been shown previously using lipophilic cations (Blaikie et al. 2006; Ross et al. 2008; Finichiu et al. 2013). It has also been demonstrated that these molecules can be used to drive the mitochondrial accumulation of larger compounds such as vitamin E (Kelso et al. 2001; James et al. 2003; Adlam et al. 2005) and superoxide dismutase (Kelso et al. 2012).

3.1.1.1. *CMCOs as mtDNA anti-genomic agents*

Prior to the initiation of this project, developmental work was carried out to determine the optimal backbone composition (the number of phosphonic ester side chains) and overall oligomer length to hybridise to complementary DNA *in vitro* (Kyriakouli 2007). A "minimal mtDNA replisome"- an *in vitro* technique that mimics mtDNA replication using human mitochondrial polγ was used to demonstrate the ability of the CMCOs to selectively bind and inhibit the replication of a mtDNA insert (Falkenberg et al. 2000; Korhonen et al. 2003; Kyriakouli 2007). Binding of the CMCO to the mtDNA template abolished the extension of the template, stalling replication at the CMCO binding site. It was also found that the optimal CMCO length for mtDNA binding and replication inhibition was a 16mer molecule with a backbone that contained 6 phosphonic ester groups spread evenly throughout the molecule.

A CMCO, complementary to *MTCO1* (nt.5979-5994), was manufactured to investigate the binding of mtDNA and mitochondrial mRNA in cultured cells. A sequence homologous to wild-type *MTCO1* was chosen as it enabled, with relative ease, the investigation of both steady state levels of COXI protein and mtDNA copy number. The CMCO, which used 2,4 dinitrophenol as a targeting molecule, was found to cause a 40% decrease in mtDNA copy number when compared to a random sequence control molecule. A significant 70% decrease in the steady state level of COXI protein was also shown following 9 days incubation with HeLa cells (Kyriakouli 2007). These results

indicated that the targeted CMCO was having an anti-genomic effect on wild-type mtDNA, which led to a decrease in protein expression, highlighting the potential use of CMCOs in the treatment of disorders caused by inherited mtDNA mutations.

Although this work showed promise, subsequent work using CMCOs derived from a similar synthesis protocol has failed to replicate these results. It was therefore decided to attempt to improve this work by developing a more robust targeting method to reliably enable the detection of the subcellular localisation of the CMCOs. This chapter will discuss the development and testing of a system to target CMCOs to mitochondria using small, lipophilic cations.

3.2. AIMS

This chapter describes work to target specific CMCOs to mitochondria. To achieve this, I addressed the following aims:

I. To investigate the efficacy of CMCO mitochondrial targeting using several "mitochondrial targeting" moieties.

II. To develop methods to detect the subcellular localisation of targeted CMCOs.

III. To develop a system to efficiently deliver CMCOs to mitochondria in live cells.

3.3. METHODS

CMCOs were produced by Ugichem GmbH using the automated process described by Koch and colleagues (Koch et al. 1997). All CMCOs were analysed using HPLC/MS (high performance liquid chromatography/ mass spectrometry) to assess the purity of the molecules and to ensure that there were no unused reagents present in the final product. CMCOs were delivered in lyophilised form.

3.3.1. CMCO preparation

Lyophilised CMCOs were stored at -20^{o}C to ensure minimal degradation. Using the mass produced and molecular mass data provided by Ugichem, CMCOs were

resuspended in a volume of PBS to generate a final concentration of 1mM. CMCO solutions were heated to 90^{o}C for 5 minutes to ensure that the molecules were fully dissolved, after which tubes were stored on ice and a 5µl aliquot was taken from each solution for further analysis.

3.3.1.1. *CMCO concentration*

Although the 1mM CMCO solutions were produced using the mass information provided by Ugichem, it was decided to confirm the concentration by calculating the optical density at 260nm using a CARY 300 Bio UV-visible spectrophotometer (Agilent technologies, USA). Using the additive monomer absorbance values (A260 EmM.cm^{-1}) for PNAs (A=13.7, C=6.06, G=11.7, T=8.6), the expected absorbance was calculated for each CMCO sequence. A 1 in 1000 dilution of the CMCO aliquots in PBS (1ml final volume) was added to a 1ml quartz cuvette and absorbance at 260nm measured. The expected and actual absorbance was used to determine the final CMCO concentration. All CMCOs were aliquoted in appropriate volumes according to the observed concentration and stored at -20^{o}C.

3.3.2. **CMCO dosing**

HeLa cells (1 x 10^{4}/well) were grown on glass bottomed dishes (WillCo Wells B.V., The Netherlands) for 24 hours prior to dosing. CMCOs were defrosted to room temperature and then briefly heated to 90^{o}C for 2 minutes to ensure they were fully dissolved, after which they were placed on ice. Each CMCO was diluted to an appropriate concentration (depending on the experiment) in the required complete media without FBS - this was to ensure the CMCOs were not sequestered by the large proteins, such as albumin, found in FBS. Media was removed and the cells washed twice in PBS, the CMCO containing media was added and incubated with cells for 2 hours. After the initial incubation, 10% (v/v) FBS was added and the cells returned to 37^{o}C in a humidified atmosphere of 5% CO_2 for the required length of time.

3.3.3. **Biotin detection**

Initial experiments in this chapter describe the use of biotin conjugated CMCOs. After incubation with biotinylated CMCOs, media was removed and cells washed three times

in PBS, after which PBS was removed and the cells fixed in ice cold 70% ethanol for 10 minutes. Ethanol was removed and the cells allowed to air dry. Cells were permeabilised 0.1% TBST for 30 minutes at room temperature, after which they were incubated with a 1 in 1000 dilution of streptavidin Alexa Fluor 488 (Invitrogen, Paisley UK) in 0.1% TBST for 30 minutes in the dark at room temperature. Following incubation, cells were washed three times in 0.1% TBST before a final wash in PBS. Cells were mounted using Vectashield hard mount with DAPI (Vector laboratories, USA) and a coverslip applied to seal the cells in the glass bottomed dishes.

3.3.4. **Microscopy**

Imaging of streptavidin conjugated biotin-CMCOs was carried out by wide-field microscopy using a Zeiss Axiovert 200M microscope. All images were captured using a 20x air objective using appropriate filter sets (DAPI: 365/445-50 Em/Ex, FITC: 475-40/530-50 Em/Ex). All other imaging was carried out using a Nikon A1R point scanning confocal microscope at 37^{o}C / 5% CO_2. Appropriate lasers were used for each dye (488nm, 561nm and 647nm for MitoTracker Green/FITC, TMRM/TAMRA and ATTO 647N respectively).

3.3.5. **Statistical analysis**

Volocity software (Perkin Elmer, USA) was used for quantitative analysis of captured images. Microsoft excel was used to collate data and Prism (GraphPad, USA) was used to generate graphs. Prior to statistical analysis, all data set were subjected to a normality test using Minitab 16 statistical software (Minitab Inc.).

3.4. RESULTS

3.4.1. CMCO targeting molecules

To drive accumulation of the CMCOs into mitochondria, several targeting molecules were selected to conjugate to the CMCOs. Previous work has shown that conjugation of TPP (triphenylphosphonium) with large molecules, such as vitamin E, can be used to force them to accumulate in mitochondria. TPP is a lipophilic cation that has the ability to cross the plasma membrane (Ross et al. 2008). However, once it enters the cytoplasm the positively charged TPP (figure 3.2) goes on to specifically accumulate in mitochondria in a membrane-potential dependent manner (Finichiu et al. 2013). This is unusual as charged molecules are generally too hydrophilic to cross plasma membranes, and would therefore not be able to enter the cell, preventing mitochondrial accumulation. TPP crosses membranes due to the delocalised positive charge generated by the phosphonium ion being distributed across the three phenyl groups. This maintains the lipophilic properties of the molecule while also enabling the positively charged ion to force accumulation down the charge gradient maintained across the inner mitochondrial membrane. These features make TPP an attractive option for use in driving the accumulation of CMCOs into mitochondria.

2, 4-dinitrophenol (DN) (figure 3.2) has been shown to increase proton leak of the inner mitochondrial membrane, dissipating the membrane potential and lowering the efficiency of oxidative phosphorylation (Weinbach and Garbus 1965). It has been postulated that it could act as an anti-obesity treatment by increasing the oxidation of fatty acids to produce ATP *in lieu* of oxidative phosphorylation (Blaikie et al. 2006), however it is too toxic to be used for this purpose as it has a very narrow therapeutic window. Although it cannot be used to treat obesity, it does target mitochondria and can cross plasma membranes. Therefore it was decided to test the ability of DN to target CMCOs to mitochondria. It was hoped that binding DN to the CMCO would disrupt its ability to act as an uncoupling protonophore (reducing its toxicity), while maintaining its ability to accumulate in mitochondria.

Due to the expense of manufacturing conjugated CMCOs, it was decided to investigate the effects of TPP and DN on mitochondrial localisation prior to testing other compounds. A CMCO conjugated to a phenyl group via a lysine molecule (Pac-K) was

also manufactured as a negative control to confirm that an uncharged phenyl group does not have the ability to cause mitochondrial accumulation. The phenyl moiety was not expected to cause mitochondrial accumulation as it lacks a positive charge and is unable to become deprotonated; therefore it acted as a negative control in these experiments. The structure of Pac-K is shown in figure 3.2.

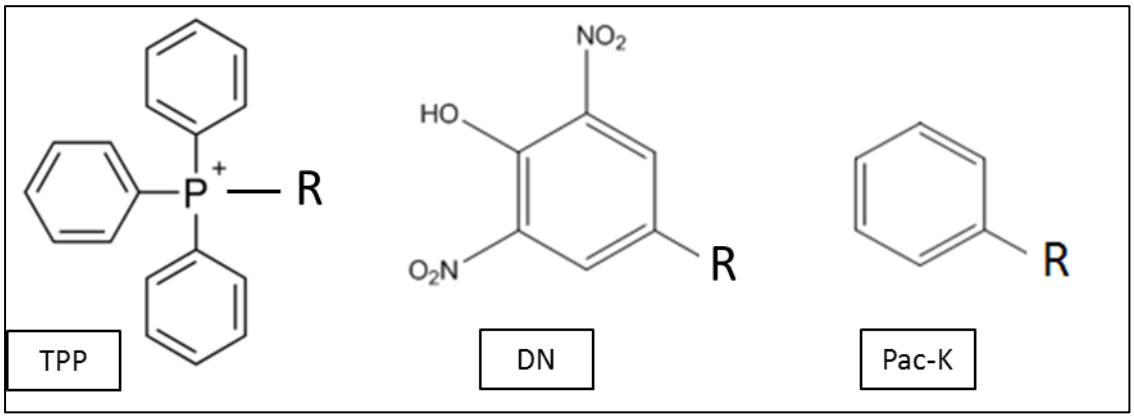

Figure 3.2 - The chemical structures of triphenylphosphonium (TPP), 2,4 dinitrophenol (DN) and phenyl (Pac-K).
The R denotes the CMCO attached via a lysine molecule

3.4.2. **Biotinylated CMCOs**

Three 16mer CMCOs were designed, each with a different targeting molecule (table 3.1). CMCOs were conjugated to the targeting molecule via a lysine residue at their N terminal. Apart from the difference in targeting molecule, all CMCOs were identical with a sequence complementary to *MTCO1* (np.5979-5994) consisting of 6 phosphonic ester containing Ugimers at nucleobase: 2, 4, 6, 12, 14 & 16. Previously it was indicated that this CMCO could accumulate in mitochondria where it went on to have an anti-genomic effect (Kyriakouli 2007). This was in comparison to several other CMCOs that targeted different regions of *MTCO1* and had different backbone structures (ratio and location of PNA:Ugimers), none of which showed an anti-genomic effect on mtDNA or led to a depletion of COXI protein.

Table 3.1 - List of sequences and targeting molecules used for biotinylated CMCOs.

Targeting molecule	Detection molecule	Sequence
2, 4 dinitrophenol	Biotin	DN-K-(Bio)-TGCCTAGGACTCCAGC
Tri-phenyl phosphonium	Biotin	TPP-K-(Bio)-TGCCTAGGACTCCAGC
Phenyl	Biotin	Pac-K-(Bio)-TGCCTAGGACTCCAGC

Red letters in the sequence information highlights Ugimer position, Black letters represent PNA monomers.

Biotin was chosen as the detection molecule for the CMCOs as it is relatively inert, uncharged and is therefore unlikely to interfere with mitochondrial targeting of the CMCO, it is also easy to detect using fluorescent conjugates of streptavidin. However, during the purification of the CMCOs there is a risk that biotin may degrade and will therefore not be detected after incubation with cells. Although there is a risk that biotin may not survive, it was still used, as conjugation of other detection molecules such as fluorescent compounds may interfere with the subcellular localisation of the CMCO. This is because many fluorophores contain charged regions which may either prevent the CMCO from crossing cell membranes due to a change in lipophilicity, or cause accumulation in another cellular compartment.

3.4.2.1. *Detection and quantification of biotin conjugated CMCO import*

The uptake of CMCOs into HeLa cells was investigated to deduce whether the targeting molecules preserved their ability to cross cell membranes, and which targeting molecule showed the best mitochondrial localisation. To determine if the CMCOs had entered the cells, changes in biotin levels were measured using streptavidin conjugated to the fluorophore; Alexa Fluor 488, in addition nuclei were stained with DAPI (section 3.3.3). If the CMCO had accumulated in the cell, it would be expected that there would be an increase in the amount of fluorescence detected; due to increased binding of streptavidin Alexa Fluor 488 (strep 488), when compared to basal fluorescence levels (due to endogenous biotin) in no dose control samples. To carry out this experiment, three repeat doses of each of the three CMCOs were performed, along with three repeats of a no dose control. The CMCOs were incubated with HeLa cells according to the

methods described in section 3.3.2 at a concentration of 10µM for 48 hours (Kyriakouli 2007). Cells were fixed and stained using the methods outlined in section 3.3.3 and imaged at 20x magnification using an inverted Zeiss Axiovert 200M microscope. Four images were taken per dose (12 in total) using filter sets appropriate for the excitation and emission spectra of DAPI and Alexa Fluor 488. Analysis of fluorescence intensity was performed using Volocity image analysis software (Perkin Elmer, USA). Median pixel intensity was used as a measure of the amount of fluorescence emitted from strep 488 for the entire image. As each image was captured using the same exposure times, changes in pixel intensity directly reflect the amount of strep 488 and therefore the amount of biotin in the sample. The median intensity values for each of the CMCOs were grouped according to targeting molecule and compared to the no dose control using a Mann-Whitney U test. It was found that there was no significant difference in the amount of biotin for any CMCO when compared to the no dose control (figure 3.3).

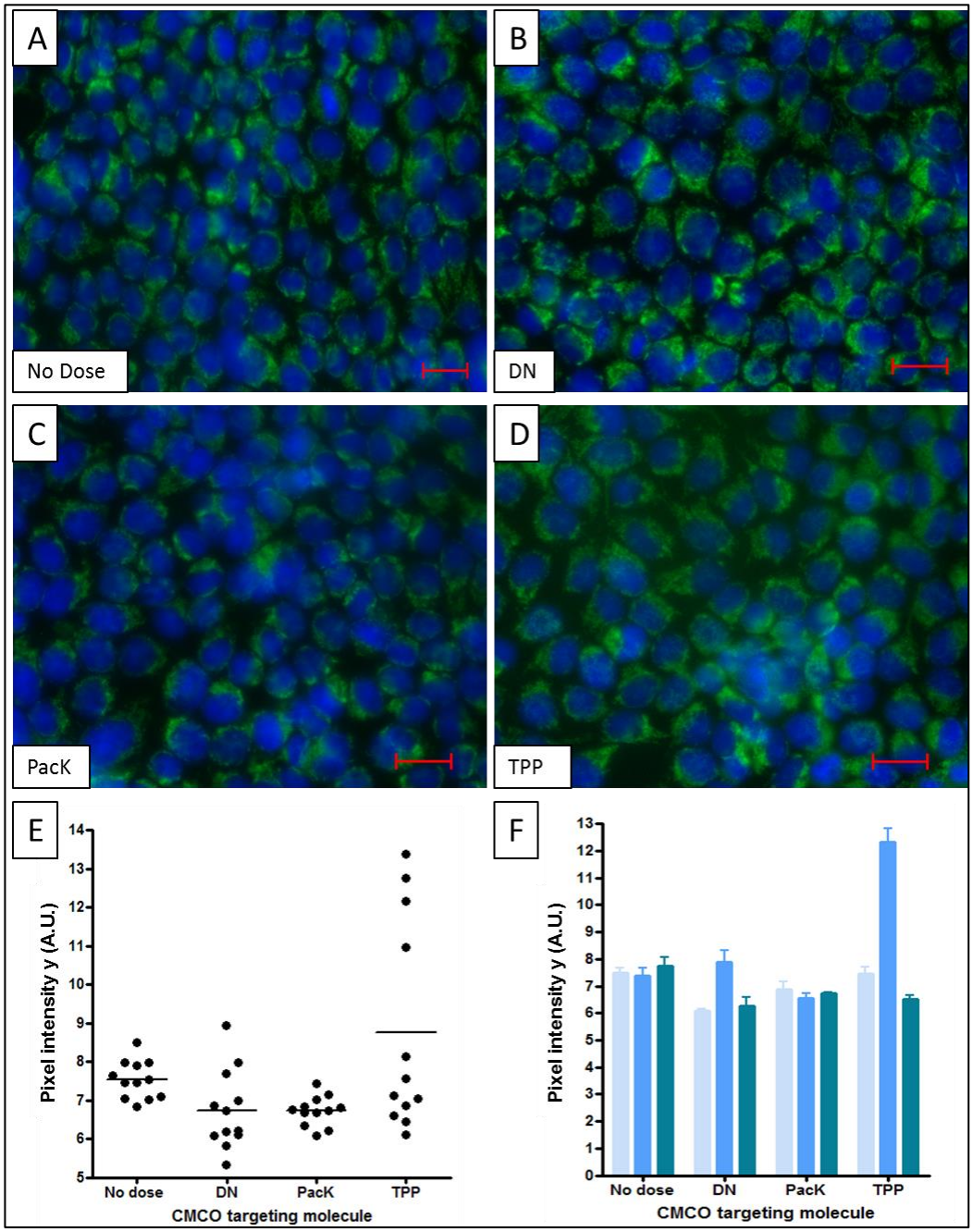

Figure 3.3 - Quantification of biotin using streptavidin conjugated Alexa Fluor 488 after HeLa cells were incubated with 10µM CMCO.
Three repeat cultures per dose were produced and 4 images captured per repeat. Panels A, B, C & D show sample images of cells that have been incubated with the relevant CMCO. **A** shows endogenous biotin levels in no dose control cells. **B, C and D** show biotin in cells incubated with DN, Pac-K and TPP conjugated CMCOs respectively. Panel **E** shows median pixel intensity for each captured image group according to CMCO (12 images per CMCO). Panel **F** shows median pixel intensities for each repeat dose (4 images per repeat). Nuclei are stained with DAPI (blue). Scale is 20µm.

3.4.2.2. *Analysis of biotinylated CMCO targeting*

Panels A-D (figure 3.3) show representative images of HeLa cells stained with streptavidin Alexa Fluor 488 either as a no dose control or after incubation with a CMCO. Analysis of median pixel intensity of the images was performed blinded to ensure that there was no bias of the results. There was no increase in the level of strep 488 in CMCO treated cells when compared to no dose controls. This was confirmed using a Mann-Whitney U test for non-parametric data, which failed to find a significant change in the sample.

The TPP conjugated CMCO showed the largest variation in median intensities. The reason for this variation is shown in panel F of figure 3.3 which shows that one repeat dose had a higher intensity than the other wells. Although this was a significant increase when compared to any of the no dose control repeats ($p=0.0044$ Mann-Whitney U test) it is unlikely to have been caused by increased levels of biotin. This is because when the outlying data is grouped with the other TPP CMCO repeats it is no longer significant, nor is there any reason for this dose to show higher levels of biotin as all repeats were dosed using the same source of CMCO which was prepared in the same way for all repeats. Therefore it is likely that the higher levels of biotin indicated by this repeat are due to experimental error rather than because of the CMCO.

Although the evidence suggests that there is no increase in biotin levels in CMCO treated cells relative to no dose controls, it does not necessarily mean that there was no import of the CMCOs. Several factors could lead to the biotinylated CMCOs not being detected, as discussed below.

Biotin degradation

As mentioned previously, there was a high probability that biotin may have degraded, either during the manufacturing process or during purification of the CMCOs. If biotin was no longer intact then it is unlikely that streptavidin would bind the CMCOs and therefore no increase in signal above endogenous levels would be detected.

Low levels of CMCO import may not be detected

There is a relatively high level of biotin endogenously expressed by cells, in particular within the mitochondria, where it acts as a cofactor in enzymatic reactions (Tong 2013). If the amount of biotin on the CMCOs is low due to degradation or because the ratio of biotin to CMCO is less than 1:1, it is possible that the extra signal caused by the CMCO biotin is not detected above endogenous levels.

CMCOs may not be retained in cells after fixation

Cells were fixed in 70% ethanol prior to staining with streptavidin; however it may be that the CMCOs are too small to be fixed sufficiently. This is a possibility as their small molecular mass may prevent them from being held in place when the cell is fixed. This could lead to a situation where the CMCOs may "leak" out of the cell membrane upon subsequent washes, lowering the amount of signal detected when stained. PFA fixation may not improve this as it covalently crosslinks proteins (Shi et al. 2001), and as the CMCOs only contain one lysine residue, it is unlikely that this method will fix them.

These factors, although possibly controllable, make biotin an unattractive option for use as a detection molecule and as a result of this experiment, it was decided to re-design the CMCOs and use a different targeting molecule.

3.4.3. **Fluorescently labelled CMCOs**

Due to the potential issues with fixation, it was decided to use a detection molecule that does not require additional labelling in order to measure its abundance and can therefore be detected in live cells. Fluorescent molecules are the best choice for this application as they emit light without the need for antibody or streptavidin based detection. They are also relatively bright when compared to background cellular auto-fluorescence which means that it should be easy to detect the presence of a molecule if it is within the cell. This will solve the issues experienced when trying to detect small increases in the level of biotin; however, several factors need to be considered when choosing a fluorophore, all of which are discussed below.

3.4.3.1. *Cellular autofluorescence*

It is important to choose a fluorescent molecule that emits light in a region of the spectrum distinct from the majority of cellular autofluorescence. This occurs primarily in the shorter wavelength regions of the spectrum (blue light) and gets progressively less common as wavelength increases (figure 3.4). NADH and FADH (two molecules that are abundant in the mitochondria) have been shown to auto-fluoresce in the blue and green region of the spectrum respectively (Andersson et al. 1998; Rodrigues et al. 2011). Green and red fluorescence is also emitted by lipofuscin, lipid containing residues of lysosomal degradation (Schnell et al. 1999).

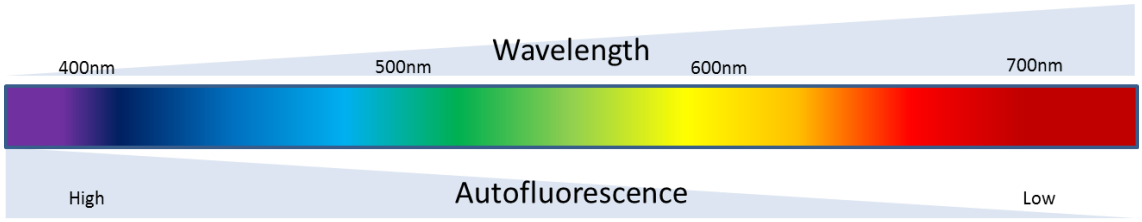

Figure 3.4 - A schematic showing the relationship between wavelength and cellular autofluorescence.
The frequency of compounds which auto-fluoresce at a given wavelength decreases as wavelength increases, causing less cellular autofluorescence.

Although most fluorophores are used at sufficient concentration to be detected above the background of cellular autofluorescence, if the conjugated CMCO shows poor accumulation within cells then it may be necessary to increase the exposure time in order to detect emitted light, thus increasing the likelihood of false positives caused by detection of autofluorescence. To minimise the likelihood of this occurring it was decided to use a fluorophore that emits light at a wavelength that is distinct from the auto-fluorescent regions of the spectrum, therefore a red or far red light emitting fluorophore was most appropriate.

3.4.3.2. *Uptake of the fluorophore into live cells and subcellular localisation*

As the fluorophore will be conjugated to CMCOs, it is important that the ability to accumulate in live cells is not compromised by the addition of the fluorophore. Furthermore it is vital that the fluorophore does not alter the ability of the CMCOs to

localise to mitochondria. The ideal fluorophore for this application therefore is a mitochondrial localising dye.

Mitochondrial dyes are a group of fluorophores that specifically stain mitochondria in live cells, generally as a function of the mitochondrial membrane potential. A list of potential dyes is shown in table 3.2.

Table 3.2 - Characteristics of commonly used live cell mitochondrial dyes.

Dye	Excitation nm	Emission nm	Optimum concentration	Fixation	Proprietary	Toxicity
MitoTracker Green	488	510	50-200nM	N/A	Y	Low
MitoTracker Orange	551	574	50-200nM	N/A	Y	Low
Mitotracker Red	577	599	100-400nM	PFA	Y	Low
Mitotracker Deep Red	643	661	100-400nM	N/A	Y	Low
TAMRA	550	576	25-100nM	N/A	N	Low
TMRM	552	578	5-20nM	N/A	N	Low
Rhodamine 123	506	527	50µM	N/A	N	High

Optimal concentrations were those given by the manufacturer or referred to in the literature (Scaduto and Grotyohann 1999). Proprietary dyes are still under patent protection and not available for use conjugation with other molecules. Toxicity is defined as the likelihood that respiration is inhibited by the dye when used at the optimal concentration.

Proprietary fluorophores were not used as they are not produced in forms that enable efficient conjugation to the CMCOs. As a result of this, none of the MitoTracker dyes were used in this assay, despite them having low toxicity and, in the case of MitoTracker Red, the ability to be fixed within mitochondria. Of the three remaining dyes, Rhodamine 123 was not selected as it emits light in the green region of the spectrum, which may overlap with cellular autofluorescence and is highly toxic. TMRM and TAMRA are derivatives of rhodamine which both show membrane potential dependent mitochondrial localisation at low concentrations. While both dyes were suitable for marking the CMCOs, it was decided to use TAMRA as it is routinely conjugated to DNA oligonucleotides for use in quantitative PCR (Heid et al. 1996). TAMRA is freely available with chemical modifications which enable the labelling of the CMCOs without disrupting its fluorescent properties.

3.4.4. **Visualisation of mitochondrially targeted CMCOs using TAMRA**

TAMRA conjugated CMCOs were manufactured with the same sequence and Ugimer:PNA ratio as described in section 3.4.1, a list of which is shown in table 3.3. Each CMCO was conjugated to TAMRA and its relevant targeting molecule in a 1:1 ratio.

Table 3.3 - List of sequences and targeting molecules used for TAMRA conjugated CMCOs.

Targeting molecule	Detection molecule	Sequence
Triphenylphosphonium	TAMRA	TPP-K-(TAMRA)-TGCCTAGGACTCCAGC
Mononitrophenol	TAMRA	MN-K-(TAMRA)-TGCCTAGGACTCCAGC
Phenyl	TAMRA	Pac-K-(TAMRA)-TGCCTAGGACTCCAGC
Acetyl	TAMRA	AC-K-(TAMRA)-TGCCTAGGACTCCAGC

Red letters in sequence information highlights Ugimers, Black letters represent PNA monomers.

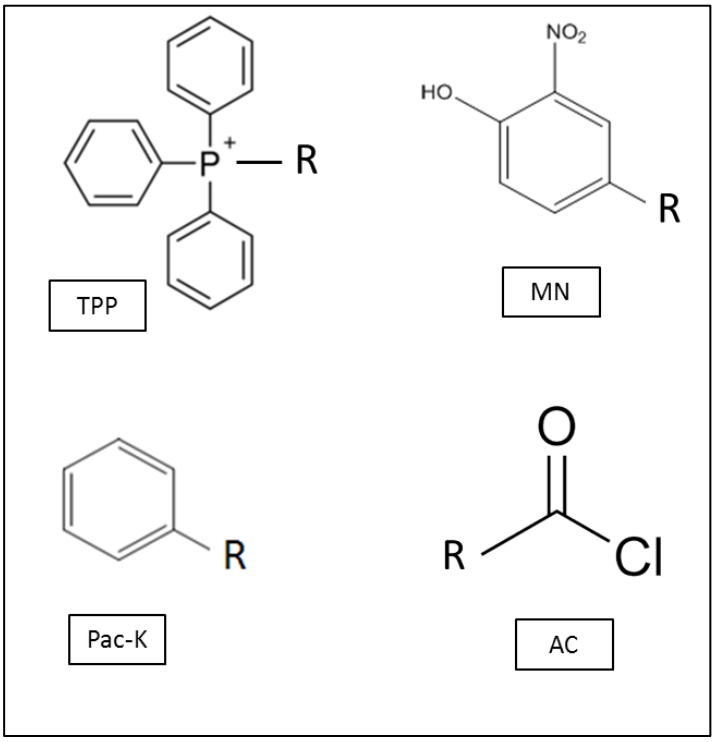

Figure 3.5 - The chemical structures of targeting molecules. Triphenylphosphonium (TPP), mononitrophenol (MN), phenyl (Pac-K) and acetyl (AC).R denotes the CMCO conjugated via a lysine molecule.

After consultation with Ugichem, it was decided to replace the targeting molecule DN with mononitrophenol (MN) due to the expense of manufacturing DN conjugated CMCOs. The ability of MN to target mitochondria is unclear; however it was decided to investigate it *in lieu* of DN. An acetyl (AC) conjugated CMCO was produced in order to test the ability of TAMRA to drive accumulation into mitochondria in the absence of a specific targeting molecule. The structures of the targeting molecules to be used in TAMRA CMCOs are shown in figure 3.5.

HeLa cells were incubated with 10µM TAMRA CMCOs for 24 hours prior to imaging according to section 3.3.2. Prior to imaging, cells were incubated with 50nM MitoTracker green for 30 minutes and subsequently washed three times in PBS before the addition of Phenol Red free complete HeLa media. Phenol red was omitted as it auto-fluoresces in the green and red regions of the spectrum. Images were captured using a Nikon A1R point scanning confocal microscope (Nikon, Japan) using the excitation and emission settings shown in table 3.2. All images were captured at 37^{o}C in a humidified atmosphere of 5% CO_2. Subcellular localisation of TAMRA-CMCOs in relation to MitoTracker Green is shown in figure 3.6.

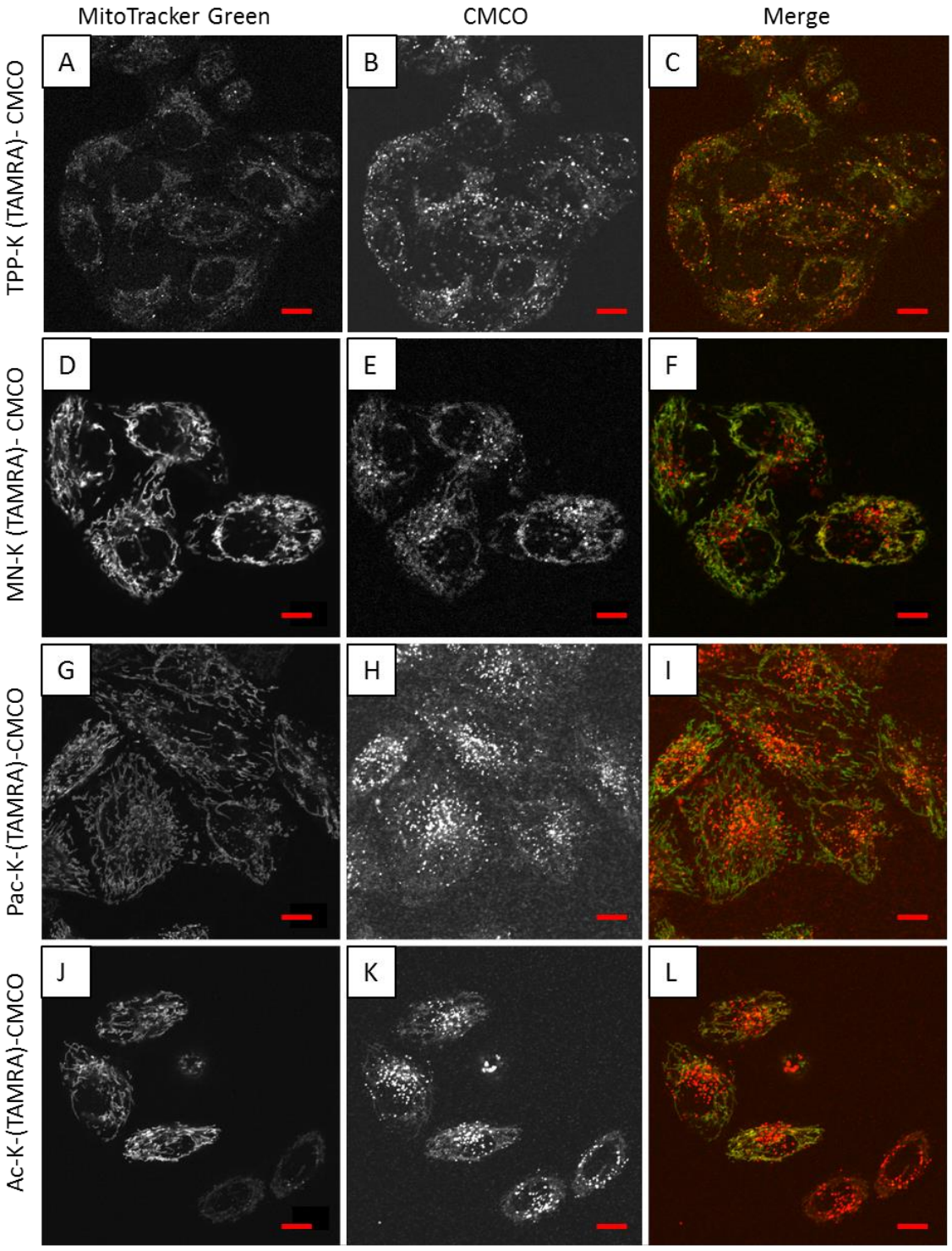

Figure 3.6 - Subcellular localisation of TAMRA conjugated CMCOs in relation to mitochondria stained with 50nM Mitotracker Green.
HeLa cells were incubated with 10µM CMCO for 24 hours prior to staining with 50nM MitoTracker Green and imaged using a point scanning confocal microscope. The left hand column shows MitoTracker Green staining; the centre column shows signal obtained from TAMRA-CMCOs and the right hand column shows the merged imaged of CMCO (red) and Mitotracker Green (green) staining – colocalisation shows up as yellow regions. Cells in panels **A-C** were incubated with triphenylphosphonium targeted CMCOs, **D-F** mononitrophenol targeted CMCOs, **G-I** were incubated with phenyl targeted CMCOs and **J-L** were incubated with acetyl targeted CMCOs. Scale bar represents 10µm.

Volocity software was used to generate a Pearson's correlation coefficient in order to quantify the degree of colocalisation of MitoTracker Green and the CMCOs. Using the method described by Costes and colleagues, regions which showed staining for both dyes (MitoTracker and TAMRA) were classed as colocalised. The proportion of these regions in relation to non-colocalised regions was then calculated – a coefficient ranging from one to zero was determined by Pearson's correlation analysis (one represents perfect colocalisation, zero represents no colocalisation).

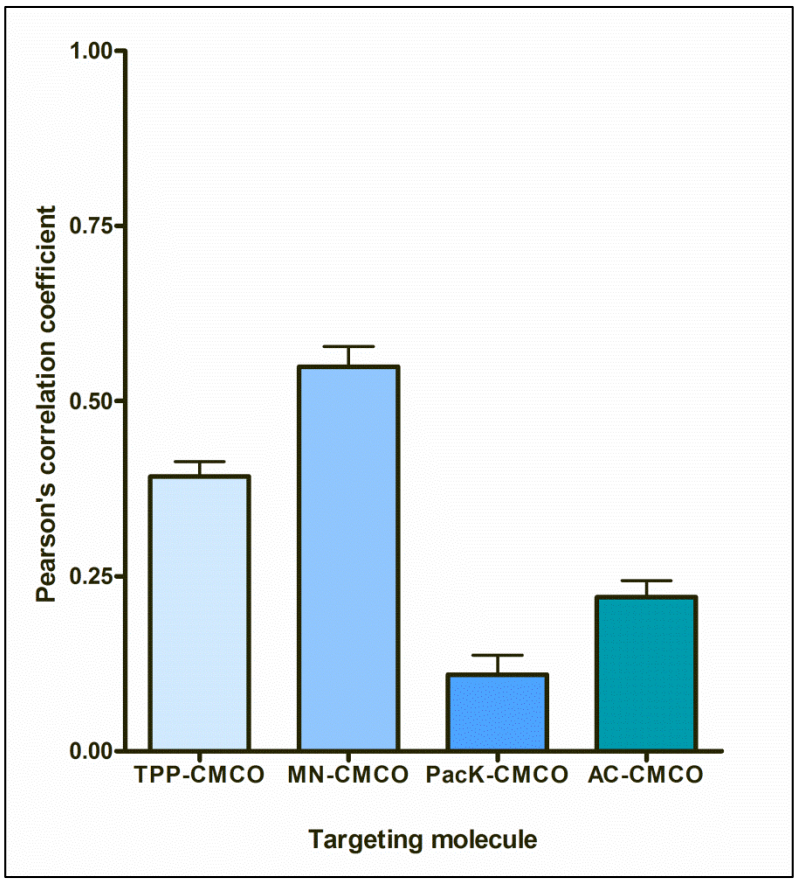

Figure 3.7 - Colocalisation coefficients of TAMRA conjugated CMCOs with MitoTracker Green.
Error bars represent standard deviation of analysed cells (n=40).

Figure 3.7 shows that the best colocalisation with mitochondria was achieved when using MN as a targeting molecule. Although TPP is regularly used to target small molecules to mitochondria, for this application the colocalisation achieved was lower than when using MN. This may have been due to the increased formation of CMCO aggregates which are visible as areas of puncta (dense white dots) seen in panel B figure 3.6, possibly leading to the sequestration of the CMCO and preventing access to

mitochondria. As expected, the use of uncharged Pac-K did not lead to mitochondrial localisation, but led to severe aggregation of the CMCO (panel H, figure 3.6). The TAMRA-AC-CMCO did show some mitochondrial localisation, however this was much lower than the TPP or MN conjugated molecules. This shows that TAMRA may have had the ability to drive accumulation of the CMCOs into mitochondria (due to its ability to localise to mitochondria in its unconjugated form), the fact that there is an increase in colocalisation when using MN or TPP compared to the non-targeting AC CMCO, indicates that the targeting molecules are essential for the CMCOs to localise to mitochondria.

3.4.4.1. *FITC conjugated CMCOs*

To understand the relationship between the fluorescent molecule and CMCO targeting, TAMRA was replaced with FITC (fluorescein isothiocyanate). This was to ascertain whether MN (the targeting molecule with the greatest mitochondrial accumulation) had the ability to drive mitochondrial localisation in the absence of TAMRA. The FITC CMCO was incubated with HeLa cells for 24 hours and imaged as described previously. As FITC emits green light (495/519nm Ex/Em), the use of MitoTracker Green to highlight mitochondria was not possible, therefore 100nM MitoTracker Deep Red (644/665nm Ex/Em) was used. To ensure mitochondrial autofluorescence was not mistaken for FITC fluorescence, a no dose control was imaged to determine the maximum possible laser power that could be used without detecting autofluorescence. These laser settings were used to image the FITC CMCO incubated cells (figure 3.8).

Figure 3.8 shows that very little fluorescence was detected from the FITC CMCO when compared to MitoTracker Deep Red. This could be due to the fluorescent properties of FITC being compromised by conjugation to the CMCO (which could inhibit the fluorescent excitation of the molecule), leading potentially to lower detected fluorescence. It could also be due to FITC decreasing the ability of the CMCO to accumulate within the cell. In order to establish the localisation of the FITC CMCO, it was necessary to increase the laser power of the microscope to increase excitation of the fluorophore. However, this was not possible as mitochondrial autofluorescence (caused by FADH) prevents the detection of the fluorescence emitted by FITC. It was therefore

decided to replace FITC with a fluorophore that has a higher quantum yield (brightness) which will enable accurate detection at lower concentrations.

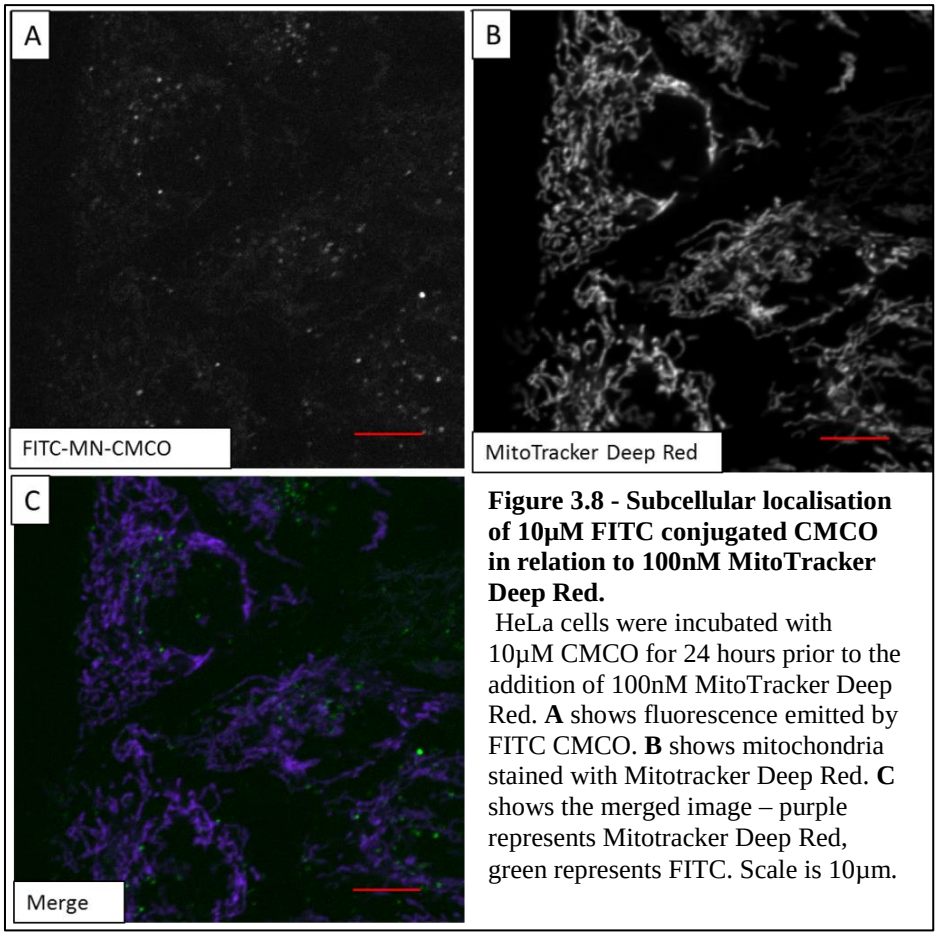

Figure 3.8 - Subcellular localisation of 10µM FITC conjugated CMCO in relation to 100nM MitoTracker Deep Red.
HeLa cells were incubated with 10µM CMCO for 24 hours prior to the addition of 100nM MitoTracker Deep Red. **A** shows fluorescence emitted by FITC CMCO. **B** shows mitochondria stained with Mitotracker Deep Red. **C** shows the merged image – purple represents Mitotracker Deep Red, green represents FITC. Scale is 10µm.

3.4.5. **ATTO 647N conjugated CMCOs**

To address the issues experienced with the FITC-MN-CMCOs, ATTO 647N (ATTO-TEC GmbH, Siegen) was used as a detection molecule as it has a high quantum yield, emits light in the far red region of the spectrum (644nm/669nm Ex/Em) and is available in forms conducive to CMCO conjugation. The use of ATTO Tec dyes was recommended by Ugichem. It was decided to manufacture ATTO conjugated CMCOs with TPP, MN or acetyl targeting groups in order to assess their targeting abilities in the absence of TAMRA (table 3.4). Pac-K was not chosen as a targeting molecule due to the poor localisation seen in figure 3.6. HeLa cells were incubated with the relevant CMCO for 24 hours prior to incubation with 50nM MitoTracker Green and imaged. Colocalisation was calculated as described previously. Captured images and colocalisation graphs are shown in figure 3.9 and figure 3.10 respectively.

Table 3.4 - List of sequences and targeting molecules used for ATTO 647N conjugated CMCOs.

Targeting molecule	Detection molecule	Sequence
Triphenylphosphonium	ATTO 647N	TPP-K-(ATTO)-TGCCTAGGACTCCAGC
Mononitrophenol	ATTO 647N	MN-K-(ATTO)-TGCCTAGGACTCCAGC
Acetyl	ATTO 647N	AC-K-(ATTO)-TGCCTAGGACTCCAGC

Red letters in the sequence information highlights Ugimers, Black letters represent PNA monomers.

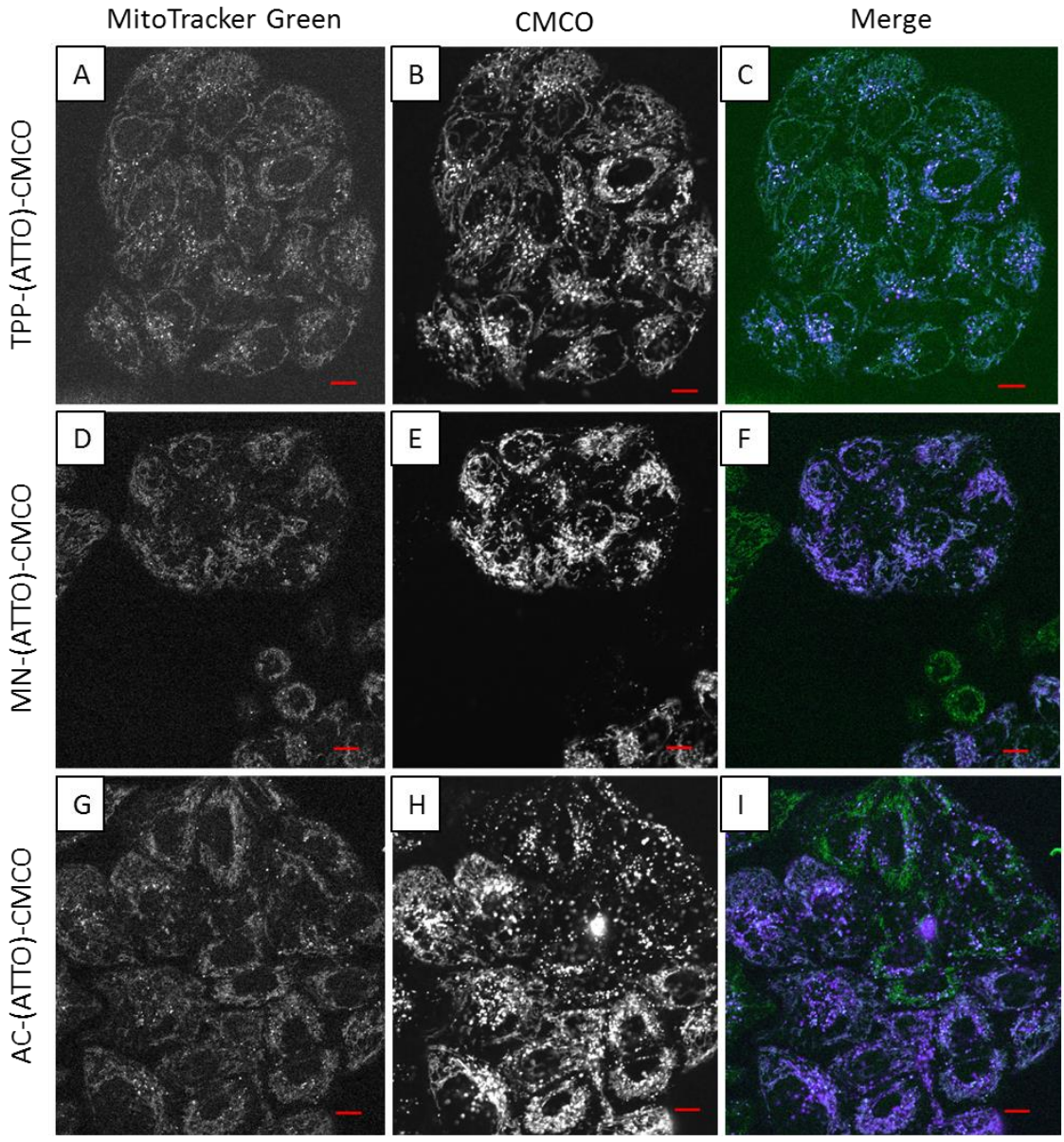

Figure 3.9 - Subcellular localisation of ATTO 647N conjugated CMCOs in relation to mitochondria stained with 50nM Mitotracker Green.
HeLa cells were incubated with 10µM CMCO for 24 hours prior to staining with 50nM MitoTracker green and imaged using a point scanning confocal microscope. The left hand column shows MitoTracker green staining; the centre column shows signal obtained from ATTO-CMCOs and the right hand column shows the merged imaged of CMCO (purple) and Mitotracker green (green) staining. Colocalisation is shown by regions of blue/light purple. Cells in panels **A-C** were incubated with triphenylphosphonium targeted CMCOs, **D-F** mononitrophenol targeted CMCOs, **G-I** were incubated with acetyl targeted CMCOs. Scale bar represents 10µm

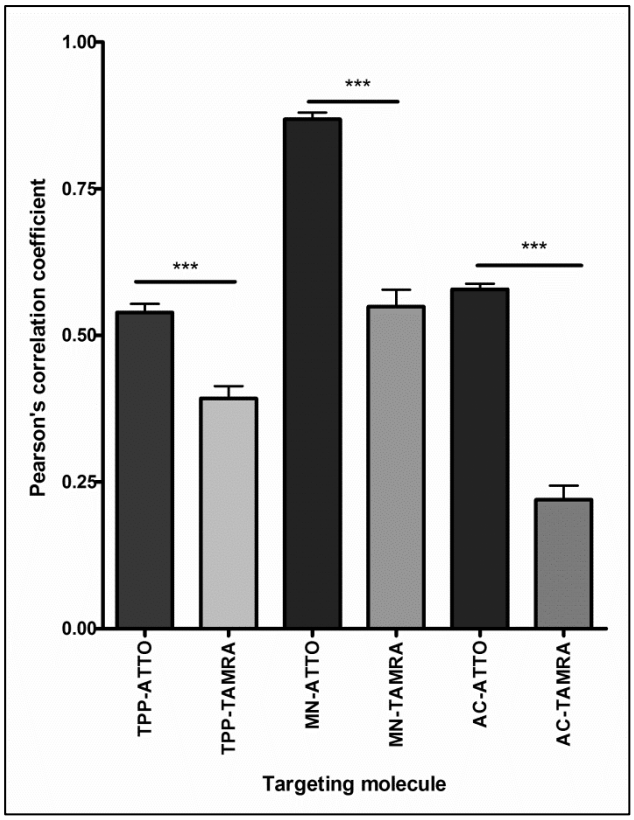

Figure 3.10 - Colocalisation coefficients of ATTO 647N conjugated CMCOs and TAMRA conjugated CMCOs with MitoTracker Green.
Error bars represent standard deviation, n=40. A Mann-Whitney U test was used to test significance, ***=p<0.0001

To determine if the ability of the CMCOs to colocalise with mitochondria was altered by the use of different detection dyes, colocalisation coefficients for both ATTO and TAMRA conjugated CMCOs were calculated by analysing 40 individual cells (figure 3.10). The graph shows that the level of colocalisation with mitochondria is significantly higher ($p<0.0001$, Mann-Whitney U test) in all ATTO 647N CMCOs when compared to TAMRA CMCOs. As with TAMRA conjugated CMCOs, the greatest colocalisation was seen when MN was used as a targeting molecule (median coefficient of 0.8645). The fact that the non-targeted AC-CMCO shows an increase in colocalisation suggests that the ATTO dye may have the ability to drive mitochondrial localisation in the absence of a targeting molecule and therefore free ATTO 647N may stain mitochondria in live cells.

3.4.5.1. *Un-conjugated ATTO 647N as a mitochondrial dye*

To investigate the ability of ATTO 647N to be used as a mitochondrial stain, 10µM of the dye was incubated with HeLa cells for 24 hours. Prior to imaging, mitochondria were labelled with 5nM TMRM, a live cell mitochondrial stain. Cells were imaged using a Nikon A1R confocal microscope and the colocalisation coefficient calculated as described previously. A sample image is shown in figure 3.11.

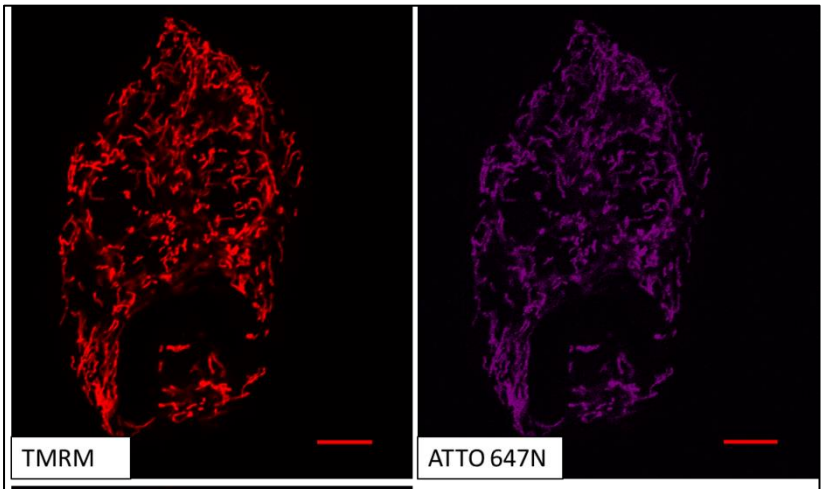

Figure 3.11 - Colocalisation of ATTO 647N dye with the specific mitochondrial stain TMRM.
HeLa cells were incubated with 10µM ATTO 647N (purple) for 24 hours before staining with 5nM TMRM (red). Images were captured using a Nikon A1R confocal microscope. Colocalisation is shown by regions of pink staining on the merged image. Scale bar represents 10µm.

The colocalisation coefficient for the ATTO 647N and TMRM had a median value of 0.8915, indicating almost perfect colocalisation between the two dyes. This finding highlights the fact that ATTO 647N has a tendency to strongly localise to mitochondria in live cells. Although the structure of the dye has not been published, the manufacturers state that it is a cationic molecule, which may enable it to specifically target mitochondria due to the relative negative charge of the organelle.

To determine if ATTO 647N accumulates in mitochondria as a function of the membrane potential, the effect of FCCP on mitochondrial localisation was investigated. FCCP is an ionophore, which transports hydrogen ions from the intermembrane space to the matrix, destroying the proton gradient and uncoupling respiration (Benz and McLaughlin 1983). Therefore, upon addition of FCCP, the mitochondrial membrane potential will dissipate and any molecules that depend on the potential to accumulate in mitochondrial will diffuse into the cytosol.

HeLa cells stained with 10µM ATTO 647N were imaged over a period of 14 seconds, after which 10µM FCCP was added and the cells imaged for a further 14 seconds (figure 3.12).

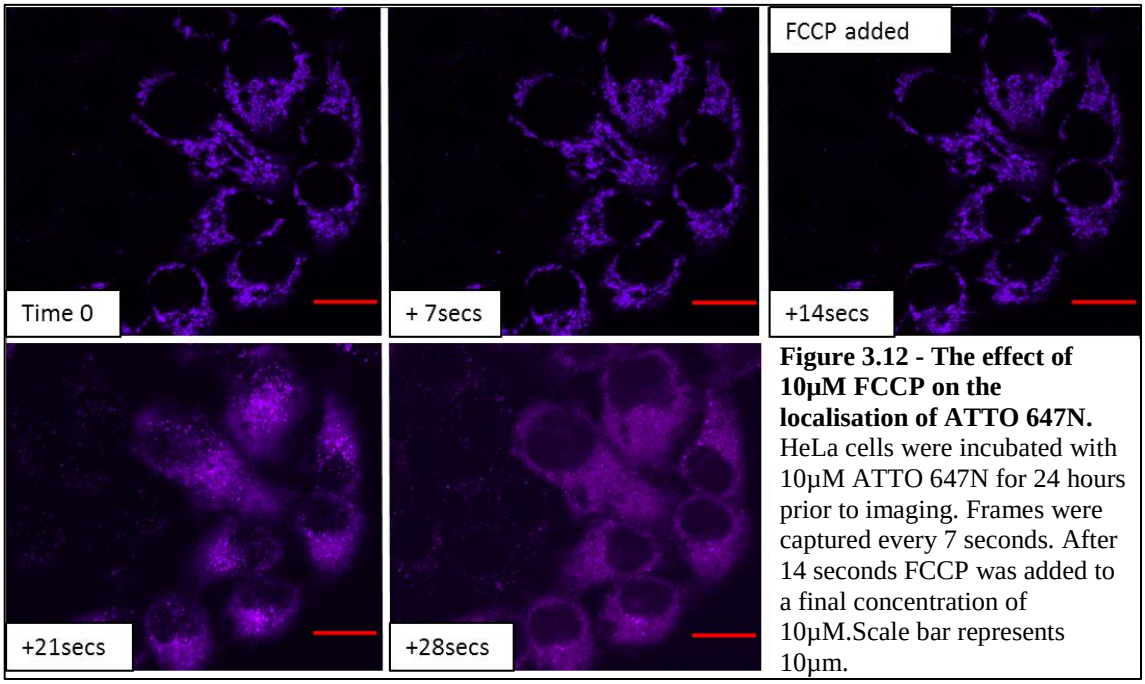

Figure 3.12 - The effect of 10µM FCCP on the localisation of ATTO 647N. HeLa cells were incubated with 10µM ATTO 647N for 24 hours prior to imaging. Frames were captured every 7 seconds. After 14 seconds FCCP was added to a final concentration of 10µM.Scale bar represents 10µm.

The effect of FCCP addition is clearly visible as the pattern of ATTO 647N staining changes from a reticular form associated with mitochondrial staining to a more diffuse cytoplasmic pattern. This indicates that ATTO 647N localises to the mitochondria as a function of the membrane potential, and highlights its potential use as a mitochondrial stain.

3.4.6. **mtDNA staining by ATTO 647N-MN-CMCOs**

In order for CMCO's to have an anti-genomic effect on mtDNA, it is essential that they have access to the mitochondrial matrix. The results presented so far suggest that ATTO conjugated CMCOs are localising to mitochondria, however their location within mitochondrial is unclear. One way to see if the CMCOs have accessed the matrix is to see if they localise with mtDNA in live cells. A 1 in 1000 dilution of Picogreen (Invitrogen, Paisley UK), a fluorescent DNA intercalator which can accumulate in mitochondria as well as the nucleus, was used to stain mtDNA in fibroblasts incubated for 24 hours with ATTO 647N-MN-CMCO. Fibroblasts were chosen due to their flat morphology which leads to mitochondria having a planar distribution, in contrast to HeLa cells which are more ovoid in structure and therefore the mitochondria overlap in 3D space, thus making it harder to accurately image mtDNA.

Although it is possible to stain mtDNA, the fact that the ATTO CMCOs localise to the entire mitochondrial network means that it is impossible to detect specific localisation to mtDNA, due to the high levels of background network staining. It was decided to add 10µM FCCP to the cells in order to equilibrate free CMCO between the network and cytosol (as it is likely to localise in a membrane potential dependent manner), thus any CMCO bound to mtDNA will remain and be expressed as regions colocalised with Picogreen staining. Prior to addition of FCCP, cells were also stained with 5nM TMRM to indicate when the membrane potential has dissipated. Images of one cell were captured every second for one minute, with FCCP added 21 seconds after the first frame was captured. Figure 3.13 shows sample images of the cell before FCCP addition and then 2 and 30 seconds post addition. A region of interest is highlighted by the white boxes; this will be investigated further in (figure 3.15).

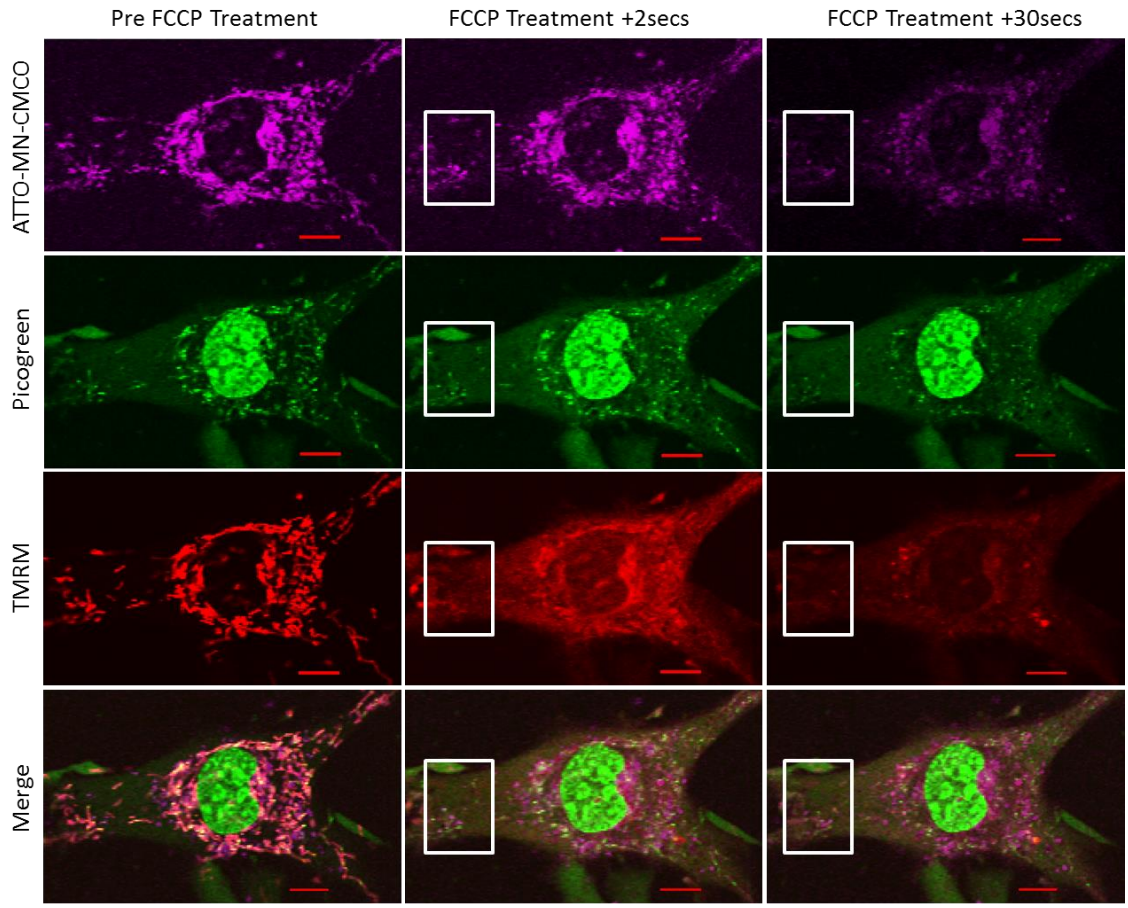

Figure 3.13 - The effect of 10μM FCCP on a fibroblast cell stained with 10μM ATTO-MN-CMCO, 1 in 1000 Picogreen (Invitrogen, UK) and 5nM TMRM.
Images show the localisation of individual dyes along with a merged image of all the dyes combined. Individual columns show the staining of the cell before the addition of FCCP, 2 seconds after the addition and 30 seconds after addition. White boxes highlight a region that will be investigated further in figure 3.15. Scale bar represents 10μm.

The staining of TMRM and ATTO-MN-CMCO shows excellent colocalisation – as highlighted by the pink regions in the merged image – before the addition of FCCP. However, after FCCP is added the TMRM staining becomes more diffuse as the dye leaves the mitochondria and equilibrates with the cytosol (2 seconds post addition), this continues until a uniform distribution of the dye is seen 28 seconds later. Interestingly the same pattern of diffusion is not shown by the CMCO, which is contrary to what was seen with both TMRM and free ATTO 647N dye (figure 3.12). 30 seconds after FCCP addition there is still some CMCO localised to mitochondria, although the proportion of mitochondrial localised CMCO and the overall intensity of the signal has decreased due to cytosolic diffusion. The time taken for it to diffuse back into the cytosol highlights

the possibility that the ATTO-MN-CMCO may not be accumulating as a function of the membrane potential and that the MN could be driving accumulation by another means. This trend is quantified in figure 3.14, which shows the effect of FCCP addition on the intensity of TMRM and ATTO fluorescence. The sharp decline seen in the intensity of TMRM staining upon FCCP addition is due to the dye entering the cytosol and becoming less concentrated, thus decreasing in intensity. Although a decrease in the intensity of ATTO fluorescence is also seen, this is far less steep than the decline in TMRM intensity.

Throughout the time course, picogreen staining has not decreased in response to FCCP addition, which will enable the analysis of the region of interest, highlighted by the white boxes shown in figure 3.13.

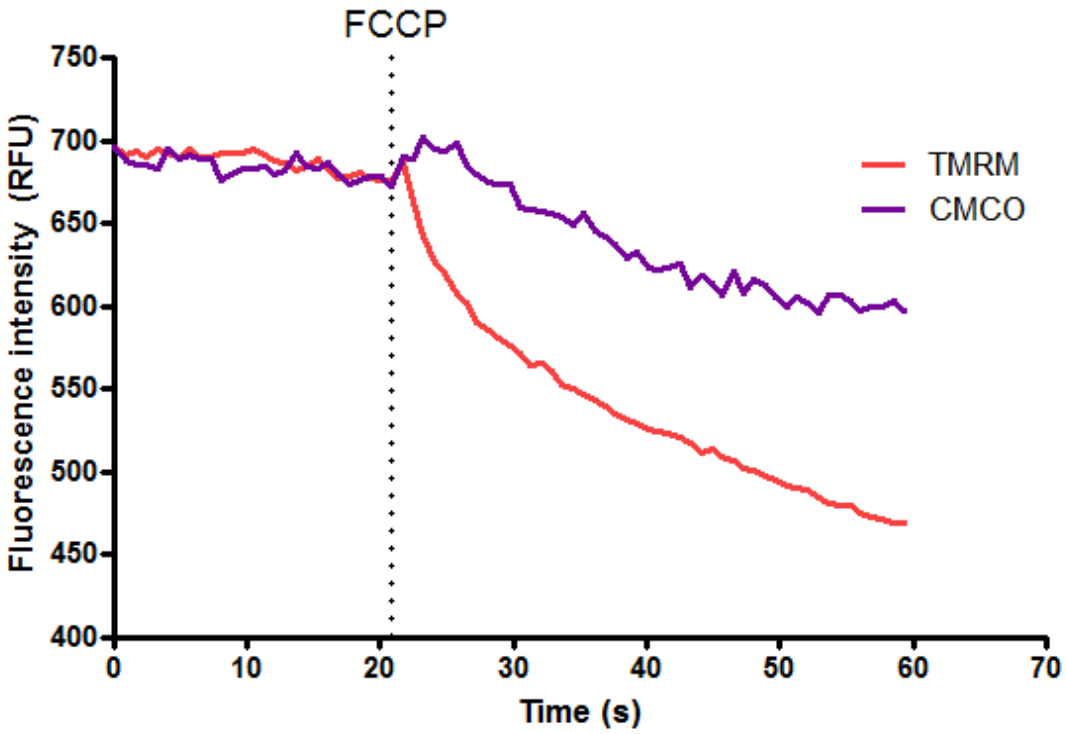

Figure 3.14 - Relative fluorescence intensity of 5nM TMRM and 10µM ATTO-MN-CMCO in fibroblast cells.
Intensity of the dye over a 60 second period was calculated using Volocity software and normalised. The addition of 10µM FCCP is shown by the dotted line.

The region of interest shown in figure 3.13 was investigated further to determine if there was colocalisation of the remaining ATTO-MN-CMCO with mtDNA stained with

picogreen. The area was monitored 40 seconds after FCCP exposure to increase the chance that unbound ATTO-MN-CMCO had dispersed into the cytoplasm. Although some reticular CMCO remained, there was a danger that imaging would either cause bleaching or photo-toxicity, therefore mtDNA binding assessment 40 seconds after FCCP addition was chosen as a compromise.

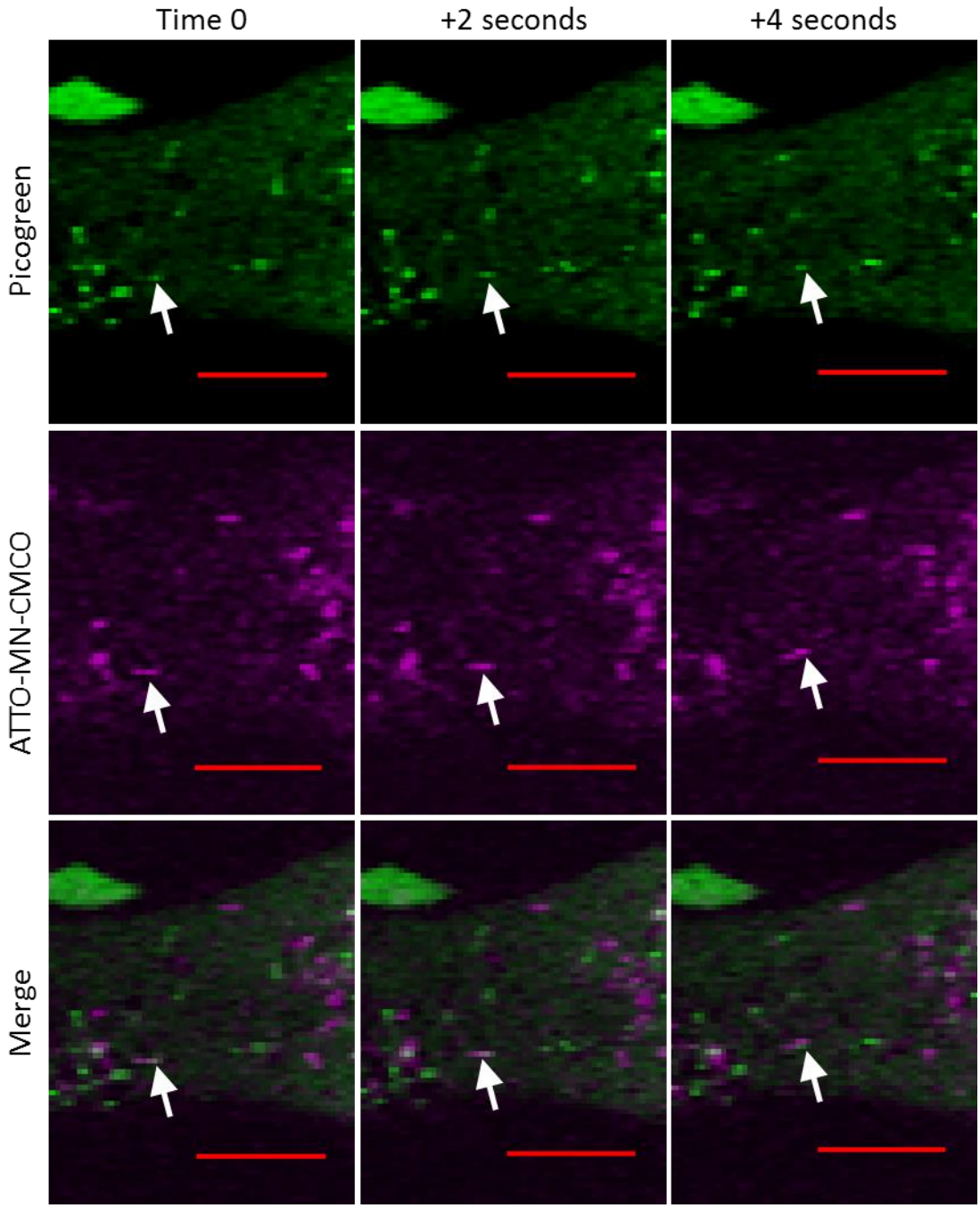

Figure 3.15 - Time lapse images of colocalised mtDNA and ATTO 647N-MN-CMCO.
Images were taken 40 seconds after FCCP exposure (figure 3.13) for 4 seconds. Individual rows show picogreen mtDNA staining, ATTO 647N-MN-CMCO, and the merge of the two stains. The arrow highlights the mtDNA nucleoid of interest. Scale bar represents 10μm.

Still images of the magnified region of interest were captured over a period of 20 seconds, a sample of these images, in which colocalisation of picogreen and ATTO647N-MN-CMCO is shown, are displayed in figure 3.15. The arrows highlight mtDNA stained with picogreen (probably in a nucleoid complex) and the corresponding region of ATTO 647N signal which colocalised. Although there are other regions of intense ATTO 647N staining on the images, these are not colocalised with picogreen and can therefore not be classed as definitely mitochondrially localised (they may be areas of aggregated CMCO). The fact that there is colocalised signal of the CMCO with picogreen could suggest that these particular molecules of mtDNA have bound CMCO and therefore prevented its diffusion from mitochondria after FCCP addition. If the CMCO has not bound mtDNA and the colocalisation is coincidental i.e. this particular region of the network has retained the CMCO and also contains mtDNA, it is still interesting as it shows CMCO retention in the mitochondrial network even after depolarisation. This provides more evidence that the CMCO does not accumulate in a membrane potential dependent manner, a potential mechanism for accumulation will be discussed in the next section. Although these results provide some evidence of CMCO binding mtDNA, at the image resolutions shown it is impossible to tell if the CMCO has accumulated in the matrix and has access to mtDNA.

3.5. DISCUSSION

3.5.1. Mitochondrial targeting of CMCOs

This work shows that CMCOs have the ability to cross the cell membrane and, with the addition of a targeting molecule, they can also specifically localise to mitochondria. The addition of fluorescent molecules (which have a inate ability to accumulate in mitochondria) enables the visualisation of CMCOs in live cells without preventing mitochondrial targeting. I have shown that the use of different targeting molecules affects the degree of mitochondrial localisation and shown that CMCOs conjugated to MN have the greatest ability to localise to mitochondria.

As the detection dyes had the ability to localise to mitochondria it was sensible to assume that the dyes may also play a role in driving the CMCO accumulation into mitochondria. This was shown to be the case as ATTO 647N conjugated CMCOs showed a much more efficient mitochondrial localisation than TAMRA conjugates. This was surprising as it had not yet been reported that free ATTO 647N localises to mitochondria in live cells. It is likely that ATTO 647N accumulates in mitochondria as a function of the membrane potential, as shown by the change in localisation of the dye after 10µM FCCP addition.

The use of targeting molecules to drive the accumulation of anti-sense therapies into mitochondria is only possible when used in conjunction with oligomers that have the ability to diffuse across plasma membranes, such as CMCOs. Although previous work had demonstrated that CMCOs could be localised to mitochondria using targeting molecules (Kyriakouli 2007) attempts to repeat this using biotinylated CMCOs failed. Therefore the use of mitochondrial dyes to aid detection and possibly localisation led to progress in understanding the differential abilities of the targeting molecules to cause localisation with the following higher order now established:

MN>TPP>AC>Pac-K

In order to create an anti-sense therapy for mtDNA disease, accumulation in the matrix to access mtDNA has to be assured. Although this work has not proven matrix localisation, I have shown that ATTO 647N-MN-CMCOs are retained and some may

colocalise with mtDNA after the dissipation of membrane potential, and while it is impossible to determine the sub-mitochondrial localisation of the CMCOs using currently available microscopy techniques, the fact that some localisation was observed provides circumstantial evidence that this CMCO can access the matrix.

The gold standard to assess the ability of the CMCOs to enter the matrix is to show that they have a functional effect on replication or translation. However, in the absence of activity it is important to show that the CMCOs are accessing the matrix (in order to understand an absence of functional effects), this will be discussed further in chapter 7.

3.5.2. **Mitochondrial accumulation of MN**

In this work CMCOs were targeted to mitochondria using MN, which was chosen as a replacement for dinitrophenol, due to the cost associated with using 2,4 DN as a targeting molecule. However, although there were no reports suggesting that MN could accumulate in mitochondria, this work has shown that there is an increased localisation to mitochondria when using MN in conjunction with either TAMRA or ATTO 647N detection systems, indicating that MN does have the ability to specifically accumulate within mitochondria.

Unlike TPP, whose mitochondrial accumulation is well studied, MN does not contain a caged positive charge so it is unlikely that it will accumulate in mitochondria as a function of membrane potential. The fact that MN is a weak acid with a pKa (dissociation constant) of 7.23 in water may explain its mitochondrial accumulation (Schwarzenbach et al. 1988). This means that it has the ability to lose a hydrogen ion under certain conditions, which changes its ability to cross cell membranes as the molecule becomes ionised and less lipophilic.

When in solutions around pH 7.4, the vast majority of MN is in a lipophilic, non-ionic form. As this is the approximately the same pH as the cytosol, MN is therefore free to cross plasma membranes including the mitochondrial membrane. However, under more alkaline conditions, such as in the matrix which has a pH of 7.8, the proportion of MN

molecules which have lost a H^+ increases. These deprotonated forms of MN can no longer cross plasma membranes and become partitioned in the matrix (figure 3.16).

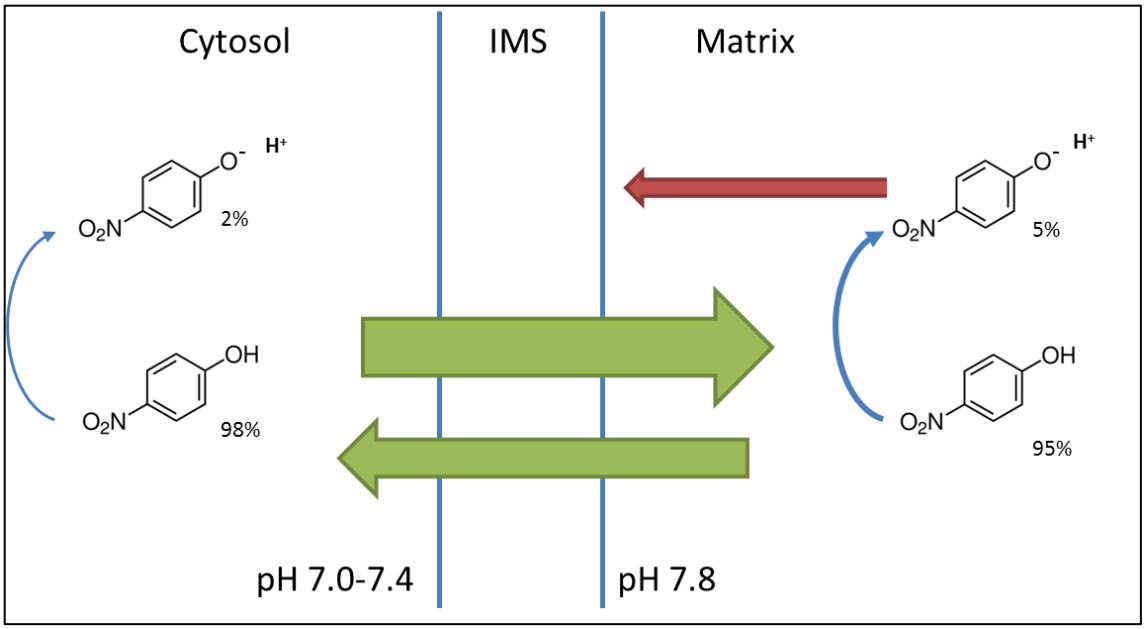

Figure 3.16 - Schematic showing the proposed mechanism of MN accumulation into the matrix. Under cytosolic pH, the majority of MN can cross the mitochondrial membranes freely (green arrows). Once in the more alkaline conditions of the matrix the proportion of deprotonated MN increases due to its weakly acidic properties. This deprotonated form cannot cross the mitochondrial membranes (red arrow) and is therefore sequestered in the matrix.

Upon addition of FCCP the inner mitochondrial membrane becomes permeable to H^+ ions, which have been transported into the intermembrane space to create an electrochemical gradient to drive ATP synthesis. The influx of H^+ ions into the matrix will lower its pH until it decreases to pH 7.4 in equilibrium with the cytosol. This is turn will cause the proportion of deprotonated MN to decrease, therefore increasing the proportion of MN that can diffuse across the mitochondrial membranes and re-enter the cytosol. However, there will still be a small amount of MN that is deprotonated and will still be retained in the matrix, which may explain why mitochondrial localisation or ATTO 647N-MN-CMCO was maintained (apart from mtDNA binding) even immediately after FCCP addition.

3.6. CONCLUSIONS

The use of fluorescent mitochondrial probes in conjunction with targeting molecules enabled real-time assessment of localisation of CMCOs within cells. Unfortunately, current live cell microscopy techniques do not offer the resolutions required to accurately assess the sub-mitochondrial localisation. Although super resolution microscopy techniques are offering insights into the fine structure of mitochondria, these currently require the cells of interest to be fixed and imaged in an oxygen scavenging environment, something that is not appropriate when using CMCOs. These techniques can also only be used in conjunction with fluorophores that can "blink" - a process by which the emitted fluorescence of the fluorophore can be repeatedly turned off and on again. This enables the location of the centre point of the fluorescent molecules to be pinpointed, offering resolutions as low as 10nm (Rust et al. 2006; Huang et al. 2008; Bates et al. 2013).

Although this work has shown mitochondrial localisation of CMCOs, the only way to prove that they have access to mtDNA or mt-mRNA is to show that there is a functional effect on either replication or translation, leading to decreased production of COXI protein. This will be discussed in the following chapter.

Chapter Four

Functional analysis of mitochondrially localised *MTCO1* complementary CMCOs

4.1. INTRODUCTION

The previous chapter described the development of targeted CMCOs and their localisation to mitochondria. Although mitochondrial targeting was achieved, sub-mitochondrial localisation was impossible to determine using imaging techniques. It was therefore decided to investigate the anti-genomic effects of the MN-CMCOs (with or without fluorescent moieties) on mtDNA copy number and COXI expression.

In order for the CMCOs to have an effect in man they must enter the cytoplasm and then specifically target and accumulate within the mitochondrial matrix before binding to mutated regions of mtDNA or mt-mRNA (figure 4.1). In order to prove the concept of CMCO anti-genomic therapies, CMCOs were designed to be complementary to wild type *MTCO1* (np.5979-5994). This enabled the use of healthy cells with wild-type mtDNA, preventing the potential difficulties associated with using heteroplasmic mutant cell lines such as mutation loss over time. In work done previously, this sequence showed the greatest efficacy at causing an apparent decline in mtDNA copy number and COXI protein expression (Kyriakouli 2007).

Previous *in vitro* work has shown that CMCO binding to mtDNA stalls replication by preventing the progress of Polγ (Kyriakouli 2007). Stalling of replication *in vivo* is likely to lead to the degradation of affected genomes, which in turn will lower copy number (Goffart et al. 2009) and as a result of this the steady state levels of all encoded proteins will decrease. If the CMCO hybridises mt-mRNA, translation is likely to be affected as the CMCO will prevent tRNA binding or ribosomal progression and therefore decrease the steady state levels of COXI without affecting mtDNA copy number. The outcomes of CMCO binding are summarised in figure 4.1.

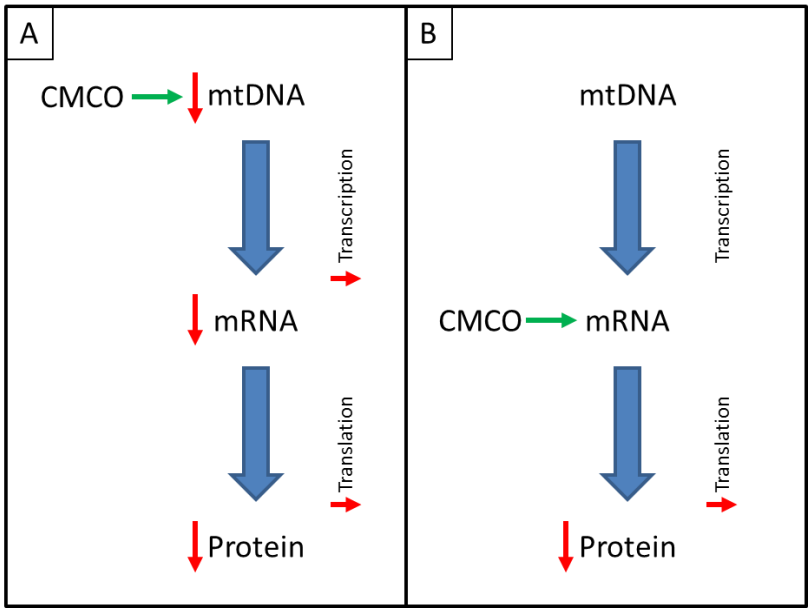

Figure 4.1- Schematic showing the downstream effects of CMCO binding to either mtDNA or mt-mRNA.
Binding of the CMCO to mtDNA (panel A) will decrease mtDNA copy number, and therefore protein expression. CMCO binding to mitochondrial mRNA (panel B) will not affect mtDNA expression, but will decrease COX1 protein expression.

This chapter focuses on the functional assessment of CMCOs targeted to mitochondria using mononitrophenol (MN) either on its own or in conjunction with a fluorophore. Any differences in the functional effect of the CMCOs will provide an insight into the most efficient method of targeting the matrix. It was also decided to test CMCOs with base substitutions to investigate their ability to bind mtDNA *in vivo*. This will primarily act as a control for CMCOs homologous to *MTCO1*; however it may also provide an insight into the ability of the CMCOs to specifically bind only one species of mtDNA and indicate the appropriateness of their use in targeting mtDNA with point mutations.

The work carried out in this chapter was severely limited by the amount of CMCO available for experiments. Ideally several repeat doses should be carried out on large numbers of cells in order to provide enough material to analyse in a statistically robust manner. This was not possible due to financial and time constraints experienced by Ugichem during production of the CMCOs used in this chapter. This was unfortunate as the functional effect of the CMCOs could not be fully elucidated or validated. The results presented in this chapter indicate the preliminary investigations and highlight problems in cell and assay variability, as well as an inability to repeat key experiments.

4.2. AIMS

In order to expand the optimisation of mitochondrially targeted CMCOs, I investigated the effect of these molecules on mtDNA and protein:

I. To investigate the effect of targeted CMCOs on COXI steady state levels and mtDNA copy number in HeLa cells.
II. To determine which targeting and detection molecule combination has the greatest functional effect.

4.3. METHODS

4.3.1. CMCO dosing

All CMCOs were prepared for incubation as described previously in section 2.6.1 and diluted to an appropriate concentration. HeLa cells were seeded in 24 well plates (1 x 10^4 cells/well) in complete media and allowed to grow overnight. Prior to CMCO addition, media was removed and the cells washed three times in PBS before the addition of FBS free HeLa media. A CMCO was added to each well to a final concentration of 10μM (calculated using the method described in section 2.6.1) and the cells placed back in the incubator in standard conditions. After 2 hours incubation, 10% FBS (v/v) was replaced and the cells placed back in the incubator (a 2 hour period was chosen as uptake experiments have shown that CMCOs accumulate within cells after 2 hours) (Kyriakouli 2007). Cells were allowed to grow until 90% confluent (roughly 4 days) after which they were passaged and seeded in fresh plates at the same density as previously (1 x 10^4 cells/well). Cells were allowed to settle and adhere to the plate for 6 hours, before media removal and CMCO addition in FBS free media as described above. 10% FBS (v/v) was added to the media after 2 hours and the cells placed back in the incubator. This process was repeated for the duration of the experiment.

4.3.2. Cell harvesting and lysate preparation

At the experiment endpoint, HeLa cells were harvested as described in section 2.2.1. Cells were placed in a universal tube and centrifuged at 160*g* for 4 minutes. The supernatant was aspirated and the pellet re-suspended in 1ml PBS, after which 500μl

was placed in a fresh universal. Both aliquots were centrifuged at 160*g* for 4 minutes. Whole cell protein lysate was prepared from one aliquot using the methods described in section 2.4.1. The concentration of the lysate was determined using the Bradford assay and diluted to an appropriate concentration of 0.5µg/µl in 10mM Tris-HCl, after which lysates were flash frozen in liquid nitrogen and stored at -80^{o}C. DNA was extracted from the second aliquot using the method described in section 2.5.1. After extraction, the concentration of DNA was determined using a Nanodrop ND1000 and the DNA preparation aliquoted in appropriate volumes and stored at -20^{o}C.

4.3.3. **Quantification of Western blots**

After signal detection by ECL Prime (GE Healthcare) and imaging, signal strength was analysed using ImageJ software. The intensity of signal for each band was calculated by using ImageJ to represent each band in graph form. This enable the measurement of area under the curve for each band, intense signal was represented by taller, wider peaks and therefore larger area under the curves. The ratio between the area under the curve for control proteins and test proteins was then calculated.

4.3.4. **Statistical analysis**

Microsoft excel was used to collate data and Prism (GraphPad, USA) was used to generate graphs. Prior to statistical analysis, all data set were subjected to a normality test using Minitab 16 statistical software (Minitab Inc.).

4.4. RESULTS

The following section will focus on each class of CMCO (fluorescent and non-fluorescent) and their functional effects separately.

4.4.1. HeLa sequencing

Prior to analysis of the CMCOs functional effects, it was decided to ensure that the region of *MTCO1* the CMCOs were designed to bind (np.5979-5994) did not contain mutations, as these could affect CMCO hybridisation. Therefore *MTCO1* in the HeLa cell line to be used for the functional analysis experiments was sequenced using the methods described in section 2.5.3. Total DNA was extracted from HeLa cells when they had reached 60% confluency in a T25cm^2 flask. A 200bp product that contained the CMCO binding region was amplified by PCR and sequenced using an ABI genetic analyser. SeqScape software was used to align the sequence to the revised Cambridge reference sequence (Andrews et al. 1999) and it was found that the HeLa cell line did not contain any mutations in this region (figure 4.2). Therefore this cell line could be used in the functional analysis experiments.

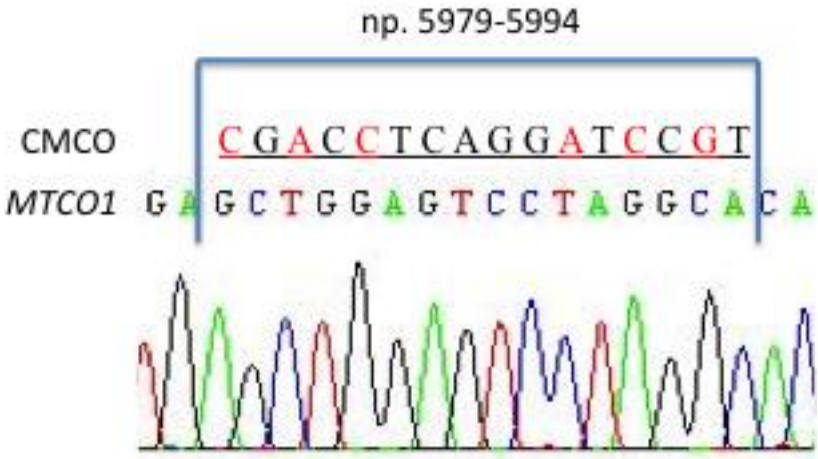

Figure 4.2 - Sequence of mtDNA (np.5979-5994).
HeLa cell mtDNA was sequenced and an electropherogram spanning the CMCO binding region was analysed for point mutations. The complementary CMCO sequence is also shown; red letters denote the position of phosphonic ester side chains.

4.4.2. **Non-fluorescently conjugated CMCOs**

In collaboration with Ugichem, several CMCOs were designed that used MN as a targeting molecule, two CMCOs that had acetyl groups in lieu of a targeting molecule were also produced (to act as a non-targeted control). A similar fluorescent molecule was not conjugated in order to ascertain whether MN alone had the ability to drive accumulation of the CMCO into the mitochondrial matrix. This was necessary as the experiments in the previous chapter showed that MN increased targeting, however it was not possible to determine if MN can target CMCOs to mitochondria in the absence of a mitochondrial dye, as the localisation experiments relied on the presence of a fluorescent moiety. If MN alone can cause accumulation, which is sufficient to have a functional effect, it is very encouraging from a financial point of view as conjugation to fluorescent molecules (particularly ATTO 647N) is very expensive.

Targeted CMCOs with different sequence homologies to np. 5979-5994 of mtDNA were designed in order to investigate specificity of binding. In order for CMCOs to treat mtDNA disease caused by point mutations the CMCOs must show differential binding to wild type and mutated mtDNA. Therefore the investigation of CMCOs with base mismatches to wild type mtDNA will indicate if they selectively bind only mtDNA to which they are 100% complementary. The various CMCOs and their sequence homologies are shown in table 4.1.

Table 4.1 - Non-fluorescently conjugated CMCOs and their sequence homology to np.5979-5994 mtDNA.

CMCO	Targeting molecule	Homology to MTCO1
Ugi 105	Mononitrophenol (MN)-Lys	Homologous
Ugi 110	Acetyl -Lys	Homologous
Ugi 192	Acetyl	Homologous
Ugi 193	MN-Lys	1bp nt.10C>G
Ugi 194	MN-Lys	2bp nt.9A>C, nt.10C>A
Ugi 195	MN-Lys	3bp nt.3C>G, nt.10C>G, nt.15G>C
Ugi 196	MN-Lys	Nonsense
Ugi 198	MN-Lys	Homologous (different backbone)

4.4.2.1. *Effect of CMCOs on mtDNA copy number*

CMCO binding of mtDNA has been shown previously to inhibit the action of polγ *in vitro* (Kyriakouli 2007), and if this occurs *in vivo* it is likely to cause a decrease in mtDNA copy number as the cells divide and cannot increase mtDNA, causing a relative fall in copy number per cell due to relaxed mtDNA replication. To determine relative copy number changes caused by CMCOs, it was decided to use quantitative PCR (qPCR) to ascertain the ratio of mtDNA to a nuclear marker gene.

As the ability of MN-CMCOs to accumulate in mitochondria is not clear, it was decided to incubate HeLa cells with 10μM CMCO for 30 days after which DNA and protein lysates were produced and analysed. Previous work indicated that this was long enough for any effect on copy number or COXI protein to be detected. mtDNA copy number was analysed by comparing the relative levels of the mitochondrial complex 1 gene *MTND1* to nuclear gene *B2M* (β2-microglobulin). The quantity of each gene was determined by comparing the Ct value to a standard curve produced from extracted HeLa DNA and diluted over a 6-log range. This is the most accurate way of determining copy number as the use of a standard curve on each reaction plate prevents variation in the *MTND1* and *B2M* reactions from being interpreted as changes in copy number. To ensure there was no bias, the dosing was blinded.

Due to the amount of CMCO available it was not possible to perform repeat doses, however if any CMCOs showed an effect these would be repeated at a later date with a new synthesis. The relative copy number of the CMCO treated HeLa cells was normalised to the average no dose control copy number (five no dose controls were set up in parallel to the CMCO incubation in a 24 well plate). This enabled relative copy number changes to be investigated, while also providing insight into the natural variation of mtDNA copy number within HeLa cells.

Figure 4.3 - Effect of CMCOs with various homologies to *MTCO1* on mtDNA copy number.
10µM of each CMCO was incubated with HeLa cells for 30 days prior to mtDNA copy number analysis by qPCR. Copy number of CMCO treated cells was normalised to the average copy number of 5 no dose controls (C1-5). The graph shows the relative copy number for each dosing regimen. Red bars denoted MN targeted CMCOs, Blue bars denote Ac-CMCOs. The black bar shows the average no dose control copy number and white bars show individual wells no dose controls. Cross-hatchings denote non-homologous CMCOs. Error bars show standard deviations of triplicate real-time PCR repeats.

CMCO	Targeting molecule	Homology to MTCO1	Normalised relative copy number
Ugi 105	Mononitrophenol (MN)-Lys	Homologous	0.9589
Ugi 110	Acetyl -Lys	Homologous	1.023
Ugi 192	Acetyl	Homologous	0.6933
Ugi 193	MN-Lys	1bp nt.10C>G	0.5137
Ugi 194	MN-Lys	2bp nt.9A>C, nt.10C>A	1.493
Ugi 195	MN-Lys	3bp nt.3C>G, nt.10C>G, nt.15G>C	0.7927
Ugi 196	MN-Lys	Nonsense	0.5729
Ugi 198	MN-Lys	Homologous (different backbone)	0.9581

Figure 4.3 shows that there is variation in the copy number of control cell lines, both within the repeat real-time PCR measurements (the average standard deviation for all controls between real-time PCR runs was 0.17) and when compared to each other (standard deviation of 0.22). This high standard deviation indicates that there is an inherent margin of error when using real-time PCR. It also indicates that there is a large natural variation in the copy number of HeLa cells, even in the absence of CMCO treatment. Therefore repeat doses of CMCO treatment are necessary in order to compensate for this variation and to be certain of any CMCO effect on mtDNA copy number.

Figure 4.3 indicates that the best performing CMCO was a MN conjugated molecule with a C>G substitution (Ugi 193) which decreased copy number by ~50%, whereas the homologous CMCO (Ugi 105) had no real effect on copy number. However, although this could suggest that the non-homologous CMCO has a greater ability to interrupt mtDNA replication, the fact that the two CMCOs that caused a similar decrease in copy number (Ugi 192 and Ugi 196) are a non-targeted and nonsense CMCO respectively suggests that the effect on copy number may be due to random variation rather than an effect of the CMCOs. It could also indicate a non-specific interaction with mtDNA causing depletion. Work in this lab has shown that real time PCR may vary by up to 20% for copy number analysis, which could also contribute to the variation seen in these results (Dr. Julie Murphy, unpublished data). If the effect of these CMCOs is real, then it is likely that in cases where there is a fall in copy number, there will be a corresponding fall in COXI levels.

4.4.2.2. *COXI expression*

After incubation with 10μM CMCO for 30 days, cytolplasmic cell protein was extracted from treated HeLa cells, along with protein from 5 no dose control cell lines. The level of COXI in relation to non-mtDNA encoded SDHA was determined by western blotting. Changes in COXI could be due to either a fall in mtDNA copy number, or a fall in the translation of mt-mRNA, which could be caused by CMCO binding of mtDNA or mt- mRNA. It is possible that a CMCO could cause a fall in COXI by binding mt-mRNA without affecting mtDNA copy number.

Figure 4.4 shows western blotting data for HeLa cells treated with the CMCOs or no dose controls. Western blots were performed using 5μg cytoplasmic cell lysate (this was limited by the number of cells available for protein extraction) and were probed using the antibody concentrations described in section 2.4. The quality of the western blots makes it difficult to infer what effect, if any, these CMCOs are having on the levels of COXI protein. This was due to the need to expose the blot for a long time in order to obtain signal from COXI, which caused overexposure of the SDHA signal, this was not suitable to easy analysis.

As with the copy number data, there was a large variation in the levels of COXI in the control cell lines. The levels of COXI do not reflect the copy number of mtDNA as C1, which had the lowest copy number of all controls actually has the highest level of COXI protein. It is very difficult to understand what effect the CMCOs are having on COXI levels without having repeat doses as there is such a high variation between controls.

The western blot did not suggest that there is a correlation between the CMCOs that caused the greatest fall in copy number and the CMCOs that indicated the largest decline in COXI. Ugi 105 – the MN targeted homologous CMCO caused the largest apparent decline in COXI – to 50% of average control levels, followed by Ugi 195 (3 nucleotide change) and Ugi 193 (1 nucleotide change)- which also indicated the largest decline in copy number. However, although there was an apparent decline caused when compared to the average no dose control COXI/SDHA ratio, when compared to individual no dose controls C2 and C4 (which had the lowest COXI/SDHA ratios), there is no difference in COXI expression.

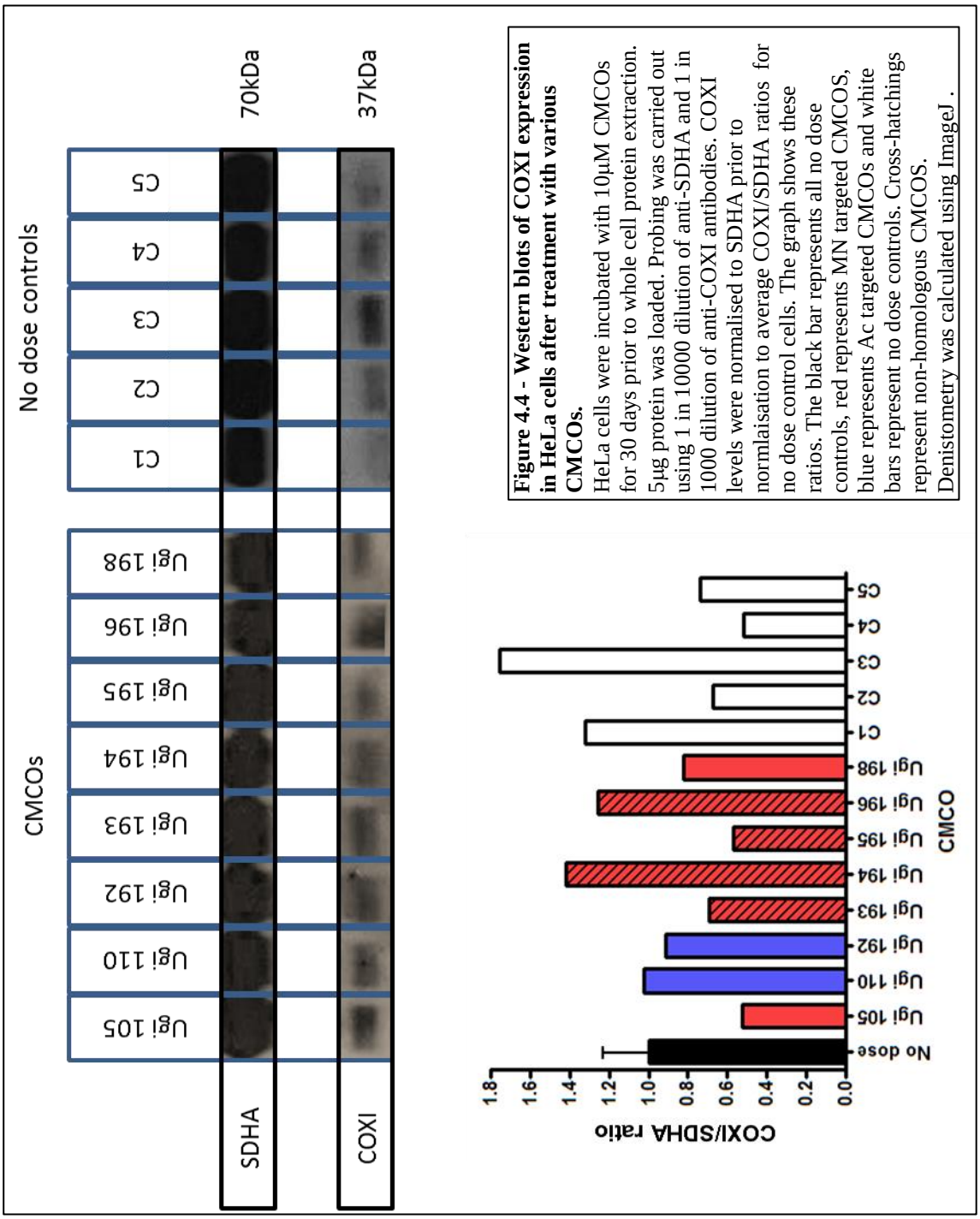

Figure 4.4 - Western blots of COXI expression in HeLa cells after treatment with various CMCOs.
HeLa cells were incubated with 10μM CMCOs for 30 days prior to whole cell protein extraction. 5μg protein was loaded. Probing was carried out using 1 in 10000 dilution of anti-SDHA and 1 in 1000 dilution of anti-COXI antibodies. COXI levels were normalised to SDHA prior to normlaisation to average COXI/SDHA ratios for no dose control cells. The graph shows these ratios. The black bar represents all no dose controls, red represents MN targeted CMCOS, blue represents Ac targeted CMCOs and white bars represent no dose controls. Cross-hatchings represent non-homologous CMCOS. Denistometry was calculated using ImageJ .

The data presented does not indicate that these CMCOs had a functional effect on mtDNA or COXI expression. It is therefore impossible to draw a firm conclusion due to the difficulty in analysing the western blots and the absence of repeat experiments. Logically the best performing CMCO should have been Ugi 105 as this was targeted using MN – the best targeting molecule (Chapter 3, figure 3.10), and also had 100% sequence homology to the targeted region. The fact that this showed the greatest decrease in COXI when compared to all no dose controls suggests that the CMCO may have bound, however further experiments are needed to fully understand any effect. These results will be discussed further in section 4.5.

4.4.3. **Fluorescently conjugated MN-CMCOs**

The previous chapter (chapter 3, figure 3.10) showed that the CMCO with the greatest mitochondrial colocalisation were MN targeted and conjugated to ATTO 647N. It was therefore decided to investigate the functional effect of these along with TAMRA conjugated CMCOs. As it is clear that fluorescently tagged MN-CMCOs colocalise to mitochondria to a certain degree, it was decided to repeat the previous dosing experiment (section 4.4.2) but for 14 days instead of 30. This change in incubation period was due to the fact that the CMCOs colocalised relatively rapidly to mitochondria and were therefore more likely to be present in higher concentration within the matrix (if they could access it), enabling a greater inhibition of mtDNA replication and COXI expression. This decision was also influenced by the obvious need to carry out repeats. Ideally it would have been more robust to dose for 30 days, however this was limited by CMCO availability. The concentration (10μM) remained the same and protein and DNA samples were extracted for each CMCO, however for these experiments there were two repeats for each CMCO. Four no-dose controls were set up in parallel to the CMCO incubations. As with the previous experiments, the dosing was blinded. Details of the CMCOs to be investigated are shown in table 4.2.

Table 4.2 - Details of fluorescently tagged CMCOs.

CMCO	Targeting molecule	Dye	Sequence	Notes
Ugi 81	Mononitrophenol (MN)-Lys	TAMRA	TGCCTAGGACTCCAGC	
Ugi 96	Acetyl -Lys	TAMRA		
Ugi 100	MN-Lys	ATTO		
Ugi 102	Acetyl -Lys	ATTO		
Ugi 199	MN-Lys	TAMRA		Different phosphonic ester side chain
Ugi 200	MN-Lys	ATTO		

All CMCOs are homologous to *MTCO1* (np. 5979-5994) and contain 6 phosphonic ester side chains. Ugi 199 and Ugi 200 contain a new proprietary side chain *in lieu* of the previously used phosphonic ester side chain, in order to investigate its functional effects. Red letters denote the position of phosphonic ester side chains, or the new side chain for Ugi 199 and 200.

It was shown in the previous chapter that mitochondrial localisation was achieved by fluorescent CMCOs in the absence of MN. Therefore it was decided to investigate the functional effects of both MN and Ac (non-targeted) CMCOs in conjunction with either TAMRA or ATTO 647N. All CMCOs contained the same ratio of phosphonic esters (6 in total) as used in the colocalisation experiments. Ugi 199 and Ugi 200 replaced the previously used side chains with a new proprietary side chain that has not been previously tested in this application – it was likely to alter the lipophilic properties and strength of DNA binding. These CMCOs were provided by Ugichem as they have shown efficacy in binding DNA in other areas of their research. Due to the proprietary nature of this side chain I am currently unable to provide details on its structure or proposed function.

4.4.3.1. *Effect of fluorescently conjugated CMCOs on mtDNA copy number*

Using the method described previously (section 2.5.2), the ratio of *MTND1* to *B2M* was used to determine the relative mtDNA copy number for each CMCO treated cell line using the standard curve method. Copy number ratios were also determined for no dose control cell lines, the average of which was used to normalise the CMCO data.

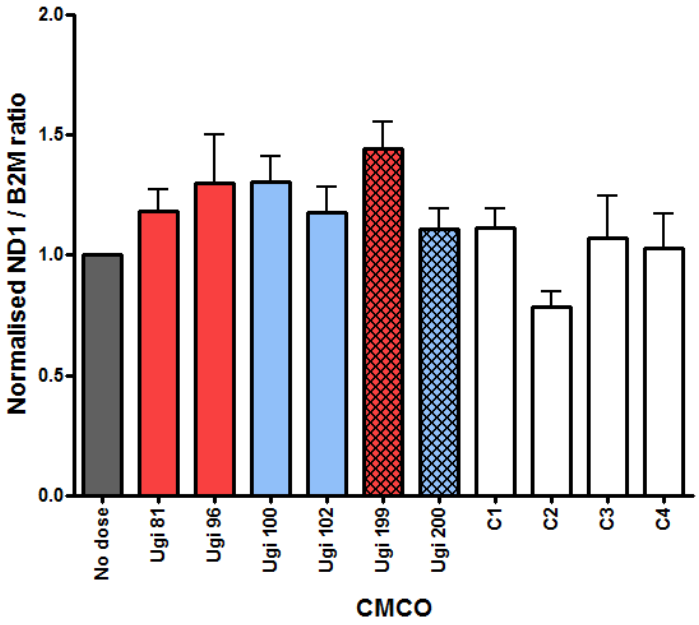

CMCO	Targeting molecule	Dye	Normalised copy number
Ugi 81	Mononitrophenol (MN)-Lys	TAMRA	1.182703
Ugi 96	Acetyl -Lys	TAMRA	1.29982
Ugi 100	MN-Lys	ATTO	1.303063
Ugi 102	Acetyl -Lys	ATTO	1.177658
Ugi 199	MN-Lys	TAMRA	1.443964
Ugi 200	MN-Lys	ATTO	1.107027

Figure 4.5 - The effect of 10μM fluorescently conjugated CMCOs on mtDNA copy number after incubation for 14 days.
Data is normalised to the mean of no dose controls (grey bar). Red bars denote TAMRA conjugated CMCOs, Blue bars denote ATTO647N conjugates CMCOs. White bars show individual no dose controls. Cross-hatchings denoted new side chain. The table shows relative mtDNA copy number normalised to controls (ND1/B2M ratio). No significance decrease in mtDNA copy number was detected (Mann-Whitney U test). Error bars represent standard deviation of dosing repeats (calculated from average of triplicate real time PCR values).

Figure 4.5 shows changes in mtDNA copy number in response to treatment with 10μM of the various fluorescent CMCOs. In this experiment, there was a much smaller variation in the copy number of real-time PCR repeats in control cells (mean standard deviation of 0.10 for all controls, compared to 0.17 in the previous experiment),

although the deviation between controls was 0.19 (relative ND1/B2M ratio), which is comparable to the previous experiment's control standard deviation. The fact that the deviation is similar indicates that the natural variation in mtDNA copy number of HeLa cells is relatively well conserved across experiments.

The data for each CMCO represents both repeat experiments and indicates that there was no evidence of decreased mtDNA copy number in treated cells. There was much less variation of copy number in all treated samples when compared to the previous experiment (figure 4.3), which could be due to the presence of repeats, therefore this data indicates that there was no inhibition of mtDNA replication.

4.4.3.2. *Effect of fluorescently conjugated CMCOs on COXI expression*

In spite of the absence of evidence of mtDNA depletion, the CMCOs may have the ability to bind COXI transcripts and prevent their translation. This was investigated by western blotting; the levels of COX in relation to SDHA in 5µg cytoplasmic protein lysate were analysed for each CMCO and normalised to the no dose control average.

Figure 4.6 shows western blots for individual repeats, along with a graph showing the relative COXI levels for each CMCO in relation to the average for the no dose controls. Although the signal obtained from the western blot is relatively diffuse, there is an obvious variation in the control levels of COXI, particularly C4 which indicated 80% lower COXI than the average controls. No CMCOs indicated an effect on COXI expression, with the possible exception of Ugi 200. This ATTO 647N-CMCO is targeted to mitochondria using MN and also contains the new, modified side chain. Although the C4 no dose control also indicated a lower level of COXI, the fact that both repeats of the Ugi 200 dose showed a decrease indicates that there could be a functional effect. This will require further investigation and more repeat doses, however after consultation with Ugichem, it is clear that this particular side-chain has led to functional effects in other areas of their research particularly in anti-viral anti-genomic therapies and as a consequence this new design is in the process of being patented.

The error bars on the graph shown in figure 4.6 represent the two repeat doses. It is clear that there was a large variation between repeats, indicating that further experiments are needed to fully investigate any effect. It is also unlikely that Ugi 96 and 100 caused an increase in COXI protein; this was probably caused by variation introduced into the quantification of the western by the low level of signal obtained during detection.

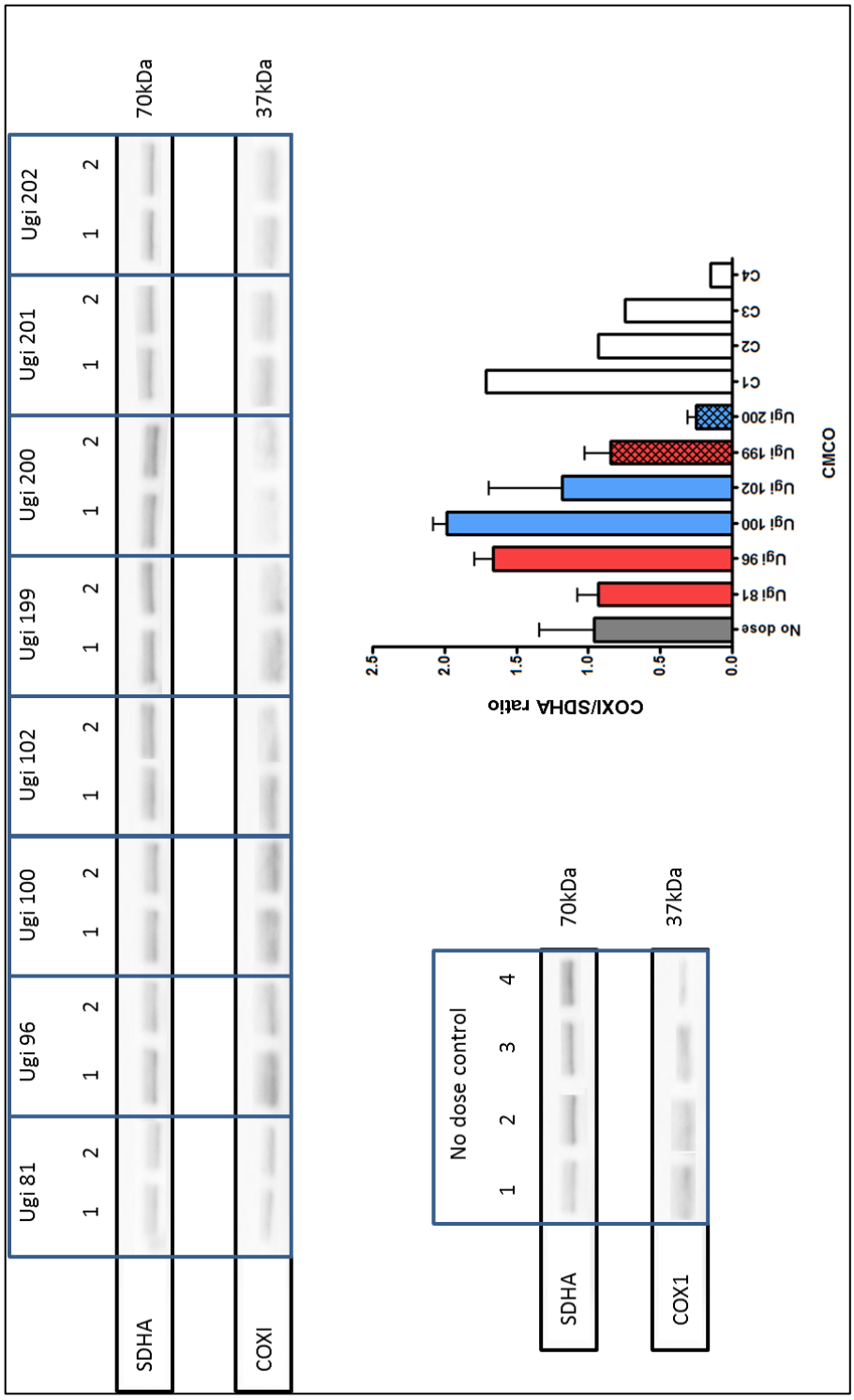

Figure 4.6 – Relative expression of COXI in response to treatment with 10μM fluorescently conjugated CMCOs for 14 days.
Western blots are shown for each CMCO repeat dosing along with 4 no dose controls. COXI levels were determined by normalising COXI signal to SDHA signal. Blots were probed using 1 in 1000 anti-COXI and 1 in 10000 anti-SDHA antibodies. The graph shows relative COXI levels normalised to the average no dose control SDHA/COXI level. The grey bar represents no dose control average, red bars TAMRA-CMCOs, Blue bars ATTO647N-CMCOs and white bars show individual no dose controls. Cross hatchings represent CMCOs with the new side chain. Error bars represent standard error of the mean. Densitometry calculated using ImageJ.

4.5. DISCUSSION

The data presented in this chapter suggests that the non-fluorescently conjugated CMCOs tended to not have a functional effect on either replication of mtDNA or expression of COXI protein, however, there is not enough data to conclusively argue that they were completely ineffective. An absence of functional effect could be due to the CMCOs not localising to the mitochondrial matrix, and therefore not having access to mtDNA, or it could be that the CMCOs could not bind mtDNA and inhibit replication. Compounds which do cause mtDNA depletion, such as ethidium bromide, can be expected to lower copy number by several orders of magnitude when compared to control molecules. This was not seen in any of the experiments carried out in this chapter by any of the CMCOs, although such a large effect may be beyond their capabilities.

4.5.1. **Non fluorescently tagged CMCOs**

The previous chapter indicated that MN had the ability to localise CMCOs to mitochondria when used in conjunction with a fluorescent mitochondrial marker. The mtDNA depletion results indicated that the CMCO which tended to cause a fall in copy number in these experiments had a one base difference to np.5979-5994 (Ugi 193), or were completely non-homologous to mtDNA (Ugi 196), whereas the homologous CMCO (Ugi 105) had no effect on mtDNA copy number, although there was not enough data to fully investigate this. Ugichem experience similar effects in other areas of CMCO research where non-homologous CMCOs show a greater effect than completely homologous oligomers although the reason for this is unclear. However, the fact that the completely random Ugi 196 also indicated a fall in copy number, suggests that the results are more likely to be due to random variation rather than an actual effect on mtDNA replication. It could also be possible that the nonsense CMCO may have a nonspecific interaction with a part of the replication machinery which causes a general decrease in replication. However, with the current data this is difficult to comment on further and may require further investigation.

The relationship between CMCO dosing and COXI expression is unclear. Detection of decreased COXI levels by western blotting relies on there being a large decrease, as quantification is difficult due to the variation seen when using the technique. Therefore

in order to reliably confirm a COXI decline, the quantity of COXI detected by western blotting needs to be substantially lower than all control cell lines. This was not the case in this experiment, and it is therefore not possible to confirm an effect on the expression of COXI by any of the non-fluorescently tagged CMCOs. The westerns presented are difficult to analyse as the signal from SDHA is substantially stronger when compared to COXI, therefore a small variation in COXI will cause a large change in the ratio of the two proteins. The reason for this is unknown as it was only experienced in this experiment, however it could be due to experimental error as unfortunately there was not sufficient protein lysate to repeat these experiments.

As discussed in the previous chapter, further investigations are needed to determine if MN-CMCOs do have the ability to accumulate within the mitochondrial matrix. If it becomes clear that MN-CMCOs can accumulate within the matrix but do not have a reproducible effect on mtDNA or protein expression, then different CMCO structures can be trialled (discussed in chapter 7).

4.5.2. **Fluorescently tagged CMCOs**

Neither the TAMRA nor ATTO 647N conjugated CMCOs showed any effect on mtDNA copy number after 14 day 10μM incubation in the two experiments completed. Although it is clear that the ATTO 647N-CMCOs localise to mitochondria, it is unknown if they accumulate within the matrix, therefore the absence of any functional effect could be due to the CMCOs not accessing the matrix, or not being able to sufficiently bind and inhibit mtDNA replication, however more experiments are needed to fully understand the activity of these CMCOs.

Western blot data also indicates that the CMCOs did not cause a decline in COXI expression in the two repeats carried out, with the possible exception of Ugi 200. Although the western blot quality is limited by the quantity of protein loaded, there is a decrease in the quantity of COXI for both repeat Ugi 200 incubations when compared to the average COXI/SDHA ratio for the no dose controls. This work will need to be repeated in order to confirm a depletion of COXI. As mentioned previously, for a COXI depletion to be confirmed, it is essential that the quantity of detected COXI is lower

than all no dose controls rather than just the average. In this case, no dose control 4 also indicates a relatively low level of COXI expression, lower in fact that seen in Ugi 200 treated cells. The lower level of COXI in no dose 4 could be due to a natural variation of endogenous protein, or it could be due to the small quantity of protein loaded increasing the variation when detecting COXI and SDHA.

The fact that both Ugi 200 repeats indicated a depletion of COXI is interesting and will require further repeat experiments to confirm any effect. The combination of MN-ATTO 647N was the most efficient at targeting mitochondria, so it was expected that if any CMCO had a functional effect on COXI levels it would be these ones. As Ugi 100, which is also MN-ATTO 647N conjugated, had no effect it is possible that the new side chain plays a role in increasing the ability of the CMCOs to bind mRNA. If this is the case, it would explain why Ugi 100 did not have an effect on COXI expression whereas Ugi 200 may have. Consultation with Ugichem has confirmed that CMCOs with the new side chain have shown efficacy in inhibiting nuclear encoded genes and viral genes and as a result of this the company no longer manufactures CMCOs with the original phosphonic ester side chain. Therefore all future experiments will be carried out using CMCOs with the new side chain.

Future work investigating the functional effects of CMCOs will require a larger quantity of oligomers to complete adequate repeats, something that was not possible in this work due to technical and financial constraints. The sensitivity of the techniques used in this chapter may prevent their use in future investigations. On-going work in this lab has highlighted the need for multiple experimental and technical repeats when using real-time PCR in order to ensure the obtained data is statistically robust. Using more repeats also enables the accurate quantification of small changes (>20%) in mtDNA copy number. This work will be applied in future investigations using CMCOs. The greater variation of copy number in cells cultured for 30 days when compared to 14 days may warrant incubating HeLa cells for less time in order to lessen the chance of inducing such a large variation.

The sensitivity of western blotting is also an issue; therefore I intend to re-optimise the technique for future work. The detection of small changes in protein using western blots is not possible; therefore the use of a different technique may be warranted. This is something that I will fully investigate prior to commencing further work; however it may be possible to use an immunocytochemical based technique to directly assess protein levels *in vivo*.

4.6. CONCLUSIONS

Although the effect of CMCOs on mtDNA replication and COXI expression is unclear, CMCOs are still an attractive option for treating mtDNA diseases, as they do not require a specific delivery mechanism to enter the cell. The variation of copy number and protein expression could be due to the genetic instability of the HeLa cells or a differential growth rate. If some of the cells did reach a slightly higher confluency than others before harvesting, the expression of mitochondrial proteins and mtDNA replication is likely to fall as the cells may enter a G_0 stage of growth, and no longer require as much energy (Martínez-Diez et al. 2006).

As there was some indication of a functional effect of Ugi 200 (MN-ATTO 647N targeted with the new side chain), it is important to repeat the mtDNA and COXI depletion experiments. However, prior to investigating this CMCO, I will analyse the variation of mtDNA copy number and COXI expression in other cell types, particularly cells that grow at a slower rate, as the risk of confluency related mtDNA depletions is smaller. In conjunction with Ugichem, I will design more targeted CMCOs with the new, active side chain in order to see if there is an effect on mtDNA copy number. I believe it is important to understand where and why the CMCOs localise within mitochondria, as until this question is answered it is difficult to analyse the functional effects of the CMCOs *in vivo*.

Chapter Five

Design and optimisation of a high throughput assay to detect changes in mitochondrial mass

5.1. INTRODUCTION

Mitochondrial dysfunction is primarily associated with mitochondrial diseases, however deficits in mitochondrial function have also been shown to be a contributing factor in numerous neurological diseases including Parkinson's (Abou-Sleiman et al. 2006) and Alzheimer's diseases (Reddy and Beal 2005; Reddy and Reddy 2011). Although the involvement of mitochondrial dysfunction in these diseases has been known for a number of years, there are currently no routinely used pharmaceuticals that target mitochondria in these diseases. Consequently there is a need to discover novel compounds that can act on mitochondria to improve their function in tissues affected by such diseases.

Although there are several interventions that could lead to an improvement in mitochondrial function in these diseases, such as causing an increase in ATP production, decreasing free radical production or increasing removal of damaged mitochondria through autophagy, it was decided to create an assay to detect changes in mitochondrial mass with the aim of detecting a compound that causes an increase in mitochondrial biogenesis. Increased mitochondrial mass was chosen as an endpoint as it is logical to assume that increases in mitochondrial biogenesis may lead to an improvement in cellular function. Recent work by Dillon and colleagues also supports this conclusion (Dillon et al. 2012). There are several ways to detect this, including; detection of increases in mitochondrial proteins by western blotting, detecting up regulation of genes driving mitochondrial biogenesis by RT PCR and network quantification using microscopy. Although these methods have all been shown to have the ability to detect changes in mitochondrial biogenesis (Medeiros 2008), none of them can be used to screen large numbers of compounds as they require too much time and resources to process each sample.

Development of an assay that is both high throughput and reproducible is essential for the screening of large numbers of compounds. Therefore an assay to detect changes in

mitochondrial biogenesis which can be applied to 96 well plates was developed. The use of fluorescent mitochondrial probes in the detection of changes in mitochondrial volume has been well characterised when used in conjunction with microscopy or fluorescently activated cell sorting (FACS) (Karbowski et al. 2001; Dingley et al. 2012) by determining the quantity of mitochondrial staining per cell, however their ability to highlight volume changes in a 96 well plate format has not been tested. This chapter focuses on the development of the assay to enable the detection of changes in mitochondrial volume in cells grown in 96 well plates using a fluorescent probe. The assay will then be used to screen compounds to see if they cause a change in cellular mitochondrial volume.

5.2. AIMS

The development of this assay involved the fulfilment of four aims:

I. To develop a 96 well plate based assay to screen compounds for effects on mitochondrial density.
II. To determine if mitochondrial dyes can be used to quantify changes in mitochondrial density.
III. To develop a plate reader based system to determine cell number per well.
IV. Investigate the benefits of automation of liquid handling and determine its suitability for the high throughput assay.

5.3. METHODS

As this chapter describes the development of a methodical approach for the mitochondrial mass detection assay and various aspects of its optimisation, the following is a brief description of the general techniques used.

5.3.1. Cell growth

All HeLa cells used were grown according to the protocol listed in section 2.2.1. Prior to seeding in clear 96 well plates they were harvested from culture flasks and counted as described in section 2.2.2. Once seeded in a plate cells were grown in appropriate media in the presence of 50 units/ml penicillin and 50µg/ml streptomycin (pen/strep). All HeLa cell cultures were incubated at 37^{o}C in a humidified atmosphere of 5% CO_2.

5.3.2. **Cell staining and fixation**

Mitochondrial dyes were diluted in complete media without Phenol Red to an appropriate concentration depending on experiment. Dye containing media was used to replace the media in each well and cells were incubated with the dye for 30 minutes at 37^{o}C. Prior to reading on a plate reader, dye media was removed and wells washed 3 times in PBS and appropriate media without Phenol Red (to prevent high background signal during imaging) added to each well. Immediately after imaging, cells were fixed in 4% PFA in their wells and washed in PBS. Plates were either stored at 4^{o}C or stained with an appropriate concentration of Hoechst 33258 and imaged.

5.3.3. **Statistical analysis**

Microsoft excel was used to collate data and Prism (GraphPad, USA) was used to generate graphs. Prior to statistical analysis, all data set were subjected to a normality test using Minitab 16 statistical software (Minitab Inc.).

5.4. RESULTS

5.4.1. Optimisation of cell seeding density

The human adenocarcinoma cell line; HeLa, was used in this assay to screen mitochondrially acting compounds. This cell line was chosen based on its short doubling time (18–24 hours) and on experience from previous chapters which shows the cells are relatively flat and have a reticular mitochondrial network that is conducive to imaging studies.

To ensure that cells did not become too confluent, it was essential to determine a seeding density that enabled sustained growth for as long as possible before confluency was reached, but also created an even layer of cells in the well. Therefore a 1:1 serial dilution of cells was performed across a 96 well plate (ranging from $1x10^4$ to 78 cells/well approximately). These cells were allowed to grow for 72 hours before the spread of the cells across the well was determined by eye using microscopy. It was found that at seeding densities below $5x10^3$ cells/well, cells were distributed unevenly across the well, whereas a $5x10^3$ cells/well seeding density led to an even distribution of around 90% confluency which equated to $8x10^4$ cells/well following 72 hours growth. To maximise the incubation length with compounds, it was decided that assayed cells will be allowed to grow for 72 hours, as any longer and the cells became over confluent.

5.4.2. Cell number normalisation

To ensure that the mitochondrial signal could be normalised to cell number, determining the number of cells per well following treatment was essential. It was decided that removing the cells from each well using trypsin and counting them manually would be too time consuming to make the assay viable and potentially not all cells would be removed, skewing the cell number data. Therefore a method to read the number of cells whilst they were still attached to the plate was developed.

Nuclear staining and counting is a technique routinely used in several assays to determine cell number for normalisation of other parameters (Chen et al. 2005; Zhou et al. 2012). However, most of these techniques require the physical counting of individual nuclei, rather than a measure of the overall fluorescent signal emitted by their staining. To stain nuclei, the DNA stain Hoechst 33258 was chosen as it has an emission and excitation spectra distinct from most live cell mitochondrial dyes (figure 5.1). It also exhibits a larger Stokes shift than other DNA stains in this emission range, meaning that it has distinct excitation and emission peaks. It is likely to have minimal background staining as the intensity of its emitted fluorescence increases 1000 fold upon intercalation into dsDNA.

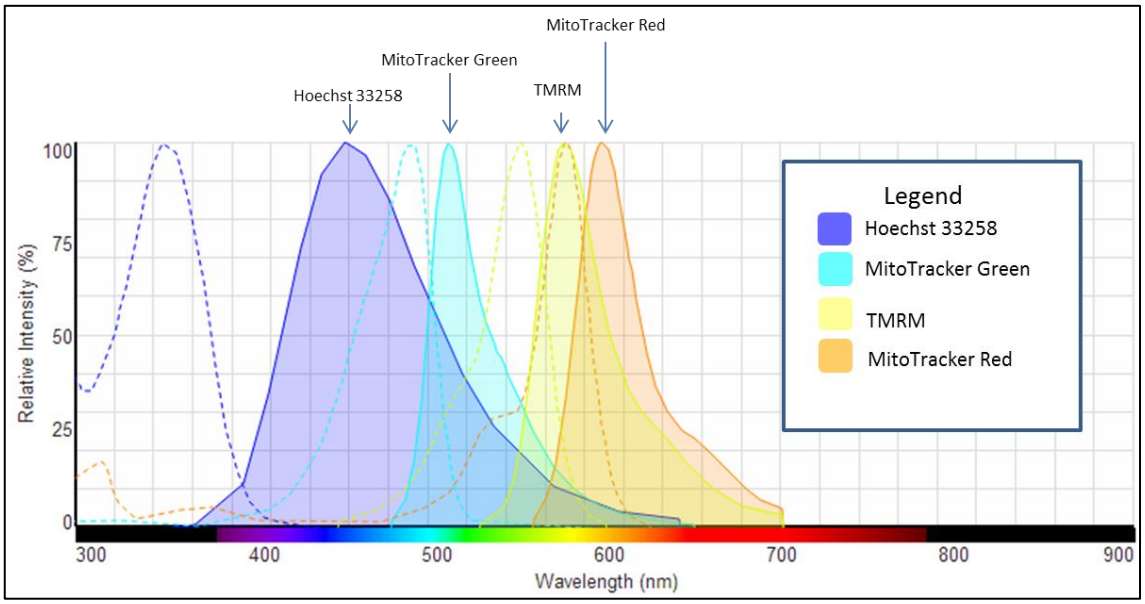

Figure 5.1 - Excitation and emission spectra of Hoechst 33258, Mitotracker Green, Mitotracker Red and TMRM.
Dotted lines represent excitation spectra, solid lines represent emission spectra. Labelled arrows denote emission peaks.

To investigate the relationship between cell number per well and whole well fluorescence emitted by a nuclear stain, a 1:1 serial dilution of HeLa cells was seeded across a 96 well plate, ranging from 0 to 8 $x10^4$ cells/well in octuplet. Cells were allowed to adhere to the plates overnight before fixation and staining with 100µl Hoechst 33258 (4µg/ml in ddH_2O) for 30 minutes. This concentration was chosen as it is recommended by the manufacturers (Sigma-Aldrich, St. Louis, USA) for staining the nuclei of fixed cells. A fluorescence plate reader using the appropriate excitation and emission filters (see materials and methods, table 2.2) was then used to measure relative

fluorescence per well and the relationship between cell number and fluorescence plotted.

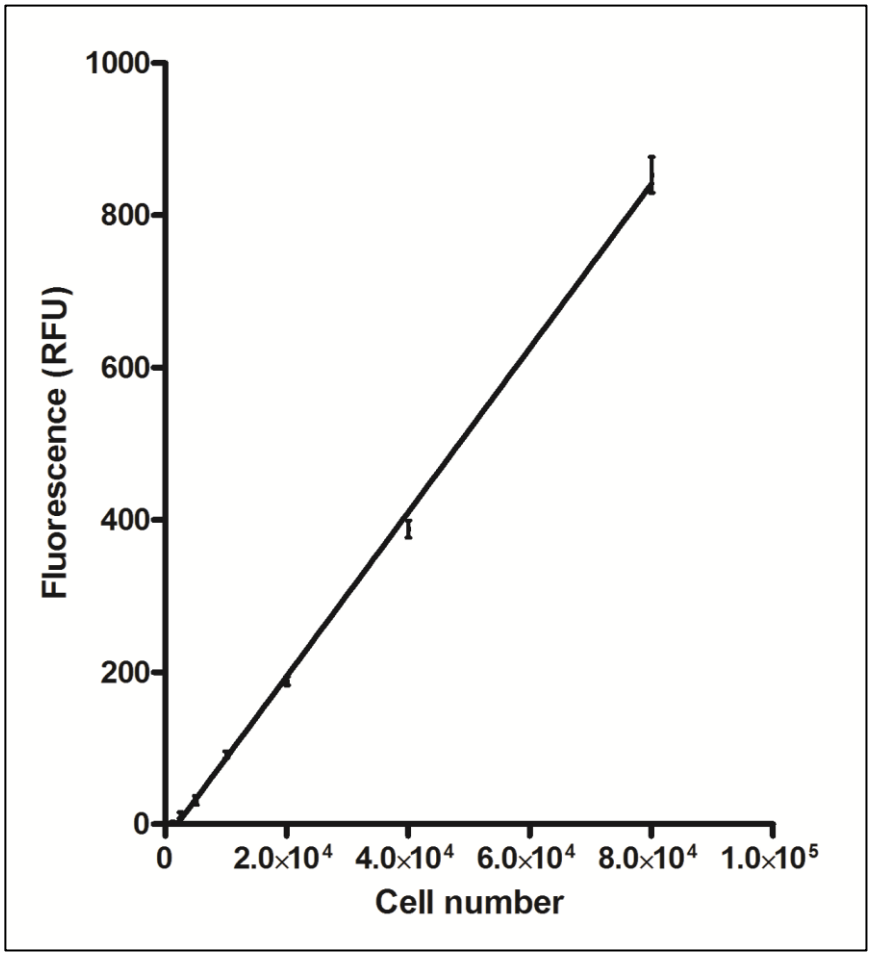

Figure 5.2 - HeLa cell number plotted against mean fluorescence emitted per well by Hoechst dye /RFU (Relative fluorescent units). Trendline shows linear regression (r^2=0.989). Error bars represent standard error of the mean for the octuplet. Cells fixed 6 hours after seeding.

Figure 5.2 shows the relationship between the number of cells seeded per well and fluorescence obtained after staining with Hoechst 33258. A trendline was generated by linear regression (r^2=0.989), demonstrating a linear relationship between Hoechst fluorescence and cell number for the cell number range investigated here. Therefore emitted Hoechst fluorescence can be used to estimate relative cell number per well.

5.4.3. **Measurement of mitochondrial density**

As with cell number counting, measurement of mitochondrial mass has to be achieved using a technique that is both reproducible and high-throughput i.e. can be achieved in a

relatively short amount of time and be carried out on a 96 well plate. Techniques used routinely in our lab include quantification of mitochondrial mass using anti-Porin antibodies as a marker with either fluorescent or chromogen visualisation. This requires the cells to be fixed and then permeablized prior to incubation with a primary and suitable secondary antibody. Samples are then imaged using microscopy and levels of staining quantified using densitometry. Although this method has been validated within the lab, it is not appropriate for this assay, primarily because of the number of steps involved and the amount of antibody required for staining a whole plate, but also the requirement of glass bottomed plates to enable accurate microscopy. These factors make the technique prohibitively expensive. Measurement of mitochondrial mass in live cells is achieved by staining mitochondria using a specific dye and analysing the total volume of the stained regions compared to a cytoplasmic stain for example Calcein Blue, enabling calculation of total mitochondrial mass per cell. Again, this method requires microscopy to be used to image the mitochondria and is therefore not appropriate for this assay. However, the use of a mitochondrial specific stain may enable the quantification of changes in mitochondrial mass using a plate reader.

5.4.3.1. *Optimisation of mitochondrial dye concentrations*

To investigate this, first the relationship between dye concentration and fluorescence was determined. Two dyes were examined, MitoTracker^{TM} Red and TMRM, both of which accumulate in mitochondria in a membrane potential dependent manner. Although MitoTracker Green also has these properties, this dye was not chosen as its excitation spectra overlaps with Hoechst (figure 5.1). A concentration gradient was prepared by diluting the dyes in PBS to create an appropriate concentration range from 300nM to 25nM decreasing in 25nM steps. This concentration range was chosen to ensure sufficient signal was picked up by the plate reader. Each concentration was set up in quadruplicate on a 96 well plate and emitted fluorescence read using a plate reader with the appropriate filter set 520nm/ 560nm (Ex/Em).

The relationship between TMRM and concentration is shown in figure 5.3. An exponential growth trendline (dashed line) has been used to illustrated the non-linear relationship across the entire concentration range, (r^2=0.9858) when compared to a linear regression trendline (solid line) with an r^2 value of 0.904. However, when

analysed it was found that for concentrations below 125nM, the interaction between TMRM concentration and fluorescence changes from a non-linear to a strongly linear relationship, as shown in figure 5.3 B, r^2= 0.9902, indicating that across this concentration range TMRM fluorescence increases in a predictable ratio against TMRM concentration.

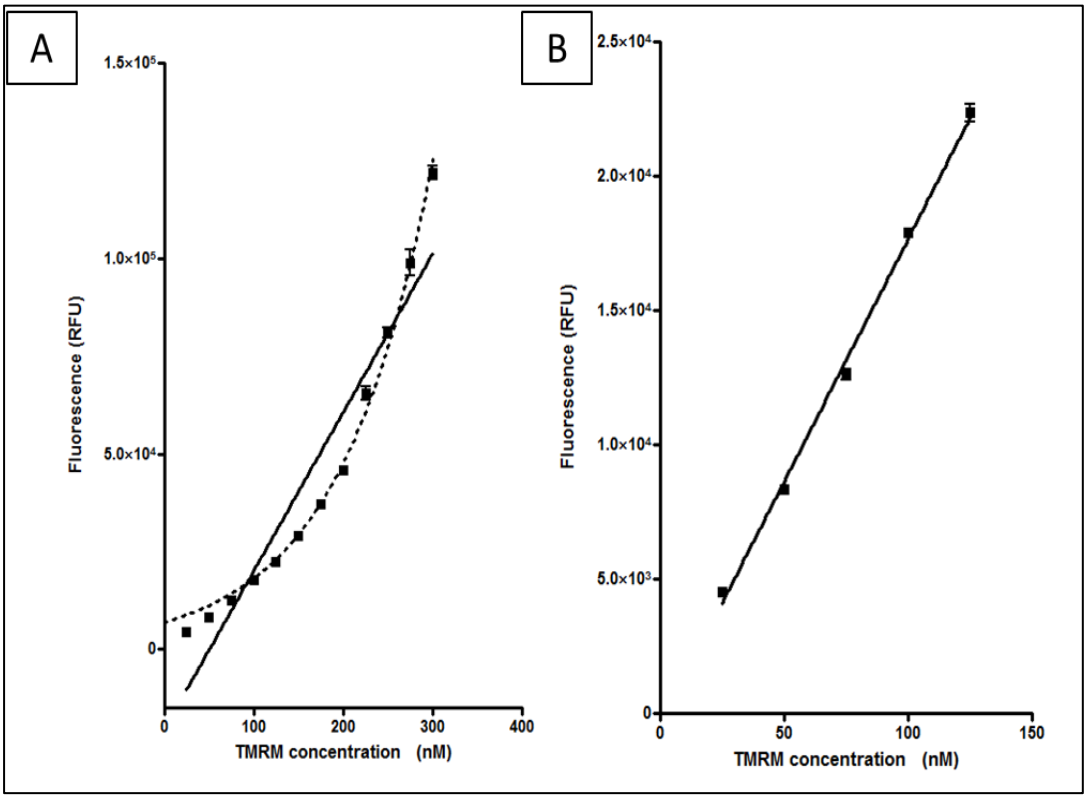

Figure 5.3 - TMRM concentration plotted against fluorescence.
A shows the relationship of fluorescence over a concentration range of TMRM from 25n-300nM. The dotted trendline is an exponential growth line (r^2=0.9858), the solid trendline a linear regression (r^2=0.9051). **B** shows the relationship between fluorescence and TMRM concentration over a range of 25-125nM, the trendline is a linear regression (r^2=0.9902). Error bars represent standard error of the mean (n=8).

The relationship between MitoTracker Red concentration and fluorescence is shown in figure 5.4. Unlike TMRM, the interaction between concentration and fluorescence was linear across the entire range of concentrations, r^2=0.9731. Although the linear relationship extends across a wider range of concentrations than TMRM, the difference in r values for MitoTracker Red and TMRM (25nM to 125nM) suggests that over this concentration range, the interaction between TMRM concentration and fluorescence is more predictable.

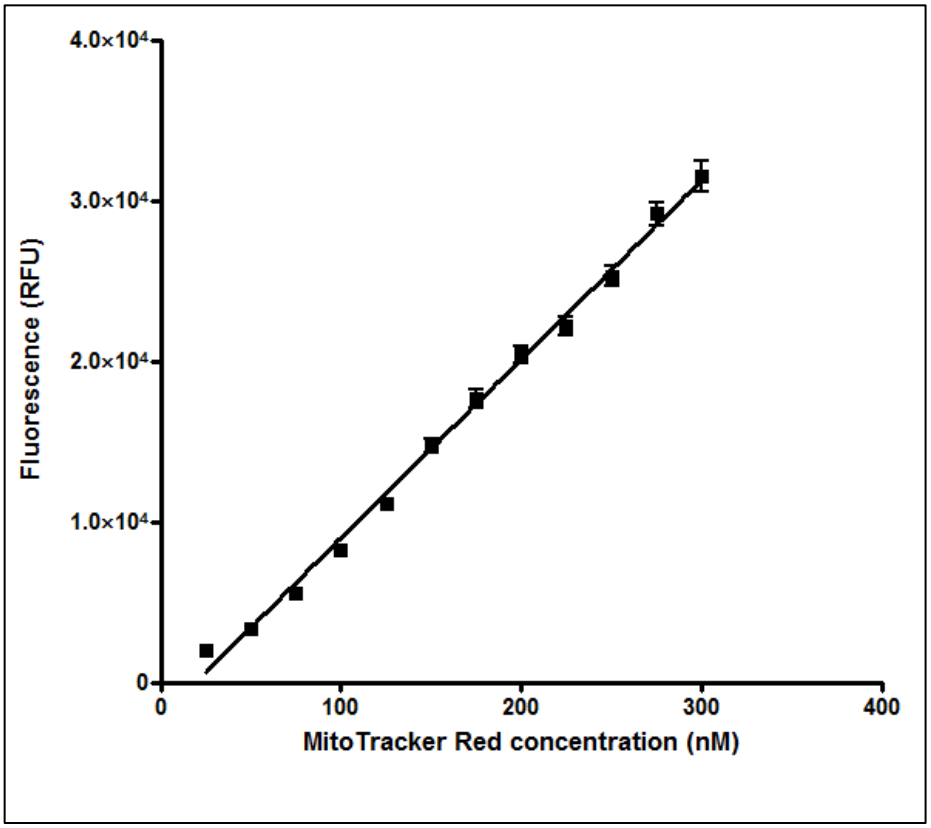

Figure 5.4 - Changes in fluorescence with increasing concentration of MitoTracker Red.
The trendline represents linear regression (r^2=0.97311). Error bars represent standard error of the mean for the octuplet.

The intensity of emitted fluorescence of TMRM is greater than Mitotracker Red, on average TMRM emits 2.25 times more relative fluorescence over a concentration range of 25nM to 125nM. This enables a reduction in sensitivity of the plate reader (a reduction in gain) which decreases the chance of picking up fluorescent signal that can be attributed to noise; in turn this increases the reproducibility of the assay. The stronger linear relationship of TMRM than MitoTracker Red across this concentration range also makes TMRM more attractive for this assay. This is because the ability to determine mitochondrial density from fluorescence is essential and TMRM behaves in a more predictable way than MitoTracker Red. Therefore TMRM was chosen for use in the assay.

The median value of the linear range of concentrations was chosen for the assay and therefore a TMRM concentration of 75nM was used for the rest of the optimization steps. This value was chosen as it enables the maximum possible changes in fluorescence over the linear range. For example, if the number of mitochondria increases, which is likely to lead to a relative increase in fluorescence, by choosing an initial TMRM concentration of 75nM this increase will be detected over this predictable range. However, if the starting concentration was 125nM, any increases in relative fluorescence would be detected outside the linear range, leading to increased variability when interpreting the results.

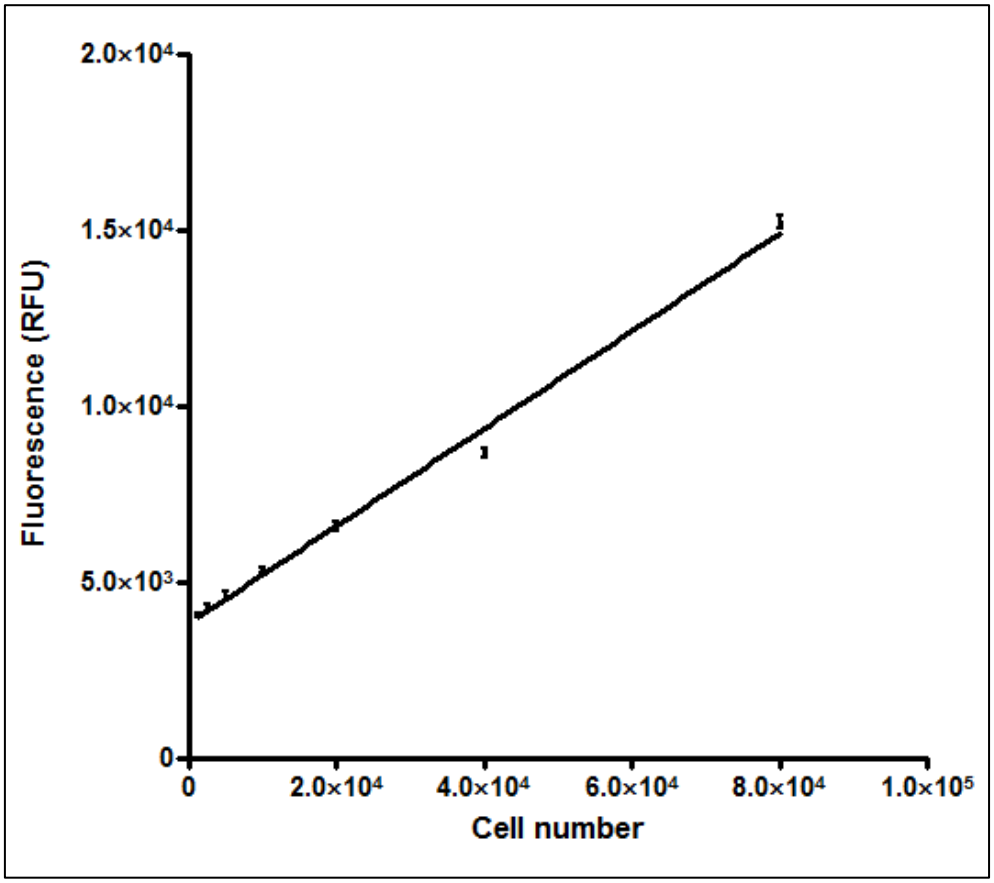

Figure 5.5 - Cell number per well plotted against fluorescence.
Measured by a plate reader after incubation with 75nM TMRM for 40 minutes. Trendline represents linear regression (r^2=0.980). Error bars represent standard error of the mean for the octuplet.

5.4.3.2. *TMRM as a marker of mitochondrial mass*

To investigate the interaction between increasing cell number and detected fluorescence emitted from 75nM TMRM, a 1:1 serial dilution of HeLa cells was prepared on a 96 well plate ranging from $8x10^4$ cells per well to 625 cells per well. Each concentration of cells was prepared in octuplets. Cells were allowed to adhere to the plate over night

before staining with 100µl 75nM TMRM for 40 minutes prior to washing 3 times in PBS and emitted fluorescence measured using a plate reader. Figure 5.5 shows the relationship cell number and TMRM fluorescence. The trendline (r^2=0.980) shows the linear relationship between the two factors, indicating that as cell number and therefore the number of mitochondria per well increases, so does fluorescence in a predictable manner. It should be noted that the level of fluorescence detected was markedly lower in this experiment than in the previous dye only experiment, however, this is likely to be because the uptake of TMRM is limited and therefore excess dye is removed during the washing stages which in turn means less fluorescence is detected. Although this is unlikely to affect the assay as the strong, linear relationship is maintained.

5.4.4. **Relationship of Hoechst and TMRM**

The interaction between Hoechst and TMRM was investigated. This was carried out to determine if as cell number increased, and therefore emitted fluorescence from Hoechst, the increase in TMRM fluorescence could be reliably predicted, i.e. is the relationship between Hoechst and TMRM fluorescence linear?

As with the previous experiments, a 1:1 serial dilution of HeLa cells was prepared ranging from $8x10^4$ to 625 cells/well in octuplet across a 96 well plate. This was then stained with 75nM TMRM as described previously. After reading, the cells were fixed in 4% PFA and stained with Hoechst prior to washes in PBS and fluorescence measured by a plate reader. The relationship between these two dyes is shown in figure 5.6. The relationship has a strongly linear characteristic, represented by a trendline of r^2=0.991. This shows that as Hoechst fluorescence increases in proportion to cell number, so does TMRM fluorescence. The predictable nature of this relationship means that if TMRM fluorescence changes due to an increase in mitochondrial mass, it would be detected as the normal relationship is so well defined.

This relationship shows that the dye choice of TMRM and Hoechst for mitochondria detection and cell number normalisation are excellent as together they enable the assessment of changes in TMRM fluorescence or cell number relative to controls.

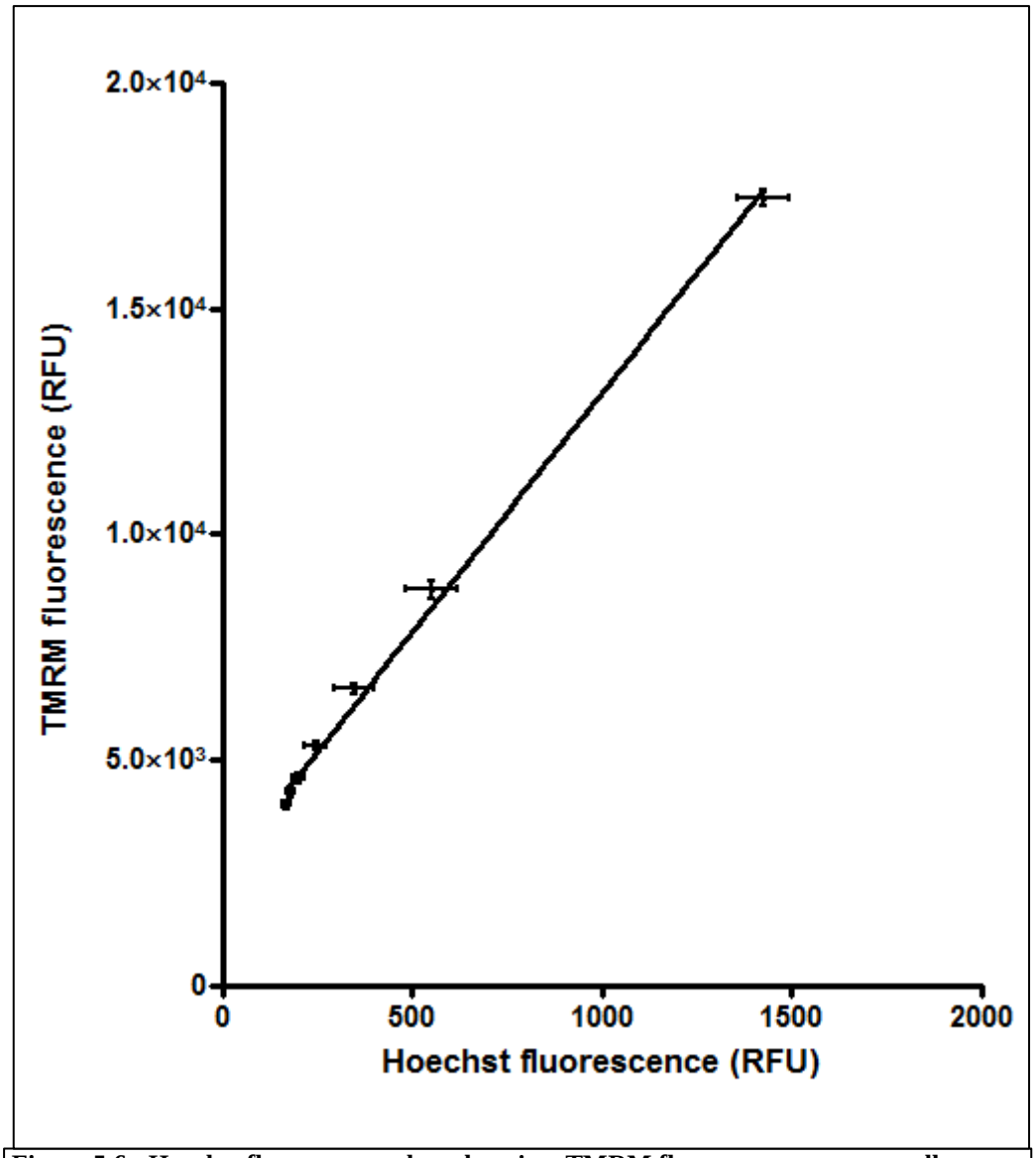

Figure 5.6 - Hoechst fluorescence plotted against TMRM fluorescence across a cell number concentration series.
A linear regression trendline is shown (r^2=0.991). Error bars represent the standard error of the mean for the octuplet.

5.4.5. **Control molecules**

Although I have shown that the assay can detect increases in mitochondrial load per well, appropriate controls are needed to show that the assay can detect both increases and decreases in mitochondrial mass per cell when compared to untreated cells. Therefore the characterisation of a positive control, which will increase mitochondria per cell, and a negative control, which will decrease mitochondria per cell will be discussed in this section.

5.4.5.1. *Negative control*

Treatment with 10µM FCCP has been shown to cause membrane depolarisation which in turn leads to the degradation of mitochondria through autophagy (Saita et al. 2013). TMRM accumulation into the mitochondria will also be prevented by this loss of

membrane potential as the dye localises to the mitochondrial matrix in a membrane potential dependant manner. To allow TMRM to accumulate, the membrane potential has to be restored by removing FCCP and allowing the proton gradient to recover. This is essential as it will ensure that any fall in detected TMRM fluorescence has not been caused by decreased dye accumulation.

To develop a protocol for FCCP removal and restoration of $\Delta\psi m$, HeLa cells were grown in glass bottomed wells in the presence of 10µM FCCP for 24 hours, a no dose control was also prepared. After incubation, one well was washed three times in PBS and placed in FCCP free media. This was then left for 1 hour at $37^{o}C$ in an atmosphere of 5% CO_2, before washing three times in FCCP free media. After this, all wells were incubated with 10nM TMRM as described in section 2.3.1, and imaged using a Zeiss Axiovert 200M fluorescent microscope. Images are shown in figure 5.7. Cells not treated with 10µM FCCP (figure 5.7 A) show normal mitochondrial TMRM staining. This is contrasted by FCCP treated cells which do not exhibit a reticular network (figure 5.7 B & C). However, in cells treated with FCCP but washed prior to staining (figure 5.7 B) there is a punctate pattern of staining not seen in the treated and unwashed cells.

Punctate staining in figure 5.7 B is likely to be the remaining mitochondria that have not degraded by autophagy. The unwashed cells show no discernible pattern of TMRM staining, it should be noted that the cell outline is visible in these cells due to the high exposure time of 1.6 seconds needed to pick up a signal in the TMRM emission range. The lack of staining was due to FCCP preventing the restoration of a normal mitochondrial membrane potential, thus inhibiting TMRM accumulation within mitochondria.

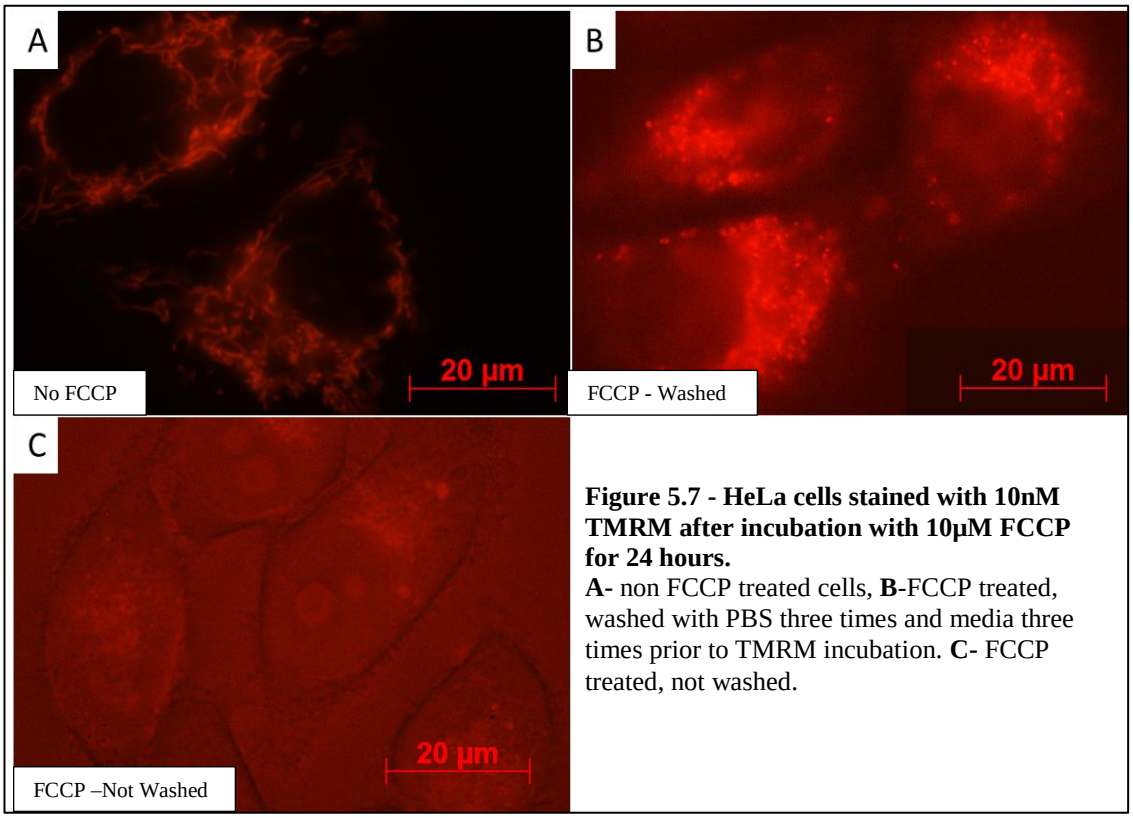

Figure 5.7 - HeLa cells stained with 10nM TMRM after incubation with 10µM FCCP for 24 hours.
A- non FCCP treated cells, **B**-FCCP treated, washed with PBS three times and media three times prior to TMRM incubation. **C-** FCCP treated, not washed.

Once it was established that staining of the mitochondrial network is possible after removal of FCCP, the effect of the negative control on TMRM fluorescence was assayed using a plate reader. $5x10^3$ cells per well were seeded on a 96 well plate and allowed to grow for 48 hours. The media of 50% of the 96 wells was replaced with complete media supplemented with 10µM FCCP and then left to incubate for 22 hours. After incubation, all cells were washed to remove FCCP. The level of TMRM and Hoechst fluorescence was measured as described previously. The level of TMRM fluorescence was normalised to cell number by dividing TMRM by Hoechst fluorescence. Normalised values for non-treated and FCCP treated cells were analysed using an unpaired Student's t-test which found a significant difference between the two populations ($p<0.0001$). A boxplot of the data is shown in figure 5.8; this shows the significant decrease in mitochondrial mass when cells are treated with 10µM FCCP for 24 hours.

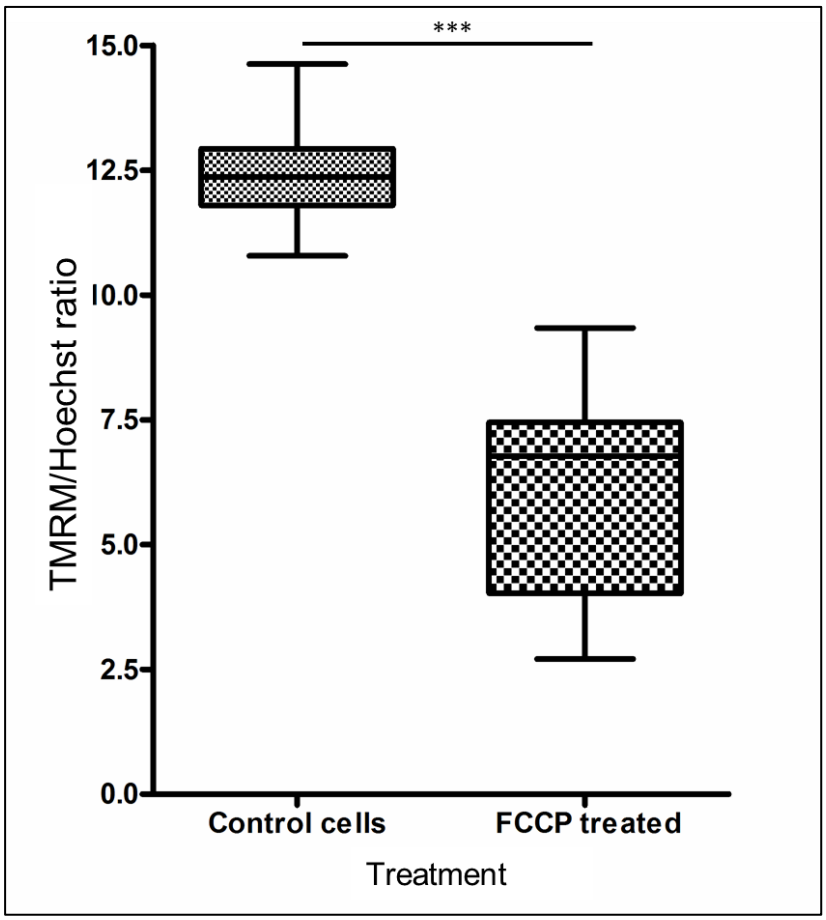

Figure 5.8 - Effect of FCCP on mitochondrial mass.
Boxplot of no dose control and 10µM FCCP treated HeLa cells against TMRM fluorescence normalised to Hoechst fluorescence. Error bars show maximum and minimum values. Significance was determined by Student's t-test (***=p<0.0001).

5.4.5.2. *Positive control*

A literature search was performed to highlight any compounds that have been shown to increase mitochondrial density that could act as a positive control for the assay. Two compounds were found; paclitaxel and bezafibrate, both of which are currently used as pharmaceutical agents and both of which have been shown to increase the density of mitochondria (Karbowski et al. 2001; Wang and Moraes 2011). The first of these, the anti-mitotic drug paclitaxel, has been shown to stabilize microtubule assembly, preventing their breakdown. Although this drug is primarily used pharmaceutically to inhibit cell division, Karbowski and colleagues have shown that stabilisation of microtubules during interphase can cause an accumulation of mitochondria in HeLa cells (Karbowski et al. 2001). Although the authors determined mitochondrial density per cell using Mitotracker Orange dye to stain mitochondria and then quantifying the

amount of dye per cell using FACS, this assay should be able to detect the change as it too quantifies mitochondria based on the amount of a mitochondrial dye per cell.

To test this, HeLa cells were synchronised in G_1/S phase of the cell cycle by double hydroxyurea block to deplete deoxyribonucleotides (Karbowski et al. 2001). Briefly, cells were cultured for 48 hours in a T75cm^2 flask before the addition of 0.1M hydroxyurea. Cells were left for 24 hours before washing in fresh media and cultured in the absence of hydroxyurea for 8 hours. After 8 hours, 0.1M hydroxyurea was added to the cells and incubated for 16 hours. The now synchronised cells were passaged and seeded on a 96 well plate ($5x10^3$ cells/well) and allowed to grow for 24 hours. Media was removed from 8 wells on the plate and replaced with media containing 2.5µM paclitaxel as described by (Karbowski et al. 2001) and left for 24 hours. A further 8 wells were incubated with 2.5µM paclitaxel for 22 hours. This was carried out on the remaining wells every two hours, 8 wells were left free of paclitaxel to act as no dose controls. The effect of incubation length with paclitaxel was investigated to determine the correct time to dose the cells as the effect of the drug is cell cycle dependant.

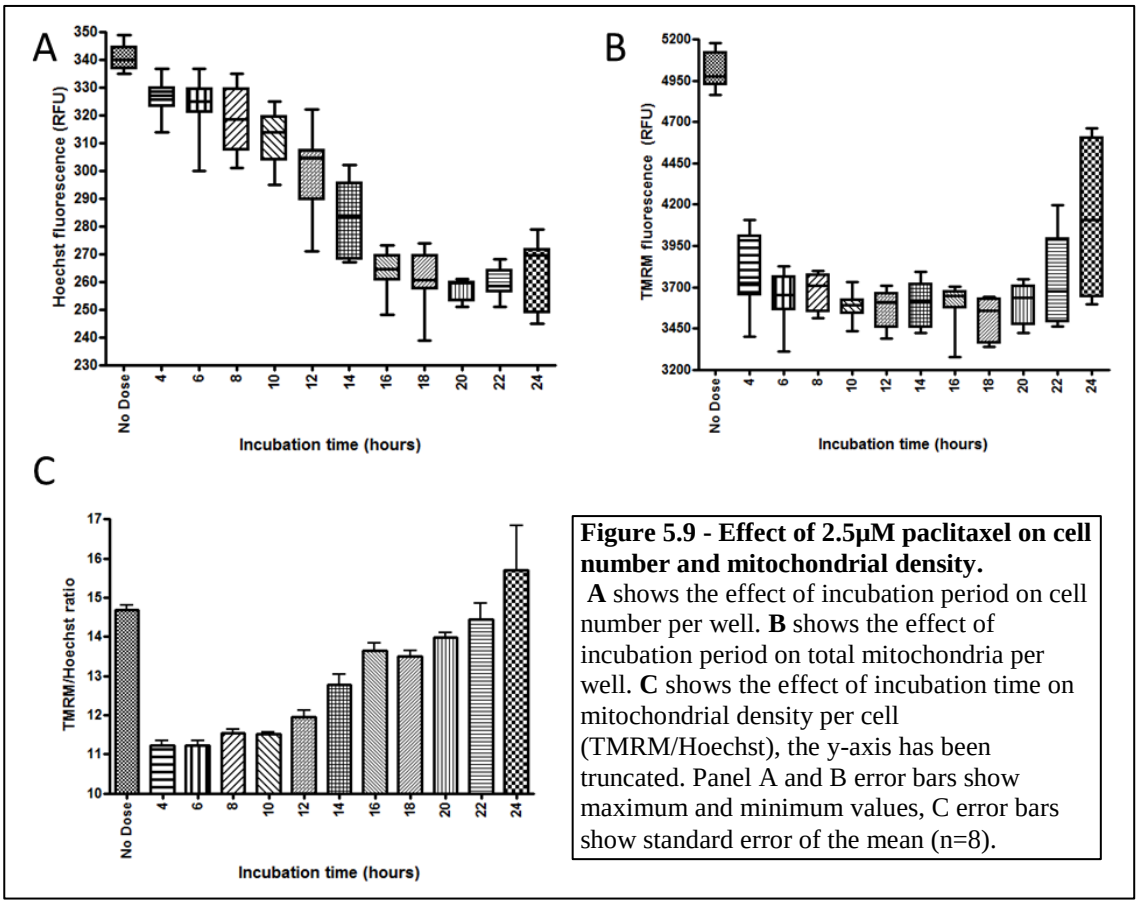

Figure 5.9 - Effect of 2.5µM paclitaxel on cell number and mitochondrial density.
A shows the effect of incubation period on cell number per well. **B** shows the effect of incubation period on total mitochondria per well. **C** shows the effect of incubation time on mitochondrial density per cell (TMRM/Hoechst), the y-axis has been truncated. Panel A and B error bars show maximum and minimum values, C error bars show standard error of the mean (n=8).

Figure 5.9 shows the effect of paclitaxel incubation length on cell number and mitochondria per well. Incubation times of longer than 14 hours limit the number of cells per well (figure 5.9 A). This is likely to be caused by either cell death induced by longer incubations with paclitaxel, or because paclitaxel has inhibited the division of cells which may have occurred 16 hours after the start of the experiment, thus limiting their number at the end of the assay. The interaction of paclitaxel with mitochondria shows that incubations shorter than 24 hours actually causes a decrease in mitochondria both per well shown by total TMRM fluorescence (figure 5.9 B) and per cell (figure 5.9 C). This is possibly because periods shorter than 24 hours limit the time available for mitochondria to accumulate during interphase. The reason that mitochondria do not increase with cell number for the shorter (<14hour) incubations could be due to paclitaxel induced toxicity during cell division preventing the biogenesis of new mitochondria.

Figure 5.9 C shows that there is an increase in the density of mitochondria per cell in cells incubated with paclitaxel for 24 hours. A Student's t test was performed to determine the significance of this increase, however it was found that this was not significant ($p=0.229$) compared to no dose controls.

Due to the lack of significance with this result, it was decided to investigate a second positive control compound; the PPAR pan agonist bezafibrate. Work by Wang and Moraes has shown that a 72 hour treatment with 400µM bezafibrate leads to an increase in mitochondrial biogenesis in HeLa cells (Wang and Moraes 2011). More recently it has been shown that bezafibrate can improve the so called "ageing" phenotype in a mtDNA mutator mouse model (Dillon et al. 2012). Both of these effects are believed to be caused by bezafibrate activating PPARs (Tenenbaum et al. 2005), which regulate transcription of genes involved in mitochondrial biogenesis (Puigserver and Spiegelman 2003). Based on this evidence it was decided to trial bezafibrate as a potential positive control.

An initial experiment was carried out to assess the optimal concentration to dose HeLa cells. Although Wang and Moraes showed a 400µM concentration caused mitochondrial biogenesis, they stated that this concentration was selected from work based on fibroblast cell lines. Therefore HeLa cells were incubated with a concentration range of 500µM to 50µM bezafibrate for 72 hours, after which their mitochondrial density and cell number was measured. This data was used to normalise the density of mitochondria to cell number which is shown in figure 5.10. A Mann-Whitney U test was performed to assess significance in changes of mitochondrial density. It was found that a concentration of 450µM gives a greater increase in mitochondrial density when compared to no dose controls ($p<0.001$). Interestingly, all concentrations of bezafibrate led to a lower cell number when compared to no dose controls, this correlates with data shown by Wang and Moraes that indicates slowed growth of HeLa cells in glucose media when exposed to bezafibrate (Wang and Moraes 2011).

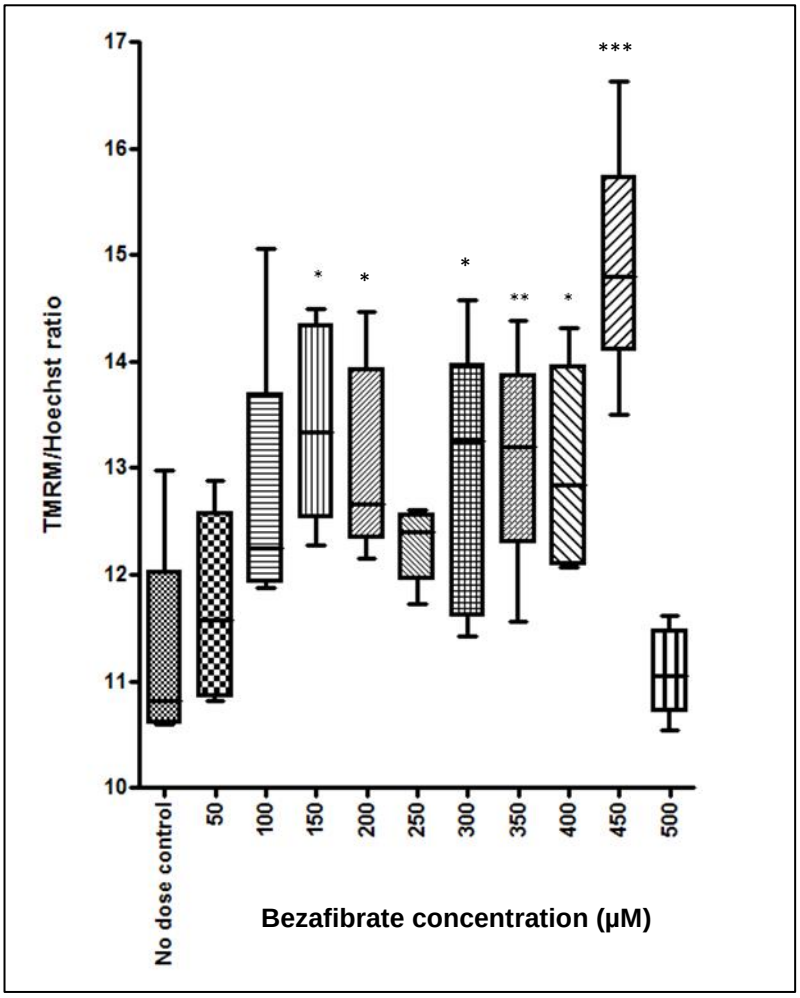

Figure 5.10 - The effect of bezafibrate concentration on mitochondrial density.
HeLa cells were incubated with various concentrations of bezafibrate for 72 hours prior to the density of mitochondria per cell being assessed using the plate reader assay. Error bars show maximum and minimum values. *=p<0.05, **=p<0.01, ***=p<0.001, one way ANOVA test.

Due to the significant increase in mitochondrial density, it was decided that bezafibrate should be used as a positive control for the assay.

5.4.6. **Automation**

To increase the throughput of the assay, it was important to develop methods to automate part of or the entire assay. Due to the large number of media changes and washes, it was decided to use a Beckman Coulter liquid handling robot equipped with a 96 well liquid handler in place of manual pipetting. Over the course of the assay this decreased the time it took to process one plate from 20 minutes to 5 minutes. Using the

robot not only increased the speed of carrying out the various steps but it also enabled the control of liquid velocity as the liquid is moved into and out of the well. This was essential as it prevents the loss of cells, which may be aspirated off the bottom of the well by over-zealous pipetting.

A comparison of manual and robotic pipetting was carried out by determining the cell number of six plates, three of which were processed manually, three by robot. Incubation times and assay length were the same for all plates and all plates were seeded using cells from the same culture. Two measures of cell number standard deviation (SD) were calculated, inter-plate SD comparing whole plates processed by robot or manually and intra-plate SD comparing deviation of 8 well columns on all plates. Graphs of this are shown in Figure 5.11.

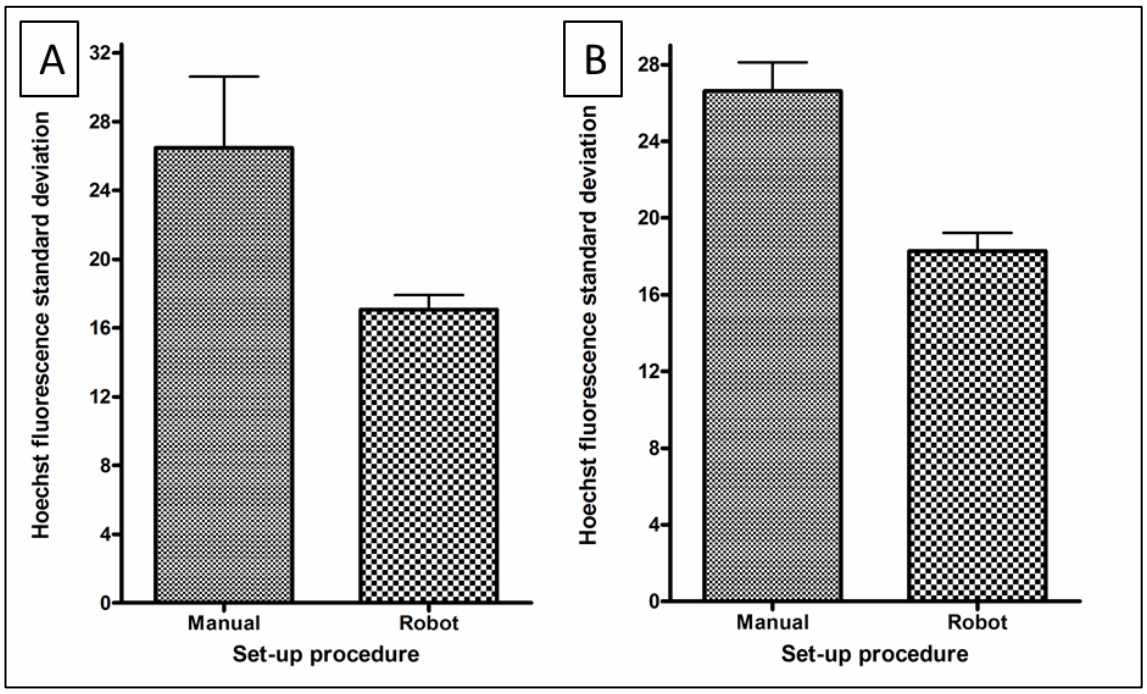

Figure 5.11 - Standard deviation of Hoechst fluorescence of 96 well plates when processed either manually or robotically.
A shows standard deviation of Hoechst fluorescence calculated from whole plates; n=3. **B** shows standard deviation of 8 well columns; n=36. Error bars show standard error of the mean.

Figure 5.11 A shows that there is smaller deviation of Hoechst fluorescence in plates set up robotically than manually. The smaller error bars also indicate that there is less variation between plates set up robotically than manually. This is also the case in figure

5.11 B which shows that the variation of Hoechst fluorescence is lower across individual plates when processed using the robot. This means that using the robot will lead to less variation between plates and also between individual wells on plates and will therefore be used to carry out all liquid handling procedures for this assay.

5.5. DISCUSSION

This chapter aimed to develop a plate reader based assay that uses fluorescent markers to detected changes in mitochondrial density in cells after treatment with test compounds. The methods in this chapter were developed to screen a large number of compounds for effects on mitochondrial density. Screening of compounds is essential for the effort to discover new drugs that can improve symptoms in diseases with mitochondrial pathologies.

Development of this assay has shown that it is possible to detect changes in mitochondrial density by detecting emitted fluorescence from mitochondria stained with TMRM and then normalising to cell number. Use of the robot has enabled the accuracy of the assay to increase while also decreasing the time taken to perform each step. Although methods exist that have been shown to be sufficient for mitochondrial density quantification, development of a higher throughput system is essential for drug screening as it enables investigation of more compounds and therefore increases the chances of discovering an active agent. The assay developed during this chapter is summarised in the schematic below (figure 5.12). The final assay protocol is shown in materials and methods section 2.7.

It should be noted that as this assay uses 75nM TMRM, a quenching effect is likely to be seen. This phenomenon occurs when high concentrations of TMRM are used and causes a decrease in the intensity of emitted fluorescence. In situations where the membrane potential dissipates and TMRM leaves mitochondria, the concentration of the dye decreases and the quench is resolved, briefly increasing the intensity of the emitted fluorescence (Scaduto and Grotyohann 1999). This will not be an issue for this assay as the membrane potential will remain stable during imaging. However, if any of the extracts cause a fall in membrane potential, it is possible that the TMRM will not

accumulate to the same concentration as other samples, and if this concentration is low enough to not be in "quench mode" then it is possible that the emitted fluorescence is more intense than other samples, creating a false positive. If this does occur, the use of microscopy to determine changes in mitochondrial mass will highlight the false positive and the extract will be removed from the investigation.

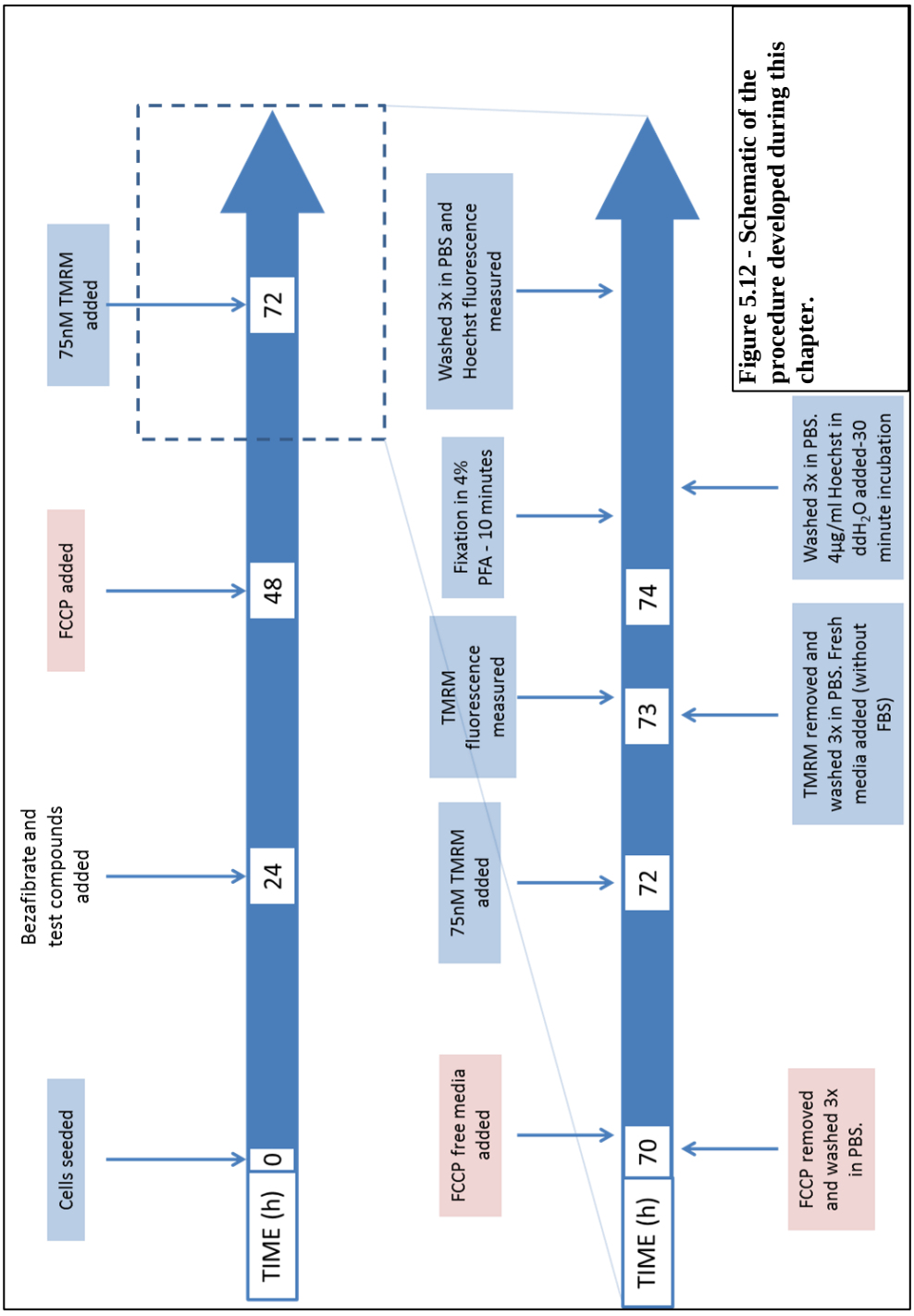

Figure 5.12 - Schematic of the procedure developed during this chapter.

Chapter Six

A high throughput screen to detect changes in mitochondrial mass caused by a library of bacterial extracts

6.1. INTRODUCTION

As discussed in the previous chapter (section 5.1), there is an essential need to develop pharmaceuticals that can improve the function of mitochondria. With recent work showing that increased mitochondrial biogenesis can lead to an improved phenotype in models of mitochondrial dysfunction (Dillon et al. 2012; Dillon et al. 2012), it was decided to use the assay developed in chapter 5 to screen a library of compounds for effects on mitochondrial mass.

6.1.1. The Library

A library of compounds secreted from actinomycetes bacteria, a major component of the phylum *Actinobacteria*, has been collated by our industrial partner Demuris Ltd. Actinomycetes are Gram-positive bacteria which are found in almost every environmental niche on Earth, ranging from marine environments to deserts (Takizawa et al. 1993; Jensen et al. 2005; Pathom-Aree et al. 2006; Montero-Calasanz Mdel et al. 2013). This success at colonising diverse habitats has been facilitated by their ability to produce and secrete a range of natural products, many of which have the ability to inhibit competing organisms such as other bacteria and fungi. The ability of actinomycetes to secrete a wide range of bioactive compounds has been exploited in the production of antibiotics, for example the widely used anti-mycobacterial Streptomycin is secreted by *Streptomyces griseus*, an actinobacterium (Waksman et al. 1946).

Although the majority of the library has not yet been properly characterised, their uses as anti-microbial agents are of primary interest to Demuris; however some compounds secreted by the bacteria have been shown to act on mitochondrial targets. One such example is chloramphenicol, a broad-spectrum antibiotic derived from the bacterium *Streptomyces venezueluae*, which decreases production of mitochondrially encoded proteins by preventing translation via reversible binding to the 55S ribosomal subunit

and inhibition of peptidyl transferase (Kuntzel 1969; Denslow and O'Brien 1974). An interaction of this type highlight the potential that other secreted compounds could also interact with mitochondria, some of which may have positive effects such as increasing mitochondrial biogenesis. It is likely that extracts will contain numerous compounds that have been secreted by the bacteria. In the event that an increase in mitochondrial mass is highlighted during the screen, the responsible extract will have to be fractionated to determine the active compound. However, prior to fractionation of any interesting extracts, further investigations using microscopy will be carried out to verify any changes in mitochondrial mass highlighted during the screen.

This chapter will focus on the screening of extracts using the methods described previously in chapter 5.

6.2. AIMS

In order to facilitate the discovery of compounds that affected mitochondrial biogenesis, this chapter fulfilled the following aims:

I. To screen and characterise changes in mitochondrial mass caused by 864 individual extracts secreted by actinomycetes bacteria.

II. Identify extracts that show a greater effect on mitochondrial mass than bezafibrate.

III. To verify increases in mitochondrial mass using microscopy techniques.

6.3. METHODS

The assay will be performed using the protocols developed in chapter 5 and detailed in materials and methods section 2.7.

6.3.1. Extract preparation

To generate the library, 864 individual actinomycetes species were grown on agar for an appropriate length of time, after which agars were crushed using sterile syringes and placed in 1.5ml tubes prior to overnight storage at -20^{o}C to further degrade the agar. Freezing of the bacteria may also lyse their cell membrane, however this is likely to be minimal and the majority of cells are likely to be intact. Tubes were thawed and centrifuged to pellet the agar; the supernatant containing aqueous and organic extracts was then taken and arrayed into 96 well plates. This generated a library of 864 unique extracts.

6.3.2. Extract dosing

Arrayed extracts were delivered by Demuris Ltd in 96 well plates, with each well containing a unique extract containing molecules secreted by one species of bacteria. Plates were stored at -80^{o}C to limit degradation of compounds that make up the extracts. Prior to screening, plates were defrosted on ice and allowed to reach room temperature. The extracts are not produced in an aseptic environment; therefore there is a chance of bacterial or fungal contamination. To minimise the chance of infection and to pellet precipitates, plates were centrifuged at 2000g for 30 minutes to pellet remaining bacteria, and fungal spores.

All pipetting steps were carried out using a Beckman Coulter liquid handling robot. 3µl of each extract was added to individual wells on a 96 well plate containing HeLa cells that were seeded 24 hours previously (original density was 5 x 10^3 cells/well). Each well contained 147µl complete media, creating a 1 in 50 dilution of extracts (the rationale for this dilution is discussed in section 6.4.1). The supernatant of each extract was added to 1 well of HeLa cells - on four separate plates - generating four repeats. The repeats were set up in this way to enable the use of the 96 well robotic liquid handler. Once dosed, plates were incubated at 37^{o}C in a humidified atmosphere of 5%

CO_2 for 48 hours. Plates containing no dose controls, FCCP (negative) controls and bezafibrate (positive) controls were also prepared in accordance with the protocols described in section 2.7.2.

6.3.3. **Excitation and emission analysis**

Extracts that indicated increases in mitochondrial mass had their fluorescence emission at 561nm measured using the plate reader. A 1 in 50 dilution in H_2O of each active extract was arrayed on a 96 well plate in triplicate (100µl/well). The plate was excited using a 520/30nm filter and emission at 561nm measured.

6.3.4. **Microscopy analysis**

To verify "hit" extracts, HeLa cells were seeded in 24 well glass bottomed plates- $5x10^3$ cells per well. After 24 hours "hit" extracts were added to the wells to a final dilution of 1 in 50 and incubated for 48 hours. Cells were stained with 10nM TMRM and Calcein Blue (20µM final concentration) for 30 minutes, after which they were washed 3 times in complete media without Phenol Red. Z-stack images were captured using a Nikon A1R confocal microscope using appropriate excitation and emission settings. The volume of mitochondrial staining (TMRM) was calculated and normalised to cell volume (Calcein blue: 360/449nm Ex/Em) using Imaris software (Bitplane, AG), to give mitochondrial mass.

6.3.5. **Statistical analysis**

All statistical analysis for the screen was performed using the statistical package R (version 2.15.2). Graphs were also produced using this package and GraphPad Prism. Microscopy analysis was quantified using Excel (Microsoft). Normality tests were performed on all data sets using Minitab 16 statistical software (Minitab, Inc.).

6.4. RESULTS

Using the assay developed in chapter 5, a library of 864 unique bacterial extracts was screened for changes in the mitochondrial mass of HeLa cells.

6.4.1. Concentration determination

Prior to screening the entire library, a sample plate of extracts was chosen at random to trial the assay. Information from this trial was used to determine an appropriate dosing concentration and likely infection rates. The extracts to be screened are likely to be heterogeneous in concentration and potency, with a range of activities and toxicity therefore likely to be seen on one plate of extracts. Due to this, choosing a concentration that represented the best range for testing for every extract in the screen was very difficult. It was decided to choose a concentration that caused the least toxicity, while maintaining the bioactivity of the extracts. It is unlikely that a change in mitochondrial mass would be found from screening just one plate of extracts, therefore bioactivity had to be determined using another marker.

One plate of extracts was chosen at random and added to HeLa cells over a range of dilutions (1 in 10, 1 in 50 and 1 in 100). Cells were incubated for 24 hours before being imaged using the protocol in section 2.7, after which they were incubated for a further 24 hours at 37^{o}C to monitor for cell death. Morphological changes in treated HeLa cells were used as a marker for bioactivity of the extracts. This was chosen as it is easy to determine and could indicate potential effects such as interactions with the cytoskeleton (Sumiya et al. 2011; Brandhagen et al. 2013), highlighting bioactivity of the extracts. A morphological change was defined as any difference in the shape of the cells that could be recognised by eye when compared to controls. All plates were examined by microscopy and it was found that one extract led to morphological changes that occurred in samples diluted 1 in 10 and 1 in 50 (figure 6.1 A & B). However this change was not observed in cells treated with a 1 in 100 dilution of the extract (figure 6.1 C). Cells were examined 24 hours after imaging and it was found that the 1 in 10 dilution had killed the cells, it was therefore decided to use a 1 in 50 dilution when dosing with the remaining extracts. Although this is a crude way of determining dosing concentration, it was decided to use this dilution initially to look for hits and in the event that no hits were found, or the toxicity was too high to try another dilution.

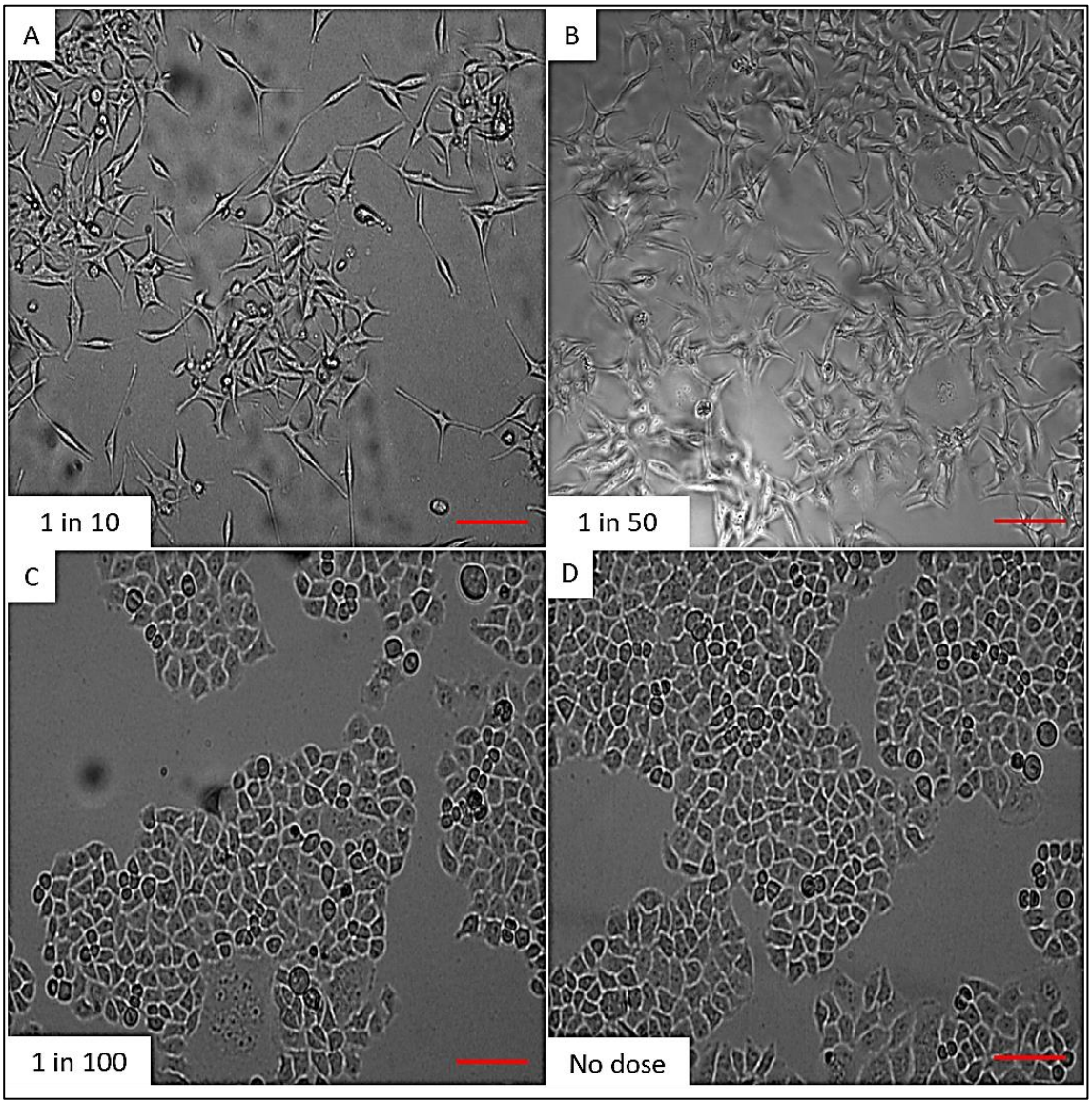

Figure 6.1 - Morphological changes induced by one extract over a dilution series.
A shows changes caused by a 1 in 10 dilution. **B** shows changes caused by a 1 in 50 dilution. **C** shows changes caused by a 1 in 100 dilution. **D** shows HeLa cells that have not been treated. Morphological changes were classed as a change in shape of the cells when compared to the no dose control.
Scale bars -100µm.

6.4.2. **The high throughput screen**

Due to the quantity of plates to be analysed (41, 96 well plates in total), it was not possible to complete all the live cell procedures at the same time, therefore the extract plates were screened in two groups, separated by one day (table 6.1).

Table 6.1 - Timings of the extract screen

Time	Group 1	Group 2
Day 1	Seeded-5 x 10^3 cells/well	N/A
Day 2	Extracts added & bezafibrate control plate produced	Seeded-5 x 10^3 cells/well
Day 3	10µM & 5µM FCCP control plates produced	Extracts added
Day 4	TMRM staining and reading. All plates fixed-stored at 4°C	10µM & 5µM FCCP control plates produced
Day 5	N/A	TMRM staining and reading. All plates fixed-stored at 4°C
Day 6	All plates stained with Hoechst and read	

Five plates of extracts were seeded in group one, four plates in group two totalling 864 individual extracts. Each extract was diluted 1 in 50 and incubated with HeLa cells for 48 hours in quadruplicate. No dose controls totalled 96 individual repeats per group, 10µM and 5µM FCCP totalled 32 wells each per group, 450µM bezafibrate control consisted of 96 individual repeats. A 5µM FCCP control was added to the assay to investigate any difference in the degradation of mitochondria when compared to 10µM FCCP. In total 3872 wells were dosed with either an extract or control and stained with both dyes (TMRM and Hoechst), generating 7744 individual data points for the entire screen. The data generated from the entire screen is discussed in the remainder of this chapter.

6.4.3. **Plate diagnostics**

Prior to analysis of changes in mitochondrial mass, the data was analysed to ensure that there was no difference in cell growth due to edge effects, which are a known issue when using a high throughput assay (Lundholt et al. 2003). They are caused by differential growth of cells based on where they are on the plate, but in general it is thought that cells seeded on the outside rows (1&8) and columns (1&12) are prone to variation in cell number (Lundholt et al. 2003). This is due to differences in evaporation rates, CO_2 exposure and temperature, in wells on the edge of the plate, with gas diffusion and exchange occurring more readily in these wells.

6.4.3.1. *No dose controls*

To check for edge effects, boxplots of Hoechst fluorescence for individual columns and rows were produced, first for no dose control plates, and then for the data set as a whole.

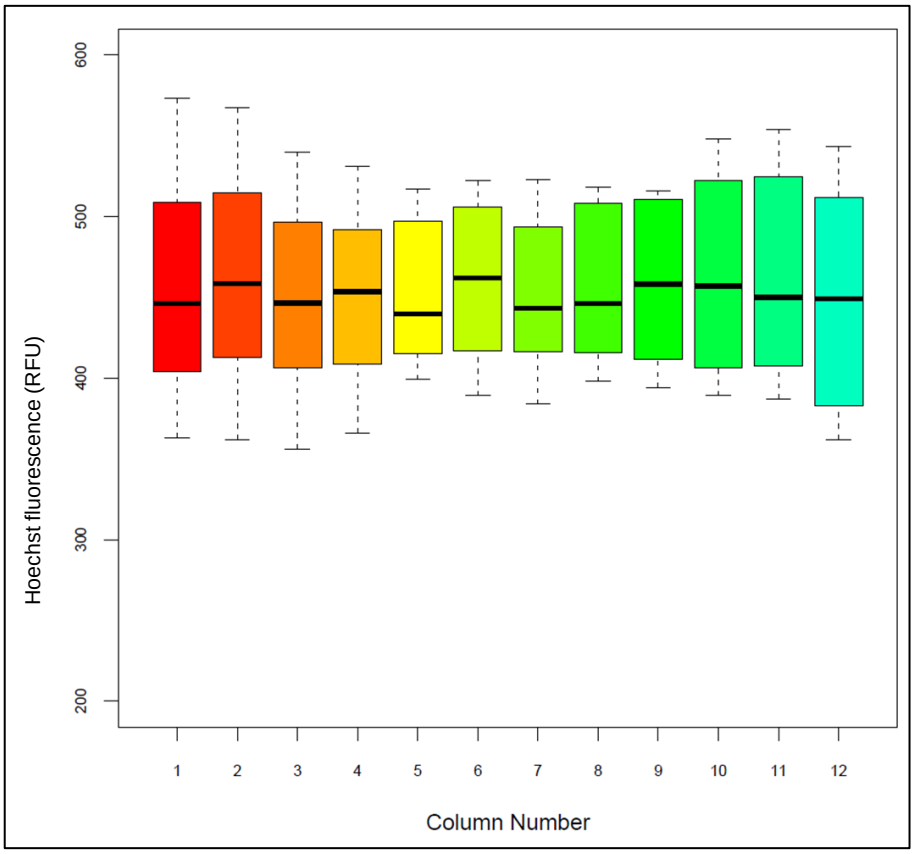

Figure 6.2 - Boxplot of Hoechst fluorescence plotted against column number for no dose controls.
Boxplot shows the interquartile range and median value, whiskers show maximum and minimum values.

Figure 6.2 shows a boxplot of Hoechst fluorescence per column for the no dose control plates. There is little variation in the median value between columns; however the interquartile range and maximum and minimum values is greater for columns on the edge of the plate (1, 2 & 11, 12), therefore a Mann-Whitney U test was performed to compare the values for the edge columns against the other columns. It was found that there was no significant difference between the two (p=0.21), indicating no edge effect associated with column number.

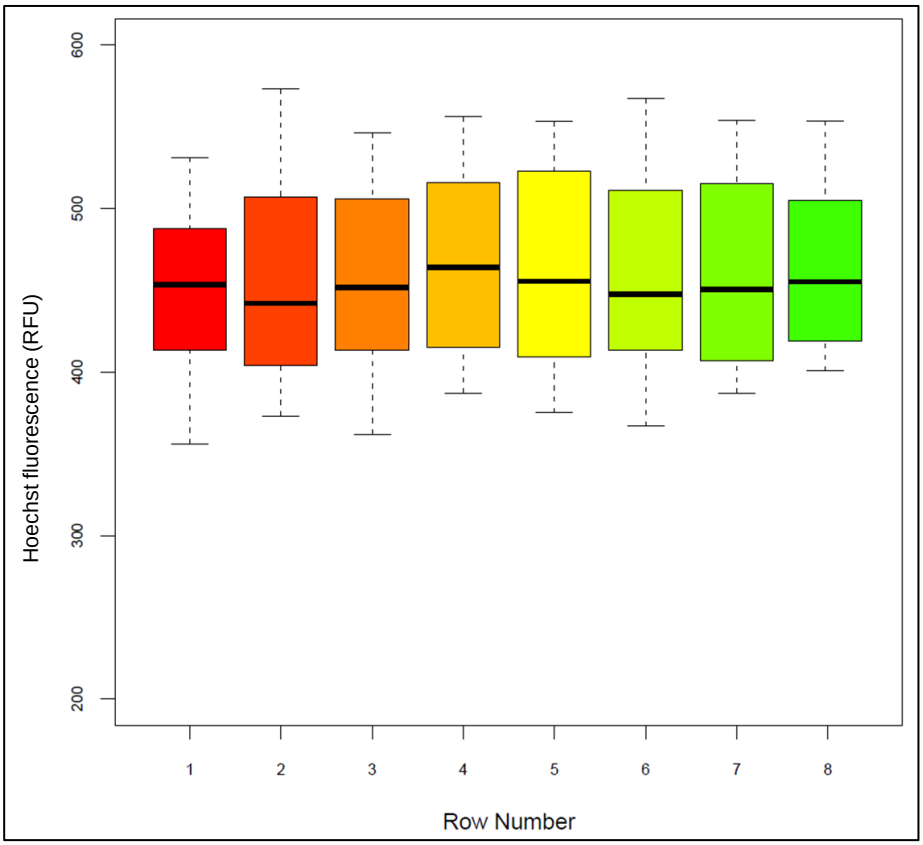

Figure 6.3 - Boxplot of Hoechst fluorescence plotted against row number for no dose controls.
Boxplot shows the interquartile range and median value, whiskers show maximum and minimum values.

Figure 6.3 shows Hoechst fluorescence plotted against row number for the same no dose control data set as represented in figure 6.2. There is less variation of Hoechst fluorescence between rows than was seen when the data was grouped according to column number, however this could be due to an increase in the number of data points represented (12) when the data is grouped in rows rather than columns (8 data points). It could also indicate that the wells with the highest variation are found in columns 1 and 12, an effect which is disguised when data is grouped by row. A Mann-Whitney U test

was performed to test for significant differences between the fluorescence of inside rows when compared to the two edge rows. As with the column data, no significant difference was found between the medians of Hoechst fluorescence (p=0.37), indicating no edge effects.

6.4.3.2. *Whole screen*

To ensure the relationship between row, column and Hoechst fluorescence was the same across the whole screen as it was for the no dose control plates, boxplots were constructed. The Hoechst fluorescence data for all plates was collated and plotted against either row number or column number, these are shown below.

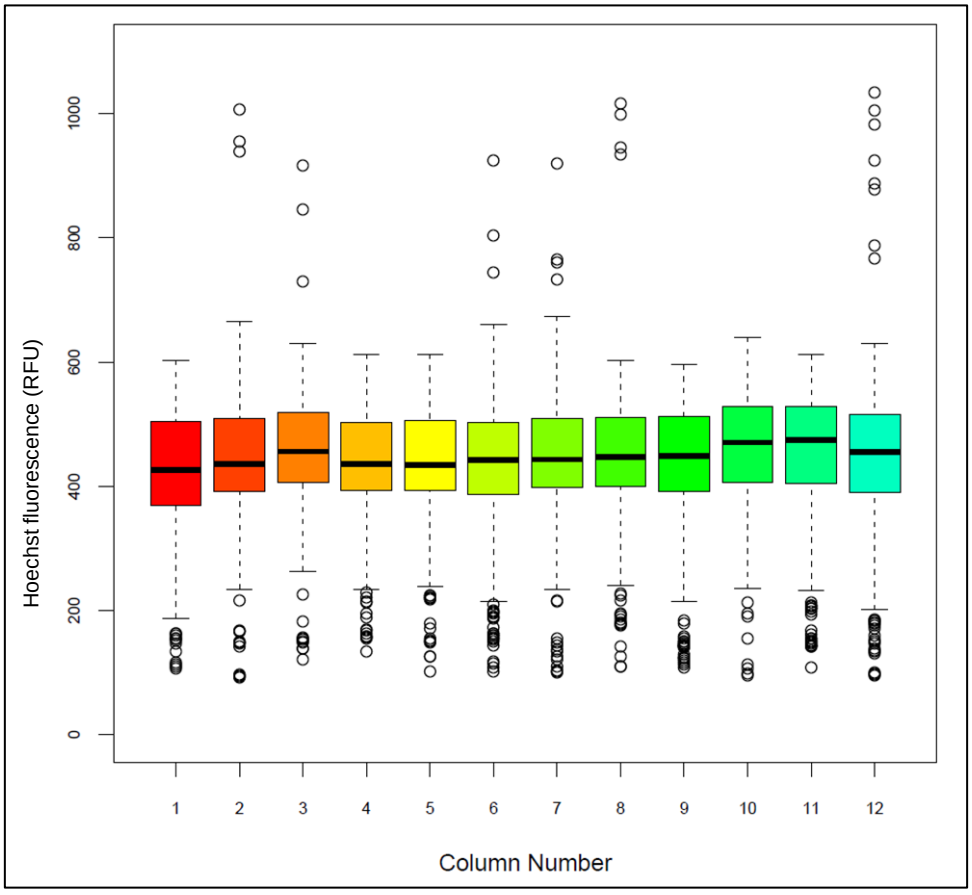

Figure 6.4 - Boxplot of Hoechst fluorescence plotted against column number for all screened plates.
Boxplot shows the interquartile range and median value, whiskers show maximum and minimum values (excluding outliers); outliers are represented by circles (values 1.5 times bigger or smaller than the quartiles).

Figure 6.4 represents collated data for the entire screen plotted against column number. The boxplot shows a uniform distribution of Hoechst fluorescence across all columns, indicating that there is not a significant difference between the edge columns and inner columns, this was confirmed using a Mann-Whitney U test (p=0.31).

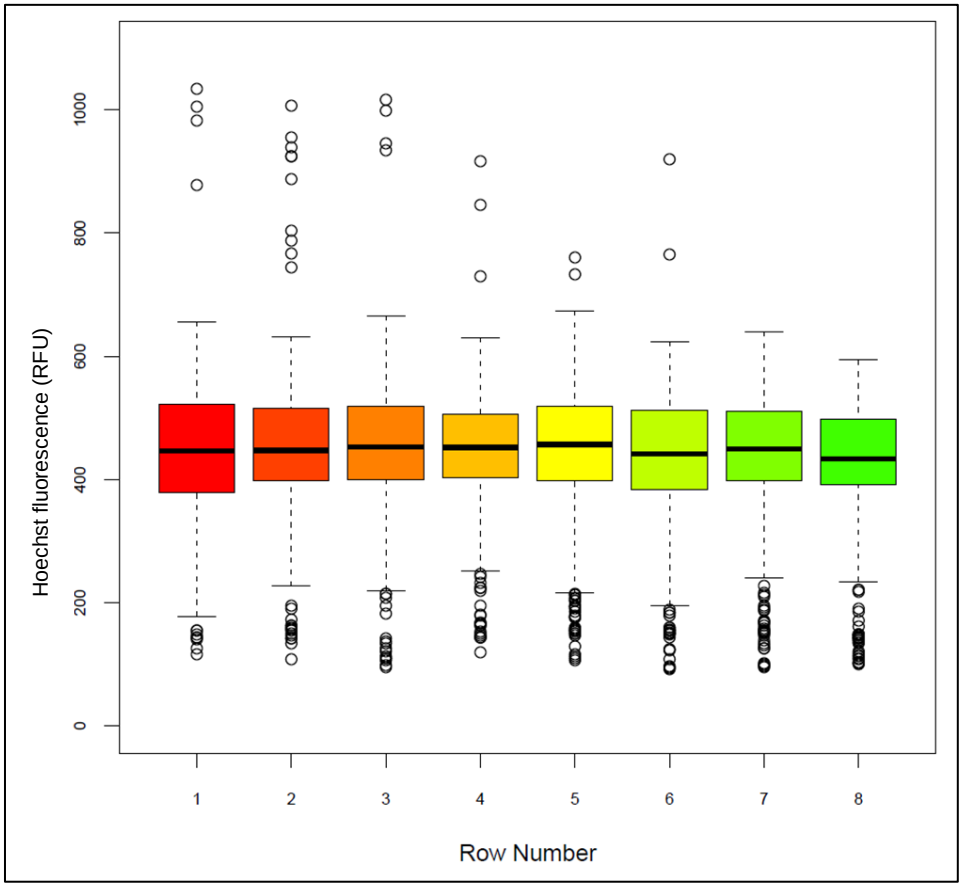

Figure 6.5 - Boxplot of Hoechst fluorescence plotted against row number for all screened plates.
Boxplot shows the interquartile range and median value, whiskers show maximum and minimum values (excluding outliers); outliers are represented by circles (values 1.5 times bigger or smaller than the quartiles).

Figure 6.5 shows the collated data for all screened extracts plotted against row number. As with the previous boxplot, there is no obvious difference in the variation of the data between row numbers, again a Mann-Whitney U test showed there was no significant difference between fluorescence detected in the wells of the edge rows when compared to the inner rows (p=0.11).

Although edge effects are common in plate based assays, the degree of any effect is dependent on the volume of liquid in the well, as this determines evaporation rates and heat retention. As this assay uses 96 well plates with 150µl of liquid per well, it is likely that this volume is sufficient prevent a severe edge effect being exhibited, whereas it is common for screens using 384 well plates to ignore the outermost wells as these are badly affected by edge effects due to the use of much smaller volumes (Lundholt et al. 2003).

6.4.4. **Normalisation**

Due to the different seeding times discussed in section 6.4.2 and shown in table 6.1, it was not possible to use cells from the same flask to seed all plates. Therefore prior to cell seeding, a culture was split into two T225cm^2 flasks to provide two batches of cells, one for each group of plates both with the same passage number.

The difference in seeding times and cultures may lead to different growth rates between the groups of cells, causing lower Hoechst fluorescence to be detected at the endpoint of the assay and consequently lower TMRM fluorescence. The Hoechst and TMRM fluorescence for the two no dose control plates – seeded on separate days- was analysed to see if there was a significant difference using a Mann-Whitney U test. The median values for both fluorophores and the significant difference between each plate are shown in Table 6.2.

Table 6.2 - Table showing the median values of Hoechst and TMRM fluorescence for day one and day two no dose control plates.

Plate	Hoechst median value	Significance (Mann-Whitney U test)	TMRM median value	Significance (Mann-Whitney U test)
Day one- ND control	508	**NA**	8209	**NA**
Day two- ND control	408.5	P<0.0001	6458	P<0.0001

Significant differences of day two plate from day one plate are shown, as calculated by a Mann-Whitney U test.

Due to the significant difference between the Hoechst and TMRM fluorescence for the control plates, it was necessary to normalise the two halves of the screen. The difference in cell number between the two plates is likely to be a constant across the entire screen, with the day one seeded plates showing a higher cell number than the day two plates after 72 hours growth. However, due to the effect the extracts may have on cell number, it is difficult to analyse the differences attributed to seeding time on an individual extract basis. Therefore a general normalisation factor was applied across the screen based on the behaviour of the no dose control plates. This factor was worked out by dividing the median value of plate one by the corresponding median of plate two to generate a factor for each dye:

Hoechst normalisation factor = 1.24

TMRM normalisation factor = 1.27

The fluorescent values obtained for all plates seeded on day two were multiplied by the appropriate factor. Due to the difference between the normalisation factors, the ratios of TMRM/Hoechst fluorescence were investigated to ensure that there was no significant difference between them after normalisation. This was important to ensure that the relationship between mitochondria and cell number was equivalent between the two seeding times, and that any changes in the level of TMRM/Hoechst are attributed to the extracts rather than being caused by normalisation.

Figure 6.6 shows the distribution of fluorescence measured from the two control plates, and the subsequent normalised fluorescence. The ratio of TMRM/Hoechst for each plate before and after normalisation is also shown. A significant difference between the day one and day two TMRM/Hoechst ratios was discovered, however this difference became non-significant after normalisation of the day 2 values ($p=0.204$) (figure 6.6 C). It is likely that this difference was due to pipetting error when preparing TMRM (due to the large volumes required to stain all plates) which could have caused an unintentional difference in concentration of the dye; this would also explain the need for a larger normalisation factor for the TMRM values. It is unlikely that there was variation in the concentration of Hoechst as all plates were stained with the dye on the same day and the same stock was used.

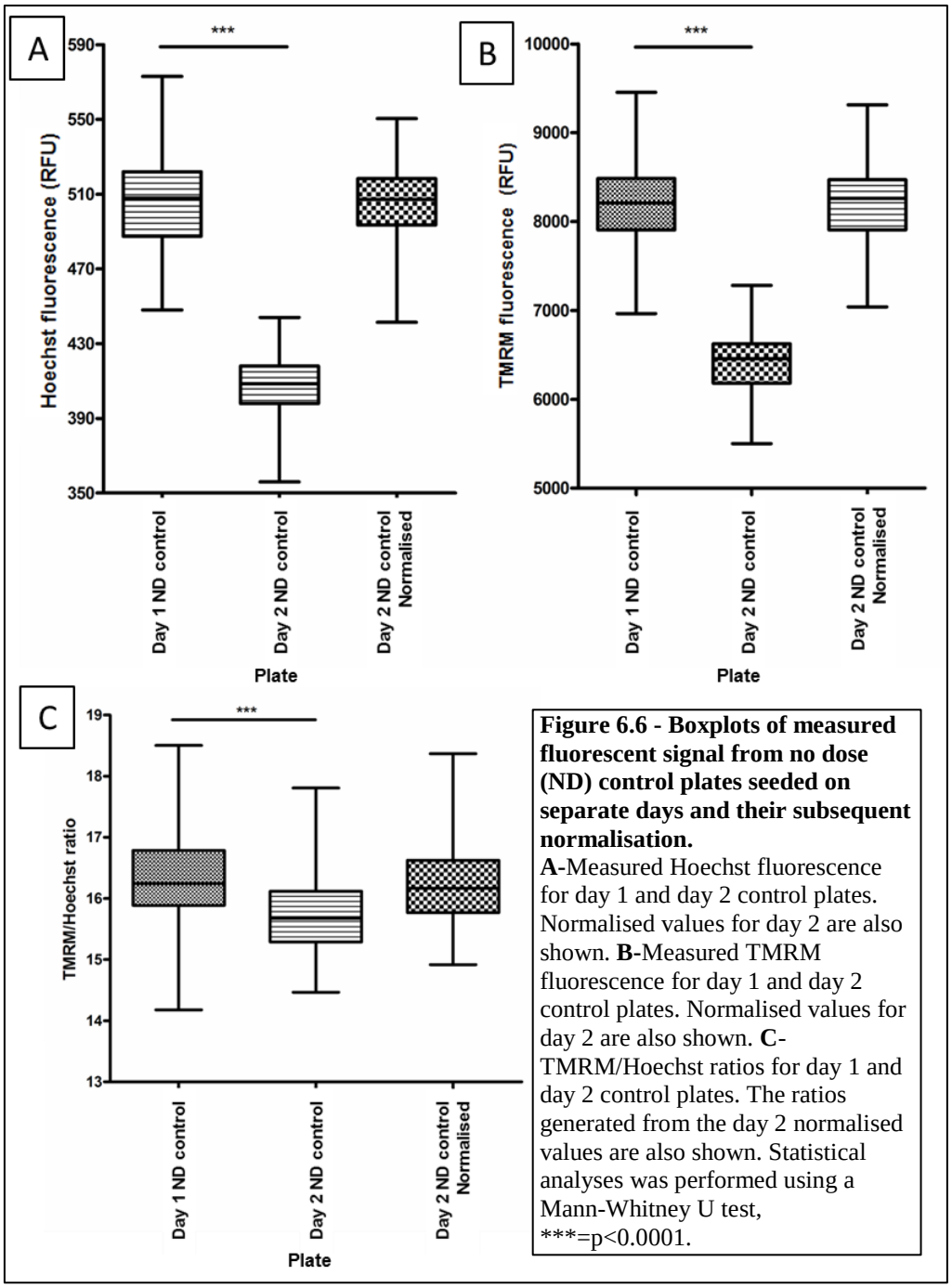

Figure 6.6 - Boxplots of measured fluorescent signal from no dose (ND) control plates seeded on separate days and their subsequent normalisation.
A-Measured Hoechst fluorescence for day 1 and day 2 control plates. Normalised values for day 2 are also shown. **B-**Measured TMRM fluorescence for day 1 and day 2 control plates. Normalised values for day 2 are also shown. **C**-TMRM/Hoechst ratios for day 1 and day 2 control plates. The ratios generated from the day 2 normalised values are also shown. Statistical analyses was performed using a Mann-Whitney U test, ***=p<0.0001.

Boxplots of fluorescence measured for individual wells were generated for each dye and arranged according to plate. Data is shown for both raw fluorescence and normalised fluorescence for Hoechst (figure 6.7) and TMRM (figure 6.8), plates contained in the boxes were subject to normalisation.

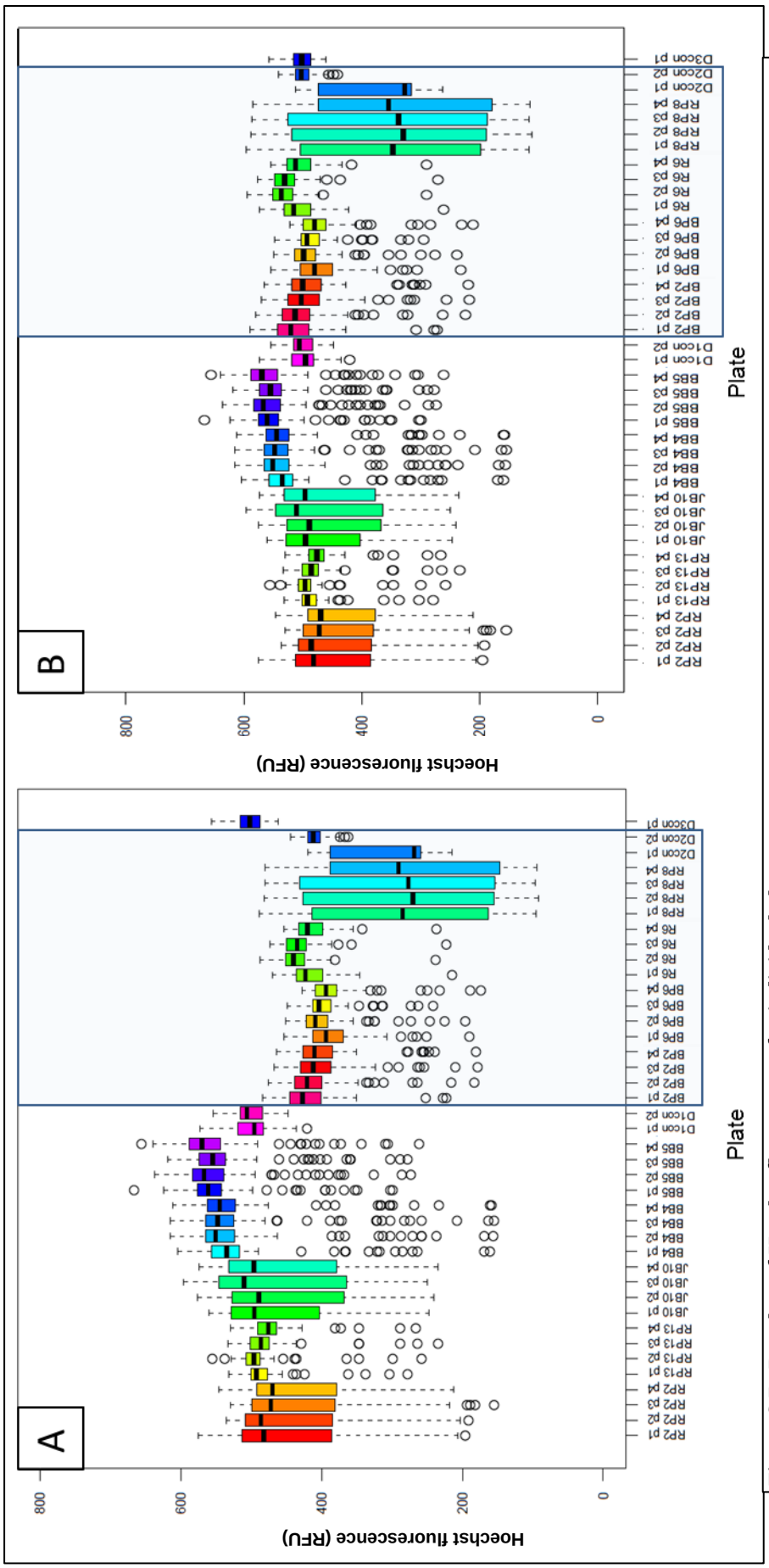

Figure 6.7 - Boxplots of Hoechst fluorescence for individual plates.
The blue box denotes plates seeded on the second day of the screen. **A** shows pre-normalisation values. **B** shows normalised values. Error bars show maximum and minimum values.

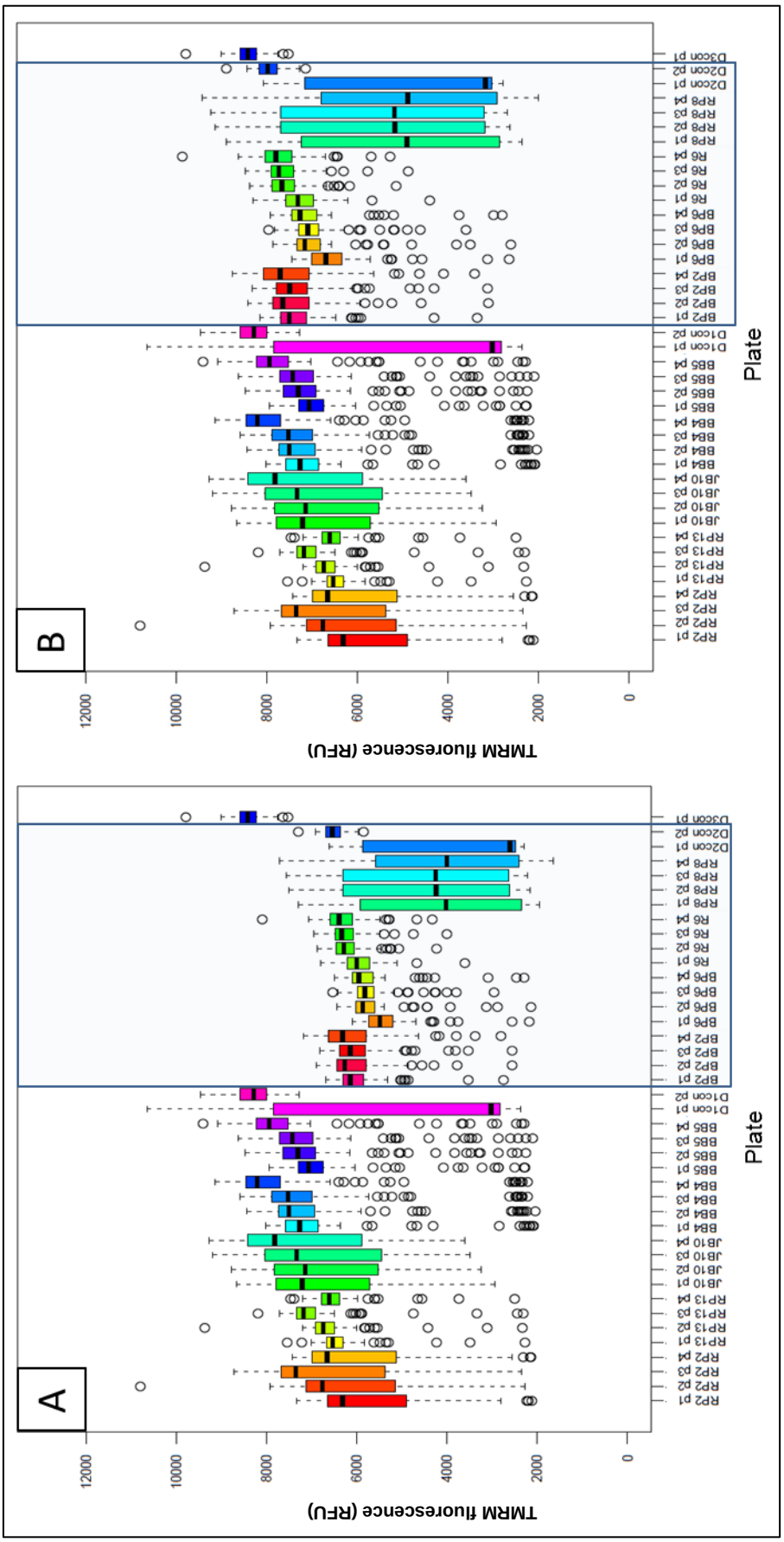

Figure 6.8 - Boxplots of TMRM fluorescence for individual plates.
The blue box denotes plates seeded on the second day of the screen. **A** shows pre-normalisation values. **B** shows normalised values. Control plate 1(Con 1) contains FCCP no dose controls, control plate 2 (Con 2) contains bezafibrate controls. Error bars show maximum and minimum values

6.4.5. **Mitochondrial mass analysis**

Following normalisation, data was analysed to assess changes in mitochondrial mass in HeLa cells. Data obtained from the plate reader was inputted into the statistical computing programme R which collated data and generated a data table containing information relevant for analysis using a code written by Dr Peter Banks (High throughput screening facility, Newcastle University) and optimised for this assay by myself. A mean RFU value for each fluorescent marker was produced for each compound screened; this included the three controls (FCCP, bezafibrate and no dose). Mean Hoechst values were plotted against mean TMRM values to investigate the relationship of mitochondrial mass to cell number for the entire screen (figure 6.9).

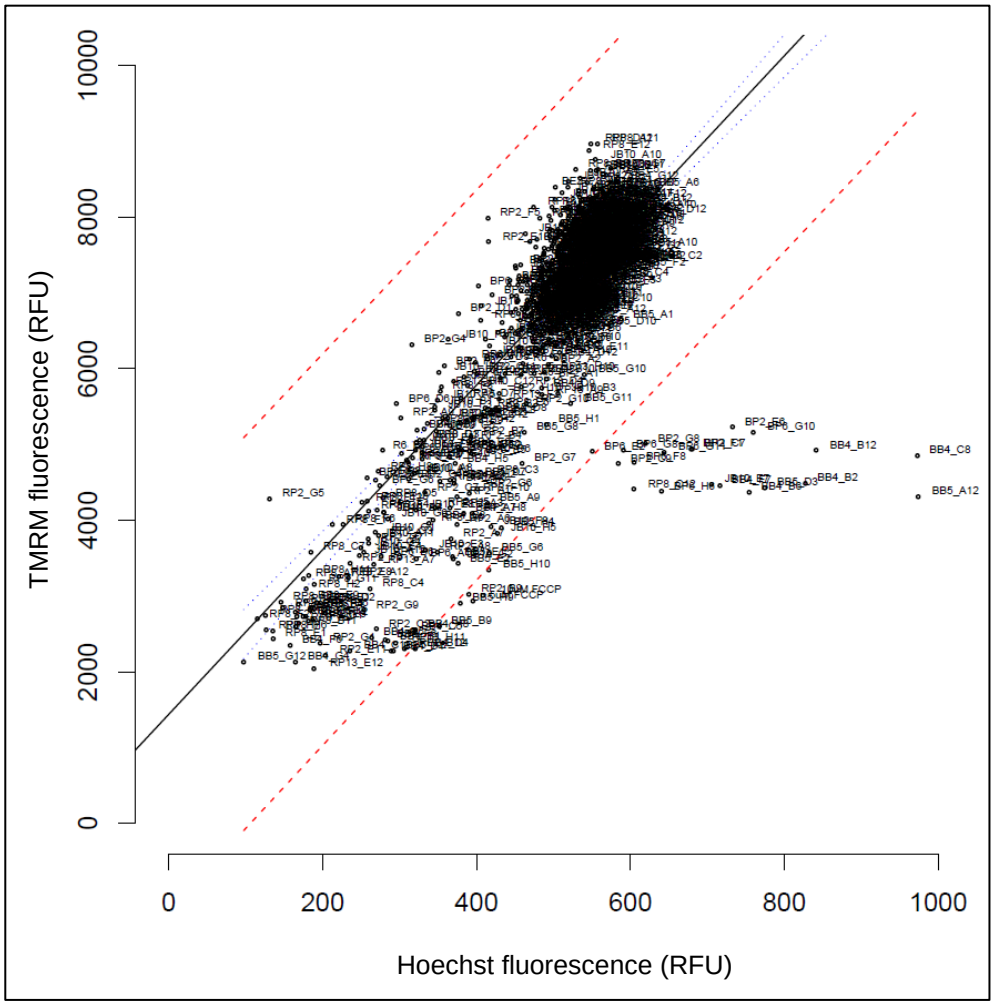

Figure 6.9 - Mean Hoechst fluorescence plotted against mean TMRM fluorescence for each compound.
Points are labelled with compound name. A trendline (black) was generated by calculating linear regression for all data points (r^2=0.571). The 99% prediction (red) and confidence (blue) intervals are also shown.

The r^2 value for the linear relationship was 0.571, which suggests that the relationship between mitochondrial mass and cell number isn't as strong as the relationship seen during assay development, where the linear relationship between the two was r^2=0.991. This difference could be due to a number of outliers that had relatively high Hoechst fluorescence; this could be caused by microbial infection- something that was monitored throughout the screen. Images were captured of cells after 24 hours incubation with the extracts during the screen. Each of these images was analysed to check for infection, in particular the wells affected by high Hoechst fluorescence. It was found that all of the wells in this outlier region had signs of bacterial contamination. Several wells showed signs of fungal infection, interestingly this type of infection caused higher TMRM fluorescence, images of two example wells are shown in (figure 6.10).

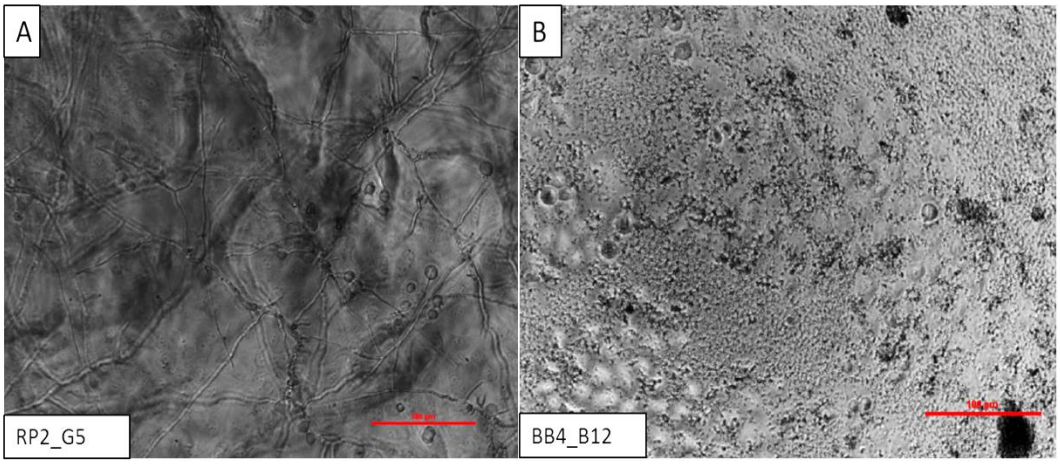

Figure 6.10 - Examples of infected wells.
A shows characteristic filament like fungal infection. **B** shows a punctate bacterial infection. Both images are labelled with the extract they were dosed with. Images were captured 24 hours after dosing. Scale 100µm.

All wells that were deemed to have been infected were removed from the analysis as the effect of the infection altered the fluorescent readings. In total 5.5% of extracts led to either a bacterial (in spite of the presence of penicillin and streptomycin in the media) or fungal infection.

The data was reanalysed and mean Hoechst fluorescence plotted against TMRM once again, this time with the infected extracts excluded (figure 6.11). The outliers have been removed and linear regression calculated from all data points. This is shown by the black trendline along with the 99% confidence (blue lines) and prediction (red lines) prediction intervals.

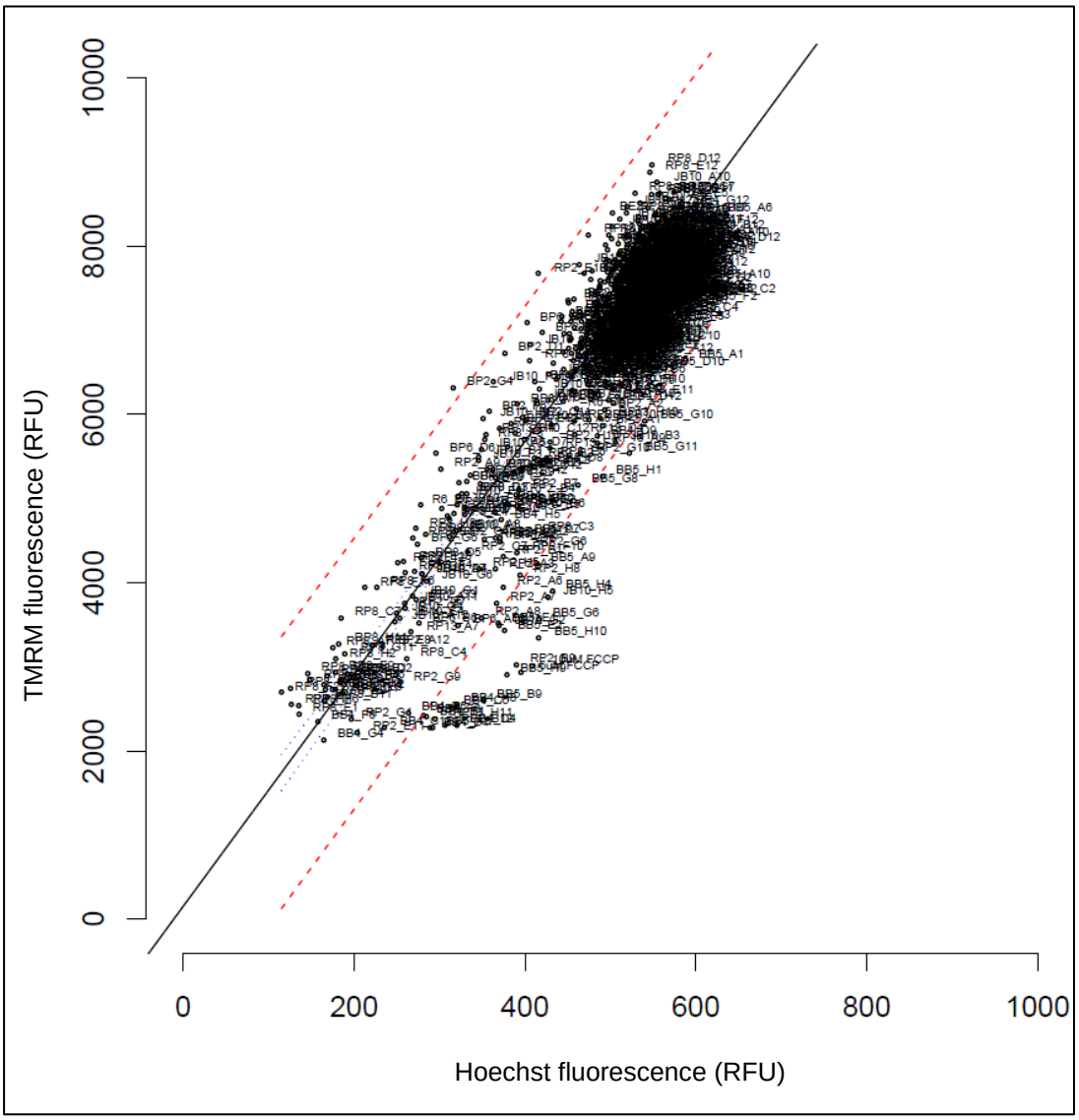

Figure 6.11 - Mean Hoechst fluorescence plotted against mean TMRM fluorescence for each compound.
Points are labelled with compound name. A trendline (black) was generated by calculating linear regression for all data points (r^2=0.8431). The 99% prediction (red) and confidence (blue) intervals are also shown.

Hoechst and TMRM fluorescence show a linear relationship (r^2=0.8431), indicating that as cell number increases so does mitochondrial mass. However, the relationship is not as strong as seen previously with different numbers of no dose control cells; however

this is likely to be because of the effect of the extracts causing a deviation from the normal relationship.

6.4.5.1. *Control molecules*

To understand graphically the distribution of the control molecules within the data obtained from extract treated wells, a graph was produced which labelled the control molecules only. The data from the extracts is shown as purple points, the control molecules; bezafibrate, no dose control, 10µM FCCP and 5µM FCCP are labelled as BEZ, EMPTY, 10uM FCCP and 5uM FCCP respectively figure 6.12. The same trendline, confidence and prediction intervals are shown as in figure 6.11.

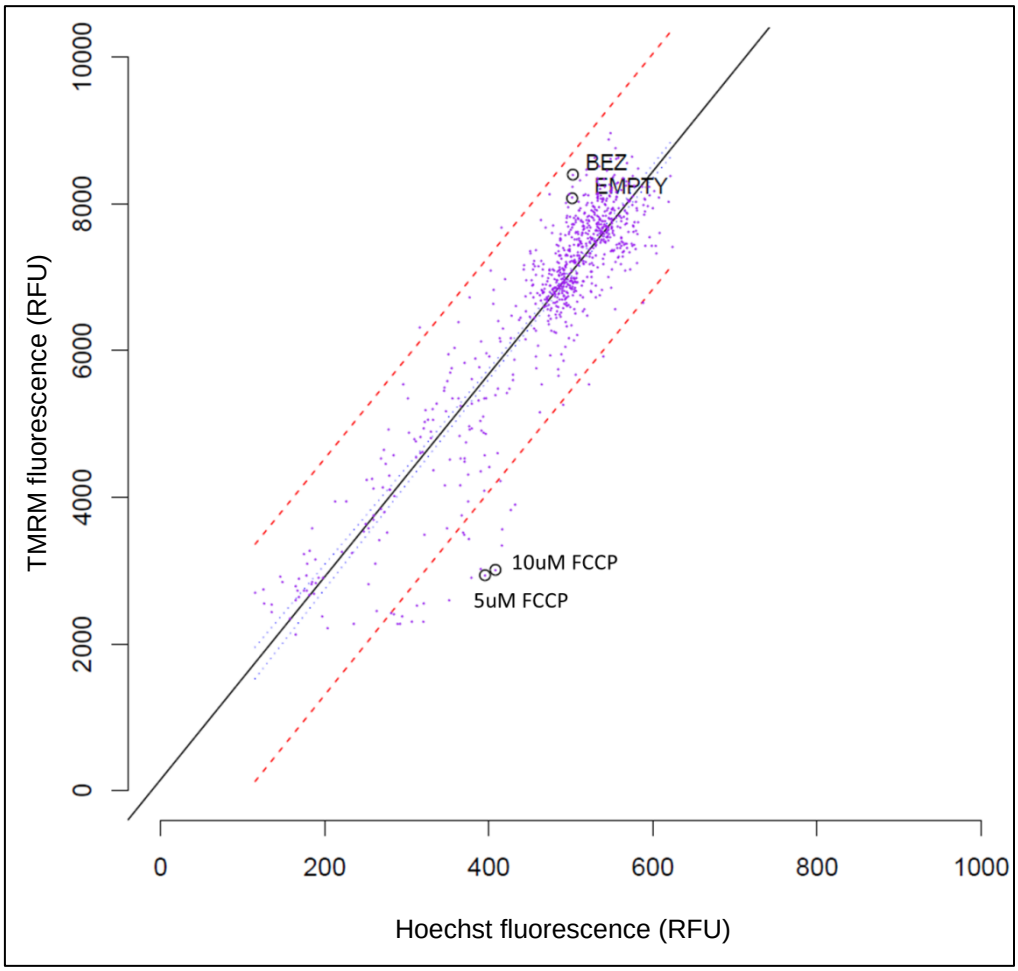

Figure 6.12 - Mean Hoechst fluorescence plotted against mean TMRM fluorescence for each compound.
Control molecules are represented by black circles and labelled accordingly. Purple points represent extract treated cells. A trendline (black) was generated by calculating linear regression for all data points (r^2=0.8431). The 99% prediction (red) and confidence (blue) intervals are also shown.

Bezafibrate and no dose controls are found in the region of the graph with the highest levels of TMRM fluorescence, with bezafibrate showing a greater level of TMRM fluorescence than the no dose control, for approximately the same cell number indicating an increase in mitochondrial mass. The FCCP controls show a relatively low amount of TMRM fluorescence for their cell number, indicating a decrease in mitochondrial mass. In general there was a lower level of TMRM fluorescence detected in cells treated with the extracts than in the no dose controls. This could be due a toxic effect caused by the extracts which leads to a lower level of TMRM fluorescence, however to investigate this fully will require further experimentation.

To verify that the positive and negative control molecules increased or decreased mitochondrial mass when compared to the no dose control, the TMRM/Hoechst ratio was calculated for individual wells treated with the control molecules (figure 6.13).

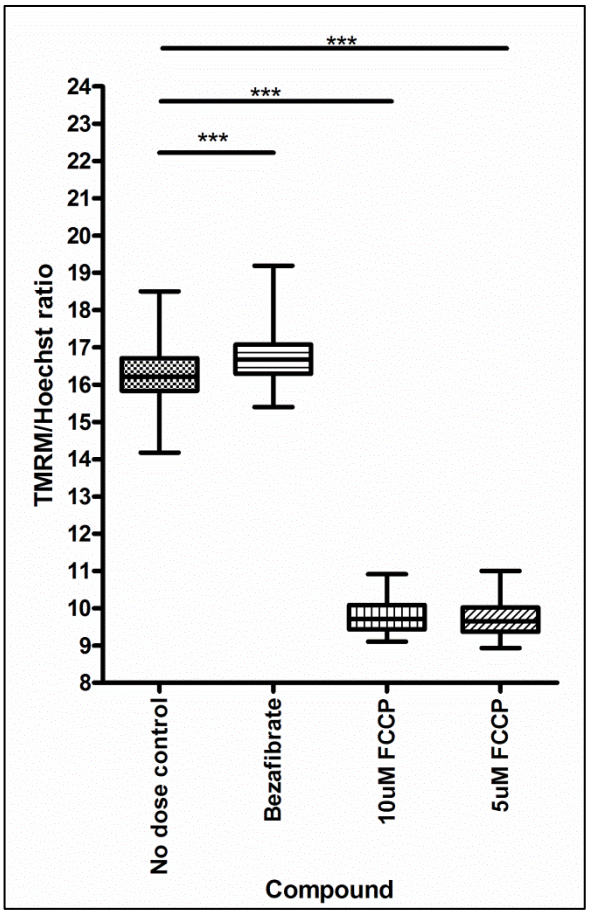

Figure 6.13 - TMRM/Hoechst ratios of HeLa cells treated with controls as part of a high throughput screen. 450µM bezafibrate was incubated with the cells for 48 hours. FCCP controls were incubated for 22 hours prior to medium changes. Significance was determined using a Mann-Whitney U test. ***=p<0.0001

There was a significant increase in mitochondrial mass caused by 450µM bezafibrate when compared to the no dose controls ($p<0.0001$, Mann-Whitney U test). A significant decrease in mitochondrial mass was found in cells treated with either the 5µM FCCP ($p<0.0001$) or 10µM FCCP ($p<0.0001$) negative controls when compared to the no dose control. Interestingly there was no significant difference in mitochondrial mass between the two FCCP controls, indicating that there was a similar effect of both concentrations on the removal of mitochondria through autophagy (Saita et al. 2013).

6.4.5.2. *Statistical analysis of changes in mitochondrial mass*

In order to determine which extracts generated the greatest increase in mitochondrial mass, a mixed model was used to investigate the effect of Hoechst fluorescence on TMRM fluorescence. A no intercept mixed model was chosen as preliminary analysis of the data indicated that the relationship between Hoechst and TMRM fluorescence was linear. This model enabled the integration of a random effect, in this case the extract or controls incubated with the cells, and its effect on the relationship between the fixed effects - Hoechst and the variable dependent -TMRM fluorescence (McLean et al. 1991). This will enable the identification of extracts that have the highest TMRM fluorescence in relation to Hoechst fluorescence, and therefore have caused an increase in mitochondrial mass.

The fixed part of the mixed model consisted of a single parameter, the gradient, defining the average relationship between Hoechst and TMRM fluorescence. The random part of the model identified the deviation for each extract or control molecule from the average gradient, allowing the identification of those extracts which had the greatest effect on the TMRM/Hoechst relationship. The residuals of this model were analysed and verified as normally distributed to validate the model.

Table 6.3 shows a list of extracts that led to an increase in mitochondrial mass, according to the mixed model, when compared to the no dose controls. The data is sorted according to the gradient value (the larger gradients indicate increases in mitochondrial mass); the mean and standard deviations for each fluorophore along with the TMRM/Hoechst ratios are also shown. Data is also shown for the FCCP controls;

which predictably led to the two largest decreases in mitochondrial mass for the entire screen. For a comprehensive list of the effects of every extract please see appendix A.

Table 6.3 - List of extracts that have increased mitochondrial mass in relation to control molecules.

Compound	Mean TMRM	TMRM SD	Mean Hoechst	Hoechst SD	TMRM/Hoechst ratio	Gradient
BP2_G4	6310.76	243.72	315.98	9.86	19.97	4.600
BP2_D1	5534.23	213.13	295.85	9.89	18.71	3.484
RP8_F2	2694.68	408.46	114.99	2.08	23.44	3.070
BP6_F4	7083.63	310.84	402.30	11.20	17.61	2.986
JB10_F11	6382.75	177.44	363.00	7.16	17.58	2.866
RP8_C10	2743.17	204.42	125.36	9.42	21.88	2.847
RP2_A9	5349.25	288.77	301.25	14.31	17.76	2.794
RP13_G5	8133.75	877.37	474.00	29.03	17.16	2.729
RP8_F11	3939.69	395.85	212.59	36.74	18.53	2.669
R6_E6	4919.96	384.35	277.86	14.31	17.71	2.666
RP8_C7	3578.57	431.05	184.53	51.71	19.39	2.642
RP8_F9	2923.73	260.09	145.79	10.18	20.05	2.627
Bezafibrate	8398.41	329.00	502.60	18.65	16.71	2.556
JB10_H7	7775.50	596.87	463.50	22.40	16.78	2.358
RP8_A7	3224.77	508.10	174.77	15.09	18.45	2.348
JB10_H12	5949.75	315.69	350.75	18.93	16.96	2.305
JB10_H4	6819.00	1941.41	406.00	123.33	16.80	2.252
RP8_H7	2544.92	303.19	126.27	4.73	20.15	2.247
RP2_E10	7669.25	2096.47	415.50	175.04	18.46	2.223
RP8_C8	2839.25	108.19	148.23	18.91	19.15	2.199
RP8_F6	3946.40	543.51	226.31	29.73	17.44	2.185
RP8_H11	3268.38	125.22	181.78	10.11	17.98	2.098
JB10_H11	8228.50	195.12	502.00	17.51	16.39	2.031
RP8_D12	8964.26	284.30	548.39	19.48	16.35	2.026
RP8_H8	4641.49	544.31	272.06	53.02	17.06	2.022
R6_H7	8134.35	385.31	498.07	16.65	16.33	1.989
JB10_H2	8462.50	285.00	519.00	12.83	16.31	1.974
RP8_B3	8624.79	680.50	528.87	47.96	16.31	1.974
RP8_B10	7671.36	261.67	469.09	22.29	16.35	1.967
No dose control	8078.38	717.86	501.59	23.30	16.11	1.963
5uM FCCP	2938.67	207.23	395.25	87.91	7.44	-6.994
10uM FCCP	3003.26	238.22	408.09	91.82	7.36	-7.110

The data is sorted by gradient size, largest to smallest. Gradients were generated using a mixed model and indicate the quantity of TMRM fluorescence in relation to Hoechst. Mean values and standard deviations for both fluorophores are also shown. Only extracts that increased mitochondrial mass in relation to the no dose control are shown. The FCCP controls are also shown.

6.4.6. **Selection of active extracts**

A set of criteria were developed to determine which extracts to investigate further. This was necessary as it was important to ensure that the effect of the extracts on mitochondrial mass was significant in order to prevent the investigation of false positives. The criteria were as follows:

- A gradient greater than that of bezafibrate.
- A TMRM/Hoechst ratio that was significantly higher (Mann-Whitney U test) than that of bezafibrate.
- A standard deviation of TMRM fluorescence smaller than 5% of the mean TMRM RFU value.

Only extracts that caused a greater increase in mitochondrial mass than the positive control, bezafibrate, were selected for continued investigation as the aim of the screen is to discover a compound that has higher efficacy than bezafibrate. It was also essential that TMRM/Hoechst ratios of treated cells were significantly increased in comparison to bezafibrate controls. Significance was calculated using ratios generated from the repeated doses. Extracts with standard deviations smaller than 5% of the total TMRM fluorescence were chosen. It was important to only pick extracts with the smallest standard deviations to ensure that the effect they had on mitochondrial mass was similar for all repeats and not just due to experimental error or a random effect on one well. Extract RP8_F2 was not taken forward as it caused excessive cell death (Hoechst value of 114). The extracts that met these criteria- "hit" extracts- are shown in table 6.4.

Table 6.4 - List of extracts that meet the criteria set out in section 6.4.6.

Compound	Mean TMRM/Mean Hoechst ratio	Gradient	SD as percentage of mean TMRM	P value
BP2_G4	19.972	4.600	3.862	p<0.0001
BP2_D1	18.706	3.484	3.851	p=0.0026
BP6_F4	17.608	2.986	4.388	p=0.0059
JB10_F11	17.583	2.866	2.780	p=0.0077
Bezafibrate	**16.710**	**2.556**	**3.917**	**N/A**

TMRM/ Hoechst ratio, gradients (generated from a mixed model) and standard deviation (SD) as a percentage of mean TMRM fluorescence are shown. P values were calculated using a Mann-Whitney U test to compare the TMRM/Hoechst ratios of extracts to bezafibrate.

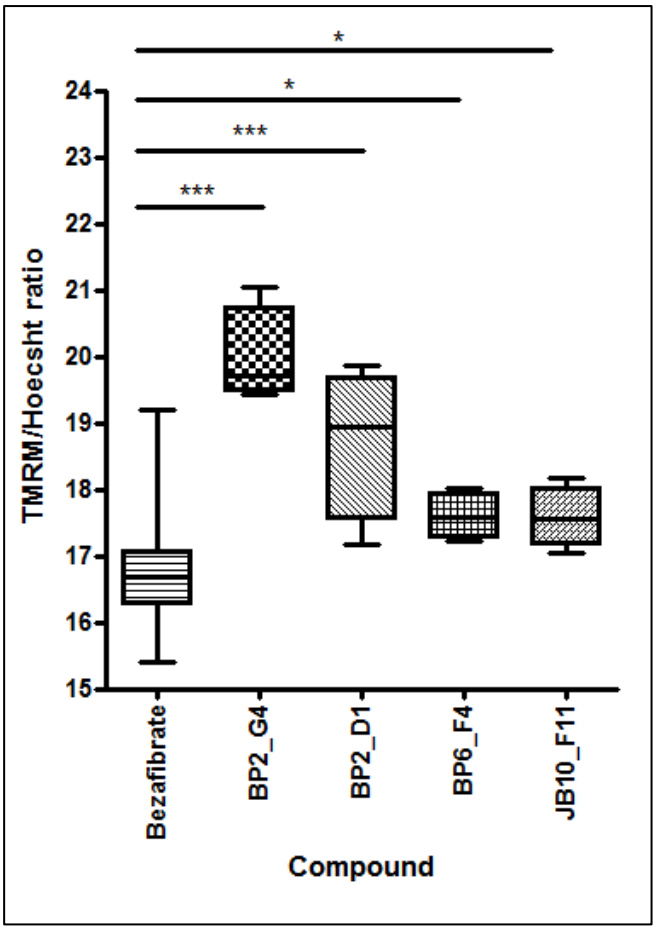

Figure 6.14 - Boxplots of TMRM/Hoechst ratios of bezafibrate and "hit" extracts.
Statistical significance was calculated using a one way ANOVA test, ***=p<0.0001, *=p<0.05.

The relationship between of mitochondrial mass per cell for each of the "hit" extracts is shown in figure 6.14; significance was calculated using a Mann-Whitney U test. The graph shows that extract BP2_G4 caused the largest increase in mitochondrial mass of any compound used in the screen, including bezafibrate ($p<0.0001$). Extract BP2_D1 also caused a significant increase in mitochondrial mass when compared to bezafibrate ($p<0.0001$). There was a large amount of variation of the TMRM/Hoechst ratios, as shown by the large spread of data in figure 6.14, even though the standard deviation of the mean met the criteria developed earlier. The variation is caused by the fact that the repeat with the lowest detected TMRM fluorescence had the highest cell number; therefore a lower TMRM/Hoechst ratio was generated. The final two selected extracts; BP6_F4 and JB10_F11 also showed a significant increase in mitochondrial mass when compared to bezafibrate.

Prior to further analysis, the fluorescent properties of the extracts were investigated to ensure that the increase in TMRM signal was not due to the extracts emitting 561nm light. The amount of emitted 561nm light was measured for a 1 in 50 dilution in ddH_2O of each extract (3 repeats of each extract) using the plate reader. A 75nM TMRM control and H_2O control was also measured (figure 6.15). None of the extracts emitted any fluorescence in the 561nm region of the spectra and it was therefore decided to confirm changes in mitochondrial mass using microscopy.

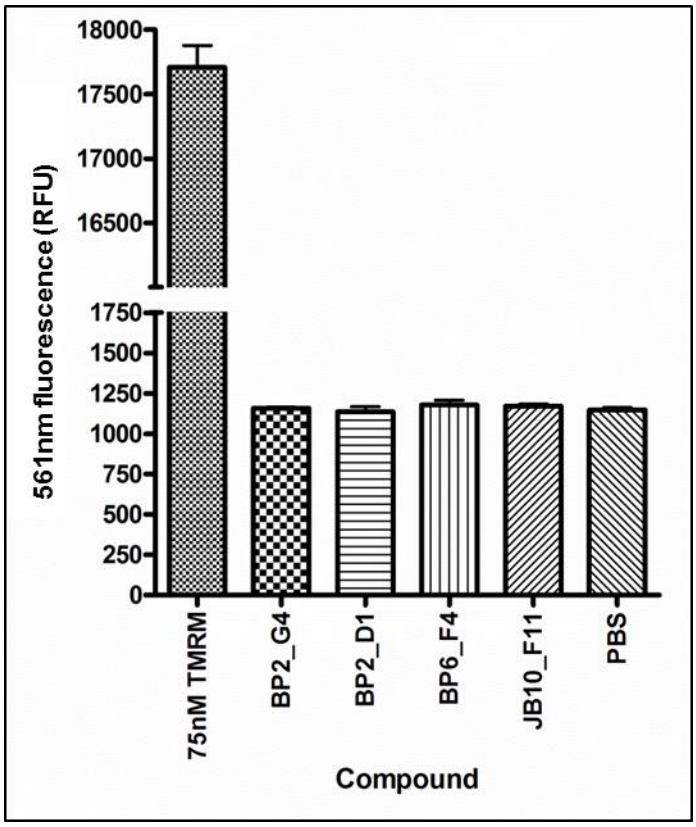

Figure 6.15 - 561nm fluorescence emitted by individual extracts, 75nM TMRM and H_2O.
Emitted fluorescence from a 1 in 50 dilution of each extract was measured in triplicate using a plate reader along with TMRM and H_2O controls. Error bars represent standard error of the mean (n=3).

6.4.7. **Mitochondrial mass quantification using microscopy**

HeLa cells were seeded on glass bottomed 96 well plates (1 x 10^5cells/well) in antibiotic containing HeLa media. Each extract was diluted 1 in 10 in media prior to sterilisation through a 0.22µm filter, after which a volume of extract was added to the first well to create a 1 in 50 dilution of the original extract concentration. A 1 in 4 serial dilution was then performed across 3 wells generating 1 in 40, 1 in 160 and 1 in 640 dilutions of the original extract. The starting dilution was chosen to ensure continuity with the drug screen. Cells were dosed with the same batch of extract that was used in the screen along with a fresh batch of extracts produced from a new bacterial culture, to ensure that any effect is reproducible and does not rely on extract batch.

After 48 hours incubation, culture cells were stained with 10nM TMRM and 2µM Calcein Blue for 45 minutes before washing in Phenol red free HeLa media and imaging using a Nikon A1R confocal microscope (60x magnification). Imaris software was used to define the area covered by each stain, TMRM stained mitochondria (Figure 6.16 panel B), Calcein Blue stained cytoplasm (Figure 6.16 panel C), and then to work out the proportion of mitochondria (TMRM) to cell volume (Calcein), a sample image is shown in figure 6.16, with the rendered computer generated image of the two stains shown in panel D. Four images per concentration were captured, each containing 5 cells; the proportion of mitochondria was calculated for each image and the data grouped together (figure 6.17). It should be noted that this experiment was blinded until after analysis of the data to prevent bias at any stage.

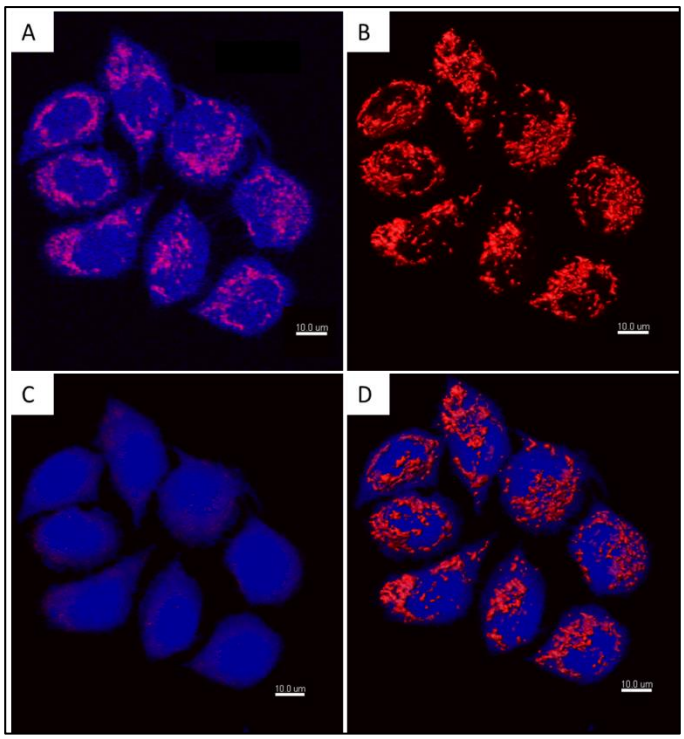

Figure 6.16 - HeLa cells stained with 10nM TMRM and 2µM Calcein Blue and the quantification of their respective areas .
Imaris software was used to detect and calculate the areas stained by each dye . The raw image is shown in panel A. Panel B shows a rendered image highlighting the TMRM staining only, C shows a rendered image of Calcein Blue cytoplasm staining only, D shows the reconstructed image which was used to calculate the proportion of mitochondria per cell area.

Figure 6.17 shows changes in mitochondrial mass after treatment with various concentrations of the selected extracts. The graph in figure 6.17 shows that only one extract, BP2_G4 had an effect on mitochondrial mass with the most concentrated dose for each batch showing a doubling in mitochondrial mass per cell. The original batch of this extract caused a dose dependent increase in mitochondrial mass, with the lowest dose (1 in 640 dilution) showing no effect. The new batch of extract showed a similar increase when used at 1 in 40, however the 1 in 160 dilution led to a greater increase in mitochondrial mass than any other. The reason for the difference in potency between batches could be due to the fact that it is impossible to know the concentration of the extract, so although the dilutions are the same, the concentration of the active compound is likely to vary between batches. Therefore the concentration range used provides an insight into the active concentration range for use in further experiments.

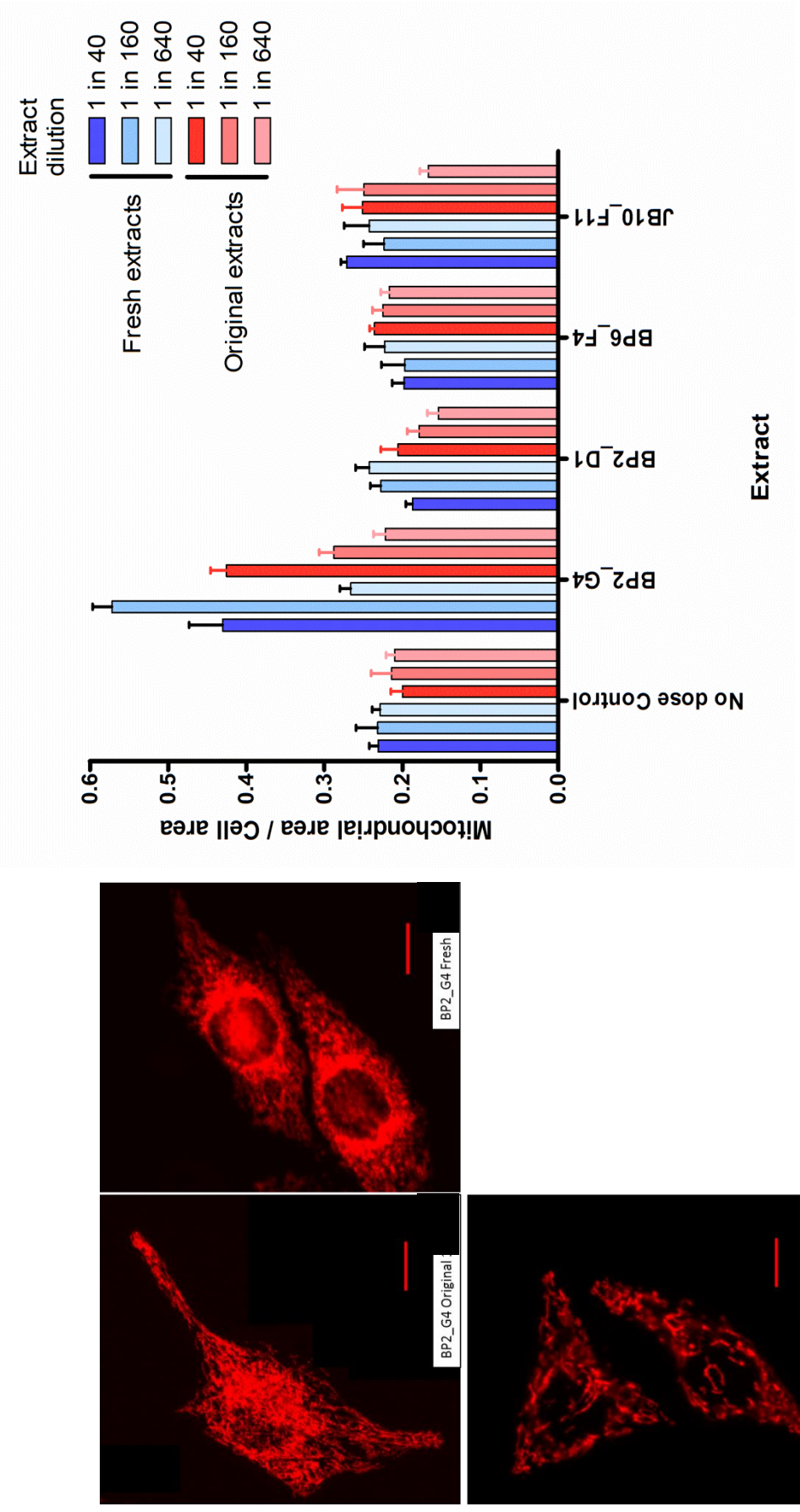

Figure 6.17- Changes in mitochondrial mass as a result of treatment with pre-screened bacterial extracts.
Sample images for the best performing extract BP2_G4 (1 in 40 dilution) along with a no dose control are shown (scale is 10µm). BP2_G4 treatment led to increases in mitochondrial mass compared to no dose control cells; no other extract had an effect on mitochondrial mass. The effect of extract dilution is also shown by the graph. Error bars represent standard error of the mean of analysed cells (n=20).

6.5. DISCUSSION

High throughout screens are an essential tool in drug discovery, enabling thousands of compounds to be investigated in a relatively short period time. The screen used in this chapter was designed to highlight compounds which increase mitochondrial mass in HeLa cells; an ability that was verified both in this chapter and the previous chapter through the use of control compounds.

By working in collaboration with our partner Demuris Ltd. it was possible to investigate a range of diverse compounds that have previously never been investigated for changes in mitochondrial mass. Many of the strains that produce the extracts are unique to this library and although 864 extracts were analysed in the final screen, the extracts are by no means homogenous with each one containing hundreds of different compounds. Therefore the screen is actually investigating potentially tens of thousands of compounds.

6.5.1. **Active extracts**

The screen was carried out with the aim of finding a compound that could increase mitochondrial mass to a greater extent than bezafibrate – a compound that has shown efficacy at improving mitochondrial function in animal models (Dillon et al. 2012). Although the screen indicated that 12 extracts achieved this (table 6.3), it was decided to exclude extracts that caused non-significant increases in mitochondrial mass or large standard deviations in cell number (this indicated that the extract was not affecting all repeats in the same manner and may not be reproducible). It was also decided to exclude extracts that exhibited high levels of toxicity (Hoechst fluorescence <200 RFU).

The remaining four extracts were investigated further by microscopy and one extract; BP2_G4, was found to cause an increase in mitochondrial mass. No increase was found in cells treated with other extracts even though the screen indicated that they had caused significant increases. This discrepancy could be due to the extracts causing an increase in mitochondrial membrane potential which in turn would enable more TMRM to accumulate in mitochondria and therefore emit a greater amount of fluorescence, indicating an increase in mitochondrial mass. Conversely the increase in TMRM

fluorescence could be due to a lower membrane potential caused by the extracts. As 75nM TMRM is likely to be in "quench mode", a decreased membrane potential may prevent the quench and cause a larger signal as the fluorescence from TMRM increases. However this is likely to require a large fall in membrane potential and both scenarios will require further investigation.

6.5.2. **BP2_G4 causes an increase in mitochondrial mass**

Extract BP2_G4 caused a significant increase in mitochondrial mass ($p<0.0001$ Mann-Whitney U test) when compared to no dose controls. Data from the original screen showed that there were fewer cells at the end of the assay than in no dose controls. This could indicate toxicity from either the active compound or another compound in the extract. The lower cell number could also be due to the fact that mitochondrial mass increased from ~20% to over 40% of total cell volume. This increase may cause a diversion of cellular resources from other areas to the growth and maintenance of mitochondria, which in turn may cause damage to accumulate in the cell, which may eventually become unviable. It is unlikely that the extract inhibits cell division as the Hoechst fluorescence was 315 RFU at the endpoint, which according to data obtained during development of the assay equates to ~2.5×10^4 cells/well. This number of cells indicates that at least 2 divisions have occurred since seeding (5×10^3 cells/well) and as HeLa cells double every 18-24 hours a division must have occurred ~24 hours after dosing with the extract.

The effect of the extract in other cell-lines also needs to be investigated in order to see if extract induced changes in mitochondrial mass is specific to HeLa cells. These experiments will be carried out using the microscopy techniques described previously and also western blots to semi-quantify changes in mitochondrial markers. If changes in mitochondrial mass are seen in other cell-lines then the extract will be fractionated in order to identify the active compound. This will enable investigation into the mechanism of mitochondrial mass increase and will also enable the creation of dose-response curves which will show the concentration range over which the compound is biologically active. The effect of the active compound on OXPHOS will also be investigated and analysed using a Seahorse XF analyser to measure oxygen consumption of OXPHOS deficient patient cell lines.

Although extensive further work is necessary, the discovery of BP2_G4 highlights the fact that there are naturally occurring compounds that have the potential to increase mitochondrial mass and possibly act to increase ATP production in patients with mitochondrial disease.

6.6. CONCLUSIONS

The need to discovery mitochondrially acting drugs is essential if mitochondrial diseases are ever going to be treated effectively. This work has shown that it is possible to develop a relatively simple screen to detect changes in mitochondrial mass. By discovering the hit extract I have shown that natural products may have the ability to act on mitochondrial biogenesis. Although the screen was relatively small compared to industrial sized screens, the use of the Demuris library, which contained mixtures of compounds within one extract, may be beneficial as it may contain synergistic compounds, the effect of which would have been missed if screening single compounds. This may also be a hindrance as the action of one compound within an extract may be inhibited by another, preventing a pharmacological action that would otherwise have been discovered if screening individual compounds. However, it is clear from this work that although the extracts are not pure, they still have the ability to have a biological effect. With future work focussing on the isolation of the active compound, it may be possible to develop a drug with the ability to improve mitochondrial function.

Final Discussion

Final Discussion

The development of treatments for mitochondrial disease is vital for improving the prognosis of patients affected by these disorders. Currently there are no effective treatments for mitochondrial dysfunction and, as a result of this deficit, clinicians can only modulate the symptoms of the disorders; it is therefore inevitable that patient's conditions progress. This project aimed to address this by investigating novel treatment options through the development of two different paradigms; a targeted, mutation specific approach using anti-genomic CMCOs, and a broad drug screen aimed at discovering compounds to increase mitochondrial mass.

7.1. CMCO DEVELOPMENT

Targeting therapeutics to mitochondria is a complex issue as the trafficking of molecules into and out of the matrix is a tightly regulated process. Therefore delivery of proteins or small molecules across the inner mitochondrial membrane is facilitated by specific carrier proteins which, in the case of peptide transport require specific recognition factors to be present on the substrate. Delivery of an anti-genomic compound to the matrix will therefore rely on manipulating one of these transport systems in order to cross the inner membrane.

Current leaders in this field utilise the TOM/TIM peptide transport system to deliver enzymes that can specifically recognise and induce a double strand break in mutated mtDNA genomes, leading to mtDNA degradation (Srivastava and Moraes 2001; Tanaka et al. 2002; Bacman et al. 2013). The use of TALENS is an approach that has shown excellent efficacy in cell models, however, delivery to the cells of a patient is difficult as it requires an efficient transfection mechanism that is currently unachievable for delivery to affected tissues in man (Bacman et al. 2013). Therefore I attempted to specifically target anti-sense oligomers – which do not require specific transfection for cellular delivery - to the mitochondrial matrix, where they would be able to recognise and hybridise to mutated mtDNA genomes, preventing their replication *in vivo*. Although the inner membrane is generally impermeable to charged molecules, lipophilic cations have been shown to accumulate within the matrix after diffusing

across the inner membrane. To exploit the ability of this class of molecules to diffuse across the inner membrane, I used CMCOs, a class of oligomers with this ability (Posch et al. 2012).

Conjugation of mitochondrial specific stains (TAMRA and ATTO 647N), along with 2,4-mononitrophenol to the CMCOs enabled the specific localisation to mitochondria, with ATTO 647N-CMCOs showing the strongest localisation (chapter 3). The sub-mitochondrial localisation of the CMCOs is unclear however as current microscopy techniques cannot resolve the fine structure of mitochondria. Super resolution techniques could be used, however these currently require fixation prior to imaging, which in the case of CMCOs is not possible as they are not retained within mitochondria after membrane depolarisation The "gold standard" test to prove matrix localisation is to detect a functional effect on the mtDNA or the levels of COXI protein, however no such effect was conclusively proven during this project (chapter 4).

Although more repeats are needed to fully understand the functionality of CMCOs, an absence of activity could be due to numerous factors, such as lack of matrix localisation or an inability of the CMCO to bind mtDNA or mt-mRNA i*n vivo*. It could also be possible that the CMCOs are in fact binding a minority of *MTCOI* mRNA and preventing its translation, but other populations of *MTCOI* mRNA could be disguising a CMCO related inhibition. However, the experiments used in this project mean that it is impossible to resolve the reason for this, as it is still unclear if the CMCO has access to mtDNA (chapter 3). Therefore it is difficult to draw firm conclusions about the effectiveness of CMCOs at selectively binding mtDNA *in vivo*, except that it was not obviously occurring during the experimentation described within this thesis (i.e. there was not a dramatic shift in mtDNA copy number). After consultation with our partners, Ugichem, who are keen to support the project, it has been decided to redesign the panel of experiments carried out on the CMCOs.

As it is difficult to infer the reasons for a lack of functional effect without knowing the sub-mitochondrial localisation of the oligomers, future experiments will focus on ascertaining this. A new batch of CMCOs, all with the new proprietary side chain, will

be produced by Ugichem, which will be incubated with cells or isolated mitochondria. After incubation, the mitochondria will be centrifuged through oil (in the case of whole cells, mitochondria will first be extracted) in order to remove any unbound CMCO from the outer mitochondrial membrane. The mitochondria will then be lysed and the contents used in a gel shift assay in order to detect the presence of the CMCOs after hybridisation with a complementary probe. This will answer the first question – are CMCOs capable of entering mitochondria, both *in vivo* and *in vitro*.

If the CMCOs are not shown to enter mitochondria, the project will be abandoned. If they are capable of entering mitochondria, the sub-mitochondrial localisation will be determined. This could be achieved by repeating the oil centrifugation experiment, after which the mitochondrial outer membrane can be shaved off and the contents of the intermembrane space removed. If CMCOs are detected in the inner membrane/matrix fraction then it is likely that the CMCO has accessed the matrix, or become sequestered in the inner membrane. Experience from using this technique to determine the sub-mitochondrial localisation of proteins has shown that it requires numerous repeats in order to be certain of the localisation as fractionation of mitochondria does not always yield 100% pure fractions, therefore CMCOs may be detected in the incorrect fraction. However, this technique will be optimised to minimise the chance of this occurring and substantial repeats will also be used.

Once the sub-mitochondrial localisation has been confirmed it will be possible to investigate the functional effects of the CMCOs. As it is clear that the CMCOs can bind and inhibit mtDNA *in vitro* (Kyriakouli 2007) and can also selectively bind nDNA targets (Unpublished data, Ugichem, GmbH) optimisation of CMCO mtDNA binding *in vivo* should also be possible. However, optimisation may require the production of CMCOs with different thermal melt temperatures by modifying the length and backbone. CMCOs designed to bind different areas of the mitochondrial genome will also be investigated in order to determine if the secondary structure of mtDNA may play a role in CMCO binding by preventing access to the mtDNA.

Although this project has not been wholly successful at decreasing the production of COXI protein via interactions with mtDNA or mt-mRNA, the creation of an anti-genomic treatment remains a viable way of treating the mtDNA disease. The use of small molecules, such as CMCOs, is attractive as they are far more likely to enter cells within a patient than large plasmid DNA (discussed in introduction, section 1.9.2). This project may have been unduly influenced by past data which affected the experimental strategies used in this work, however the completion of further investigations mentioned previously, along with set goals and endpoints will answer the question of the whether CMCOs have potential in this field.

7.2. HIGH THROUGHPUT DRUG SCREEN

Recently, evidence has pointed to improvements in mitochondrial function caused by biogenesis of the organelle. This has been caused both pharmacologically, using the PPAR pan agonist bezafibrate, and by exercise. This work is interesting, particularly in the case of mtDNA diseases where heteroplasmy has not been shown to increase, highlighting the safety of the techniques in patients. Although there is evidence to show that pharmacological intervention can improve the disease phenotype by acting on biogenesis pathways (Dillon et al. 2012; Dillon et al. 2012), the efficacies of the drugs that achieve this are relatively poor. Therefore I set out to develop a simple screen to discover compounds that can increase mitochondrial mass – a marker of biogenesis.

The screen was developed using the fluorescent markers TMRM and Hoechst, which stain mitochondria and nuclei respectively. The relationship between cell number (Hoechst intensity) and mitochondria (TMRM intensity) was shown to be linear. This enabled deviations in the proportion of mitochondria per cell to be determined using a plate reader to measure the intensity of the two fluorescent markers. Control molecules (FCCP and bezafibrate) were used to cause decreases and increases in the proportion of mitochondria per cell respectively.

Screening of hundreds of thousands of compounds was not practical as I did not have easy access to a large library of single molecules, nor is there appropriate equipment to enable a screen of this many compounds within Newcastle University. Therefore I

decided to screen 846 extracts from discrete strains of bacteria within the Actinomycetes family. This library, which was compiled by Demuris Ltd (Newcastle, UK), contains rare species of bacteria of diverse origins, enabling the screening of compounds that may not be present elsewhere in nature or other molecule libraries. The number of compounds in each extract is likely to number in the hundreds or thousands, therefore the screen of molecules is actually several orders of magnitude larger than the 846 extracts suggests.

Using the screen I was able to identify an extract (BP2_G4) which caused the volume of mitochondria per cell to increase from 20% to 40% after 48 hours incubation. Although this is promising, there are many factors that could be causing this such as an inhibition of mitophagy, inhibition of fission or increased fusion. There is also evidence to suggest that preventing the breakdown of microtubules can also increase mitochondrial volume (Karbowski et al. 2001), although to date I have not found an article discussing a pharmaceutical that can increase the volume of mitochondria to this degree.

The effect of the active extract on mitochondrial volume will be investigated in other cell lines (fibroblasts and sarcoma cells – both of which are conducive to imaging studies) to see if there is an increase detected using microscopy and also to see if there is an increase in the proportion of mitochondrial markers (matrix, inner and outer membrane proteins) when compared to a cell based control protein. If these results confirm an increase, the extract will be fractionated in order to determine the active compound. As the extract will be separated into multiple fractions, it is likely that the designed high-throughput assay will be used to assess their activities as this is the most practical method. Upon fractionation, the mechanism of the increase will be investigated by determining changes in the level of biogenesis and mitophagy associated transcripts. The toxicity of the compound in relation to fission and fusion changes will also be investigated. Changes in OXPHOS will also be investigated in control and patient cell lines to quantify changes in relation to mitochondrial mass. This will also highlight the potential benefits of the compound for improving the function of OXPHOS complexes in patient cell lines.

7.3. FINAL CONCLUSIONS

It is clear that there is a need to invest in the discovery of mitochondrially acting pharmaceuticals if there is ever going to be a viable treatment for mitochondrial dysfunction. Although there is the will to do this in academia, the facilities and funds available do not necessarily make it possible. Therefore a focused approach or a screen of completely novel compounds like those used in this project, are the only options viable for academia when working alone. The use of two approaches is necessary as targeted therapies such as CMCOs are only applicable for treating mtDNA diseases, whereas improving the function of mitochondria can be used to treat mitochondrial diseases caused by mutations in both nDNA and mtDNA. It could be argued that the focus should be on developing treatments for all mitochondrial diseases; however the fact that targeted treatments, which remove mutated mtDNA molecules, can offer a cure in affected patients means that apart from the academic and patient benefits of developing such a treatment, there is an economic incentive to do so as well.

The capacity of mitochondrial research in industry has been traditionally focused on mitochondrial toxicology; however, in collaboration with Novartis (Basel, Switzerland), this lab is developing assays in order to screen for mitochondrially acting therapeutics. This collaboration is ideal as it combines the resources of a large pharmaceutical company with the specialist knowledge that an academic lab can provide. Therefore it is hoped that with the involvement of industry, the development of practical therapies for mitochondrial disease may finally become a reality.

Addendum

Subsequent to the completion of this thesis, repeat experiment have shown that Ugi200 does not cause a decrease in the expression of COXICOXI protein.

Appendix

Appendix A

9.1. COMPLETE DRUG SCREEN DATA SET

Compound	Mean TMRM	TMRM SD	Mean Hoechst	Hoechst SD	TMRM/Hoechst ratio	Gradient
BP2_G4	6310.755	243.720	315.980	9.861	19.972	4.600
BP6_D6	5534.225	213.128	295.850	9.886	18.706	3.484
RP8_F2	2694.675	408.464	114.985	2.084	23.435	3.070
BP6_F4	7083.625	310.843	402.295	11.198	17.608	2.986
BP2_D1	6725.860	723.059	376.370	80.252	17.870	2.909
JB10_F11	6382.750	177.444	363.000	7.165	17.583	2.866
RP8_C10	2743.170	204.421	125.355	9.417	21.883	2.847
RP2_A9	5349.250	288.774	301.250	14.315	17.757	2.794
RP13_G5	8133.750	877.366	474.000	29.029	17.160	2.729
RP8_F11	3939.685	395.850	212.585	36.740	18.532	2.669
R6_E6	4919.955	384.350	277.855	14.310	17.707	2.666
RP8_C7	3578.565	431.046	184.525	51.706	19.393	2.642
RP8_F9	2923.730	260.095	145.790	10.183	20.054	2.627
BEZAFIBRATE	8398.406	329.004	502.600	18.646	16.710	2.556
JB10_H7	7775.500	596.870	463.500	22.398	16.776	2.358
RP8_A7	3224.765	508.099	174.765	15.086	18.452	2.348
JB10_H12	5949.750	315.694	350.750	18.927	16.963	2.305
JB10_H4	6819.000	1941.409	406.000	123.329	16.796	2.252
RP8_H7	2544.920	303.191	126.270	4.725	20.155	2.247
RP2_E10	7669.250	2096.471	415.500	175.038	18.458	2.223
RP8_C8	2839.245	108.195	148.230	18.913	19.154	2.199
RP8_F6	3946.395	543.510	226.310	29.726	17.438	2.185
RP8_H11	3268.380	125.219	181.780	10.110	17.980	2.098
JB10_H11	8228.500	195.121	502.000	17.512	16.391	2.031
RP8_D12	8964.255	284.296	548.390	19.482	16.346	2.026
RP8_H8	4641.490	544.314	272.060	53.020	17.061	2.022
R6_H7	8134.350	385.310	498.065	16.650	16.332	1.989
JB10_H2	8462.500	285.005	519.000	12.832	16.305	1.974
RP8_B3	8624.790	680.495	528.870	47.964	16.308	1.974
RP8_B10	7671.360	261.668	469.090	22.285	16.354	1.967
NO DOSE	8078.377	717.863	501.586	23.300	16.106	1.963
JB10_C1	8317.750	444.737	511.000	19.096	16.277	1.945
RP8_E11	4526.200	179.095	268.705	21.741	16.844	1.939
RP8_E12	8874.890	476.311	545.950	20.475	16.256	1.933
BP2_H5	6965.895	812.866	419.985	87.932	16.586	1.923
RP8_F10	6633.140	585.360	405.345	35.336	16.364	1.920
BP2_F6	6029.545	847.206	358.070	93.426	16.839	1.917
RP8_F12	4230.960	355.190	251.015	22.371	16.855	1.905
R6_D1	8014.180	1376.380	494.100	48.412	16.220	1.902
RP8_H6	2540.955	281.411	135.115	8.762	18.806	1.885

JB10_F12	7319.500	460.321	450.750	15.735	16.238	1.869
BP2_H10	7359.345	289.196	450.485	48.508	16.336	1.868
RP8_A3	8393.295	768.545	518.805	54.917	16.178	1.845
BP2_C1	7156.520	292.978	443.165	16.104	16.149	1.768
BP2_D2	7371.240	288.840	457.195	11.504	16.123	1.766
JB10_G5	7703.500	360.430	478.500	21.331	16.099	1.744
RP8_H2	3088.430	245.511	178.425	3.504	17.309	1.730
RP13_H4	5755.250	158.895	354.500	9.849	16.235	1.728
BP2_G1	7107.720	288.376	442.555	10.418	16.061	1.695
RP8_B12	7957.145	455.718	496.845	40.184	16.015	1.677
RP8_F8	5702.585	248.402	352.885	12.175	16.160	1.662
RP8_E10	4242.855	430.768	257.725	32.848	16.463	1.630
JB10_A3	8508.500	142.027	534.750	20.516	15.911	1.607
JB10_G11	7595.750	437.471	477.000	8.287	15.924	1.596
RP8_E1	2439.390	327.549	135.420	5.364	18.014	1.591
RP8_D9	2891.400	260.403	168.360	15.528	17.174	1.555
RP8_H5	4883.050	365.997	302.560	28.245	16.139	1.526
BP2_H1	7222.095	390.902	455.060	29.533	15.871	1.526
BP2_G6	4452.695	176.115	274.195	20.081	16.239	1.519
BP2_H4	7833.620	458.861	495.625	22.282	15.806	1.513
JB10_A10	8753.250	537.877	554.500	23.798	15.786	1.513
JB10_A5	5580.500	195.873	349.250	8.694	15.979	1.512
RP8_E2	4575.915	312.116	283.650	13.457	16.132	1.494
JB10_B4	7808.750	681.284	494.750	22.081	15.783	1.490
JB10_B1	5500.000	419.659	345.750	15.521	15.907	1.461
R6_H6	8022.415	305.472	509.350	26.682	15.750	1.457
RP8_G11	3152.480	160.830	188.795	10.929	16.698	1.452
R6_G11	8112.085	349.380	515.450	15.891	15.738	1.450
RP8_B5	7752.795	1248.674	494.710	62.799	15.671	1.432
R6_H11	8126.115	283.375	517.585	17.549	15.700	1.420
RP8_A12	8608.625	415.292	548.085	50.019	15.707	1.393
JB10_D11	8349.250	371.226	532.750	12.685	15.672	1.392
RP8_H9	2781.905	234.042	164.395	18.566	16.922	1.367
RP8_B8	7178.175	669.472	454.450	68.700	15.795	1.364
JB10_D1	8305.750	540.491	531.750	30.412	15.620	1.361
BP2_E1	7098.265	592.904	453.840	20.293	15.640	1.350
BP2_C4	7823.860	237.287	498.675	31.648	15.689	1.349
RP8_H1	5834.955	216.357	370.270	22.595	15.759	1.343
JB10_F3	5456.250	1619.122	345.500	108.433	15.792	1.318
JB10_F10	8108.750	696.008	521.000	18.673	15.564	1.315
RP8_A1	6117.385	795.229	390.705	32.238	15.657	1.303
JB10_C4	7584.000	833.496	487.750	12.010	15.549	1.294
RP8_D11	8613.505	417.805	555.100	24.319	15.517	1.272
RP8_E9	2930.745	211.102	177.815	15.508	16.482	1.257
RP8_C11	5271.620	165.600	336.110	7.875	15.684	1.251
RP2_G2	7152.500	606.881	456.250	36.936	15.677	1.247

BP2_H6	7937.015	129.179	511.485	17.379	15.518	1.241
RP8_A8	8453.380	609.101	543.815	64.228	15.545	1.237
BP2_C10	7912.920	396.928	510.265	20.880	15.507	1.233
BB4_F2	5191.500	411.516	322.750	74.011	16.085	1.229
BP6_B9	5195.675	298.303	331.535	16.410	15.672	1.224
BP2_H7	7901.330	325.080	509.960	28.612	15.494	1.223
BP2_G5	7833.010	273.399	505.995	7.140	15.480	1.222
R6_H4	7805.560	392.076	503.555	37.263	15.501	1.219
JB10_F7	6957.750	334.776	445.750	51.629	15.609	1.219
RP8_D8	4124.210	491.680	259.555	38.751	15.890	1.215
BP2_F2	7142.185	367.105	460.550	27.416	15.508	1.214
JB10_B11	8621.750	365.965	557.750	10.996	15.458	1.214
BB4_G9	8258.250	643.589	534.250	18.536	15.458	1.199
R6_H1	7692.710	312.343	496.845	37.063	15.483	1.186
RP8_H3	2733.410	436.478	166.530	13.749	16.414	1.185
BP6_B10	6393.715	445.370	411.445	34.955	15.540	1.180
JB10_F1	5021.000	307.455	321.750	14.660	15.605	1.176
JB10_B9	8338.250	186.325	540.500	18.788	15.427	1.170
BP6_B12	7444.745	489.529	482.510	19.044	15.429	1.166
RP2_D12	7532.000	413.396	487.250	24.350	15.458	1.162
BP6_E1	7505.440	186.874	487.085	8.533	15.409	1.147
JB10_G3	5061.750	251.139	325.750	7.228	15.539	1.128
BP2_H8	8006.250	201.628	520.330	24.267	15.387	1.126
BP2_B7	7988.560	143.068	519.110	18.054	15.389	1.124
BP2_E2	7713.755	305.297	501.420	24.257	15.384	1.122
BP2_F7	7775.975	149.745	505.690	12.815	15.377	1.119
RP2_G3	7178.750	524.944	466.750	22.911	15.380	1.119
BP2_E7	7216.910	762.089	463.905	86.396	15.557	1.114
BP2_F9	6959.185	269.169	452.010	14.724	15.396	1.112
R6_H8	7805.255	182.306	508.435	10.418	15.352	1.102
BP2_E12	7514.895	58.622	487.390	34.065	15.419	1.100
BP6_H12	7034.520	154.226	457.500	17.567	15.376	1.089
JB10_B5	8204.250	310.192	535.750	10.935	15.314	1.082
BP2_F5	7711.925	182.917	502.640	13.585	15.343	1.081
BP2_H9	7795.495	254.725	508.740	17.339	15.323	1.078
BP6_F6	7566.440	475.607	493.185	8.474	15.342	1.075
BP2_H12	7712.840	199.765	503.555	11.461	15.317	1.064
BP6_G9	7424.920	192.500	484.950	1.220	15.311	1.057
JB10_D10	8132.250	426.654	531.750	19.602	15.293	1.053
R6_G2	7619.205	238.768	498.065	18.566	15.298	1.048
R6_F11	8141.365	480.440	533.140	19.545	15.271	1.042
RP2_G8	7669.000	489.518	501.500	20.486	15.292	1.034
BP6_E12	5884.365	560.257	383.690	22.507	15.336	1.024
R6_H3	7743.340	119.879	505.995	34.613	15.303	1.021
BP2_D11	7880.895	604.838	516.670	14.792	15.253	1.017
R6_E12	7641.165	335.970	499.895	29.740	15.286	1.016

RP8_H10	8127.030	112.445	532.835	16.945	15.252	1.009
JB10_F9	8009.000	394.939	525.500	15.610	15.241	1.004
RP2_D6	7102.000	522.895	465.750	9.535	15.249	0.999
BP2_B5	7869.000	148.182	516.365	20.228	15.239	0.996
R6_C1	7591.145	412.424	497.455	40.590	15.260	0.993
R6_G9	8104.155	326.484	532.835	11.504	15.210	0.985
RP8_H4	8228.290	610.643	541.375	25.089	15.199	0.984
JB10_C8	6600.000	323.098	433.000	6.633	15.242	0.974
JB10_F4	4930.000	362.712	320.500	9.110	15.382	0.973
RP8_F1	4787.585	294.118	309.270	36.769	15.480	0.972
RP2_F2	7329.000	619.355	481.500	11.504	15.221	0.969
JB10_E10	8369.000	684.776	551.500	15.610	15.175	0.956
JB10_G8	8078.000	329.164	532.250	11.026	15.177	0.942
BP2_B3	7774.755	280.475	512.400	17.454	15.173	0.940
JB10_E12	7358.750	413.273	485.000	17.010	15.173	0.933
BP6_C1	6904.895	530.983	453.840	44.325	15.214	0.931
BP2_D5	7767.130	318.842	512.400	16.757	15.158	0.929
RP8_A5	8070.300	589.820	532.835	40.135	15.146	0.923
RP13_G3	6879.500	330.122	453.000	16.432	15.187	0.918
R6_F7	8115.440	552.370	536.495	22.036	15.127	0.918
JB10_A4	8394.500	202.011	553.000	39.387	15.180	0.912
R6_H9	7968.735	227.510	527.040	11.574	15.120	0.899
BP6_D1	6742.940	509.377	444.690	35.978	15.163	0.896
JB10_D9	8263.000	526.519	547.000	4.243	15.106	0.895
RP8_E4	4768.675	106.550	311.100	22.319	15.328	0.892
BB4_G5	7972.750	418.561	527.250	16.641	15.121	0.877
JB10_A2	8033.750	261.320	532.500	11.818	15.087	0.862
BP6_H11	7403.570	318.842	490.440	22.976	15.096	0.857
RP8_D1	5060.255	271.130	331.840	21.108	15.249	0.854
JB10_H1	7750.500	481.760	514.500	26.602	15.064	0.851
JB10_G12	6467.750	319.272	427.750	15.650	15.120	0.850
BP2_D4	7549.360	428.279	501.115	7.804	15.065	0.848
R6_G6	8076.705	255.231	536.495	9.779	15.055	0.838
RP8_E5	8551.590	194.888	568.520	6.829	15.042	0.836
R6_F1	7618.595	283.130	506.300	16.216	15.048	0.829
BP6_B11	7014.085	393.807	465.430	24.833	15.070	0.826
BP2_D7	7946.165	216.566	528.565	13.040	15.033	0.822
RP8_F7	4815.340	466.422	316.590	38.919	15.210	0.820
RP8_G7	8636.075	202.111	574.620	13.402	15.029	0.818
BP2_B2	7604.565	281.797	505.690	15.058	15.038	0.816
JB10_E11	7914.000	128.735	525.250	30.913	15.067	0.814
RP8_D5	4287.690	537.821	278.465	56.642	15.398	0.804
BB4_F10	8073.500	590.174	538.500	11.561	14.993	0.798
JB10_D2	6292.500	368.306	417.000	39.606	15.090	0.795
RP8_G12	2728.835	121.370	174.460	12.561	15.642	0.784
RP8_A10	6777.405	308.403	450.790	30.321	15.035	0.782

BP6_H8	7298.650	158.677	486.170	15.319	15.013	0.778
R6_F10	7773.840	481.671	518.805	25.618	14.984	0.778
RP8_F4	4137.630	307.434	270.535	33.163	15.294	0.773
R6_H2	7815.015	231.510	520.330	36.769	15.019	0.769
BB4_G7	7927.000	319.487	529.500	14.731	14.971	0.763
JB10_H9	7288.750	157.085	485.750	22.589	15.005	0.763
BP2_H2	7612.190	410.464	508.435	16.916	14.972	0.761
BP2_D6	7892.790	188.482	527.345	7.804	14.967	0.757
JB10_D8	8070.750	636.153	539.500	17.823	14.960	0.749
JB10_C2	5342.250	433.690	355.750	17.462	15.017	0.743
RP8_A9	2644.960	167.565	168.665	19.530	15.682	0.742
R6_D2	7692.405	300.083	514.535	15.667	14.950	0.741
JB10_H3	7701.250	318.394	515.000	22.730	14.954	0.740
RP2_H4	7288.250	546.411	487.750	19.856	14.943	0.738
R6_D11	7832.095	301.032	521.855	49.269	15.008	0.732
JB10_E9	8049.250	542.628	539.500	13.528	14.920	0.730
RP8_B11	2595.245	146.963	164.700	22.385	15.757	0.728
BP2_H11	8218.530	136.286	550.220	15.750	14.937	0.727
RP2_E1	7084.250	515.518	474.000	11.690	14.946	0.723
RP2_C10	7364.250	479.629	492.000	22.906	14.968	0.723
BP6_F12	7099.485	359.406	473.970	25.985	14.979	0.720
RP8_F5	2838.330	408.495	184.525	3.643	15.382	0.711
BP2_G9	8025.465	299.677	538.325	15.086	14.908	0.708
RP2_C11	5955.250	408.980	397.000	28.694	15.001	0.706
JB10_A9	8191.500	321.499	549.750	19.397	14.900	0.704
BP2_A9	8053.525	115.260	538.630	37.517	14.952	0.703
BP2_B12	7696.065	160.464	516.060	24.703	14.913	0.689
RP8_B4	2819.420	258.220	183.610	13.567	15.355	0.685
JB10_B10	8172.000	281.978	547.750	38.690	14.919	0.682
BB5_F1	7953.250	176.296	534.250	18.410	14.887	0.681
BB4_G2	8273.250	188.952	555.500	18.628	14.893	0.681
RP8_F3	7200.135	403.145	483.730	19.251	14.885	0.681
BP2_A8	7586.875	161.650	509.045	20.081	14.904	0.680
JB10_E6	6169.000	404.272	413.250	20.123	14.928	0.680
BP2_B10	7822.030	221.639	524.905	21.787	14.902	0.679
BP2_B6	7876.930	121.374	528.565	29.857	14.902	0.678
JB10_B12	7909.750	273.231	531.750	12.920	14.875	0.676
BP2_G11	8285.935	348.460	557.540	9.911	14.862	0.666
R6_G7	8160.885	222.605	549.305	4.152	14.857	0.665
RP2_E2	7427.000	214.777	498.500	23.445	14.899	0.665
R6_B12	7771.705	205.609	521.550	30.711	14.901	0.663
R6_E2	7760.420	305.910	522.160	20.942	14.862	0.660
BP2_E10	8075.180	590.740	543.815	11.633	14.849	0.659
BP2_G2	7733.580	461.603	520.330	35.784	14.863	0.649
BP6_E9	7101.010	350.863	477.935	0.610	14.858	0.649
BP6_H7	7508.490	240.043	504.775	32.696	14.875	0.647

RP2_D7	7045.000	351.461	473.500	15.264	14.879	0.644
R6_G10	8109.950	255.075	546.865	9.041	14.830	0.640
BP6_G7	7373.070	355.619	496.540	14.158	14.849	0.639
BP6_G12	7252.900	226.017	488.610	13.159	14.844	0.638
JB10_C5	5177.500	360.112	347.500	7.141	14.899	0.635
BB4_H1	7852.000	276.595	529.000	19.765	14.843	0.626
R6_F8	8035.530	453.212	542.900	14.741	14.801	0.618
JB10_A6	8351.750	285.823	563.500	16.623	14.821	0.617
BP6_C12	7194.340	427.350	485.255	25.089	14.826	0.616
RP8_G9	6903.675	1001.195	465.735	66.371	14.823	0.613
BP2_B8	7647.265	124.847	515.145	33.786	14.845	0.607
R6_G1	7605.175	286.892	513.620	28.646	14.807	0.602
JB10_C12	5768.500	411.127	388.250	30.956	14.858	0.598
R6_H5	7370.935	327.800	498.065	24.931	14.799	0.596
JB10_B2	8093.750	100.739	547.250	20.172	14.790	0.591
RP8_B7	7654.890	725.719	516.365	64.421	14.825	0.590
BB4_H7	8003.000	418.687	541.500	13.404	14.779	0.584
BP2_B4	7605.175	59.571	514.230	18.729	14.789	0.583
JB10_G9	4892.250	245.075	329.250	8.098	14.859	0.582
JB10_D7	6128.000	470.184	414.250	23.599	14.793	0.578
R6_E3	7674.410	568.561	519.720	30.000	14.766	0.570
R6_E1	7530.450	191.517	509.655	21.650	14.776	0.569
BP6_H4	6979.010	186.184	472.445	17.379	14.772	0.567
R6_D12	7803.120	176.337	526.735	40.246	14.814	0.565
BP6_F7	7443.830	236.863	503.555	22.148	14.783	0.564
RP8_H12	2724.260	67.693	178.120	20.728	15.295	0.564
RP13_H7	7093.500	267.602	479.500	25.331	14.794	0.564
R6_A1	7506.355	448.913	507.215	50.335	14.799	0.562
RP2_F1	6724.500	489.793	454.500	20.290	14.795	0.560
BP6_D5	7036.350	382.893	476.715	20.951	14.760	0.560
RP2_C1	6535.500	1510.335	445.000	62.199	14.687	0.557
R6_F12	7302.920	376.898	494.710	20.524	14.762	0.557
RP8_G2	7576.505	112.286	513.315	18.512	14.760	0.556
RP13_F10	6783.750	169.183	459.250	16.153	14.771	0.548
RP2_G4	7381.500	944.108	498.250	26.750	14.815	0.547
RP8_B1	2906.040	121.817	192.455	8.986	15.100	0.544
R6_E8	7832.705	340.165	531.920	16.817	14.725	0.543
JB10_D5	5911.250	398.545	400.500	16.862	14.760	0.539
R6_D6	7345.315	457.124	498.370	21.881	14.739	0.536
R6_G8	7779.635	306.954	528.260	15.107	14.727	0.535
BB4_H4	7977.750	388.726	542.250	8.421	14.712	0.532
BP6_A5	7293.770	314.874	493.795	41.124	14.771	0.528
BP2_G10	8163.020	490.759	555.405	21.673	14.697	0.524
RP8_D7	5606.815	210.813	379.115	28.722	14.789	0.516
BP2_A7	7699.725	396.127	522.160	47.250	14.746	0.515
R6_F3	7502.390	321.427	510.265	6.008	14.703	0.514

BP6_F1	7287.365	93.982	495.930	12.969	14.694	0.502
R6_E7	7824.775	526.805	533.750	17.553	14.660	0.490
BP6_B8	6936.310	132.468	471.530	24.532	14.710	0.481
BP2_B1	7137.000	151.165	486.170	16.564	14.680	0.480
RP8_D6	2827.960	308.331	189.100	11.048	14.955	0.479
BP6_H10	6892.390	81.795	469.700	10.775	14.674	0.477
RP8_B2	6821.935	143.568	464.515	14.754	14.686	0.476
RP2_C8	5342.000	376.736	362.750	20.123	14.726	0.474
BP6_F11	7595.110	334.284	518.195	10.513	14.657	0.473
RP2_E9	6438.500	404.442	438.750	10.935	14.675	0.459
R6_G3	7668.615	192.725	523.990	8.769	14.635	0.457
R6_H10	7445.660	264.377	508.740	17.167	14.635	0.451
BP6_B1	6814.615	750.629	465.430	50.719	14.642	0.451
BP2_D3	7490.190	203.684	512.095	10.370	14.627	0.449
RP8_G8	8296.610	303.108	567.605	11.844	14.617	0.443
R6_G12	7633.235	214.864	522.160	10.110	14.619	0.436
JB10_F6	6751.500	578.904	462.250	21.077	14.606	0.434
BP2_E5	7443.830	141.136	509.350	17.524	14.614	0.427
RP13_B6	6834.500	291.541	467.750	11.442	14.611	0.425
RP2_H3	6410.500	708.809	436.750	42.797	14.678	0.424
BP6_E8	7469.145	395.882	511.485	4.712	14.603	0.424
BB4_H9	7897.750	420.345	541.500	18.285	14.585	0.417
RP13_G8	7086.000	355.409	485.500	7.767	14.595	0.412
BP6_G6	7430.410	245.820	509.045	13.816	14.597	0.412
BB4_G12	8476.500	485.330	581.750	25.277	14.571	0.410
BP6_H9	7202.575	337.954	494.100	18.178	14.577	0.404
BB4_A2	8096.750	432.434	555.500	16.422	14.576	0.402
JB10_D4	4099.750	281.750	279.500	10.017	14.668	0.401
BP6_G5	7102.840	166.126	486.780	15.907	14.591	0.401
JB10_A7	4098.000	287.414	279.250	9.708	14.675	0.394
BB5_A2	8251.500	478.136	567.000	26.038	14.553	0.393
R6_F6	7791.225	350.321	534.665	15.636	14.572	0.392
BB4_G10	8084.500	508.069	555.500	22.942	14.554	0.388
RP8_G10	8375.300	73.653	575.535	7.676	14.552	0.387
R6_B5	7940.980	70.781	545.340	17.196	14.562	0.386
JB10_C11	8179.750	439.374	561.250	24.240	14.574	0.385
BB4_H2	7733.250	408.364	531.500	3.109	14.550	0.383
BP6_A4	7437.730	367.011	509.960	40.549	14.585	0.379
BP6_E7	7281.570	437.182	500.200	7.907	14.557	0.377
BP2_C5	7582.300	141.769	520.940	18.609	14.555	0.375
BP2_F3	6797.230	275.577	466.955	19.402	14.556	0.374
R6_B1	7784.820	383.823	535.580	15.496	14.535	0.370
BP6_A3	7071.730	259.831	483.730	49.512	14.619	0.369
BP6_D7	7117.175	355.288	489.525	8.237	14.539	0.369
BP2_E11	8032.175	586.212	552.355	24.224	14.542	0.367
BP2_C6	7836.975	269.132	538.935	13.452	14.542	0.366

RP13_G4	6775.500	376.573	465.500	25.645	14.555	0.365
RP8_D2	2909.090	300.857	197.640	9.811	14.719	0.363
R6_A3	7459.080	109.393	512.705	22.238	14.548	0.363
RP8_E8	3248.250	83.820	220.820	9.811	14.710	0.361
BP2_D10	7723.820	396.927	531.615	14.171	14.529	0.359
BB4_F6	2348.500	94.016	157.750	2.630	14.887	0.359
BP2_C3	7772.925	267.284	535.275	12.849	14.521	0.354
JB10_G10	4808.000	173.038	329.500	10.083	14.592	0.354
BP2_D12	7908.040	365.721	544.120	11.445	14.534	0.354
BP2_E8	8057.490	118.256	554.795	14.788	14.523	0.352
JB10_B8	7746.750	321.793	533.250	10.275	14.527	0.351
RP2_C4	4537.250	847.654	311.500	13.102	14.566	0.349
BP6_E10	6889.645	388.983	474.580	5.977	14.517	0.347
RP8_G1	2666.615	331.577	181.170	12.815	14.719	0.342
BP6_F3	6631.615	299.490	456.890	11.379	14.515	0.342
JB10_A1	4602.000	366.336	316.500	12.793	14.540	0.335
BP6_A8	7164.450	298.280	493.795	20.593	14.509	0.329
RP8_D3	8267.635	455.015	570.655	28.514	14.488	0.327
RP13_H9	6976.000	271.003	480.250	20.887	14.526	0.326
RP2_H9	7178.250	479.444	495.000	11.605	14.502	0.320
BP6_H1	6885.375	101.127	474.885	18.459	14.499	0.315
BP6_H5	7291.025	210.808	503.555	8.416	14.479	0.314
RP2_H7	7055.500	580.381	487.250	8.770	14.480	0.314
BP6_E11	7142.185	408.030	493.185	9.150	14.482	0.312
BP6_A9	7282.790	201.320	500.200	40.155	14.560	0.306
JB10_G4	3632.750	351.088	249.750	8.421	14.546	0.304
RP13_D8	7030.250	360.653	485.250	15.521	14.488	0.304
BP6_C9	7021.710	618.714	485.865	23.156	14.452	0.294
BB4_H6	7722.250	424.143	534.500	17.020	14.448	0.294
JB10_C7	7837.750	458.722	542.500	16.258	14.447	0.288
BP2_E3	7526.485	257.555	520.940	15.074	14.448	0.286
R6_D8	7683.255	374.159	532.225	9.470	14.436	0.281
R6_H12	7104.975	596.590	491.355	13.192	14.460	0.279
RP2_F3	7127.500	570.237	493.750	13.865	14.435	0.278
JB10_A8	4619.750	352.828	319.250	4.573	14.471	0.274
BP6_G1	7095.215	117.511	491.355	12.964	14.440	0.271
JB10_B7	6165.500	308.463	427.000	15.122	14.439	0.269
BP6_D9	7096.740	270.158	491.660	8.627	14.434	0.268
R6_E10	7929.390	418.196	549.915	12.964	14.419	0.263
JB10_F2	7227.250	237.036	501.000	19.305	14.426	0.261
BP6_A11	6954.000	473.128	482.510	13.007	14.412	0.259
BP2_E9	7759.200	157.441	538.020	13.026	14.422	0.255
BP6_C8	7204.405	276.062	498.980	17.708	14.438	0.253
JB10_G7	7549.500	362.882	524.000	9.487	14.407	0.252
JB10_H8	7415.750	337.900	514.750	13.598	14.407	0.249
BP2_A11	7404.790	517.459	513.315	45.434	14.425	0.247

BB4_A4	7932.750	392.268	550.750	4.272	14.404	0.245
RP8_G3	6683.465	217.138	463.295	17.521	14.426	0.243
R6_E9	7593.280	492.266	527.650	24.613	14.391	0.239
JB10_A11	3754.000	135.691	259.250	6.185	14.480	0.238
R6_C8	7680.510	268.765	533.445	16.769	14.398	0.231
JB10_C10	7924.750	292.544	550.250	21.203	14.402	0.229
RP2_E6	7036.500	438.615	489.000	13.292	14.390	0.227
BP2_C2	6954.305	176.172	483.425	6.928	14.385	0.226
BB4_D6	7624.250	551.278	530.250	3.500	14.379	0.225
R6_A11	7759.810	467.066	538.935	38.675	14.398	0.221
BB4_G8	7885.750	504.627	548.500	21.048	14.377	0.219
JB10_D12	7938.750	306.508	551.500	27.441	14.395	0.218
BP2_B9	7640.555	286.622	530.700	27.497	14.397	0.218
RP8_G4	7456.030	1045.737	518.500	72.265	14.380	0.212
BB4_F12	7864.250	460.019	547.500	33.601	14.364	0.208
RP2_F8	7342.750	473.513	508.500	46.148	14.440	0.205
RP8_B9	5250.880	656.794	365.390	38.483	14.371	0.205
BB5_D9	6728.750	964.285	470.500	29.183	14.301	0.197
BP6_D10	7042.755	360.939	490.745	18.646	14.351	0.192
RP2_H12	7299.000	308.209	508.750	14.198	14.347	0.190
R6_C10	7712.230	238.206	537.105	23.559	14.359	0.189
BP2_E4	7635.980	288.412	532.530	13.857	14.339	0.189
RP2_E3	6926.000	309.077	482.500	12.261	14.354	0.182
RP2_F11	7239.500	453.085	504.500	14.248	14.350	0.177
BP2_G12	7527.400	180.365	524.905	17.293	14.340	0.176
BP6_A7	7287.365	313.862	507.520	31.673	14.359	0.173
BP6_C4	6454.715	437.927	449.875	35.630	14.348	0.172
R6_A5	7767.130	170.912	541.680	30.524	14.339	0.169
BP2_F4	7213.860	279.558	503.860	13.102	14.317	0.168
RP13_H8	7045.500	337.818	491.500	24.678	14.335	0.168
R6_F2	7336.775	231.916	512.705	9.150	14.310	0.162
RP13_D12	7208.000	214.544	503.250	14.198	14.323	0.158
RP2_E7	6846.250	370.233	478.000	11.804	14.323	0.155
RP13_H6	6794.750	240.088	474.250	24.622	14.327	0.150
RP8_G5	7628.355	1147.873	535.580	30.589	14.243	0.150
BB4_A1	7907.750	214.882	553.250	13.048	14.293	0.144
R6_G4	7514.895	243.184	525.820	12.200	14.292	0.144
R6_F9	7290.110	360.722	510.265	13.852	14.287	0.142
RP13_C5	6851.750	381.979	479.500	13.229	14.289	0.142
R6_B4	7512.150	112.039	525.210	23.667	14.303	0.141
BP6_C2	7043.975	384.816	492.575	31.913	14.300	0.141
BP2_G3	6822.545	350.136	477.325	25.306	14.293	0.140
BP6_F5	7202.880	275.790	504.165	1.535	14.287	0.140
BB5_E11	8244.250	365.127	577.250	2.217	14.282	0.139
RP8_A2	7802.205	688.676	545.950	50.445	14.291	0.139
R6_B8	7480.735	69.110	522.770	24.103	14.310	0.137

R6_D7	7681.120	413.582	538.325	10.418	14.269	0.130
RP13_E2	6820.000	394.109	477.750	9.251	14.275	0.130
R6_C12	7428.885	355.414	518.805	41.461	14.319	0.128
RP8_E3	2684.000	294.321	186.965	3.050	14.356	0.127
BP6_C11	7523.435	192.485	526.430	19.251	14.291	0.127
BP6_C7	7210.505	408.736	505.690	9.986	14.259	0.119
BP2_C11	7467.925	360.850	522.770	22.196	14.285	0.119
JB10_C6	6851.000	646.707	481.000	14.765	14.243	0.116
JB10_G1	3834.500	276.722	268.500	10.017	14.281	0.115
RP13_E3	6691.500	464.247	468.250	19.015	14.290	0.113
RP2_D5	6967.250	533.736	488.500	11.561	14.263	0.106
JB10_B6	7787.000	330.424	546.750	12.606	14.242	0.100
RP13_D11	7007.750	366.643	492.000	13.038	14.243	0.093
BP2_A4	7258.695	1010.141	511.180	40.987	14.200	0.091
R6_B11	7654.890	195.610	534.665	53.997	14.317	0.090
JB10_A12	3538.750	75.332	247.750	9.287	14.284	0.089
BP6_D2	6713.660	581.499	470.920	50.919	14.256	0.085
R6_A6	7721.990	248.162	541.070	44.330	14.272	0.084
RP13_D7	6854.000	481.455	481.750	14.660	14.227	0.084
RP13_H1	6735.250	227.900	472.750	20.918	14.247	0.082
R6_C7	6971.995	334.044	490.440	10.682	14.216	0.076
BP6_B5	7194.950	204.049	505.080	25.533	14.245	0.073
R6_E5	7683.560	342.625	539.850	40.358	14.233	0.067
RP2_G7	3693.000	141.579	259.500	9.147	14.231	0.067
BB4_E7	7568.000	355.249	532.750	12.842	14.206	0.066
BB4_H3	7655.250	400.790	538.750	12.945	14.209	0.063
BB5_F10	7934.750	654.436	558.500	10.376	14.207	0.061
RP13_G9	6877.250	362.010	484.250	9.179	14.202	0.055
BB4_G6	7705.250	489.098	543.000	7.394	14.190	0.055
R6_D3	7623.170	471.607	536.800	32.797	14.201	0.053
BP6_A12	6997.310	356.381	491.965	37.595	14.223	0.053
BB4_F8	7788.750	539.358	549.000	17.569	14.187	0.053
R6_C4	7243.140	370.758	510.265	23.027	14.195	0.052
BP2_F12	6699.935	108.387	471.530	22.241	14.209	0.044
JB10_F5	7611.500	514.995	537.250	8.461	14.168	0.039
BP2_D9	7687.220	165.294	541.985	19.171	14.183	0.037
BB4_G11	7987.250	600.649	564.000	10.551	14.162	0.037
R6_F4	7505.440	323.512	529.175	21.069	14.183	0.035
BP6_C5	7224.840	184.008	509.960	8.274	14.167	0.030
RP2_D4	6760.000	496.406	477.250	8.539	14.164	0.028
BP6_D4	6797.230	345.600	479.765	21.581	14.168	0.027
RP13_B10	7086.000	410.803	500.500	11.818	14.158	0.025
BB4_F11	7798.500	296.029	550.500	18.717	14.166	0.024
BB4_A5	8057.250	314.173	569.250	4.193	14.154	0.021
RP2_D10	6896.750	518.644	487.000	16.021	14.162	0.018
BP6_D11	6665.165	193.565	470.920	17.339	14.153	0.004

RP13_G7	6921.500	325.455	489.750	9.535	14.133	0.001
RP2_C9	6439.250	1037.744	455.500	66.796	14.137	0.000
RP13_F7	6789.750	302.552	479.750	15.756	14.153	-0.002
R6_D4	7387.100	319.868	522.770	20.231	14.131	-0.002
R6_A8	7482.565	207.207	528.870	24.186	14.148	-0.003
BB5_E9	7680.250	430.521	543.750	7.632	14.125	-0.007
RP13_E8	6896.000	419.321	488.000	15.684	14.131	-0.008
JB10_E4	3580.750	133.315	253.250	9.287	14.139	-0.011
R6_C11	7593.280	155.533	535.885	42.031	14.170	-0.011
RP13_H3	6955.500	148.653	492.500	6.137	14.123	-0.013
RP13_F6	6782.500	311.254	480.250	8.995	14.123	-0.014
JB10_G6	4016.250	340.408	284.750	17.173	14.104	-0.014
BP2_D8	7612.495	294.655	538.935	14.171	14.125	-0.023
RP13_E1	6856.500	325.603	485.750	10.782	14.115	-0.024
BP6_A2	6819.800	368.448	482.815	37.143	14.125	-0.024
BP6_E6	6924.110	396.426	491.050	9.048	14.101	-0.024
BP6_C10	7040.010	157.541	498.065	29.405	14.135	-0.026
BB4_D7	6849.750	712.012	485.000	48.436	14.123	-0.029
R6_A9	7594.805	202.602	536.190	46.140	14.164	-0.034
BB4_C12	7762.000	432.807	550.000	41.288	14.113	-0.038
BP6_D12	6584.340	291.543	467.565	12.457	14.082	-0.045
BB4_D10	7810.250	571.247	555.000	19.149	14.073	-0.053
R6_B3	7520.080	130.218	533.445	28.496	14.097	-0.056
RP13_H12	6927.500	235.811	492.000	14.071	14.080	-0.057
BB4_A3	8103.250	370.622	575.500	15.330	14.080	-0.058
BB4_G1	7156.250	760.315	509.000	30.232	14.059	-0.059
BB4_H11	8027.000	344.746	570.500	20.728	14.070	-0.060
BP2_F10	7677.155	346.602	545.645	14.987	14.070	-0.063
JB10_E2	7292.750	261.899	518.250	13.817	14.072	-0.063
BP6_G4	6911.300	150.260	491.355	15.347	14.066	-0.064
BB5_A11	8034.000	611.527	571.750	21.061	14.052	-0.064
RP2_F7	7163.500	432.492	509.500	11.902	14.060	-0.072
BP6_B4	6976.570	381.678	495.930	30.614	14.068	-0.073
BB5_A7	8231.250	695.473	586.750	25.078	14.029	-0.080
BB4_D5	7593.500	485.292	540.250	10.532	14.056	-0.080
RP2_G11	7226.750	498.241	514.500	8.347	14.046	-0.081
RP13_E7	6763.750	361.118	481.000	20.510	14.062	-0.082
R6_G5	6598.675	206.343	469.700	11.488	14.049	-0.084
BP6_D3	6918.925	277.791	491.965	36.045	14.064	-0.087
BP6_B7	6841.150	529.085	486.780	26.524	14.054	-0.089
R6_C2	7467.925	98.744	531.005	32.833	14.064	-0.094
JB10_D3	7636.500	348.926	544.000	22.435	14.038	-0.094
BP6_C3	6867.380	526.717	488.915	43.253	14.046	-0.096
RP2_H6	6738.500	446.899	480.500	8.699	14.024	-0.097
R6_C3	7622.255	319.824	542.900	33.677	14.040	-0.101
BB4_H10	7842.250	460.649	559.500	11.030	14.017	-0.103

BB4_F1	7841.500	336.113	558.500	17.311	14.040	-0.104
BP6_C6	6925.635	366.230	494.405	21.350	14.008	-0.110
R6_D10	7427.055	179.696	529.785	14.065	14.019	-0.111
R6_B9	7726.870	159.792	550.220	33.203	14.043	-0.113
R6_B2	7444.745	251.548	531.005	27.880	14.020	-0.117
BP2_F11	7391.065	217.049	527.345	16.886	14.016	-0.120
BB5_D5	7645.500	272.335	545.500	22.825	14.016	-0.122
BB4_E12	7691.500	554.568	549.750	23.085	13.991	-0.123
BP6_B3	7326.100	97.514	522.465	24.550	14.022	-0.128
JB10_C3	7519.000	304.432	537.250	18.998	13.995	-0.132
RP13_C4	6613.500	452.363	473.250	9.639	13.975	-0.134
BP6_H3	6872.260	76.104	491.050	14.418	13.995	-0.135
R6_E11	7324.270	514.750	523.990	17.665	13.978	-0.141
BP2_H3	6843.895	303.376	489.830	13.964	13.972	-0.142
RP2_A11	7553.250	418.082	539.000	21.510	14.013	-0.143
JB10_C9	7601.000	402.950	543.750	12.500	13.979	-0.146
RP13_A5	6987.250	353.240	500.250	16.460	13.968	-0.149
RP13_B8	6769.250	297.554	484.750	12.971	13.964	-0.156
BB4_C1	7903.000	457.234	565.750	5.909	13.969	-0.158
BP6_H2	7190.375	54.627	515.145	8.705	13.958	-0.162
R6_C6	7499.950	379.868	537.410	19.225	13.956	-0.163
BB4_G3	7680.000	571.732	550.250	19.923	13.957	-0.171
RP2_H2	5270.250	624.444	379.250	20.023	13.897	-0.175
RP13_A1	7182.000	410.820	515.500	10.472	13.932	-0.181
RP13_D5	6775.250	349.916	485.500	15.610	13.955	-0.182
JB10_E1	7475.500	463.243	536.250	40.302	13.940	-0.186
BB5_G7	7653.000	391.388	549.750	14.660	13.921	-0.191
BP6_D8	6938.445	561.035	498.980	23.720	13.905	-0.191
RP2_G12	7211.500	524.877	518.000	12.247	13.922	-0.193
RP2_E12	7062.500	377.695	507.000	14.306	13.930	-0.199
RP13_G2	6807.000	178.675	489.250	9.605	13.913	-0.199
BP6_B2	7285.535	103.652	523.075	26.680	13.928	-0.205
R6_E4	7507.880	373.620	539.850	11.891	13.907	-0.207
RP13_F3	6560.000	442.679	471.750	15.607	13.906	-0.209
RP13_A8	6950.750	308.088	500.000	12.517	13.902	-0.212
RP13_C6	6900.500	286.312	496.500	9.883	13.898	-0.213
BP2_A12	3243.675	156.155	233.020	26.147	13.920	-0.214
RP13_C7	6720.750	258.758	483.750	5.679	13.893	-0.214
RP2_D2	6657.000	462.550	478.750	11.236	13.905	-0.217
RP13_C10	6984.250	407.655	503.000	6.481	13.885	-0.220
RP8_C2	6892.695	452.342	496.235	32.757	13.890	-0.226
BB4_C6	7805.500	318.457	561.500	13.279	13.901	-0.226
BB4_E8	7586.000	409.009	546.500	7.047	13.881	-0.229
BB4_E9	7559.750	576.998	544.750	14.080	13.877	-0.230
BP6_E3	6866.465	273.259	494.710	19.785	13.880	-0.233
BB5_B7	7828.000	442.792	564.250	21.670	13.873	-0.242

BB5_A4	8029.250	453.399	579.250	24.268	13.861	-0.247
BB4_E1	7982.500	481.776	574.750	18.154	13.889	-0.251
RP8_C1	7038.790	385.443	507.215	37.476	13.877	-0.251
BB5_F11	7879.500	723.283	568.000	7.874	13.872	-0.253
R6_C9	7546.615	177.423	543.510	32.985	13.885	-0.254
BP6_F10	6152.155	392.319	444.690	18.218	13.835	-0.255
RP13_F1	6780.500	277.625	489.500	4.359	13.852	-0.256
BB4_H12	7547.750	382.110	544.750	25.526	13.855	-0.257
BB4_B4	7486.250	414.766	540.500	9.950	13.851	-0.262
RP13_C12	6806.000	315.608	491.750	16.800	13.840	-0.263
RP13_D2	6657.000	415.387	481.000	6.377	13.840	-0.266
RP8_B6	6939.055	519.438	501.725	25.772	13.830	-0.270
BB4_D8	7629.000	491.998	551.500	17.078	13.833	-0.273
BB5_B8	7865.250	711.500	569.000	10.360	13.823	-0.274
RP2_H11	6982.250	514.257	504.750	10.905	13.833	-0.283
BB5_H7	7766.750	260.529	561.500	15.330	13.832	-0.285
RP13_A4	6974.000	269.734	504.750	8.655	13.817	-0.286
BB5_F12	8229.750	454.690	595.500	12.342	13.820	-0.295
BB5_G1	7485.500	389.853	542.250	27.256	13.805	-0.305
JB10_H6	6574.750	100.970	476.000	23.022	13.813	-0.306
RP13_B11	6927.250	358.426	502.250	3.594	13.792	-0.308
RP2_A5	6990.250	335.709	506.750	8.180	13.794	-0.309
BB5_H6	7597.750	398.518	550.750	6.238	13.795	-0.311
RP13_F5	6661.250	214.301	483.000	9.832	13.791	-0.313
BP6_A1	6291.540	463.029	455.365	33.118	13.816	-0.315
BB4_D11	7472.250	403.844	542.000	18.601	13.786	-0.319
RP2_B10	7268.250	346.566	526.500	20.404	13.805	-0.320
RP2_B8	6931.000	381.961	502.500	15.780	13.793	-0.321
RP2_D11	6881.500	445.734	499.000	23.137	13.791	-0.332
RP13_B5	6543.500	312.676	475.500	12.450	13.761	-0.333
BB4_E4	7685.500	708.238	557.000	14.765	13.798	-0.333
RP13_E6	6692.000	187.682	486.250	10.178	13.762	-0.340
BB4_F9	7503.250	507.317	545.500	6.952	13.755	-0.343
RP13_F11	6944.250	271.976	505.000	3.742	13.751	-0.348
BP6_E4	6856.095	387.213	498.980	19.444	13.740	-0.352
BP2_A6	6910.385	432.809	502.335	35.713	13.757	-0.364
RP13_D3	6798.500	410.481	494.750	10.626	13.741	-0.367
RP2_E5	6750.000	526.205	491.500	9.399	13.733	-0.368
RP2_C12	7183.500	425.871	523.000	14.832	13.735	-0.375
BB4_F3	7549.750	535.917	547.750	26.887	13.783	-0.377
RP2_F4	6266.250	516.474	457.500	10.247	13.697	-0.377
RP2_B11	7289.750	423.076	530.500	15.330	13.741	-0.381
RP13_A3	6929.500	383.157	505.500	19.122	13.708	-0.381
BB4_B9	7797.750	527.834	568.500	11.676	13.716	-0.383
RP13_F9	6738.750	189.222	491.500	7.594	13.711	-0.383
BB5_C6	7572.250	353.806	552.750	9.287	13.699	-0.398

BB5_A5	7937.250	593.238	580.000	23.466	13.685	-0.402
BB5_G9	7669.000	262.041	560.000	10.677	13.695	-0.403
BP6_G3	6872.260	183.274	502.030	14.925	13.689	-0.403
BP2_C12	5318.285	509.887	387.350	53.740	13.730	-0.405
RP13_B12	6779.500	352.491	495.750	13.475	13.675	-0.408
RP13_G1	6838.250	337.485	500.250	14.104	13.670	-0.414
BP2_A5	6693.225	280.201	489.220	23.699	13.681	-0.416
RP13_E9	6599.250	271.796	482.500	13.379	13.677	-0.416
R6_A2	7196.475	169.433	525.515	34.035	13.694	-0.428
RP13_B2	6930.000	336.366	507.000	12.356	13.669	-0.430
BB4_A8	8063.500	176.152	590.000	11.576	13.667	-0.434
RP13_F4	6469.000	316.466	473.000	22.760	13.677	-0.438
RP8_A6	5878.875	281.390	430.965	25.129	13.641	-0.440
RP2_C6	6841.500	481.487	501.250	9.430	13.649	-0.444
RP2_C3	3791.000	1158.305	272.500	82.124	13.912	-0.453
BB5_E12	8050.250	456.853	590.250	8.180	13.639	-0.468
BP6_G2	6836.880	47.366	502.030	12.180	13.618	-0.469
BB5_H5	7711.500	385.989	566.250	10.340	13.619	-0.474
BP6_F2	5354.275	147.593	394.365	11.886	13.577	-0.476
RP2_F12	6923.500	568.377	508.250	8.057	13.622	-0.477
BB4_B11	7905.000	406.623	580.750	22.692	13.612	-0.479
RP13_B3	6724.500	251.362	494.500	12.342	13.599	-0.479
BB5_H8	7730.750	255.450	568.000	8.406	13.610	-0.481
BB4_A11	8114.000	368.836	596.000	19.528	13.614	-0.482
RP13_G6	6715.250	316.242	493.750	14.315	13.601	-0.496
RP13_G10	6694.500	248.346	492.750	11.177	13.586	-0.498
BB4_C4	7163.750	561.024	527.250	24.891	13.587	-0.500
R6_A4	6586.170	192.862	484.645	29.151	13.590	-0.506
RP13_G12	6855.500	231.244	505.000	14.468	13.575	-0.510
BB5_E10	7988.250	505.649	588.500	9.883	13.574	-0.521
RP2_E8	6408.250	579.271	472.250	37.053	13.570	-0.522
RP13_D1	6731.750	325.916	496.750	8.461	13.552	-0.526
BB5_B12	8169.750	376.640	601.750	13.326	13.577	-0.527
RP13_C9	6427.500	269.822	475.250	12.842	13.524	-0.543
BB4_C7	7311.000	264.997	540.750	8.500	13.520	-0.560
RP13_F8	6531.000	362.342	483.000	10.424	13.522	-0.561
RP13_G11	6948.750	259.521	514.500	4.435	13.506	-0.567
RP2_D1	5348.500	329.653	396.750	21.793	13.481	-0.570
RP13_F12	6640.250	361.141	492.000	13.089	13.496	-0.572
BP2_B11	6818.275	310.388	504.470	28.982	13.516	-0.574
RP2_B3	7072.250	332.966	524.250	8.180	13.490	-0.587
RP13_E5	6796.000	495.504	503.750	19.670	13.491	-0.588
BB5_A6	8376.500	713.035	621.250	28.628	13.483	-0.594
RP13_A10	7004.500	284.975	519.750	13.226	13.477	-0.595
BB4_G4	2132.750	90.345	164.500	5.066	12.965	-0.598
R6_A12	6481.555	645.135	481.595	43.023	13.459	-0.614

RP13_C1	6757.750	418.247	502.500	13.102	13.448	-0.616
RP13_H5	6358.000	293.472	473.250	7.805	13.435	-0.626
BB4_F5	7252.750	673.180	539.250	2.754	13.450	-0.627
R6_B6	6937.530	171.697	515.450	15.254	13.459	-0.627
RP2_A4	7073.000	267.294	525.500	15.199	13.460	-0.627
R6_B7	6656.625	264.288	494.710	27.434	13.456	-0.628
RP13_B7	6806.000	219.399	506.500	17.673	13.437	-0.641
BB5_C7	7547.500	202.268	561.250	15.735	13.448	-0.642
RP13_A11	6888.250	273.278	513.500	14.201	13.414	-0.652
BB5_F8	7747.500	683.049	577.500	19.053	13.416	-0.660
BB5_B11	7966.500	464.854	593.750	8.808	13.417	-0.663
R6_A7	6580.375	323.686	490.440	36.478	13.417	-0.667
RP2_B2	5473.500	963.066	411.250	38.222	13.309	-0.670
BB4_E3	7370.000	674.825	550.000	5.099	13.400	-0.678
BB5_D6	7353.000	452.279	548.750	12.971	13.400	-0.680
RP13_C8	6613.750	343.529	494.000	19.950	13.388	-0.684
BB4_F4	7534.750	639.642	561.500	18.484	13.419	-0.687
BB5_E7	7442.750	371.920	555.750	13.817	13.392	-0.688
R6_C5	6442.820	283.772	482.205	8.297	13.361	-0.691
RP13_C3	6518.750	365.148	488.000	2.828	13.358	-0.699
BB5_C1	7702.000	409.341	576.000	4.397	13.372	-0.702
RP13_D10	6493.750	241.892	486.250	17.289	13.355	-0.708
RP2_C5	4837.750	407.941	364.250	6.238	13.281	-0.711
BB5_C12	7891.000	814.965	590.250	6.131	13.369	-0.714
R6_F5	6610.570	210.474	495.320	18.716	13.346	-0.718
BB5_D11	7490.750	530.184	562.000	16.104	13.329	-0.731
R6_A10	7131.205	234.141	532.530	51.765	13.391	-0.735
BB5_H3	7610.500	385.309	570.000	21.649	13.352	-0.736
BB5_F4	7368.250	437.898	552.500	12.069	13.336	-0.737
BB4_E5	7456.500	433.238	558.500	16.941	13.351	-0.737
BB4_B3	7686.500	222.034	576.250	8.016	13.339	-0.739
BB4_B7	7349.000	303.326	551.250	12.148	13.332	-0.742
RP2_E4	6616.250	416.570	497.250	3.775	13.306	-0.744
BB5_H11	7455.000	216.962	559.500	9.678	13.324	-0.748
BP2_C8	5387.520	1388.036	407.785	95.894	13.212	-0.758
BB4_A10	8085.750	207.924	607.250	9.811	13.315	-0.765
BB4_A9	7846.000	257.873	589.500	13.000	13.310	-0.768
BB4_D2	6995.000	489.294	525.000	21.954	13.324	-0.770
BB5_D2	7172.500	308.269	539.500	27.767	13.295	-0.778
BB4_A12	7745.000	262.028	582.000	24.125	13.308	-0.780
BB4_E6	4962.000	287.935	376.000	12.055	13.197	-0.782
BB4_D3	7397.000	363.132	556.750	22.940	13.286	-0.795
BB4_E11	7472.500	476.264	563.750	27.439	13.255	-0.806
RP13_E4	6460.750	321.118	487.750	16.761	13.246	-0.820
RP2_H10	5671.250	288.132	429.500	9.950	13.204	-0.823
RP2_C7	4363.750	417.927	332.500	10.149	13.124	-0.831

BB5_F7	7430.500	443.099	561.500	7.937	13.233	-0.833
R6_D5	6067.365	398.467	459.940	25.338	13.192	-0.834
BB5_B5	7618.000	457.089	576.250	8.655	13.220	-0.841
BB4_E10	7400.500	582.703	560.250	25.158	13.209	-0.841
R6_D9	6758.495	125.125	511.485	15.636	13.213	-0.845
BB4_A6	7934.750	190.989	599.750	14.175	13.230	-0.849
RP13_A2	6584.250	154.675	499.500	13.404	13.182	-0.866
RP2_D3	6271.500	326.133	476.250	19.619	13.169	-0.878
RP2_B6	6670.750	510.539	507.500	9.678	13.144	-0.891
BB5_F9	7434.250	416.294	564.750	7.411	13.164	-0.896
BB5_C5	7458.250	402.434	566.750	16.721	13.160	-0.898
RP13_C11	6912.500	256.349	525.500	12.923	13.154	-0.902
BB5_C8	7632.500	589.308	579.500	16.114	13.171	-0.907
RP8_D10	4921.175	426.107	376.675	46.375	13.065	-0.940
BB5_G3	7449.500	581.824	567.750	10.689	13.121	-0.942
RP2_B5	4931.250	653.441	379.250	5.377	13.003	-0.963
RP2_A1	6726.250	203.800	514.750	5.737	13.067	-0.967
RP13_A7	3409.000	260.427	266.500	8.386	12.792	-0.972
RP13_F2	5590.250	268.516	429.500	5.972	13.016	-0.976
RP13_D6	6251.000	367.937	479.750	7.228	13.030	-0.990
RP2_B7	5102.000	262.657	393.000	14.720	12.982	-0.997
BB5_B10	7277.500	853.972	558.500	42.681	13.030	-0.998
BB5_C9	7265.250	489.584	557.250	10.046	13.038	-1.002
BB5_C11	7582.250	472.068	581.250	11.354	13.045	-1.011
RP2_B4	5038.500	352.525	389.500	4.655	12.936	-1.012
BB5_C3	7336.750	398.486	563.000	20.785	13.032	-1.013
BP2_A3	6556.280	420.327	504.165	13.563	13.004	-1.024
BB5_H2	7353.250	428.093	564.250	25.145	13.032	-1.035
BB5_D4	7403.250	212.625	568.250	19.225	13.028	-1.037
BB5_H12	7459.750	261.223	574.000	9.092	12.996	-1.054
RP2_D8	5925.000	309.099	457.500	11.387	12.951	-1.062
BB4_C2	7206.750	265.305	554.250	36.207	13.003	-1.066
RP2_A10	6887.000	313.323	530.500	26.851	12.982	-1.074
RP13_B9	6236.000	191.465	481.750	20.056	12.944	-1.074
RP13_C2	6387.750	355.948	493.750	16.174	12.937	-1.084
BB5_G5	6806.500	254.570	524.250	37.044	12.983	-1.086
RP2_A12	6802.000	208.290	524.750	33.540	12.962	-1.089
BB5_D12	8026.000	442.640	619.250	7.719	12.961	-1.099
BB5_E4	7280.750	496.701	563.250	11.587	12.926	-1.111
RP8_E6	5480.240	704.475	425.170	63.553	12.890	-1.112
BB5_D8	5415.750	699.388	422.000	12.884	12.834	-1.118
RP13_A6	4506.750	228.323	352.500	18.877	12.785	-1.120
BB5_B1	7419.000	565.085	574.750	25.131	12.908	-1.129
BB5_E8	7102.000	373.092	550.250	17.821	12.907	-1.132
BB5_C10	7447.250	457.333	577.250	10.874	12.901	-1.148
BB4_H5	4741.750	164.441	372.000	6.683	12.747	-1.159

RP8_D4	6498.940	523.734	505.385	45.183	12.859	-1.172
BB4_C9	7001.500	274.210	545.500	11.561	12.835	-1.190
BB5_F3	7334.500	440.803	571.250	27.837	12.839	-1.194
RP13_D9	6330.500	256.068	494.750	14.818	12.795	-1.214
BB5_E5	7183.250	370.924	560.750	5.377	12.810	-1.221
RP2_G1	2374.500	171.617	196.750	11.206	12.069	-1.227
JB10_E5	6567.250	473.815	516.500	9.256	12.715	-1.283
BB5_G4	7380.250	429.299	579.000	17.474	12.747	-1.295
BB4_E2	4912.500	774.735	390.750	11.758	12.572	-1.298
BB5_D1	6830.750	317.267	538.000	6.325	12.697	-1.313
JB10_H10	6343.000	257.802	500.500	11.902	12.673	-1.324
BB4_C3	6529.250	173.492	514.750	26.437	12.684	-1.331
RP13_A12	6718.250	355.369	530.250	22.202	12.670	-1.332
RP2_H5	4162.750	2427.047	346.250	151.364	12.022	-1.370
RP13_D4	5761.000	224.228	458.000	10.296	12.579	-1.381
RP8_E7	6754.225	342.907	535.275	13.304	12.618	-1.386
BB5_G2	7540.750	369.345	595.750	38.612	12.658	-1.398
BP6_B6	3512.075	878.978	276.025	98.880	12.724	-1.408
RP13_H2	4534.250	1583.669	370.500	96.186	12.238	-1.427
BB5_B4	7422.500	459.418	590.750	14.728	12.565	-1.451
BB4_B10	5928.250	486.492	475.000	13.292	12.481	-1.465
RP2_A2	4520.750	471.820	365.500	9.000	12.369	-1.488
JB10_D6	4872.500	223.030	393.500	11.619	12.382	-1.495
BB5_F5	7087.250	312.642	566.250	11.786	12.516	-1.501
BB4_C10	6856.500	397.305	549.000	16.753	12.489	-1.503
BP6_A6	4488.685	2067.808	370.575	137.730	12.113	-1.505
BB5_B6	6467.000	533.491	519.750	20.370	12.443	-1.528
BB5_A10	7595.750	515.773	608.250	24.744	12.488	-1.534
BB5_A3	7105.250	504.641	572.250	23.754	12.416	-1.579
BP2_A10	6170.455	286.125	497.455	34.020	12.404	-1.586
BP6_E5	4858.650	264.312	396.195	17.033	12.263	-1.594
BB5_C4	7189.500	359.244	580.750	17.671	12.380	-1.620
BB5_B3	7424.500	296.344	598.500	25.801	12.405	-1.621
RP8_C4	3090.870	284.602	261.385	17.149	11.825	-1.659
BP2_A2	6052.725	250.044	493.185	16.379	12.273	-1.687
BB5_B2	7421.750	369.088	603.250	32.387	12.303	-1.717
RP13_E11	6209.000	224.627	507.750	11.177	12.228	-1.733
BB4_D12	6143.250	526.620	503.500	21.810	12.201	-1.735
RP13_H10	5947.500	47.226	488.500	19.672	12.175	-1.775
BB5_F2	7330.000	456.849	604.250	22.157	12.131	-1.885
RP2_G10	5532.750	1284.629	464.500	70.382	11.911	-1.898
RP2_E11	2220.750	109.804	203.500	7.937	10.913	-1.972
BP2_A1	5859.965	218.575	491.050	28.359	11.934	-1.990
BB4_D9	5736.500	398.103	484.500	15.969	11.840	-2.050
BB5_D10	6558.750	495.790	554.000	11.662	11.839	-2.101
RP2_G9	2812.250	36.573	253.250	5.852	11.105	-2.139

BB5_D7	4568.500	686.597	394.750	20.123	11.573	-2.156
BB5_C2	7411.750	350.058	624.000	41.110	11.878	-2.160
RP2_B1	4311.750	526.435	374.750	17.595	11.506	-2.188
RP13_A9	5651.000	299.890	485.000	7.528	11.652	-2.226
RP2_A3	4155.500	749.372	365.250	6.185	11.377	-2.308
RP8_C3	4597.265	278.419	410.530	6.719	11.198	-2.538
RP2_F10	4350.000	335.438	390.250	32.108	11.147	-2.609
BP6_A10	3490.115	270.314	321.470	13.083	10.857	-2.628
BB5_A1	6645.250	678.250	588.000	16.269	11.301	-2.637
BB5_G8	5159.750	239.109	462.000	17.029	11.168	-2.646
JB10_B3	5669.750	166.748	505.750	18.927	11.211	-2.655
RP2_G6	4413.250	409.867	400.750	26.750	11.012	-2.667
BB5_G10	5922.750	556.200	539.750	16.701	10.973	-2.885
BB5_A9	4222.750	2462.129	414.250	132.588	10.194	-2.919
RP2_A6	3940.000	482.010	374.750	8.500	10.514	-3.051
RP2_H8	4089.500	1261.897	394.250	58.631	10.373	-3.064
BB4_C11	2276.750	70.287	235.250	23.329	9.678	-3.070
BB5_H1	5259.500	207.898	490.750	16.601	10.717	-3.074
RP2_A8	3579.250	357.692	349.000	5.774	10.256	-3.170
BB5_G11	5537.500	271.871	522.000	20.510	10.608	-3.212
RP2_A7	3751.000	445.664	366.750	6.602	10.228	-3.268
BB4_B5	2449.500	124.265	263.500	7.047	9.296	-3.499
BB5_E1	3513.750	760.030	368.750	12.894	9.529	-3.818
JB10_G2	3483.500	559.589	369.750	9.500	9.421	-3.926
BB5_F6	2422.750	123.716	281.000	17.833	8.622	-4.150
BB5_E2	3423.500	144.549	375.750	25.979	9.111	-4.248
BB4_B1	2398.750	90.669	284.500	13.964	8.431	-4.298
BB5_H4	3897.750	215.290	432.000	11.165	9.023	-4.468
JB10_H5	3823.000	157.654	427.000	13.711	8.953	-4.517
RP13_H11	2374.000	106.496	294.500	7.681	8.061	-4.648
BB4_C5	2526.750	109.463	312.250	6.946	8.092	-4.742
BB4_D1	2268.750	105.256	288.750	9.069	7.857	-4.752
BB5_A8	2278.750	45.353	291.750	12.633	7.811	-4.816
BB5_G6	3561.000	100.701	416.500	13.699	8.550	-4.841
BB4_H8	2554.000	187.378	320.750	9.032	7.963	-4.891
RP2_B12	2308.000	75.714	306.250	10.720	7.536	-5.139
BB5_H10	3342.500	357.104	416.000	14.652	8.035	-5.270
RP2_B9	3023.750	218.971	390.000	12.111	7.753	-5.434
BB5_H9	2903.500	69.467	378.750	19.889	7.666	-5.459
BB4_D4	2308.500	159.203	320.000	1.414	7.214	-5.485
BB5_B9	2601.500	202.824	351.500	19.434	7.401	-5.532
5uM FCCP	2938.672	207.228	395.246	87.905	7.435	-6.994
10uM FCCP	3003.263	238.224	408.086	91.823	7.359	-7.110

References

References

Abou-Sleiman, P. M., M. M. Muqit, et al. (2006). "Expanding insights of mitochondrial dysfunction in Parkinson's disease." Nat Rev Neurosci **7**(3): 207-219.

Abramov, A. Y. and M. R. Duchen (2010). "Impaired mitochondrial bioenergetics determines glutamate-induced delayed calcium deregulation in neurons." Biochim Biophys Acta **1800**(3): 297-304.

Adlam, V. J., J. C. Harrison, et al. (2005). "Targeting an antioxidant to mitochondria decreases cardiac ischemia-reperfusion injury." FASEB J **19**(9): 1088-1095.

Agostino, A., L. Valletta, et al. (2003). "Mutations of ANT1, Twinkle, and POLG1 in sporadic progressive external ophthalmoplegia (PEO)." Neurology **60**(8): 1354-1356.

Akimoto, T., S. C. Pohnert, et al. (2005). "Exercise stimulates Pgc-1alpha transcription in skeletal muscle through activation of the p38 MAPK pathway." Journal of Biological Chemistry **280**(20): 19587-19593.

Al Rawi, S., S. Louvet-Vallee, et al. (2011). "Postfertilization autophagy of sperm organelles prevents paternal mitochondrial DNA transmission." Science **334**(6059): 1144-1147.

Alberts, B., J. H. Wilson, et al. (2008). Molecular biology of the cell. New York, Garland Science.

Albring, M., J. Griffith, et al. (1977). "Association of a protein structure of probable membrane derivation with HeLa cell mitochondrial DNA near its origin of replication." Proc Natl Acad Sci U S A **74**(4): 1348-1352.

Alcolado, J. C., J. A. Rees, et al. (1994). "Selection of control subjects in genetic studies of diabetes mellitus." Diabetologia **37**(6): 639-640.

Alexeyev, M. F., N. Venediktova, et al. (2008). "Selective elimination of mutant mitochondrial genomes as therapeutic strategy for the treatment of NARP and MILS syndromes." Gene Ther **15**(7): 516-523.

Alston, C. L., J. Lowe, et al. (2010). "A novel mitochondrial tRNAGlu (MTTE) gene mutation causing chronic progressive external ophthalmoplegia at low levels of heteroplasmy in muscle." Journal of the Neurological Sciences **298**(1–2): 140-144.

Anderson, S., A. T. Bankier, et al. (1981). "Sequence and organization of the human mitochondrial genome." Nature **290**(5806): 457-465.

Andersson, H., T. Baechi, et al. (1998). "Autofluorescence of living cells." Journal of Microscopy-Oxford **191**: 1-7.

Andersson, S. G. E., A. Zomorodipour, et al. (1998). "The genome sequence of Rickettsia prowazekii and the origin of mitochondria." Nature **396**(6707): 133-140.

Andreux, P. A., R. H. Houtkooper, et al. (2013). "Pharmacological approaches to restore mitochondrial function." Nat Rev Drug Discov **12**(6): 465-483.

Andrews, R. M., I. Kubacka, et al. (1999). "Reanalysis and revision of the Cambridge reference sequence for human mitochondrial DNA." Nature Genetics **23**(2): 147-147.

Ashley, M. V., P. J. Laipis, et al. (1989). "Rapid segregation of heteroplasmic bovine mitochondria." Nucleic Acids Res **17**(18): 7325-7331.

Bacman, S. R., S. L. Williams, et al. (2013). "Specific elimination of mutant mitochondrial genomes in patient-derived cells by mitoTALENs." Nat Med.

Baradaran, R., J. M. Berrisford, et al. (2013). "Crystal structure of the entire respiratory complex I." Nature **494**(7438): 443-448.

Barrell, B. G., S. Anderson, et al. (1980). "Different pattern of codon recognition by mammalian mitochondrial tRNAs." Proc Natl Acad Sci U S A **77**(6): 3164-3166.

Bates, M., S. A. Jones, et al. (2013). "Stochastic optical reconstruction microscopy (STORM): a method for superresolution fluorescence imaging." Cold Spring Harb Protoc **2013**(6): 498-520.

Benz, R. and S. McLaughlin (1983). "The molecular mechanism of action of the proton ionophore FCCP (carbonylcyanide p-trifluoromethoxyphenylhydrazone)." Biophys J **41**(3): 381-398.

Bereiter-Hahn, J. (1978). "Intracellular motility of mitochondria: role of the inner compartment in migration and shape changes of mitochondria in XTH-cells." J Cell Sci **30**: 99-115.

Berg, J., Tymoczko, J. and Stryer, L. (2011). The Citric Acid Cycle. Biochemistry. New York, W.H. Freeman and Company.

Berg, J., Tymoczko, J. and Stryer, L. (2011). Glycolysis and Gluconeogenesis. Biochemistry. New York, W.H. Freeman and Company.

Berg, J., Tymoczko, J. and Stryer, L. (2011). Oxidative Phosphorylation. Biochemistry. New York, W.H. Freeman and Company.

Biswas, S., N. S. Dodwadkar, et al. (2011). "Surface modification of liposomes with rhodamine-123-conjugated polymer results in enhanced mitochondrial targeting." Journal of Drug Targeting **19**(7): 552-561.

Blaikie, F. H., S. E. Brown, et al. (2006). "Targeting dinitrophenol to mitochondria: limitations to the development of a self-limiting mitochondrial protonophore." Biosci Rep **26**(3): 231-243.

Bleazard, W., J. M. McCaffery, et al. (1999). "The dynamin-related GTPase Dnm1 regulates mitochondrial fission in yeast." Nature Cell Biology **1**(5): 298-304.

Bogenhagen, D. and D. A. Clayton (1977). "Mouse L-Cell Mitochondrial-DNA Molecules Are Selected Randomly for Replication Throughout Cell-Cycle." Cell **11**(4): 719-727.

Bonnet, D., P. Rustin, et al. (2001). "Heart transplantation in children with mitochondrial cardiomyopathy." Heart **86**(5): 570-573.

Brand, M. D. (2010). "The sites and topology of mitochondrial superoxide production." Exp Gerontol **45**(7-8): 466-472.

Brandhagen, B., C. Tieszen, et al. (2013). "Cytostasis and morphological changes induced by mifepristone in human metastatic cancer cells involve cytoskeletal filamentous actin reorganization and impairment of cell adhesion dynamics." BMC Cancer **13**(1): 35.

Brown, T. A., A. N. Tkachuk, et al. (2011). "Superresolution fluorescence imaging of mitochondrial nucleoids reveals their spatial range, limits, and membrane interaction." Molecular and Cellular Biology **31**(24): 4994-5010.

Camara, Y., J. Asin-Cayuela, et al. (2011). "MTERF4 regulates translation by targeting the methyltransferase NSUN4 to the mammalian mitochondrial ribosome." Cell Metab **13**(5): 527-539.

Canto, C., Z. Gerhart-Hines, et al. (2009). "AMPK regulates energy expenditure by modulating NAD+ metabolism and SIRT1 activity." Nature **458**(7241): 1056-1060.

Cao, W., K. W. Daniel, et al. (2004). "p38 mitogen-activated protein kinase is the central regulator of cyclic AMP-dependent transcription of the brown fat uncoupling protein 1 gene." Molecular and Cellular Biology **24**(7): 3057-3067.

Carrodeguas, J. A., R. Kobayashi, et al. (1999). "The accessory subunit of Xenopus laevis mitochondrial DNA polymerase gamma increases processivity of the catalytic subunit of human DNA polymerase gamma and is related to class II

aminoacyl-tRNA synthetases." Molecular and Cellular Biology **19**(6): 4039-4046.

Carrodeguas, J. A., K. G. Pinz, et al. (2002). "DNA binding properties of human pol gamma B." Journal of Biological Chemistry **277**(51): 50008-50014.

Carrozzo, R., A. Tessa, et al. (2001). "The T9176G mtDNA mutation severely affects ATP production and results in Leigh syndrome." Neurology **56**(5): 687-690.

Chang, D. D. and D. A. Clayton (1984). "Precise Identification of Individual Promoters for Transcription of Each Strand of Human Mitochondrial-DNA." Cell **36**(3): 635-643.

Chang, D. D. and D. A. Clayton (1987). "A Novel Endoribonuclease Cleaves at a Priming Site of Mouse Mitochondrial-DNA Replication." Embo Journal **6**(2): 409-417.

Chase, J. W. and K. R. Williams (1986). "Single-Stranded-DNA Binding-Proteins Required for DNA-Replication." Annual Review of Biochemistry **55**: 103-136.

Chen, H., J. Kovar, et al. (2005). "A cell-based immunocytochemical assay for monitoring kinase signaling pathways and drug efficacy." Analytical Biochemistry **338**(1): 136-142.

Chen, H. C., S. A. Detmer, et al. (2003). "Mitofusins Mfn1 and Mfn2 coordinately regulate mitochondrial fusion and are essential for embryonic development." Journal of Cell Biology **160**(2): 189-200.

Chi, C. S., H. F. Lee, et al. (2010). "Clinical manifestations in children with mitochondrial diseases." Pediatr Neurol **43**(3): 183-189.

Chinnery, P. F., M. A. Johnson, et al. (2000). "The epidemiology of pathogenic mitochondrial DNA mutations." Annals of Neurology **48**(2): 188-193.

Chinnery, P. F., R. W. Taylor, et al. (1999). "Peptide nucleic acid delivery to human mitochondria." Gene Therapy **6**(12): 1919-1928.

Chomyn, A., A. Martinuzzi, et al. (1992). "Melas Mutation in Mtdna Binding-Site for Transcription Termination Factor Causes Defects in Protein-Synthesis and in Respiration but No Change in Levels of Upstream and Downstream Mature Transcripts." Proceedings of the National Academy of Sciences of the United States of America **89**(10): 4221-4225.

Ciafaloni, E., E. Ricci, et al. (1992). "MELAS: clinical features, biochemistry, and molecular genetics." Annals of Neurology **31**(4): 391-398.

Cipolat, S., O. Martins de Brito, et al. (2004). "OPA1 requires mitofusin 1 to promote mitochondrial fusion." Proc Natl Acad Sci U S A **101**(45): 15927-15932.

Clayton, D. A. (1982). "Replication of animal mitochondrial DNA." Cell **28**(4): 693-705.

Comte, C., Y. Tonin, et al. (2013). "Mitochondrial targeting of recombinant RNAs modulates the level of a heteroplasmic mutation in human mitochondrial DNA associated with Kearns Sayre Syndrome." Nucleic Acids Res **41**(1): 418-433.

Costes, S. V., D. Daelemans, et al. (2004). "Automatic and quantitative measurement of protein-protein colocalization in live cells." Biophys J **86**(6): 3993-4003.

Crane, F. L. (1977). "Hydroquinone dehydrogenases." Annual Review of Biochemistry **46**: 439-469.

Craven, L., H. A. Tuppen, et al. (2010). "Pronuclear transfer in human embryos to prevent transmission of mitochondrial DNA disease." Nature **465**(7294): 82-U89.

Crick, F. H. (1966). "Codon--anticodon pairing: the wobble hypothesis." Journal of Molecular Biology **19**(2): 548-555.

D'Souza, G. G. M., R. Rammohan, et al. (2003). "DQAsome-mediated delivery of plasmid DNA toward mitochondria in living cells." Journal of Controlled Release **92**(1-2): 189-197.

de Grey, A. D. (1997). "A proposed refinement of the mitochondrial free radical theory of aging." Bioessays **19**(2): 161-166.

Denslow, N. D. and T. W. O'Brien (1974). "Susceptibility of 55S mitochondrial ribosomes to antibiotics inhibitory to prokaryotic ribosomes, lincomycin, chloramphenicol and PA114A." Biochem Biophys Res Commun **57**(1): 9-16.

Dillon, L. M., A. Hida, et al. (2012). "Long-Term Bezafibrate Treatment Improves Skin and Spleen Phenotypes of the mtDNA Mutator Mouse." Plos One **7**(9): e44335.

Dillon, L. M., S. L. Williams, et al. (2012). "Increased mitochondrial biogenesis in muscle improves aging phenotypes in the mtDNA mutator mouse." Hum Mol Genet **21**(10): 2288-2297.

Dingley, S., K. A. Chapman, et al. (2012). "Fluorescence-activated cell sorting analysis of mitochondrial content, membrane potential, and matrix oxidant burden in human lymphoblastoid cell lines." Methods Mol Biol **837**: 231-239.

Dorn, G. W., 2nd, C. F. Clark, et al. (2011). "MARF and Opa1 control mitochondrial and cardiac function in Drosophila." Circulation Research **108**(1): 12-17.

Dubrovsky, E. B., V. A. Dubrovskaya, et al. (2004). "Drosophila RNase Z processes mitochondrial and nuclear pre-tRNA 3' ends in vivo." Nucleic Acids Res **32**(1): 255-262.

Duchen, M. R. (2000). "Mitochondria and calcium: from cell signalling to cell death." J Physiol **529 Pt 1**: 57-68.

Efremov, R. G., R. Baradaran, et al. (2010). "The architecture of respiratory complex I." Nature **465**(7297): 441-445.

Elson, J. L., D. C. Samuels, et al. (2001). "Random intracellular drift explains the clonal expansion of mitochondrial DNA mutations with age." Am J Hum Genet **68**(3): 802-806.

Falkenberg, M., M. Gaspari, et al. (2002). "Mitochondrial transcription factors B1 and B2 activate transcription of human mtDNA." Nature Genetics **31**(3): 289-294.

Falkenberg, M., N. G. Larsson, et al. (2007). "DNA replication and transcription in mammalian mitochondria." Annual Review of Biochemistry **76**: 679-699.

Falkenberg, M., N. G. Larsson, et al. (2007). "DNA replication and transcription in mammalian mitochondria." Annual Review of Biochemistry **76**: 679-699.

Falkenberg, M., I. R. Lehman, et al. (2000). "Leading and lagging strand DNA synthesis in vitro by a reconstituted herpes simplex virus type 1 replisome." Proc Natl Acad Sci U S A **97**(8): 3896-3900.

Faraci, M., D. Cuzzubbo, et al. (2007). Allogeneic bone marrow transplantation for Pearson's syndrome, Bone Marrow Transplant. 2007 May;39(9):563-5. Epub 2007 Mar 5.

Faxen, K., G. Gilderson, et al. (2005). "A mechanistic principle for proton pumping by cytochrome c oxidase." Nature **437**(7056): 286-289.

Filipovska, A., M. R. Eccles, et al. (2004). "Delivery of antisense peptide nucleic acids (PNAs) to the cytosol by disulphide conjugation to a lipophilic cation." Febs Letters **556**(1-3): 180-186.

Finichiu, P. G., A. M. James, et al. (2013). "Mitochondrial accumulation of a lipophilic cation conjugated to an ionisable group depends on membrane potential, pH gradient and pK(a): implications for the design of mitochondrial probes and therapies." J Bioenerg Biomembr **45**(1-2): 165-173.

Fisher, R. P. and D. A. Clayton (1988). "Purification and characterization of human mitochondrial transcription factor 1." Molecular and Cellular Biology **8**(8): 3496-3509.

Fisher, R. P., T. Lisowsky, et al. (1992). "DNA Wrapping and Bending by a Mitochondrial High Mobility Group-Like Transcriptional Activator Protein." Journal of Biological Chemistry **267**(5): 3358-3367.

Fukuhara, N., S. Tokiguchi, et al. (1980). "Myoclonus epilepsy associated with ragged-red fibres (mitochondrial abnormalities): disease entity or a syndrome? Light- and electron-microscopic studies of two cases and review of literature." Journal of the Neurological Sciences **47**(1): 117-133.

Garone, C., S. Tadesse, et al. (2011). "Clinical and genetic spectrum of mitochondrial neurogastrointestinal encephalomyopathy." Brain **134**(Pt 11): 3326-3332.

Garrido, N., L. Griparic, et al. (2003). "Composition and dynamics of human mitochondrial nucleoids." Molecular Biology of the Cell **14**(4): 1583-1596.

Ghafourifar, P. and E. Cadenas (2005). "Mitochondrial nitric oxide synthase." Trends in Pharmacological Sciences **26**(4): 190-195.

Giles, R. E., H. Blanc, et al. (1980). "Maternal Inheritance of Human Mitochondrial-DNA." Proceedings of the National Academy of Sciences of the United States of America-Biological Sciences **77**(11): 6715-6719.

Goffart, S., H. M. Cooper, et al. (2009). "Twinkle mutations associated with autosomal dominant progressive external ophthalmoplegia lead to impaired helicase function and in vivo mtDNA replication stalling." Hum Mol Genet **18**(2): 328-340.

Golubitzky, A., P. Dan, et al. (2011). "Screening for active small molecules in mitochondrial complex I deficient patient's fibroblasts, reveals AICAR as the most beneficial compound." Plos One **6**(10): e26883.

Goto, Y., I. Nonaka, et al. (1990). "A mutation in the tRNA(Leu)(UUR) gene associated with the MELAS subgroup of mitochondrial encephalomyopathies." Nature **348**(6302): 651-653.

Graham, B. H., K. G. Waymire, et al. (1997). "A mouse model for mitochondrial myopathy and cardiomyopathy resulting from a deficiency in the heart/muscle isoform of the adenine nucleotide translocator." Nature Genetics **16**(3): 226-234.

Gray, H. and T. W. Wong (1992). "Purification and Identification of Subunit Structure of the Human Mitochondrial-DNA Polymerase." Journal of Biological Chemistry **267**(9): 5835-5841.

Hagerhall, C. (1997). "Succinate: quinone oxidoreductases. Variations on a conserved theme." Biochim Biophys Acta **1320**(2): 107-141.

Hales, K. G. and M. T. Fuller (1997). "Developmentally regulated mitochondrial fusion mediated by a conserved, novel, predicted GTPase." Cell **90**(1): 121-129.

Halter, J., W. M. Schupbach, et al. (2011). "Allogeneic hematopoietic SCT as treatment option for patients with mitochondrial neurogastrointestinal encephalomyopathy

(MNGIE): a consensus conference proposal for a standardized approach." Bone Marrow Transplant **46**(3): 330-337.

Handschin, C., J. Rhee, et al. (2003). "An autoregulatory loop controls peroxisome proliferator-activated receptor gamma coactivator 1alpha expression in muscle." Proc Natl Acad Sci U S A **100**(12): 7111-7116.

Hartzog, P. E. and B. D. Cain (1993). "The aleu207-->arg mutation in F1F0-ATP synthase from Escherichia coli. A model for human mitochondrial disease." Journal of Biological Chemistry **268**(17): 12250-12252.

Hauswirth, W. W. and P. J. Laipis (1982). "Mitochondrial DNA polymorphism in a maternal lineage of Holstein cows." Proc Natl Acad Sci U S A **79**(15): 4686-4690.

Hawlitschek, G., H. Schneider, et al. (1988). "Mitochondrial protein import: identification of processing peptidase and of PEP, a processing enhancing protein." Cell **53**(5): 795-806.

Heid, C. A., J. Stevens, et al. (1996). "Real time quantitative PCR." Genome Res **6**(10): 986-994.

Herzig, S., F. Long, et al. (2001). "CREB regulates hepatic gluconeogenesis through the coactivator PGC-1." Nature **413**(6852): 179-183.

Hirano, M., E. Ricci, et al. (1992). "Melas: an original case and clinical criteria for diagnosis." Neuromuscul Disord **2**(2): 125-135.

Hirst, J., J. Carroll, et al. (2003). "The nuclear encoded subunits of complex I from bovine heart mitochondria." Biochim Biophys Acta **1604**(3): 135-150.

Hixson, J. E. and D. A. Clayton (1985). "Initiation of Transcription from Each of the 2 Human Mitochondrial Promoters Requires Unique Nucleotides at the Transcriptional Start Sites." Proceedings of the National Academy of Sciences of the United States of America **82**(9): 2660-2664.

Hockemeyer, D., H. Wang, et al. (2011). "Genetic engineering of human pluripotent cells using TALE nucleases." Nat Biotechnol **29**(8): 731-734.

Holme, E., N. G. Larsson, et al. (1993). "Multiple symmetric lipomas with high levels of mtDNA with the tRNA(Lys) A-->G(8344) mutation as the only manifestation of disease in a carrier of myoclonus epilepsy and ragged-red fibers (MERRF) syndrome." American Journal of Human Genetics **52**(3): 551-556.

Holt, I. J., H. E. Lorimer, et al. (2000). "Coupled leading- and lagging-strand synthesis of mammalian mitochondrial DNA." Cell **100**(5): 515-524.

Holzmann, J., P. Frank, et al. (2008). "RNase P without RNA: identification and functional reconstitution of the human mitochondrial tRNA processing enzyme." Cell **135**(3): 462-474.

Hoppins, S., L. Lackner, et al. (2007). "The machines that divide and fuse mitochondria." Annual Review of Biochemistry **76**: 751-780.

Horvath, R. (2012). "Update on clinical aspects and treatment of selected vitamin-responsive disorders II (riboflavin and CoQ 10)." J Inherit Metab Dis **35**(4): 679-687.

Horvath, R., G. Gorman, et al. (2008). "How can we treat mitochondrial encephalomyopathies? Approaches to therapy." Neurotherapeutics **5**(4): 558-568.

Houtkooper, R. H., C. Canto, et al. (2010). "The secret life of NAD+: an old metabolite controlling new metabolic signaling pathways." Endocr Rev **31**(2): 194-223.

Huang, B., W. Wang, et al. (2008). "Three-dimensional super-resolution imaging by stochastic optical reconstruction microscopy." Science **319**(5864): 810-813.

Hyvarinen, A. K., J. L. Pohjoismaki, et al. (2007). "The mitochondrial transcription termination factor mTERF modulates replication pausing in human mitochondrial DNA." Nucleic Acids Res **35**(19): 6458-6474.

Inoue, K., K. Nakada, et al. (2000). "Generation of mice with mitochondrial dysfunction by introducing mouse mtDNA carrying a deletion into zygotes." Nature Genetics **26**(2): 176-181.

Jacobson, J. and M. R. Duchen (2004). "Interplay between mitochondria and cellular calcium signalling." Mol Cell Biochem **256-257**(1-2): 209-218.

Jager, S., C. Handschin, et al. (2007). "AMP-activated protein kinase (AMPK) action in skeletal muscle via direct phosphorylation of PGC-1alpha." Proc Natl Acad Sci U S A **104**(29): 12017-12022.

James, A. M., F. H. Blaikie, et al. (2003). "Specific targeting of a DNA-alkylating reagent to mitochondria. Synthesis and characterization of [4-((11aS)-7-methoxy-1,2,3,11a-tetrahydro-5H-pyrrolo[2,1-c][1,4]benzodiazepin-5-o n-8-oxy)butyl]-triphenylphosphonium iodide." Eur J Biochem **270**(13): 2827-2836.

James, A. M., M. S. Sharpley, et al. (2007). "Interaction of the mitochondria-targeted antioxidant MitoQ with phospholipid bilayers and ubiquinone oxidoreductases." Journal of Biological Chemistry **282**(20): 14708-14718.

Jensen, P. R., E. Gontang, et al. (2005). "Culturable marine actinomycete diversity from tropical Pacific Ocean sediments." Environ Microbiol **7**(7): 1039-1048.

Jeppesen, M. G., T. Navratil, et al. (2005). "Crystal structure of the bovine mitochondrial elongation factor Tu.Ts complex." Journal of Biological Chemistry **280**(6): 5071-5081.

Jorgensen, S. B., J. F. Wojtaszewski, et al. (2005). "Effects of alpha-AMPK knockout on exercise-induced gene activation in mouse skeletal muscle." FASEB J **19**(9): 1146-1148.

Jouaville, L. S., P. Pinton, et al. (1999). "Regulation of mitochondrial ATP synthesis by calcium: evidence for a long-term metabolic priming." Proc Natl Acad Sci U S A **96**(24): 13807-13812.

Karbowski, M., J. H. Spodnik, et al. (2001). "Opposite effects of microtubule-stabilizing and microtubule-destabilizing drugs on biogenesis of mitochondria in mammalian cells." Journal of Cell Science **114**(2): 281-291.

Karicheva, O. Z., O. A. Kolesnikova, et al. (2011). "Correction of the consequences of mitochondrial 3243A > G mutation in the MT-TL1 gene causing the MELAS syndrome by tRNA import into mitochondria." Nucleic Acids Research **39**(18): 8173-8186.

Katunin, V. I., A. Savelsbergh, et al. (2002). "Coupling of GTP hydrolysis by elongation factor G to translocation and factor recycling on the ribosome." Biochemistry **41**(42): 12806-12812.

Kelso, G. F., A. Maroz, et al. (2012). "A Mitochondria-Targeted Macrocyclic Mn(II) Superoxide Dismutase Mimetic." Chem Biol **19**(10): 1237-1246.

Kelso, G. F., C. M. Porteous, et al. (2001). "Selective targeting of a redox-active ubiquinone to mitochondria within cells: antioxidant and antiapoptotic properties." Journal of Biological Chemistry **276**(7): 4588-4596.

Kirichok, Y., G. Krapivinsky, et al. (2004). "The mitochondrial calcium uniporter is a highly selective ion channel." Nature **427**(6972): 360-364.

Kirino, Y. and T. Suzuki (2005). "Human mitochondrial diseases associated with tRNA wobble modification deficiency." RNA Biol **2**(2): 41-44.

Kirino, Y., T. Yasukawa, et al. (2004). "Codon-specific translational defect caused by a wobble modification deficiency in mutant tRNA from a human mitochondrial disease." Proc Natl Acad Sci U S A **101**(42): 15070-15075.

Koc, E. C., W. Burkhart, et al. (2001). "The large subunit of the mammalian mitochondrial ribosome. Analysis of the complement of ribosomal proteins present." Journal of Biological Chemistry **276**(47): 43958-43969.

Koch, T., H. F. Hansen, et al. (1997). "Improvements in automated PNA synthesis using Boc/Z monomers." J Pept Res **49**(1): 80-88.

Koga, Y., Y. Akita, et al. (2005). "L-arginine improves the symptoms of strokelike episodes in MELAS." Neurology **64**(4): 710-712.

Koga, Y., N. Povalko, et al. (2012). "Molecular pathology of MELAS and L-arginine effects." Biochim Biophys Acta **1820**(5): 608-614.

Kolesnikova, O. A., N. S. Entelis, et al. (2004). "Nuclear DNA-encoded tRNAs targeted into mitochondria can rescue a mitochondrial DNA mutation associated with the MERRF syndrome in cultured human cells." Hum Mol Genet **13**(20): 2519-2534.

Korhonen, J. A., M. Gaspari, et al. (2003). "TWINKLE Has 5' -> 3' DNA helicase activity and is specifically stimulated by mitochondrial single-stranded DNA-binding protein." Journal of Biological Chemistry **278**(49): 48627-48632.

Korhonen, J. A., X. H. Pham, et al. (2004). "Reconstitution of a minimal mtDNA replisome in vitro." Embo Journal **23**(12): 2423-2429.

Koshiba, T., S. A. Detmer, et al. (2004). "Structural basis of mitochondrial tethering by mitofusin complexes." Science **305**(5685): 858-862.

Krishnan, K. J., A. K. Reeve, et al. (2008). "What causes mitochondrial DNA deletions in human cells?" Nature Genetics **40**(3): 275-279.

Kruse, B., N. Narasimhan, et al. (1989). "Termination of transcription in human mitochondria: identification and purification of a DNA binding protein factor that promotes termination." Cell **58**(2): 391-397.

Kuntzel, H. (1969). "PROTEINS OF MITOCHONDRIAL AND CYTOPLASMIC RIBOSOMES FROM NEUROSPORA-CRASSA." Nature (London) **222**(5189): 142-146.

Kussmaul, L. and J. Hirst (2006). "The mechanism of superoxide production by NADH:ubiquinone oxidoreductase (complex I) from bovine heart mitochondria." Proc Natl Acad Sci U S A **103**(20): 7607-7612.

Kyriakouli, D. S. (2007). Manipulation of the mitochondrial genome : generating models and exploring an antigenomic approach for treating mitochondrial DNA disorders PhD Thesis, University of Newcastle.

Lagouge, M., C. Argmann, et al. (2006). "Resveratrol improves mitochondrial function and protects against metabolic disease by activating SIRT1 and PGC-1alpha." Cell **127**(6): 1109-1122.

Land, E. J. and A. J. Swallow (1970). "One-electron reactions in biochemical systems as studied by pulse radiolysis. 3. Ubiquinone." Journal of Biological Chemistry **245**(8): 1890-1894.

Larsson, N. G., J. Wang, et al. (1998). "Mitochondrial transcription factor A is necessary for mtDNA maintenance and embryogenesis in mice." Nature Genetics **18**(3): 231-236.

Leigh, D. (1951). "Subacute necrotizing encephalomyelopathy in an infant." J Neurol Neurosurg Psychiatry **14**(3): 216-221.

Lerin, C., J. T. Rodgers, et al. (2006). "GCN5 acetyltransferase complex controls glucose metabolism through transcriptional repression of PGC-1alpha." Cell Metab **3**(6): 429-438.

Lestienne, P. and G. Ponsot (1988). Kearns-Sayre syndrome with muscle mitochondrial DNA deletion, Lancet. 1988 Apr 16;1(8590):885.

Lightowlers, R. N. (2011). "Mitochondrial transformation: time for concerted action." Embo Reports **12**(6): 480-481.

Litonin, D., M. Sologub, et al. (2010). "Human mitochondrial transcription revisited: only TFAM and TFB2M are required for transcription of the mitochondrial genes in vitro." Journal of Biological Chemistry **285**(24): 18129-18133.

Lodeiro, M. F., A. Uchida, et al. (2012). "Transcription from the second heavy-strand promoter of human mtDNA is repressed by transcription factor A in vitro." Proc Natl Acad Sci U S A **109**(17): 6513-6518.

Loschen, G., L. Flohe, et al. (1971). "Respiratory chain linked H(2)O(2) production in pigeon heart mitochondria." Febs Letters **18**(2): 261-264.

Lundholt, B. K., K. M. Scudder, et al. (2003). "A Simple Technique for Reducing Edge Effect in Cell-Based Assays." Journal of Biomolecular Screening **8**(5): 566-570.

Luo, S. M., Z. J. Ge, et al. (2013). "Unique insights into maternal mitochondrial inheritance in mice." Proc Natl Acad Sci U S A **110**(32): 13038-13043.

Lyrawati, D., A. Trounson, et al. (2011). "Expression of GFP in the Mitochondrial Compartment Using DQAsome-Mediated Delivery of an Artificial Mini-mitochondrial Genome." Pharmaceutical Research **28**(11): 2848-2862.

Ma, J. and L. L. Spremulli (1996). "Expression, purification, and mechanistic studies of bovine mitochondrial translational initiation factor 2." Journal of Biological Chemistry **271**(10): 5805-5811.

Malecki, M. T., J. Skupien, et al. (2006). "Maternally inherited diabetes with deafness and obesity: body weight reduction response to treatment with insulin analogues." Rev Diabet Stud **3**(4): 205-207.

Mannella, C. A., M. Marko, et al. (1994). "The internal compartmentation of rat-liver mitochondria: tomographic study using the high-voltage transmission electron microscope." Microsc Res Tech **27**(4): 278-283.

Margulis, L. (1971). "Symbiosis and evolution." Sci Am **225**(2): 48-57.

Martin, W. and M. Muller (1998). "The hydrogen hypothesis for the first eukaryote." Nature **392**(6671): 37-41.

Martínez-Diez, M., G. Santamaría, et al. (2006). "Biogenesis and Dynamics of Mitochondria during the Cell Cycle: Significance of 3′UTRs." Plos One **1**(1): e107.

Masucci, J. P., M. Davidson, et al. (1995). "In vitro analysis of mutations causing myoclonus epilepsy with ragged-red fibers in the mitochondrial tRNA(Lys)gene: two genotypes produce similar phenotypes." Molecular and Cellular Biology **15**(5): 2872-2881.

McCormack, J. G., A. P. Halestrap, et al. (1990). "Role of calcium ions in regulation of mammalian intramitochondrial metabolism." Physiol Rev **70**(2): 391-425.

McFarland, R., R. W. Taylor, et al. (2002). "The neurology of mitochondrial DNA disease." Lancet Neurology **1**(6): 343-351.

McFarland, R. and D. M. Turnbull (2009). "Batteries not included: diagnosis and management of mitochondrial disease." J Intern Med **265**(2): 210-228.

McLean, R. A., W. L. Sanders, et al. (1991). "A Unified Approach to Mixed Linear Models." The American Statistician **45**(1): 54-64.

Medeiros, D. M. (2008). "Assessing mitochondria biogenesis." Methods **46**(4): 288-294.

Meeusen, S., Q. Tieu, et al. (1999). "Mgm101p is a novel component of the mitochondrial nucleoid that binds DNA and is required for the repair of oxidatively damaged mitochondrial DNA." Journal of Cell Biology **145**(2): 291-304.

Michael, L. F., Z. Wu, et al. (2001). "Restoration of insulin-sensitive glucose transporter (GLUT4) gene expression in muscle cells by the transcriptional coactivator PGC-1." Proc Natl Acad Sci U S A **98**(7): 3820-3825.

Milder, J. and M. Patel (2012). "Modulation of oxidative stress and mitochondrial function by the ketogenic diet." Epilepsy Res **100**(3): 295-303.

Minczuk, M., M. A. Papworth, et al. (2006). "Sequence-specific modification of mitochondrial DNA using a chimeric zinc finger methylase." Proceedings of the National Academy of Sciences **103**(52): 19689-19694.

Minczuk, M., M. A. Papworth, et al. (2008). "Development of a single-chain, quasi-dimeric zinc-finger nuclease for the selective degradation of mutated human mitochondrial DNA." Nucleic Acids Research **36**(12): 3926-3938.

Mitchell, P. (1961). "Coupling of phosphorylation to electron and hydrogen transfer by a chemi-osmotic type of mechanism." Nature **191**: 144-148.

Mitchell, P. (1976). "Possible Molecular Mechanisms of Protonmotive Function of Cytochrome Systems." J Theor Biol **62**(2): 327-367.

Montero-Calasanz Mdel, C., M. Goker, et al. (2013). "Geodermatophilus africanus sp. nov., a halotolerant actinomycete isolated from Saharan desert sand." Antonie Van Leeuwenhoek **104**(2): 207-216.

Montoya, J., T. Christianson, et al. (1982). "Identification of initiation sites for heavy-strand and light-strand transcription in human mitochondrial DNA." Proc Natl Acad Sci U S A **79**(23): 7195-7199.

Morgan-Hughes, J. A., M. G. Sweeney, et al. (1995). "Mitochondrial DNA (mtDNA) diseases: correlation of genotype to phenotype." Biochim Biophys Acta **1271**(1): 135-140.

Mozdy, A. D., J. M. McCaffery, et al. (2000). "Dnm1p GTPase-mediated mitochondrial fission is a multi-step process requiring the novel integral membrane component Fis1p." Journal of Cell Biology **151**(2): 367-380.

Murphy, J. L., E. L. Blakely, et al. (2008). "Resistance training in patients with single, large-scale deletions of mitochondrial DNA." Brain **131**: 2832-2840.

Murphy, M. P. (2009). "How mitochondria produce reactive oxygen species." Biochemical Journal **417**: 1-13.

Naviaux, R. K., W. L. Nyhan, et al. (1999). "Mitochondrial DNA polymerase gamma deficiency and mtDNA depletion in a child with Alpers' syndrome." Annals of Neurology **45**(1): 54-58.

Nielsen, P. E., M. Egholm, et al. (1991). "Sequence-Selective Recognition of DNA by Strand Displacement with a Thymine-Substituted Polyamide." Science **254**(5037): 1497-1500.

Noji, H., R. Yasuda, et al. (1997). "Direct observation of the rotation of F1-ATPase." Nature **386**(6622): 299-302.

Nunnari, J., W. F. Marshall, et al. (1997). "Mitochondrial transmission during mating in Saccharomyces cerevisiae is determined by mitochondrial fusion and fission and the intramitochondrial segregation of mitochondrial DNA." Molecular Biology of the Cell **8**(7): 1233-1242.

O'Brian, T. (1971). "The general occurrence of 55S ribosomes in mammalian liver mitochondria." Journal of Biological Chemistry **246**: 3409-3417.

Ohkubo, K., A. Yamano, et al. (2001). "Mitochondrial gene mutations in the tRNA(Leu(UUR)) region and diabetes: prevalence and clinical phenotypes in Japan." Clinical Chemistry **47**(9): 1641-1648.

Ojala, D., J. Montoya, et al. (1981). "tRNA punctuation model of RNA processing in human mitochondria." Nature **290**(5806): 470-474.

Otera, H., C. Wang, et al. (2010). "Mff is an essential factor for mitochondrial recruitment of Drp1 during mitochondrial fission in mammalian cells." Journal of Cell Biology **191**(6): 1141-1158.

Palade, G. E. (1952). "The fine structure of mitochondria." Anat Rec **114**(3): 427-451.

Paradkar, P. N., K. B. Zumbrennen, et al. (2009). "Regulation of mitochondrial iron import through differential turnover of mitoferrin 1 and mitoferrin 2." Molecular and Cellular Biology **29**(4): 1007-1016.

Park, C. B., J. Asin-Cayuela, et al. (2007). "MTERF3 is a negative regulator of mammalian mtDNA transcription." Cell **130**(2): 273-285.

Park, C. B. and N. G. Larsson (2011). "Mitochondrial DNA mutations in disease and aging." Journal of Cell Biology **193**(5): 809-818.

Pathom-Aree, W., J. E. Stach, et al. (2006). "Diversity of actinomycetes isolated from Challenger Deep sediment (10,898 m) from the Mariana Trench." Extremophiles **10**(3): 181-189.

Pavlakis, S. G., P. C. Phillips, et al. (1984). "Mitochondrial myopathy, encephalopathy, lactic acidosis, and strokelike episodes: a distinctive clinical syndrome." Annals of Neurology **16**(4): 481-488.

Pellegrini, M., J. Asin-Cayuela, et al. (2009). "MTERF2 is a nucleoid component in mammalian mitochondria." Biochim Biophys Acta **1787**(5): 296-302.

Persikov, A. V., R. Osada, et al. (2009). "Predicting DNA recognition by Cys2His2 zinc finger proteins." Bioinformatics **25**(1): 22-29.

Pfaff, E. and M. Klingenberg (1968). "Adenine nucleotide translocation of mitochondria. 1. Specificity and control." Eur J Biochem **6**(1): 66-79.

Pfanner, N., F. U. Hartl, et al. (1988). "Import of proteins into mitochondria: a multi-step process." Eur J Biochem **175**(2): 205-212.

Posch, W., S. Piper, et al. (2012). "Inhibition of human immunodeficiency virus replication by cell membrane-crossing oligomers." Mol Med **18**: 111-122.

Puigserver, P. and B. M. Spiegelman (2003). "Peroxisome Proliferator-Activated Receptor-γ Coactivator 1α (PGC-1α): Transcriptional Coactivator and Metabolic Regulator." Endocrine Reviews **24**(1): 78-90.

Puigserver, P., Z. Wu, et al. (1998). "A cold-inducible coactivator of nuclear receptors linked to adaptive thermogenesis." Cell **92**(6): 829-839.

Rebelo, A. P., S. L. Williams, et al. (2009). "In vivo methylation of mtDNA reveals the dynamics of protein-mtDNA interactions." Nucleic Acids Res **37**(20): 6701-6715.

Reddy, P. H. and M. F. Beal (2005). "Are mitochondria critical in the pathogenesis of Alzheimer's disease?" Brain Res Brain Res Rev **49**(3): 618-632.

Reddy, P. H. and T. P. Reddy (2011). "Mitochondria as a therapeutic target for aging and neurodegenerative diseases." Curr Alzheimer Res **8**(4): 393-409.

Reeve, A. K. (2007). "The molecular basis of neurodegeneration : the role of mitochondrial DNA mutations."

Rhee, S. G., Y. S. Bae, et al. (2000). "Hydrogen peroxide: a key messenger that modulates protein phosphorylation through cysteine oxidation." Sci STKE **2000**(53): pe1.

Rodgers, J. T., C. Lerin, et al. (2005). "Nutrient control of glucose homeostasis through a complex of PGC-1alpha and SIRT1." Nature **434**(7029): 113-118.

Rodgers, J. T. and P. Puigserver (2007). "Fasting-dependent glucose and lipid metabolic response through hepatic sirtuin 1." Proc Natl Acad Sci U S A **104**(31): 12861-12866.

Rodrigues, R. M., P. Macko, et al. (2011). "Autofluorescence microscopy: a non-destructive tool to monitor mitochondrial toxicity." Toxicol Lett **206**(3): 281-288.

Rorbach, J., R. Richter, et al. (2008). "The human mitochondrial ribosome recycling factor is essential for cell viability." Nucleic Acids Res **36**(18): 5787-5799.

Ross, M. F., T. A. Prime, et al. (2008). "Rapid and extensive uptake and activation of hydrophobic triphenylphosphonium cations within cells." Biochem J **411**(3): 633-645.

Russo, A., C. Cirulli, et al. (2008). "cis-acting sequences and trans-acting factors in the localization of mRNA for mitochondrial ribosomal proteins." Biochimica Et Biophysica Acta-Gene Regulatory Mechanisms **1779**(12): 820-829.

Rust, M. J., M. Bates, et al. (2006). "Sub-diffraction-limit imaging by stochastic optical reconstruction microscopy (STORM)." Nat Methods **3**(10): 793-795.

Sacconi, S., L. Salviati, et al. (2008). "A functionally dominant mitochondrial DNA mutation." Hum Mol Genet **17**(12): 1814-1820.

Saita, S., M. Shirane, et al. (2013). "Selective escape of proteins from the mitochondria during mitophagy." Nat Commun **4**: 1410.

Saneto, R. P., B. H. Cohen, et al. (2013). "Alpers-Huttenlocher syndrome." Pediatr Neurol **48**(3): 167-178.

Sazanov, L. A. (2007). "Respiratory complex I: mechanistic and structural insights provided by the crystal structure of the hydrophilic domain." Biochemistry **46**(9): 2275-2288.

Scaduto, R. C., Jr. and L. W. Grotyohann (1999). "Measurement of mitochondrial membrane potential using fluorescent rhodamine derivatives." Biophys J **76**(1 Pt 1): 469-477.

Schaefer, A. M., R. McFarland, et al. (2008). "Prevalence of mitochondrial DNA disease in adults." Annals of Neurology **63**(1): 35-39.

Schnell, S. A., W. A. Staines, et al. (1999). "Reduction of lipofuscin-like autofluorescence in fluorescently labeled tissue." J Histochem Cytochem **47**(6): 719-730.

Schwartz, M. and J. Vissing (2002). "Paternal inheritance of mitochondrial DNA." N Engl J Med **347**(8): 576-580.

Schwarzenbach, R. P., R. Stierli, et al. (1988). "COMPOUND PROPERTIES RELEVANT FOR ASSESSING THE ENVIRONMENTAL PARTITIONING OF NITROPHENOLS." Environmental Science & Technology **22**(1): 83-92.

Sciacco, M., E. Bonilla, et al. (1994). "Distribution of wild-type and common deletion forms of mtDNA in normal and respiration-deficient muscle fibers from patients with mitochondrial myopathy." Hum Mol Genet **3**(1): 13-19.

Sena, L. A. and N. S. Chandel (2012). "Physiological roles of mitochondrial reactive oxygen species." Molecular Cell **48**(2): 158-167.

Sgarbi, G., A. Baracca, et al. (2006). "Inefficient coupling between proton transport and ATP synthesis may be the pathogenic mechanism for NARP and Leigh

syndrome resulting from the T8993G mutation in mtDNA." Biochem J **395**(3): 493-500.

Shi, S. R., R. J. Cote, et al. (2001). "Antigen retrieval immunohistochemistry and molecular morphology in the year 2001." Appl Immunohistochem Mol Morphol **9**(2): 107-116.

Shi, Y., A. Dierckx, et al. (2012). "Mammalian transcription factor A is a core component of the mitochondrial transcription machinery." Proc Natl Acad Sci U S A **109**(41): 16510-16515.

Shin, H. W., C. Shinotsuka, et al. (1997). "Identification and subcellular localization of a novel mammalian dynamin-related protein homologous to yeast Vps1p and Dnm1p." J Biochem **122**(3): 525-530.

Shoffner, J. M., M. T. Lott, et al. (1990). "MYOCLONIC EPILEPSY AND RAGGED-RED FIBER DISEASE (MERRF) IS ASSOCIATED WITH A MITOCHONDRIAL-DNA TRANSFER RNALYS MUTATION." Cell **61**(6): 931-937.

Shoffner, J. M., M. T. Lott, et al. (1989). "Spontaneous Kearns-Sayre/chronic external ophthalmoplegia plus syndrome associated with a mitochondrial DNA deletion: a slip-replication model and metabolic therapy." Proc Natl Acad Sci U S A **86**(20): 7952-7956.

Shoubridge, E. A. and T. Wai (2007). "Mitochondrial DNA and the mammalian oocyte." Curr Top Dev Biol **77**: 87-111.

Shutt, T. E., M. F. Lodeiro, et al. (2010). "Core human mitochondrial transcription apparatus is a regulated two-component system in vitro." Proc Natl Acad Sci U S A **107**(27): 12133-12138.

Sies, H. (1993). "Strategies of antioxidant defense." Eur J Biochem **215**(2): 213-219.

Sinnathuray, A. R., V. Raut, et al. (2003). "A review of cochlear implantation in mitochondrial sensorineural hearing loss." Otol Neurotol **24**(3): 418-426.

Skulachev, V. P. (2001). "Mitochondrial filaments and clusters as intracellular power-transmitting cables." Trends in Biochemical Sciences **26**(1): 23-29.

Smith, O. P., I. M. Hann, et al. (1995). "Pearson's marrow/pancreas syndrome: haematological features associated with deletion and duplication of mitochondrial DNA." Br J Haematol **90**(2): 469-472.

Smits, P., J. Smeitink, et al. (2010). "Mitochondrial translation and beyond: processes implicated in combined oxidative phosphorylation deficiencies." J Biomed Biotechnol **2010**: 737385.

Soleimanpour-Lichaei, H. R., I. Kuhl, et al. (2007). "mtRF1a is a human mitochondrial translation release factor decoding the major termination codons UAA and UAG." Molecular Cell **27**(5): 745-757.

Sologub, M., S. N. Kochetkov, et al. (2009). "[Transcription and its regulation in mammalian and human mitochondria]." Mol Biol (Mosk) **43**(2): 215-229.

Southgate, R. J., C. R. Bruce, et al. (2005). "PGC-1alpha gene expression is down-regulated by Akt- mediated phosphorylation and nuclear exclusion of FoxO1 in insulin-stimulated skeletal muscle." FASEB J **19**(14): 2072-2074.

Srivastava, S. and C. T. Moraes (2001). "Manipulating mitochondrial DNA heteroplasmy by a mitochondrially targeted restriction endonuclease." Hum Mol Genet **10**(26): 3093-3099.

St-Pierre, J., J. A. Buckingham, et al. (2002). "Topology of superoxide production from different sites in the mitochondrial electron transport chain." Journal of Biological Chemistry **277**(47): 44784-44790.

St-Pierre, J., S. Drori, et al. (2006). "Suppression of reactive oxygen species and neurodegeneration by the PGC-1 transcriptional coactivators." Cell **127**(2): 397-408.

Steffann, J., N. Frydman, et al. (2006). "Analysis of mtDNA variant segregation during early human embryonic development: a tool for successful NARP preimplantation diagnosis." Journal of Medical Genetics **43**(3): 244-247.

Stein, C. A., J. B. Hansen, et al. (2010). "Efficient gene silencing by delivery of locked nucleic acid antisense oligonucleotides, unassisted by transfection reagents." Nucleic Acids Res **38**(1): e3.

Sumiya, E., H. Shimogawa, et al. (2011). "Cell-morphology profiling of a natural product library identifies bisebromoamide and miuraenamide A as actin filament stabilizers." ACS Chem Biol **6**(5): 425-431.

Sutovsky, P., R. D. Moreno, et al. (2000). "Ubiquitinated sperm mitochondria, selective proteolysis, and the regulation of mitochondrial inheritance in mammalian embryos." Biol Reprod **63**(2): 582-590.

Suzuki, T., M. Terasaki, et al. (2001). "Proteomic analysis of the mammalian mitochondrial ribosome - Identification of protein components in the 28 S small subunit." Journal of Biological Chemistry **276**(35): 33181-33195.

Taanman, J. W. (1999). "The mitochondrial genome: structure, transcription, translation and replication." Biochim Biophys Acta **1410**(2): 103-123.

Tachibana, M., M. Sparman, et al. (2009). "Mitochondrial gene replacement in primate offspring and embryonic stem cells." Nature **461**(7262): 367-372.

Taivassalo, T., J. L. Gardner, et al. (2006). "Endurance training and detraining in mitochondrial myopathies due to single large-scale mtDNA deletions." Brain **129**: 3391-3401.

Takeuchi, K., S. Shibamoto, et al. (2001). "Signaling pathways leading to transcription and translation cooperatively regulate the transient increase in expression of c-Fos protein." Journal of Biological Chemistry **276**(28): 26077-26083.

Takizawa, M., R. R. Colwell, et al. (1993). "Isolation and diversity of actinomycetes in the chesapeake bay." Appl Environ Microbiol **59**(4): 997-1002.

Tanaka, M., H. J. Borgeld, et al. (2002). "Gene therapy for mitochondrial disease by delivering restriction endonuclease SmaI into mitochondria." J Biomed Sci **9**(6 Pt 1): 534-541.

Tarassov, I., P. Kamenski, et al. (2007). "Import of nuclear DNA-encoded RNAs into mitochondria and mitochondrial translation." Cell Cycle **6**(20): 2473-2477.

Tatuch, Y., J. Christodoulou, et al. (1992). "Heteroplasmic mtDNA mutation (T----G) at 8993 can cause Leigh disease when the percentage of abnormal mtDNA is high." American Journal of Human Genetics **50**(4): 852-858.

Taylor, R. W., P. F. Chinnery, et al. (1997). "Selective inhibition of mutant human mitochondrial DNA replication in vitro by peptide nucleic acids." Nature Genetics **15**(2): 212-215.

Taylor, R. W. and D. M. Turnbull (2005). "Mitochondrial DNA mutations in human disease." Nature Reviews Genetics **6**(5): 389-402.

Tein, I., S. DiMauro, et al. (1993). "Valproic acid impairs carnitine uptake in cultured human skin fibroblasts. An in vitro model for the pathogenesis of valproic acid-associated carnitine deficiency." Pediatr Res **34**(3): 281-287.

Temperley, R. J., M. Wydro, et al. (2010). "Human mitochondrial mRNAs-like members of all families, similar but different." Biochimica Et Biophysica Acta-Bioenergetics **1797**(6-7): 1081-1085.

Tenenbaum, A., M. Motro, et al. (2005). "Dual and pan-peroxisome proliferator-activated receptors (PPAR) co-agonism: the bezafibrate lessons." Cardiovasc Diabetol **4**: 14.

Terzioglu, M., B. Ruzzenente, et al. (2013). "MTERF1 binds mtDNA to prevent transcriptional interference at the light-strand promoter but is dispensable for rRNA gene transcription regulation." Cell Metab **17**(4): 618-626.

Thyagarajan, D., S. Shanske, et al. (1995). "A novel mitochondrial ATPase 6 point mutation in familial bilateral striatal necrosis." Annals of Neurology **38**(3): 468-472.

Tong, L. (2013). "Structure and function of biotin-dependent carboxylases." Cell Mol Life Sci **70**(5): 863-891.

Tong, W. H., G. N. Jameson, et al. (2003). "Subcellular compartmentalization of human Nfu, an iron-sulfur cluster scaffold protein, and its ability to assemble a [4Fe-4S] cluster." Proc Natl Acad Sci U S A **100**(17): 9762-9767.

Tong, W. H. and T. Rouault (2000). "Distinct iron-sulfur cluster assembly complexes exist in the cytosol and mitochondria of human cells." Embo Journal **19**(21): 5692-5700.

Tonks, N. K. (2005). "Redox redux: revisiting PTPs and the control of cell signaling." Cell **121**(5): 667-670.

Trifunovic, A., A. Wredenberg, et al. (2004). "Premature ageing in mice expressing defective mitochondrial DNA polymerase." Nature **429**(6990): 417-423.

Tsuboi, M., H. Morita, et al. (2009). "EF-G2mt is an exclusive recycling factor in mammalian mitochondrial protein synthesis." Molecular Cell **35**(4): 502-510.

Tsukihara, T., H. Aoyama, et al. (1996). "The whole structure of the 13-subunit oxidized cytochrome c oxidase at 2.8 angstrom." Science **272**(5265): 1136-1144.

Tucker, E. J., S. G. Hershman, et al. (2011). "Mutations in MTFMT underlie a human disorder of formylation causing impaired mitochondrial translation." Cell Metab **14**(3): 428-434.

Tuppen, H. A., E. L. Blakely, et al. (2010). "Mitochondrial DNA mutations and human disease." Biochim Biophys Acta **1797**(2): 113-128.

Tyynismaa, H., K. P. Mjosund, et al. (2005). "Mutant mitochondrial helicase Twinkle causes multiple mtDNA deletions and a late-onset mitochondrial disease in mice." Proc Natl Acad Sci U S A **102**(49): 17687-17692.

Tzoulis, C., B. A. Engelsen, et al. (2006). "The spectrum of clinical disease caused by the A467T and W748S POLG mutations: a study of 26 cases." Brain **129**(Pt 7): 1685-1692.

Vionnet, N., P. Passa, et al. (1993). "Prevalence of mitochondrial gene mutations in families with diabetes mellitus." Lancet **342**(8884): 1429-1430.

Waksman, S. A., H. C. Reilly, et al. (1946). "Isolation of Streptomycin-producing Strains of Streptomyces griseus." J Bacteriol **52**(3): 393-397.

Walker, J. E., J. M. Arizmendi, et al. (1992). "Sequences of 20 subunits of NADH:ubiquinone oxidoreductase from bovine heart mitochondria. Application of a novel strategy for sequencing proteins using the polymerase chain reaction." Journal of Molecular Biology **226**(4): 1051-1072.

Wallace, D. C. (1992). "Mitochondrial genetics: a paradigm for aging and degenerative diseases?" Science **256**(5057): 628-632.

Wallace, D. C. (2001). "Mouse models for mitochondrial disease." American Journal of Medical Genetics **106**(1): 71-93.

Wang, C. and R. J. Youle (2009). "The role of mitochondria in apoptosis*." Annu Rev Genet **43**: 95-118.

Wang, G., H.-W. Chen, et al. (2010). "PNPASE Regulates RNA Import into Mitochondria." Cell **142**(3): 456-467.

Wang, G., E. Shimada, et al. (2012). "Correcting human mitochondrial mutations with targeted RNA import." Proceedings of the National Academy of Sciences.

Wang, X. and C. T. Moraes (2011). "Increases in mitochondrial biogenesis impair carcinogenesis at multiple levels." Mol Oncol **5**(5): 399-409.

Wang, Y. and D. F. Bogenhagen (2006). "Human mitochondrial DNA nucleoids are linked to protein folding machinery and metabolic enzymes at the mitochondrial inner membrane." Journal of Biological Chemistry **281**(35): 25791-25802.

Wang, Y. E., G. K. Marinov, et al. (2013). "Genome-Wide Analysis Reveals Coating of the Mitochondrial Genome by TFAM." Plos One **8**(8): e74513.

Wanrooij, P. H., J. P. Uhler, et al. (2010). "G-quadruplex structures in RNA stimulate mitochondrial transcription termination and primer formation." Proc Natl Acad Sci U S A **107**(37): 16072-16077.

Wanrooij, S. and M. Falkenberg (2010). "The human mitochondrial replication fork in health and disease." Biochim Biophys Acta **1797**(8): 1378-1388.

Wanrooij, S., J. M. Fuste, et al. (2008). "Human mitochondrial RNA polymerase primes lagging-strand DNA synthesis in vitro." Proc Natl Acad Sci U S A **105**(32): 11122-11127.

Watt, I. N., M. G. Montgomery, et al. (2010). "Bioenergetic cost of making an adenosine triphosphate molecule in animal mitochondria." Proc Natl Acad Sci U S A **107**(39): 16823-16827.

Wei, M. C., W. X. Zong, et al. (2001). "Proapoptotic BAX and BAK: a requisite gateway to mitochondrial dysfunction and death." Science **292**(5517): 727-730.

Weinbach, E. C. and J. Garbus (1965). "The Interaction of Uncoupling Phenols with Mitochondria and with Mitochondrial Protein." Journal of Biological Chemistry **240**: 1811-1819.

Weiss, M. J., J. R. Wong, et al. (1987). "Dequalinium, a Topical Antimicrobial Agent, Displays Anticarcinoma Activity Based on Selective Mitochondrial Accumulation." Proceedings of the National Academy of Sciences of the United States of America **84**(15): 5444-5448.

Weissig, V., J. Lasch, et al. (1998). "DQAsomes: A novel potential drug and gene delivery system made from Dequalinium (TM)." Pharmaceutical Research **15**(2): 334-337.

Wenz, T., C. Luca, et al. (2009). "mTERF2 regulates oxidative phosphorylation by modulating mtDNA transcription." Cell Metab **9**(6): 499-511.

Willis, S. N., J. I. Fletcher, et al. (2007). "Apoptosis initiated when BH3 ligands engage multiple Bcl-2 homologs, not Bax or Bak." Science **315**(5813): 856-859.

Wittenhagen, L. M. and S. O. Kelley (2002). "Dimerization of a pathogenic human mitochondrial tRNA." Nat Struct Biol **9**(8): 586-590.

Wittig, I. and H. Schagger (2008). "Structural organization of mitochondrial ATP synthase." Biochim Biophys Acta **1777**(7-8): 592-598.

Wittig, I., J. Velours, et al. (2008). "Characterization of domain interfaces in monomeric and dimeric ATP synthase." Molecular & Cellular Proteomics **7**(5): 995-1004.

Wolfe, S. A., L. Nekludova, et al. (2000). "DNA recognition by Cys2His2 zinc finger proteins." Annu Rev Biophys Biomol Struct **29**: 183-212.

Wredenberg, A., M. Lagouge, et al. (2013). "MTERF3 regulates mitochondrial ribosome biogenesis in invertebrates and mammals." Plos Genetics **9**(1): e1003178.

Xia, D., C. A. Yu, et al. (1997). "Crystal structure of the cytochrome bc1 complex from bovine heart mitochondria." Science **277**(5322): 60-66.

Xu, B. and D. A. Clayton (1992). "Assignment of a yeast protein necessary for mitochondrial transcription initiation." Nucleic Acids Res **20**(5): 1053-1059.

Xu, B. and D. A. Clayton (1996). "RNA-DNA hybrid formation at the human mitochondrial heavy-strand origin ceases at replication start sites: an implication for RNA-DNA hybrids serving as primers." Embo Journal **15**(12): 3135-3143.

Yakubovskaya, E., E. Mejia, et al. (2010). "Helix unwinding and base flipping enable human MTERF1 to terminate mitochondrial transcription." Cell **141**(6): 982-993.

Yamada, Y., R. Furukawa, et al. (2011). "Dual function MITO-Porter, a nano carrier integrating both efficient cytoplasmic delivery and mitochondrial macromolecule delivery." Mol Ther **19**(8): 1449-1456.

Yamada, Y. and H. Harashima (2012). "Delivery of bioactive molecules to the mitochondrial genome using a membrane-fusing, liposome-based carrier, DF-MITO-Porter." Biomaterials **33**(5): 1589-1595.

Yasukawa, T., A. Reyes, et al. (2006). "Replication of vertebrate mitochondrial DNA entails transient ribonucleotide incorporation throughout the lagging strand." Embo Journal **25**(22): 5358-5371.

Yasukawa, T., T. Suzuki, et al. (2001). "Wobble modification defect in tRNA disturbs codon-anticodon interaction in a mitochondrial disease." Embo Journal **20**(17): 4794-4802.

Yasukawa, T., T. Suzuki, et al. (2000). "Defect in modification at the anticodon wobble nucleotide of mitochondrial tRNA(Lys) with the MERRF encephalomyopathy pathogenic mutation." Febs Letters **467**(2-3): 175-178.

Yoneda, M., A. Chomyn, et al. (1992). "Marked replicative advantage of human mtDNA carrying a point mutation that causes the MELAS encephalomyopathy." Proc Natl Acad Sci U S A **89**(23): 11164-11168.

Yoneda, M., Y. Tanno, et al. (1990). "A common mitochondrial DNA mutation in the t-RNA(Lys) of patients with myoclonus epilepsy associated with ragged-red fibers." Biochem Int **21**(5): 789-796.

Yoon, T. and J. A. Cowan (2003). "Iron-sulfur cluster biosynthesis. Characterization of frataxin as an iron donor for assembly of [2Fe-2S] clusters in ISU-type proteins." Journal of the American Chemical Society **125**(20): 6078-6084.

Yoshida, M., E. Muneyuki, et al. (2001). "ATP synthase--a marvellous rotary engine of the cell." Nat Rev Mol Cell Biol **2**(9): 669-677.

Zeviani, M., C. T. Moraes, et al. (1988). "Deletions of mitochondrial DNA in Kearns-Sayre syndrome." Neurology **38**(9): 1339-1346.

Zeviani, M., S. Servidei, et al. (1989). "An autosomal dominant disorder with multiple deletions of mitochondrial DNA starting at the D-loop region." Nature **339**(6222): 309-311.

Zhou, W., M. Choi, et al. (2012). "HIF1alpha induced switch from bivalent to exclusively glycolytic metabolism during ESC-to-EpiSC/hESC transition." Embo Journal **31**(9): 2103-2116.

Zollo, O., V. Tiranti, et al. (2012). "Transcriptional requirements of the distal heavy-strand promoter of mtDNA." Proc Natl Acad Sci U S A **109**(17): 6508-6512.

Zweier, J. L., J. T. Flaherty, et al. (1987). "Direct Measurement of Free-Radical Generation Following Reperfusion of Ischemic Myocardium." Proceedings of the National Academy of Sciences of the United States of America **84**(5): 1404-1407.